Using Affimers to dissect a multiprotein complex in living cells

James Shelford

Supervisors: Prof. Stephen Royle and Prof. Richard Bayliss

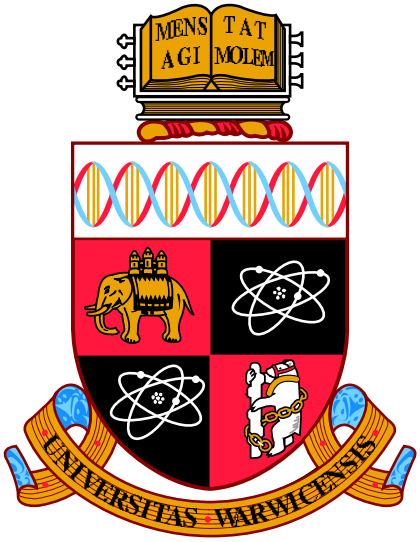

Thesis submitted to the University of Warwick in partial fulfilment for the degree of Doctor of Philosophy in Life Sciences

December 2021

Contents

List of Figures

List of Tables

Acknowledgements

Firstly, I would like to thank my supervisor, Steve Royle, for his support and valuable scientific advice throughout the course of my PhD. In particular, thank you for the inspiration and guidance to write my own code for the quantitative aspects of my project. I would also like to thank my second supervisor, Richard Bayliss, for the useful discussion of my project during lab meetings.

I am grateful to all members of the Royle lab past and present for their support, and for providing me the opportunity to learn. I am especially thankful to Gabrielle, Miguel, Cansu and Laura for the beers and laughter, that flowed in equal measure. A special thanks to Laura for her kindness, always being on hand with a sweet treat or two, or three!

To Mum, thank you for simultaneously being my biggest fan and critic, but for always encouraging me to be the best that I can be. Thanks also for your recommendation of Trevor Nelson's rhythm nation, which made the many hours of analysis even more enjoyable! Most importantly, thank you Emma - without your kindness, support and incredible Sunday roasts, this thesis would not have been possible.

Finally, I am grateful to the MIBTP and the BBSRC for funding my PhD.

Declaration

This thesis is submitted to the University of Warwick in support of my application for the degree of Doctor of Philosophy. It has been composed by myself and has not been submitted in any previous application for any degree.

The work presented in this thesis was carried out by myself, except in the case of figures 3.5 and 3.6, which were carried out by Selena Burgess. This is acknowledged within the figure legends.

The model presented in figure 1.6 in the introduction section has been published (Ryan et al. 2021), and the paper is included at the end of this thesis in Appendix 2. In this article, I contributed to the validation of CRISPR/Cas9-mediated knock-in cell lines, and carried out experiments investigating the recruitment of GTSE1 to the TACC3–ch-TOG–clathrin complex.

Summary

Accurate cell division depends on the precise segregation of chromosomes to generate two genetically identical daughter cells. High fidelity in this process is achieved by the formation of a bipolar mitotic spindle, an array of microtubules that are organised and regulated by the concerted action of motor and non-motor proteins. One known non-motor protein complex composed of TACC3, ch-TOG, clathrin and GTSE1, has been implicated in mitotic spindle stability. This complex is important for the organisation of microtubules that form the kinetochore fibres, which facilitate the movement of chromosomes during mitosis. Owing to the importance of this complex in ensuring accurate mitosis, it is an attractive target to disrupt in a cancer context.

Affimers are novel synthetic binding proteins based on the consensus sequence of a phytocystatin cysteine protease inhibitor found in plants. Here, we used Affimers as a research tool to dissect the TACC3–ch-TOG–clathrin–GTSE1 complex in human cells, with a goal of developing specific inhibitors to disrupt cell division in an anti-cancer context. Expression of Affimers in HeLa cells as mCherry-fusion proteins led to specific disruption of the TACC3–ch-TOG interaction at the mitotic spindle, displacing ch-TOG while leaving the localisation of the other complex components intact. Inhibition of TACC3–ch-TOG had no effect on a number of functions previously ascribed to these proteins, such as MT growth and plus-end tracking. Inhibition of this interaction led to unexpected fragmentation of the pericentriolar material (PCM) in metaphase cells following the formation of a bipolar spindle, coupled with a delayed transition to anaphase. This effect was not observed with a control Affimer. Thus, this work has uncovered a novel role of TACC3–ch-TOG in maintaining PCM integrity during mitosis to ensure timely cell division. More broadly, this thesis demonstrates that Affimers are useful tools for dissecting the functional properties of multiprotein complexes in living cells.

Abbreviations

+TIP	microtubule plus-end tracking protein
γ-TuRC	γ-tubulin ring complex
ANOVA	analysis of variance
APC	anaphase promoting complex
BSA	bovine serum albumin
CDK	cyclin-dependent kinase
ch-TOG	colonic and hepatic tumor overexpressed gene protein
CHC	clathrin heavy chain
CID	clathrin interaction domain
CRISPR	clustered regularly interspaced short palindromic repeats
DMEM	Dulbecco's Modified Eagle's Medium
dTdT	deoxythymidine dinucleotide
EB	end-binding
EB1	end-binding protein 1
EB3	end-binding protein 3
ELISA	enzyme-linked immunosorbent assay
ESCRT-III	endosomal sorting complex required for transport III
FBS	fetal bovine serum
FKBP	FK506-binding protein
FRAP	fluorescence recovery after photobleaching
FRB	FKBP and rapamycin-binding
GDP	guanosine diphosphate
GTP	guanosine triphosphate
GTSE1	G2 and S-phase expressed protein 1
IF	immunofluorescence
IRES	internal ribosome entry site
K-fibre	kinetochore-fibre
KS	knocksideways
LB	lysogeny broth
MAP	microtubule-associated protein

MCAK	mitotic centromere-associated kinesin
MT	microtubule
NTD	N-terminal domain
PBS	phosphate buffered saline
PCM	pericentriolar material
PCR	polymerase chain reaction
PFA	paraformaldehyde
ROI	region of interest
SAC	spindle assembly checkpoint
siRNA	small interfering RNA
TACC3	transforming acidic coiled-coil containing protein 3
TBS	tris buffered saline
TBS-T	tris buffered saline with tween 20
WT	wild-type
XMAP215	*Xenopus* microtubule-associated protein 215

Chapter 1

Introduction

1.1 The cell cycle

To give rise to two genetically identical daughter cells, the mother cell must go through a highly coordinated process of events known as the cell cycle. In eukaryotic cells, the cell cycle can be separated into two stages: interphase and mitosis. Interphase can be further separated into three phases: G1 (gap-1), the cell undergoes growth and duplication of its organelles; S (synthesis), the cell duplicates its genome; G2 (gap-2), the cell continues to grow and synthesises proteins in preparation for the next stage, mitosis. For a typical dividing human cell in tissue culture, the cell cycle is approximately 24 h, with the majority of this time spent in interphase, and only an hour required for mitosis, where the mother cell physically divides into two daughters.

The progression of the cell cycle is controlled by cyclin-dependent kinases (CDKs), serine threonine kinases that are activated by the binding of their co-factors, cyclins. Once activated, cyclin-CDK complexes phosphorylate substrates to promote DNA synthesis and entry into mitosis. The importance of CDKs in promoting cell cycle progression was first realised from work carried out in yeast (Nurse et al. 1976; Hartwell et al. 1970), while the discovery of cyclins that are synthesised and degraded at various points of the cell cycle, occurred from work in sea urchins (Evans et al. 1983).

Based on decades of research on cyclin-CDK complexes and their substrates, we now have a general framework to describe how the cell cycle in mammalian systems is regulated (Fig. 1.1). In dividing cells, mitogens stimulate the production of cyclin D proteins, enabling the subsequent formation of cyclin D-CDK4/6 complexes in G1. These complexes are responsible for the

phosphorylation of retinoblastoma (Rb) proteins, that function to control the activity of transcription factors (Sherr and Roberts 1999). This phosphorylation event promotes DNA transcription, leading to the production of cyclin E and cyclin E-CDK2 complexes that irreversibly inactivate Rb proteins (Malumbres and Barbacid 2005). Once this point is reached, the cell no longer needs encouragement from mitogens to divide, resulting in entry to S phase. Since the activity of cyclin E-CDK2 initiates DNA replication, it must be inactivated through degradation of cyclin E during S phase to prevent the re-replication of DNA (Hwang and Clurman 2005). CDK2 is now able to bind the newly synthesised cyclin A proteins, enabling the cyclin A-CDK2 complexes to drive progression through S phase by phosphorylating various substrates required to complete S phase (Malumbres and Barbacid 2005). Moreover, A-type cyclins activate CDK1, but their degradation and the synthesis of cyclin B proteins during G2 leads to the formation of cyclin B-CDK1 complexes that ultimately permit entry into mitosis. Destruction of cyclin B and the reactivation of phosphatases leads to the inactivation of CDK1, driving mitotic exit (Holder et al. 2019).

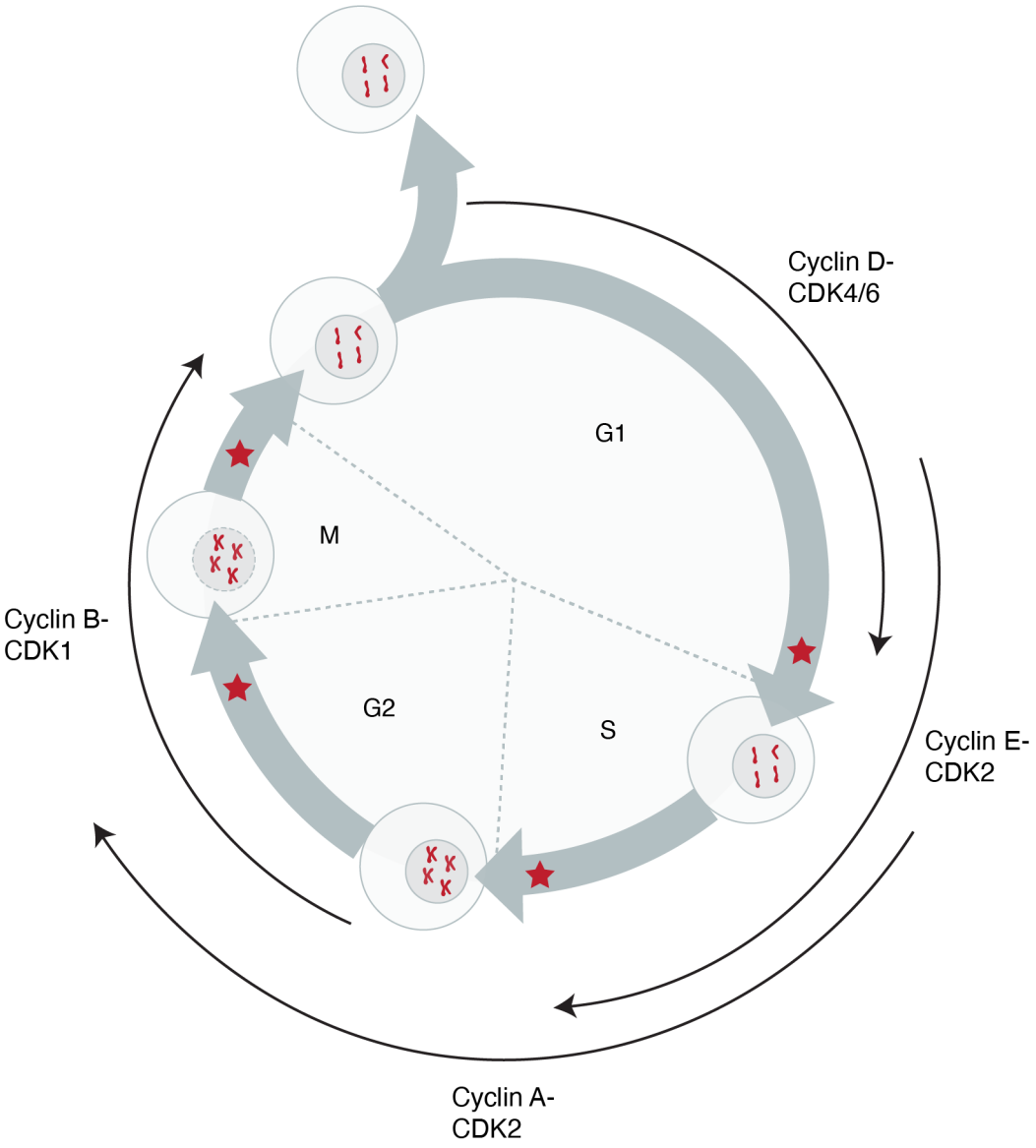

Figure 1.1. The cell cycle. A schematic to illustrate the stages of the cell cycle and the contribution of cyclin-CDK complexes, where activation and inactivation of these complexes drives progression to each stage. Checkpoints (indicated by red stars) can pause progression through the cell cycle by promoting signalling events that control the activity of cyclin-CDK complexes, thus preventing uncontrolled proliferation.

1.1.1 Cell cycle checkpoints

Errors during stages of the cell cycle can result in the activation of checkpoints, surveillance mechanisms that ensure the accurate and coordinated progression of the cell cycle. For example, DNA damage activates cell cycle checkpoints in G1, S phase and at the G2/M transition, to stop cell cycle progression and initiate the repair of damaged DNA (Visconti et al. 2016; Kastan and Bartek 2004). During mitosis, the segregation of sister chromatids at the onset of anaphase must only occur once each pair has formed a bipolar attachment to the mitotic spindle. Errors associated with this task are detected by proteins of the spindle assembly

checkpoint (SAC), and arrests the cell in metaphase (Cheeseman 2014).

1.2 The stages of mitosis

The first descriptions of the subcellular details of cell division in animal cells were published by Walther Flemming between 1874-1876 and later summarised in his book in 1882, in which the term mitosis was used to describe this process for the first time (Paweletz 2001). Flemming described the rearrangement of 'nuclear threads' during progressive and regressive phases of cell division. Here, the progressive phase was defined by the appearance of threads within the nucleus that were subsequently arranged in the centre of the cell, while the regressive phase was defined as the separation of these threads to form two daughter nuclei. In 1888, Heinrich Wilhelm Waldeyer coined the term chromosomes, to describe these nuclear threads (Paweletz 2001). Thanks to the pioneering work of many researchers, and the development of technology to manipulate and visualise this process in intricate detail, we now define mitosis as the process in which a mother cell equally segregates its duplicated genome to form two genetically identical daughter cells (Fig. 1.2).

1.2.1 Prophase

Prophase is the first stage of mitosis and is defined by the visible compaction of chromatin into condensed chromosomes, each consisting of two identical sister chromatids. How the cell manages to package several metres of DNA into micrometre-sized chromosomes appropriate for cell division is still an active area of investigation. However, research into this area has shown that condensin proteins are required for this process (Thadani et al. 2012), and that postranslational modifications of chromatin are also likely to play a role in its compaction (McIntosh 2016). During this stage, the interphase microtubules (MTs) are rapidly disassembled (Rusan et al. 2002), whilst new MTs begin to grow from the centrosomes. The newly formed MTs will later form the mitotic spindle (McIntosh 2016). Concomitant with this structural reorganisation, the cell rounds up which provides symmetry to encourage the equal distribution of the cells contents during the later stages of mitosis. In mammalian cells, the end of prophase is marked by the rupture of the nuclear envelope and subsequent release of the chromosomes into the cytoplasm.

1.2.2 Prometaphase

The goal of prometaphase is to align the now freely accessible chromosomes at the cell equator, ensuring that the sister chromatids are attached to opposite poles. To achieve this, the cell builds the mitotic spindle, composed of dynamic MTs that emanate from the centrosomes present at either pole. Via this process, MTs grow out into the region occupied by the chromosomes and capture them by binding the kinetochore, a large multiprotein structure present on each chromatid (Cheeseman 2014). This is made possible by the rapid transition between growing and shrinking states that MTs undergo, known as dynamic instability (Mitchison and Kirschner 1984). In essence, growth and shrinkage provides MTs with multiple chances to capture chromosomes at the kinetochore, where they are then stabilised. Mathematical modelling has suggested that this search and capture method alone is not sufficient to carry out this task (Wollman et al. 2005), thus the cell uses other mechanisms to assist spindle assembly. For example, MTs assembled from chromatin or even from the MTs themselves, helps to increase the density of MTs within the cell (Prosser and Pelletier 2017).

Alignment of chromosomes at the cell equator is achieved in part by bi-orientation, when sister kinetochores are stably attached to MTs emanating from opposite poles (Maiato et al. 2017). However, chromosomes located further away from the cell equator, for example at the poles, require the coordinated activity of motor proteins that transport the chromosomes along MTs to achieve bi-orientation (Maiato et al. 2017). Prometaphase is thought to be complete once all chromosomes are aligned at the cell equator.

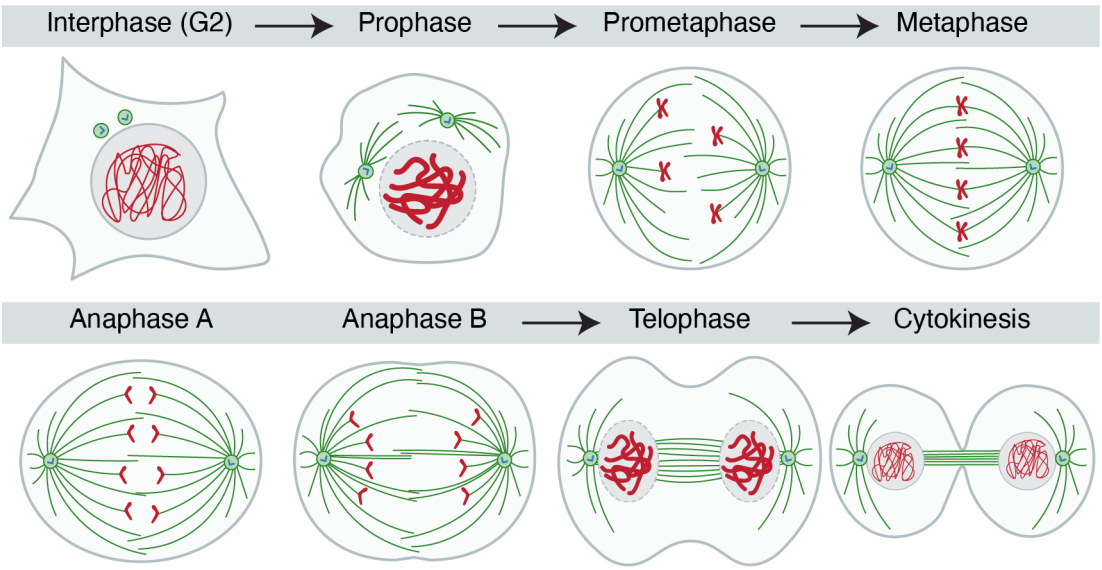

Figure 1.2. The stages of mitosis. A schematic to illustrate the cellular changes associated with each stage of mitosis, as shown by the DNA (red) and microtubules (green). Note that anaphase is often described as two mechanisms: anaphase A and B, though their timings and relative contributions vary depending on the species and cell type (see main text for details).

1.2.3 Metaphase

Metaphase begins once all of the chromosomes have congressed at the cell equator, otherwise known as the metaphase plate. Sister chromatids are held in place at the metaphase plate by virtue of their attachment to bundles of parallel MTs, collectively referred to as a kinetochore-fibre (K-fibre), that typically span from the kinetochore to the spindle pole. The number of MTs within a K-fibre increases as it matures through prometaphase and metaphase, with human cell lines containing 20-40 MTs per K-fibre by anaphase (Nixon et al. 2015). To progress to anaphase and separate the chromosomes, the SAC must be silenced. This is thought to be achieved by having sufficient tension between all pairs of sister kinetochores as a result of the opposing forces generated by their respective K-fibres (Cheeseman 2014). Silencing of the SAC leads to a cascade of events where the anaphase promoting complex (APC), an E3 Ubiquitin ligase, is activated and targets multiple regulatory proteins for degradation (Peters 2006). Importantly, the degradation of securin and subsequent activation of separase, leads to the irreversible cleavage of the cohesin complex, which functions to hold the sister chromatids together (Nasmyth and Haering 2009). As a result, sister chromatid separation can now occur.

1.2.4 Anaphase

Following cleavage of the cohesin complex, the sister chromatids are segregated to opposite poles, in a process called anaphase. This stage is often described as two mechanisms: the poleward movement of chromosomes as anaphase A and elongation of the spindle as anaphase B. In each case, the dynamic change in the length of various types of MTs is coupled to chromosome movement. During anaphase A, shortening of the K-fibres via the loss of tubulin from the kinetochore associated MT plus-ends, is partly responsible for the poleward movement of chromosomes (Asbury 2017). The disassembly of MT minus-ends at the poles is also thought to contribute to the velocity of poleward chromosome movement (Rogers et al. 2004).

The forces required for anaphase B spindle elongation to separate the spindle poles, can be generated by pulling from the outside of the spindle, or pushing from the inside of the spindle. However, determining which mechanism is the dominant force is still under investigation, made more complicated by the fact that this can differ between organisms (Vukušić and Tolić 2021). From outside of the spindle, force can be generated via the direct contact of astral MTs and the cell cortex. In this context, force can be generated by the action of a minus-end directed motor protein or the depolymerisation of the plus-ends of astral MTs anchored at the cortex, both of which would result in pulling the poles towards the cortex (Vukušić and Tolić 2021). Forces inside of the spindle are thought to arise from the pushing of antiparallel, overlapping interpolar MTs of the central spindle within the spindle midzone. Here, plus-end directed motors function to slide apart the interpolar MTs, thereby generating pushing forces onto the poles. This can occur directly, by the sliding minus-ends pushing the poles, or indirectly, by sliding minus-ends into K-fibres that are connected to the poles (Vukušić and Tolić 2021).

1.2.5 Telophase

The goal of telophase is to take the cell from a mitotic state back to an interphase state, in preparation for the abscission into two daughter cells. To do this, pieces of the reorganised ER network contact the chromatin mass and fuse together, reforming the nuclear envelope (Schooley et al. 2012). Shortly after this, the chromatin starts to decondense to resemble a functional interphase nucleus that is capable of DNA transcription. This is thought to occur via the action of phosphatases that function to undo the work carried out by the mitotic kinases at the start of mitosis (Qian et al. 2011). Moreover, removal of the mitotic kinase Aurora B from chromatin is a requirement for decondensation (Ramadan et al.

2007).

At the onset of anaphase, bundling of antiparallel MTs within the spindle midzone leads to the formation of the central spindle (Lee et al. 2012). MT bundling is achieved in part by the recruitment of PRC1 to the spindle midzone (Mollinari et al. 2002), and the action of the centralspindlin complex (Mishima et al. 2002).

1.2.6 Cytokinesis

Though not recognised as a stage in mitosis, cytokinesis is the final stage of cell division, and is defined by the formation of two new daughter cells, equally sharing the cellular contents of the mother cell. As per the stages of mitosis, it must be completed without errors, as failure can lead to aneuploidy, a hallmark of cancer (Lens and Medema 2019).

The driving force of this process is the actomyosin ring, which contracts at the cell equator to draw in the plasma membrane and form a cleavage furrow (Glotzer 2017). Cleavage furrow ingression helps form the intracellular bridge, by compacting together the MT bundles that are present between the nascent daughter cells. Upon completion, the midbody is formed. This refers to the bundled MTs that are present at the intracellular bridge (Lee et al. 2012).

Abscission of the membrane to physically separate the daughter cells, is mediated by the endosomal sorting complex required for transport III (ESCRT-III) protein complex (Carlton and Martin-Serrano 2007). To complete the abscission, the ESCRT-III complex recruits spastin, a MT severing enzyme, that leads to the disassembly of bundled MTs in the midbody (Yang et al. 2008).

1.3 Microtubules

Microtubules are an essential component of all eukaryotic cells, performing crucial functions during both interphase and mitosis. They provide tracks for the motor protein driven transport of vesicles and organelles around the cell, and along with actin and intermediate filaments, form the cytoskeleton that serves to maintain cell shape and structure. During mitosis, MTs form the mitotic spindle, responsible for the distribution of the cells genome to two daughter cells with high precision.

1.3.1 Structure and assembly

The term microtubule was coined in 1963 following the observation of 'small tubules' present in the cytoplasm of cells by electron microscopy (Slautterback 1963; Ledbetter and Porter 1963). A few years later, the core component of MTs was identified by colchicine binding experiments in sea urchin eggs (Borisy and Taylor 1967), and later given the name tubulin (Mohri 1968). As their naming suggests, MTs are hollow tubes composed of tubulin proteins assembled in linear strands called protofilaments. In mammalian cells, MTs contain 13 laterally connected protofilaments, each assembled from a head-to-tail arrangement of α,β-tubulin heterodimers (Meunier and Vernos 2012). By virtue of this organisation, MTs are polar, with a minus-end that contains exposed α-tubulin, and a plus-end with exposed β-tubulin. Importantly, the minus-ends are characterised by slow MT growth and are typically embedded at the centrosome where there are nucleated, whereas the plus-end is characterised by fast MT growth and explores the volume of the cell.

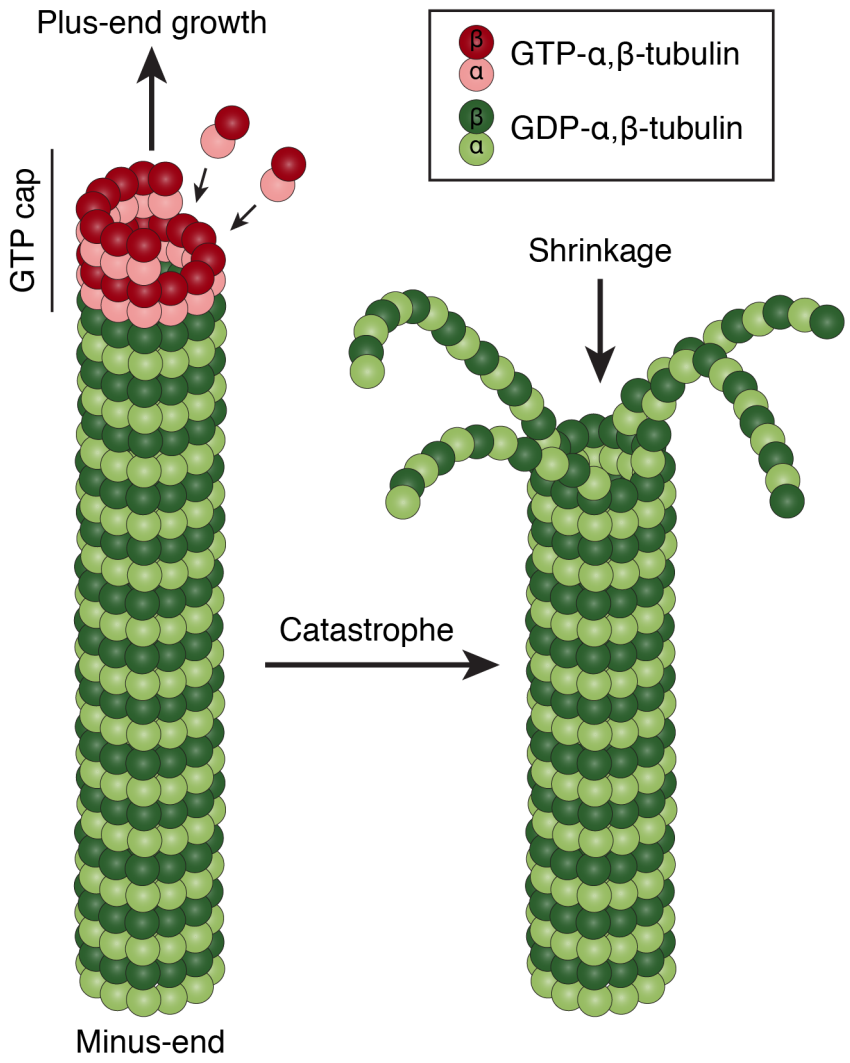

Figure 1.3. Microtubules transition between periods of growth and shrinkage. A cartoon representation of microtubule dynamic instability. The presence of a GTP-cap at the plus-end is proposed to stabilise the remaining GDP-tubulin containing filament and enable growth. Loss of the GTP-cap results in shrinkage (catastrophe).

The intrinsic behaviour of MTs is attributed to their dynamic instability, which was discovered by Mitchison and Kirschner and explained by their GTP cap model, where the behaviour of MTs depends on the hydrolysis of guanosine triphosphate (GTP) to guanosine diphosphate (GDP) (Mitchison and Kirschner 1984). This model proposes that since tubulin bound to GTP is the predominant form in solution, MTs are assembled using this form of tubulin. Once GTP-tubulin is assembled into a MT, the GTP is hydrolysed to GDP, forming GDP-tubulin (Carlier and Pantaloni 1981). This means that after a short period of growth, the majority of the MT contains GDP-tubulin, with a small GTP-cap at the plus-end that functions to stabilise the entire structure (Fig. 1.3). The size of the GTP-cap is dependent on the rate in which GTP-tubulin is added compared to the rate in which it dissociates, and the hydrolysis rate of GTP-tubulin. If

the GTP-cap becomes too small, the MT transitions to a period of shortening (Gudimchuk and McIntosh 2021). Therefore, a key feature of dynamic instability is that MTs will stochastically switch from a period of growth to shrinkage, termed a 'catastrophe', or from a period of shortening to growth, termed 'rescue'. Although the turnover of MTs is an energetically expensive process, it is necessary to allow cells to adapt to changes in the environment, and those brought about by the cell cycle, e.g. to search and capture chromosomes during mitosis.

MTs serve as binding sites for a group of functionally diverse proteins known as microtubule-associated proteins (MAPs). In this regard, MAPs can be grouped based on their function to nucleate MTs, promote MT growth by polymerisation or stabilisation, destabilise MTs via depolymerisation, crosslink MTs or provide transport in the case of molecular motors (Petry 2016).

1.3.2 Microtubule plus-end binding proteins

Since the plus-end of MTs is the predominant site of growth, it is an important site of MT regulation by MAPs. This function is carried out by a broad group of functionally diverse proteins, known collectively as microtubule plus-end tracking proteins (+TIPs), characterised by their comet-like appearance at the ends of growing MTs (Schuyler and Pellman 2001).

The XMAP215 family

The so-called XMAP215 family refers to a highly conserved group of microtubule-associated proteins, where at least one member is present in all eukaryotic organisms (Gard et al. 2004). *Xenopus* microtubule-associated protein 215 (XMAP215) was first isolated from *Xenopus* egg extract, where it was found to dramatically promote MT elongation at the plus-end *in vitro* (Gard and Kirschner 1987). Therefore, the XMAP215 family, which includes the human homologue colonic and hepatic tumor overexpressed gene protein (ch-TOG), are a well studied class of +TIP that function as MT polymerases to promote MT growth (Brouhard et al. 2008). Their MT polymerase activity comes via conserved N-terminal TOG domains, which have been shown to directly bind tubulin dimers *in vitro* (Brouhard et al. 2008; Widlund et al. 2011). Of note, ch-TOG and its *Xenopus* homologue XMAP215 are monomeric proteins, containing five N-terminal TOG domains, while the yeast member Stu2 is dimeric and contains two TOG domains on each protein (Akhmanova and Steinmetz 2015). Recently, a putative sixth TOG domain (TOG6) has been identified in the C-terminal region of human ch-TOG by nuclear magnetic resonance (NMR), alongside a helical domain termed '4α', due to the presence of four α-helices

(Rostkova et al. 2018). In addition to its TOG domains, *in vitro* assays using deletion mutants of XMAP215, identified a basic linker region between TOG4 and TOG5 that acts as a MT lattice binding domain (Widlund et al. 2011). Together, it is thought that TOG proteins bind to the MT plus-end via a lattice binding domain and catalyse the addition of tubulin by way of the TOG domains. It is intriguing that TOG proteins selectively bind MT plus-ends, and do so regardless of the growing or shrinking state (Brouhard et al. 2008). The current explanation for this comes from structural work using the yeast XMAP215 member Stu2, that found TOG1 and TOG2 selectively binds a curved conformation of α,β-tubulin, likely to exist only at the extreme plus-end of MTs (Ayaz et al. 2014).

Studies investigating the role of ch-TOG in complex with its binding partner TACC3 in cells will be discussed in section 1.5.3.

End-binding proteins

Another group of extensively studied +TIPs are the highly conserved end-binding (EB) proteins: EB1, EB2 and EB3 (Akhmanova and Steinmetz 2015). Unlike TOG proteins that bind the extreme tip of the plus-end, EB proteins bind at a site approximately 100 nm downstream (Maurer et al. 2014; Gutierrez-Caballero et al. 2015). Moreover, they autonomously track growing MT plus and minus-ends. It is thought that EB proteins recognise the nucleotide state of tubulin, as they preferentially bind to GTP-tubulin, found at the MT tip, over the GDP-tubulin lattice (Zanic et al. 2009). MT binding is mediated by a calponin homology domain at the N-terminus (Hayashi and Ikura 2003). The key feature of EB proteins is their ability to act as an adaptor and recruit other +TIP proteins to the growing ends. This was realised by the finding that the majority of +TIPs contain a Ser-x-Ile-Pro (SxIP, where x denotes any amino acid) amino acid motif that is recognised by the EB homology domain of EB proteins (Honnappa et al. 2009). It is now clear that EB proteins recruit a plethora of functionally diverse proteins to growing MT ends to regulate a variety of cellular processes including cell migration, mitotic spindle positioning and kinetochore MT attachment (Akhmanova and Steinmetz 2015).

It has long been recognised that phosphorylation of residues in close proximity to SxIP motifs on +TIPs directly affects their affinity to EB proteins, and therefore serves as a mechanism to regulate their localisation at MT ends (Honnappa et al. 2009). However, more evidence for the cell-cycle regulation of +TIPs is emerging. One example of a +TIP regulated in this way is G2 and S-phase expressed protein 1 (GTSE1), which has previously been shown to be recruited to the MT plus-end by EB1 to promote cell migration (Scolz et al. 2012). More recently,

it was discovered that GTSE1 is hyperphosphorylated by CDK1 at the onset of mitosis, which abolishes its interaction with EB1 (Singh et al. 2020). This regulation is required to destabilise astral MTs to enable spindle reorientation during prometaphase (Singh et al. 2020).

1.4 The mitotic spindle

The mitotic spindle is a MT based structure, defined by 3 subclasses of MT (Fig. 1.4), that functions to separate the mitotic chromosomes into two daughter cells. This essential task is achieved through the concerted action of MAPs, that help build the spindle and provide the stability and forces needed to separate the chromosomes.

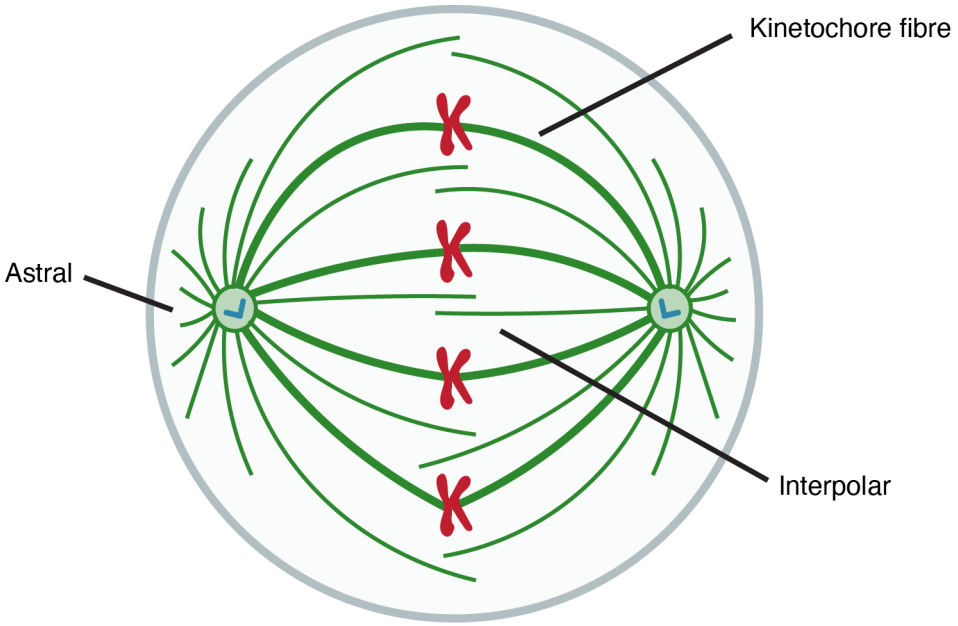

Figure 1.4. The metaphase spindle. A schematic diagram to illustrate the three subclasses of microtubules that form the metaphase spindle: kinetochore fibres (bundles of kinetochore microtubules), interpolar and astral.

1.4.1 Astral microtubules

Astral MTs emanate from the mitotic centrosomes toward the cell cortex to create a link that is responsible for spindle orientation. This is thought to occur via the recruitment of the minus-end directed motor protein complex, dynein, that walks along the MT to generate force required to reorient the spindle during mitosis (O'Connell and Wang 2000). It is also thought that the force generated by the dynein motor complex pulling the astral MTs towards the cell cortex contributes to spindle elongation during anaphase B (Vukušić and Tolić 2021).

1.4.2 Interpolar microtubules

Interpolar MTs extend from the centrosome to the metaphase spindle body, and during anaphase they overlap with MTs of the same class from the opposite pole in an antiparallel fashion (Mastronarde et al. 1993). They are the most abundant class of spindle MT, providing structure to maintain a bipolar spindle (Meunier and Vernos 2012). Moreover, they are the most dynamic class of spindle MT, with an estimated half-life of 1 minute in metaphase and anaphase spindles (Zhai et al. 1995). As the cell progresses to anaphase, overlapping interpolar MTs at the cell equator form bundles between the segregating chromosomes, referred to as the central spindle (Lee et al. 2012). However, some interpolar MTs are much shorter and do not extend to the metaphase plate (Mastronarde et al. 1993).

1.4.3 Kinetochore fibres

According to the textbook definition, kinetochore-fibres (K-fibres) are bundles of parallel kinetochore MTs that extend from the centrosome to the metaphase plate, where they are attached to kinetochores present on sister chromatids. As such, K-fibres begin to form during spindle assembly, when MTs emanating from the centrosome grow out and are captured by kinetochores where they are stabilised. Additionally, MTs can grow out from the kinetochore where they are captured by centrosome MTs, and incorporated into the developing spindle by the action of motor proteins (Maiato et al. 2004). However, recent electron tomography data shows that only half of the kinetochore MTs within K-fibres of a HeLa cell in metaphase reach the spindle pole (Kiewisz et al. 2021). Moreover, this study found that many kinetochore nucleated MTs are short in length, with their minus-ends positioned away from the poles. In these instances, the kinetochore MTs of the K-fibre are indirectly linked to the pole by interpolar MTs (Kiewisz et al. 2021). Nonetheless, the K-fibres function to physically link sister chromatids to opposite poles to ensure faithful segregation.

Within the metaphase spindle, K-fibres are more stable than interpolar or astral MTs, as demonstrated by the fact that they do not immediately depolymerise in cells exposed to low temperature (Rieder 1981). During metaphase, MTs within the K-fibre display a so-called ‘flux’, where polymerisation occurs at the kinetochore attached plus-end, and depolymerisation occurs at the spindle pole focussed minus-end (Mitchison 1989). During anaphase in human cells, the majority of chromatid poleward movement is thought to occur through disassembly of the kinetochore attached plus-end, though how the plus-end can disassemble whilst maintaining an attached chromosome is unclear (Asbury 2017). K-fibres are therefore not only a physical link between the chromosome and the

spindle pole, but a force-generating unit that powers chromosome movement during mitosis. Despite this, it has been shown that K-fibres without a direct link to the pole can still move chromosomes poleward during anaphase (Sikirzhytski et al. 2014). This is thought to occur via the dynein-driven poleward transport of a K-fibre connected to an adjacent K-fibre or interpolar MT (Sikirzhytski et al. 2014).

How are K-fibres maintained as coherent units to ensure accurate chromosome segregation? A clue was revealed from early 2D electron microscopy studies that identified inter-MT bridges between the kinetochore MTs in HeLa cells (Hepler et al. 1970). More recently, work using 3D electron microscopy revealed that the inter-MT bridges resemble an interconnected 'mesh' that links multiple MTs within the K-fibre (Nixon et al. 2015). Moreover, a multiprotein complex containing TACC3, clathrin, ch-TOG and GTSE1 has been identified as one component of the mesh (Booth et al. 2011; Nixon et al. 2015). Disruption of this complex leads to fewer inter-MT bridges and a delayed mitosis (Booth et al. 2011; Nixon et al. 2015). Therefore, this complex is required to maintain the structure of the K-fibre and enable chromosome movement to occur efficiently. The TACC3–ch-TOG–clathrin–GTSE1 complex will be discussed in section 1.5.6.

1.4.4 Centrosomes

Centrosomes are membraneless organelles that serve as a major site of MT nucleation in most animal cells, and are often referred to as the dominant microtubule-organising centre (MTOC). At the core of the centrosome are two barrel-like structures called the centrioles, a mother and a daughter, arranged at a right angle to one another. Each centriole consists of a distinctive organisation of nine triplet MTs arranged in a circular fashion around a cartwheel-like structure with nine spokes (Nigg and Stearns 2011). Surrounding the centrioles is the pericentriolar material (PCM), a matrix containing hundreds of proteins that function to nucleate, organise and stabilise MTs (Conduit et al. 2015).

During mitosis, the two centrosomes are localised at opposite poles of the bipolar spindle. As the cell divides, each daughter cell receives one centrosome containing a pair of centrioles. Therefore to repeat this process, the centrosome undergoes duplication and maturation steps, known as the centrosome cycle (Fig. 1.5). This cycle of events is tightly coupled with the cell cycle and is regulated by kinases such as polo-like kinase 4 (PLK4), a critical factor in controlling centriole number (Nigg and Holland 2018). Centrosome amplification, that is cells with too many centrosomes, can lead to multipolar spindle formation and chromosome mis-segregation, thus leading to aneuploidy (Raff and Basto 2017). Though

centrosome amplification is a common feature of many types of cancer and is often correlated with an increase in aneuploidy, it is unclear what role centrosome amplification has in driving tumourigenesis, and how this could differ between cancers of different origins (Raff and Basto 2017; Godinho and Pellman 2014).

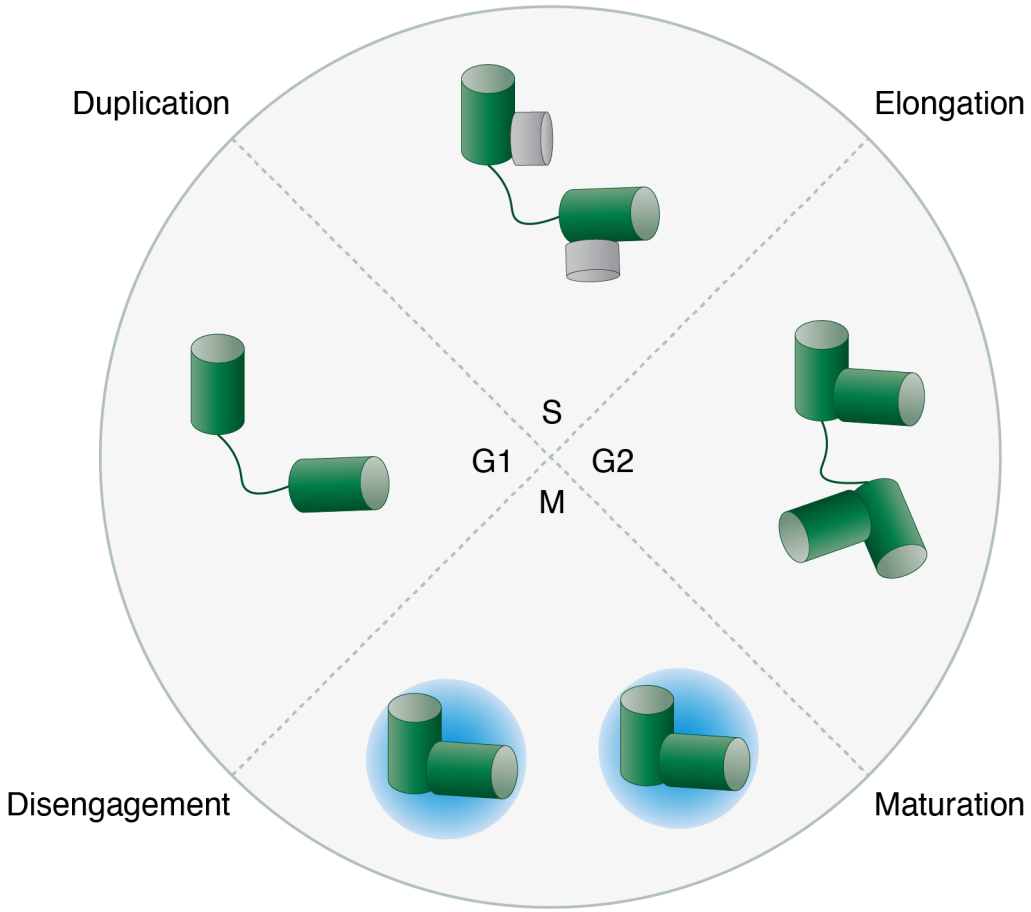

Figure 1.5. The centrosome cycle. In late mitosis, the link between the centrioles (shown in green) is severed during a process called disengagement that requires the activity of polo-like kinase 1 and separase. This process is a primer for centriole duplication in the next cycle. Therefore in G1, a cell has one centrosome that contains two closely associated centrioles, the mother and daughter, that are only loosely attached by a fibrous connection. Alongside DNA replication, the centrioles undergo duplication in S phase, where polo-like kinase 4 plays a key role. Here, a procentriole (shown in grey) assembles at an angle perpendicular to each parent centriole, which elongates through G2. The tether between the mother and daughter centriole is lost. At the end of G2 and continuing throughout early mitosis, the centrosome matures, leading to a rapid accumulation of pericentriolar material (shown in blue) around the centrioles. A process that is promoted by Aurora A and polo-like kinase 1.

The pericentriolar material

The PCM is a complex assortment of proteins that surrounds the centrioles. Owing to its main function, MT nucleation, it is rapidly recruited by the centrioles in late G2 and early mitosis in order to build the mitotic spindle. This process of expansion is known as centrosome maturation, and is driven by the kinase activity

of polo-like kinase 1 (PLK1) and Aurora A, and the action of their substrates. For example, PLK1 phosphorylates pericentrin, a coiled-coil containing protein that constitutes a core component of the PCM, and acts as a scaffold to recruit other proteins. Upon phosphorylation, pericentrin contributes to the recruitment and anchorage of γ-tubulin ring complex (γ-TuRC) to the PCM, where it nucleates MTs (Lee and Rhee 2011; Zimmerman et al. 2004). Although assembled in the cytoplasm from multiple copies of γ-tubulin and γ-tubulin complex proteins, γ-TuRCs are activated at the PCM via the action of CDK5RAP2 in a PLK1 and Aurora A dependent manner (Conduit et al. 2015; Choi et al. 2010; Farache et al. 2018). Once activated, MTs are assembled using the 13-fold symmetry of the γ-TuRC as a template, which then functions as a cap at the minus-end (Prosser and Pelletier 2017). Though γ-tubulin is a member of the tubulin superfamily and is required for the nucleation of MTs in cells, it does not assemble into MTs.

Unsurprisingly, disruption of these pathways, for example through inhibiting PLK1 function, leads to a drastic reduction in centrosome MT nucleation due to reduced γ-tubulin complexes at the PCM (Lane and Nigg 1996). Moreover, Eg5-mediated centrosome separation is also impaired, as loss of PLK1 function frequently results in the formation of monopolar spindles (McInnes et al. 2006). Loss of Aurora A function results in similar phenotypes (Barr and Gergely 2007).

Upon entry to mitosis, it is clear that cells rapidly increase the amount of PCM around the centrioles in order to promote MT nucleation. However, it is less clear how this material, containing hundreds of proteins, is actually organised to carry out this function. Unlike centrioles that display an intricate structure, the mitotic PCM is an electron-dense material lacking any discernable structure asides from the ring-like structures of γ-TuRCs (Moritz et al. 1995). More recently, super-resolution imaging has shown that pericentrin, along with CEP152, form a small layer of PCM around the centrioles in interphase cells that represents a somewhat ordered structure (Fry et al. 2017). They do this by binding to the centrioles by virtue of their C-terminal domains, and extend outwards in a radial manner, creating elongated filaments. Proteins such as CDK5RAP2 essentially fill in the gaps defined by the filaments, creating a 'branched matrix' that serves as a surface to recruit other proteins, including γ-TuRCs. At the onset of mitosis, phosphorylation events drive the recruitment of significant amounts of these proteins, forming an outer layer of PCM that is less ordered. However, it contains so-called 'scaffolds' that recruit components necessary for the concomitant increase in MT nucleation. An interesting observation is that many PCM organising proteins, such as pericentrin, contain multiple coiled-coil domains, a structural motif consisting of a number of α-helices coiled together

that mediate protein-protein interactions (Salisbury 2003). Hence it is thought that these domains might help to assemble the complex protein-rich environment of the PCM (Salisbury 2003; Woodruff et al. 2014). How the PCM selectively concentrates proteins to carry out MT nucleation, without sequestering those not important for this function, is not known.

One somewhat controversial idea is that the mitotic PCM is a liquid-like state that can form through liquid-liquid phase-separation, as has been described for other membraneless compartments within the cell (Woodruff et al. 2017; Banani et al. 2017; Raff 2019). In this sense, the centrosome serves as a liquid droplet that demixes its components from the cytoplasm, like the separation of oil and water. This idea was born from *in vitro* reconstitution experiments using the *C. elegans* SPD-5 protein that is required for mitotic PCM assembly in this system (Woodruff et al. 2017). Here, the authors showed that *in vitro*, purified SPD-5 can self-assemble into condensates when the crowding agent polyethylene glycol is added. Moreover, these condensates are similar in size and shape to the mitotic PCM observed *in vivo*, and are amorphous by cryoelectron microscopy. Although the condensates initially exhibit liquid properties, that is they coalesce and internally rearrange, after around 10 min they lose this ability, which the authors describe as the structure solidifying into a gel-like state. Interestingly, addition of PLK1, but not a kinase dead version, promoted the formation of SPD-5 condensates in conditions with low levels of crowding agent, consistent with the role of phosphorylation in PCM expansion. The key finding from this study was that while the condensates could nucleate MT asters following the recruitment of PCM effector proteins ZYG-9 and TPXL-1 (the *C. elegans* homologues of ch-TOG and TPX-2, respectively), the condensates were unable to efficiently sequester EB1. This data suggests that the SPD-5 condensate can filter out non-centrosomal proteins, thus functions as a scaffold (Woodruff et al. 2017). Investigating the biophysical properties of mitotic PCM *in vivo* is now necessary to determine if the PCM truly does behave in a liquid like manner, and whether this concept applies to human cells (Woodruff 2018).

Much attention has been paid to understanding PCM maturation at the onset of mitosis, with considerably less paid to understanding how it disassembles at the end of mitosis. Since the assembly of the PCM requires phosphorylation events, it is intuitive to think that this work needs to be undone via the action of phosphatases in order to break it apart. Indeed, work carried out in *C. elegans* embryos suggests that the action of protein phosphatase 2, combined with MT-dependent pulling forces, is required for PCM disassembly (Enos et al. 2018).

1.5 The TACC3–ch-TOG–clathrin–GTSE1 complex

A complex consisting of TACC3, clathrin and ch-TOG was previously identified as an inter-MT bridge, where it physically crosslinks kinetochore MTs to provide K-fibre stability (Booth et al. 2011; Nixon et al. 2015). More recently, work provided evidence to support the idea that GTSE1 is also a member of this complex (Rondelet et al. 2020; Ryan et al. 2021; Hubner et al. 2010). The following sections will briefly describe each protein individually, the proposed roles of TACC3–ch-TOG, and our current understanding of the TACC3–ch-TOG–clathrin–GTSE1 complex.

1.5.1 TACC3

Transforming acidic coiled-coil containing protein 3 (TACC3) is one of three TACC proteins present in mammalian cells that all share a highly conserved C-terminal coiled-coil region known as the TACC domain (Peset and Vernos 2008). The TACC family of proteins were initially identified during a search of genomic regions that are amplified in breast cancer (Still et al. 1999a). Stemming from this, it was discovered that the gene encoding TACC3 is upregulated in various human cancer cell lines (Still et al. 1999b). TACC3 contains a conserved serine 558 (S558) residue that is phosphorylated by Aurora A to permit mitotic spindle localisation (Kinoshita et al. 2005; LeRoy et al. 2007). Here, TACC3 is part of a multiprotein complex that stabilises the K-fibres. The interactions within the complex and its role in human cells will be discussed in section 1.5.6.

The role of TACC3 in cells was first studied in the early embryo of *Drosophila*, where its homologue D-TACC was shown to interact with centrosomes and spindle MTs via its TACC domain (Gergely et al. 2000b). In the same study, inhibition of D-TACC through antibody injection revealed a shortening of the spindle MTs and chromosome segregation defects, indicating a role in MT stability. Later it was identified that D-TACC interacts with and targets Msps, the *Drosophila* homologue of ch-TOG, to the centrosome to stabilise MTs (Lee et al. 2001). Similarly, TACC3 and ch-TOG have been identified as binding partners at the growing MT plus-end in human cells (Gutierrez-Caballero et al. 2015). The role of TACC3–ch-TOG in these contexts will be covered in section 1.5.3.

Although the majority of work concerning TACC3 points to a role in regulating MT stability, a role in MT nucleation has been reported (Singh et al. 2014). Here, the authors found that TACC3 depletion inhibited MT nucleation in interphase

cells, as demonstrated by a MT regrowth assay. Consistent with that, they showed that depletion of TACC3 affected assembly of the γ-TuRC (Singh et al. 2014).

1.5.2 ch-TOG

As described in section 1.3.2, ch-TOG is the human homologue of XMAP215, with a molecular mass of approximately 218 kDa (Charrasse et al. 1995). Based on results from *in vitro* experiments, it is thought to function as a polymerase by loading tubulin dimers onto the growing MT plus-end. However, there have been conflicting reports regarding the effect of ch-TOG depletion on MT dynamics at the plus-end in cells, as determined by tracking EB proteins (Stiff et al. 2020; Herman et al. 2020; van der Vaart et al. 2011). This is likely due to differences in experimental setup, including different expression levels of EB proteins that may affect growth parameters, and perhaps unintended off-target effects of siRNA. Thus, firm evidence to support the idea that ch-TOG is a MT polymerase in human cells is needed.

In interphase cells, ch-TOG is localised at the centrosome and MT plus-ends, while during mitosis it is observed at the centrosomes, kinetochores, MT plus-ends and on the spindle MTs as part of inter-MT bridge complexes (Gutierrez-Caballero et al. 2015). With the exception of the kinetochore, the role of ch-TOG at these intracellular locations has been studied in the context of an interaction with its binding partner TACC3. This work will be summarised in the following section.

It has previously been identified that ch-TOG localises to the kinetochore in human cells (Gutierrez-Caballero et al. 2015). Recently, it has been determined that this occurs via an interaction with the Hec1 subunit of the Ndc80 kinetochore complex, in a manner that is independent from its localisation at MT plus-ends (Herman et al. 2020). Here, the authors identified a conserved pair of basic amino acid residues present in a linker region between TOG4 and TOG5 in ch-TOG that is required for error correction, where it destabilises low-tension attachments independently of Aurora B. To show this, the authors generated a doxycycline-inducible HeLa cell line with siRNA-resistant alleles of ch-TOG, where the pair of conserved residues are mutated to alanine (K1142, 1143A), which they refer to as the basic pair mutant. Using this mutant, the authors found that MT dynamics and bipolar spindle formation were restored following depletion of endogenous ch-TOG. However, they observed an increase in mitotic index due to erroneous kinetochore-MT attachments, and chromosome alignment defects where chromosomes were frequently clustered at the poles. Moreover, fewer Mad1-positive kinetochores in cells expressing the mutant were observed,

indicating stabilised erroneous attachments. Using the Eg5 inhibitor STLC to arrest cells in a monopolar state and enrich syntelic attachments, they found that washout of the inhibitor in the presence of wild-type (WT) ch-TOG resulted in bipolar spindle formation with aligned chromosomes, whereas the mutant failed to properly align its chromosomes. Furthermore, they found an additive chromosome alignment defect in cells expressing the mutant and an inhibitor of Aurora B, compared to cells treated with the inhibitor only. Thus, the authors conclude that ch-TOG operates independently of Aurora B to correct erroneous kinetochore-MT attachments by destabilising them (Herman et al. 2020).

1.5.3 TACC3–ch-TOG

Early work investigating the function of TACC3 was carried out in the early embryo of *Drosophila*, where its D-TACC homologue is a centrosome and spindle MT associated protein (Gergely et al. 2000b). Here, D-TACC is required for the proper centrosome localisation of its binding partner Msps, the ch-TOG homologue (Lee et al. 2001). In this study, the authors showed that immunoprecipitation of either protein using embryo extract revealed a direct interaction. Interestingly, overexpression of the C-terminal TACC domain resulted in the formation of large MT asters, but not in Msps mutant cells. Since the level of Msps was unaltered in the WT cells, the authors speculated that D-TACC may activate the MT stabilising activity of Msps. Similarly, work in *Drosophila* oocytes that lack centrosomes, identified that D-TACC is required to anchor Msps at the acentrosomal poles (Cullen and Ohkura 2001). Another study in *Drosophila* showed that Aurora A phosphorylation of D-TACC is required to target it to the minus-end of spindle MTs that have been released from the centrosomes, as a phosphorylation mutant failed to show this localisation pattern (Barros et al. 2005). Moreover, the authors found that the mutant could still localise to the centrosomes, albeit slightly reduced. This led to the idea that Aurora A phosphorylates the centrosome pool of D-TACC to enable it to interact with and stabilise MT-minus ends in complex with Msps (Barros et al. 2005). Additionally, the authors proposed that unphosphorylated D-TACC is present on the MT plus-ends with Msps, as had been suggested previously (Barros et al. 2005; Lee et al. 2001). In both instances, D-TACC could function to promote MT stability via its interaction with Msps which opposes the MT destabilising activity of mitotic centromere-associated kinesin (MCAK).

The *Xenopus* egg extract system has also been used to study the MT function of the TACC3–ch-TOG complex, using purified Maskin and XMAP215 protein, the *Xenopus* homologues of TACC3 and ch-TOG, respectively. By MT sedimentation

assay, it was found that increasing the amount of purified Maskin added to XMAP215 and MCAK increased the amount of pelleted tubulin, suggesting Maskin increases the activity of XMAP215 to counteract the MT destabilising behaviour of MCAK (Kinoshita et al. 2005). Furthermore, the authors looked specifically at mitotic centrosomes by adding centrosomes to interphase *Xenopus* egg extracts along with cyclin B to drive the cells into mitosis. Using this system, it was found that immunodepletion of Maskin resulted in fewer centrosome MTs, and growth could be stimulated to normal levels upon addition of MCAK inhibitory antibodies. Suggesting that Maskin functions to increase the activity of XMAP215 at the centrosome to counteract MCAK. To investigate the role of Aurora A phosphorylation on the localisation of Maskin, the authors used Maskin depleted extract and compared the effect of adding back WT Maskin or a non-phosphorylatable version. This revealed that the Maskin mutant was barely detectable at the centrosome, and although an interaction with XMAP215 was preserved, it too was not efficiently targeted to the centrosome. Thus, the authors proposed a model where Aurora A targets Maskin and in turn, XMAP215 to the mitotic centrosomes, where Maskin can enhance activity of XMAP215 to counteract MCAK and stabilise centrosome MTs (Kinoshita et al. 2005). In line with this idea, a separate study carried out using *Xenopus* extract identified that Maskin enhanced the *in vitro* MT binding activity of XMAP215 (Peset et al. 2005).

In summary, work carried out in *Drosophila* and *Xenopus* systems suggests that one function of the TACC3–ch-TOG complex is to stabilise centrosome MTs, and this is likely to occur through activation of ch-TOG by TACC3. This could occur at the minus-end of spindle MTs or at the plus-end of nascent MTs, or a combination of both.

In comparison, TACC3 in human cells is enriched on the mitotic spindle and at a diffuse area around the centrosome, whereas ch-TOG is clearly enriched at the centrosome in addition to its distribution along spindle MTs. Phosphorylation at S558 by Aurora A is necessary to target TACC3 to the mitotic spindle (LeRoy et al. 2007). Moreover, TACC3 is required for the spindle localisation rather than the centrosome localisation of ch-TOG, as depletion of TACC3 or expression of a mutant deficient in binding ch-TOG, both result in a reduction of spindle ch-TOG, while the centrosome pool is unaffected (Gergely et al. 2003; Gutierrez-Caballero et al. 2015). The observation that ch-TOG requires TACC3 for its spindle localisation is somewhat surprising given that ch-TOG is thought to bind tubulin directly via its TOG domains, and also contains a MT lattice-binding motif (Widlund et al. 2011). The ch-TOG binding region

on TACC3 has been mapped to a predicted 3-aa stutter in the C-terminal coiled-coil region of the TACC domain, where deletion of amino acids 678-681 or 682-688 in the full-length TACC3 protein disrupts the interaction with ch-TOG biochemically and in cells (Hood et al. 2013; Gutierrez-Caballero et al. 2015). Moreover, the TACC3 binding site on ch-TOG has been mapped to a pair of leucine residues within the C-terminus (L1939 and L1942), and mutation of either residue to alanine blocks the interaction with TACC3 biochemically. In HeLa cells, a full-length construct of ch-TOG with both of the leucine residues mutated to alanine is unable to localise at the spindle MTs, but is localised at the centrosome (Gutierrez-Caballero et al. 2015).

Studies investigating TACC3–ch-TOG function in human cells have mostly relied on the use of siRNA to deplete either protein. A hallmark of ch-TOG depletion is the formation of disorganised multipolar spindles that arise largely due to compromised MT assembly at the centrosome (Gergely et al. 2003; Cassimeris and Morabito 2004; Barr and Bakal 2015), but partly due to the compensation of other spindle assembly pathways in the absence of ch-TOG, such as chromatin-mediated MT nucleation (Barr and Bakal 2015). Coupled with that, cells display severe chromosome alignment defects and a delayed mitosis (Gergely et al. 2003). In comparison, TACC3 depletion results in a much smaller increase in the number of cells containing multipolar spindles, suggesting that unlike ch-TOG, TACC3 does not have an essential role in bipolar spindle formation (Gergely et al. 2003). Furthermore, loss of TACC3 results in mild chromosome congression defects and a delayed mitosis (Gergely et al. 2003; Lin et al. 2010).

Interestingly, TACC3–ch-TOG has been identified as a potential target to inhibit the clustering of supernumerary centrosomes present in some cancer cell lines (Fielding et al. 2011). In this study, the authors found that siRNA-mediated depletion of TACC3 or ch-TOG in a breast cancer (BT549) and prostate cancer cell line (PC3) led to an increase in the proportion of cells containing de-clustered centrosomes, which can lead to multipolar divisions, mitotic arrest and cell death, thus inhibiting proliferation (Fielding et al. 2011).

Interaction at the microtubule plus-end

Our understanding of ch-TOG as a MT polymerase acting at the MT plus-end has been developed from various *in vitro* studies, with the general view that it catalyses the addition of tubulin via its conserved TOG domains (Spittle et al. 2000; Brouhard et al. 2008; Widlund et al. 2011). However, the idea that TACC3–ch-TOG might be able to bind the MT plus-end in cells, originated from work in *Drosophila* embryos that observed GFP-tagged D-TACC and Msps

display comet-like behaviour in the vicinity of the centrosomes (Lee et al. 2001). More recently, work carried out in *Xenopus* neuronal growth cones identified that TACC3 tracks the growing MT plus-ends and may function to regulate dynamics (Nwagbara et al. 2014). Here, the authors observed a modest 11% reduction in MT plus-end growth speed in TACC3-depleted cells compared to the control, as determined by tracking EB1. Similarly, overexpression of TACC3 was found to increase growth speed by the same magnitude, suggestive of a role in regulating MT polymerisation. Moreover, the authors found that TACC3 localises to the distal tip of the MT end, ahead of the EB proteins and colocalises with ch-TOG, consistent with the idea that these proteins track the plus-ends in a complex (Nwagbara et al. 2014).

TACC3–ch-TOG has also been observed to track the plus-ends of MTs in HeLa cells during interphase and mitosis, independently of EB proteins (Gutierrez-Caballero et al. 2015). An interaction between TACC3 and ch-TOG in this context was demonstrated in live cells using the knocksideways (KS) method, where removal of GFP-FKBP-TACC3 to the mitochondria resulted in co-rerouting of ch-TOG but not EB1. Importantly, this study highlighted that TACC3 tracks the plus-ends by virtue of its interaction with ch-TOG, as TACC3 mutants deficient in binding ch-TOG did not display a comet-like localisation in live cells, while a ch-TOG mutant deficient in binding TACC3 maintained +TIP activity. The finding that a non-phosphorylatable TACC3 mutant can track MT plus-ends suggests that the +TIP activity of TACC3–ch-TOG is not dependent on Aurora A phosphorylation. Similarly, a TACC3 mutant deficient in binding clathrin was observed to track the plus-ends like the WT protein, suggesting that this function of TACC3 is distinct from its role at the K-fibres with clathrin. Despite TACC3 displaying clear +TIP activity, manipulation of its expression, either by siRNA-mediated depletion or overexpression, failed to show any detectable change on MT dynamics, as determined by tracking growing MT tips in interphase RPE-1 cells stably expressing EB3 (Gutierrez-Caballero et al. 2015).

A role for TACC3 in regulating MT plus-end growth has recently been identified in SK-N-SH cells, a human neuroblastoma cell line (Furey et al. 2020). In this study, the authors showed that TACC3 depletion led to an increase in stable MT networks in interphase cells, as determined by the detyrosinated state of tubulin, a post-translational modification of tubulin that is typically associated with long lived stable MTs. In contrast, depletion of EB1 had no effect. The authors also observed a reduction in EB1 comet number in fixed TACC3-depleted cells and by live-cell imaging they observed a reduction in the velocity of CLIP170, a protein

that tracks the MT plus-ends. Surprisingly, the authors found an increased nuclear signal for ch-TOG in TACC3-depleted interphase cells compared to the control, leading them to suggest that TACC3 controls the localisation of ch-TOG. The authors showed that entry of the herpes simplex virus type 1 (HSV-1) into TACC3-depleted cells was slower, and once in the cell, it was trafficked to the nucleus with significant delay. Thus, the authors propose that TACC3 is an important regulator of the interphase MT network in SK-N-SH cells that could control the trafficking of cargo (Furey et al. 2020).

1.5.4 Clathrin

Our structural understanding of clathrin is thanks to a plethora of studies that have sought to investigate the role of this protein in the internalisation of cargo at the plasma membrane, a process referred to as clathrin-mediated endocytosis. This process was first described by Roth and Porter who observed yolk protein uptake in mosquito oocytes by electron microscopy, and noticed invagination of the plasma membrane and vesicles that appeared to be coated (Roth and Porter 1964). A few years later, the coated vesicles were isolated using pig brain, where it was discovered that the coat consisted of a lattice-like network (Kanaseki and Kadota 1969). The subsequent purification of the vesicles revealed its main protein constituent, clathrin (Pearse 1976).

Clathrin consists of a heavy chain (190 kDa) and a light chain (25 kDa), that self assembles into a triskelion structure composed of three heavy chains that are each associated with a single light chain (Kirchhausen and Harrison 1981). The three clathrin heavy chains are non-covalently joined at their C-terminus to form the 'legs' of the triskelia, while the light chains bind the proximal region of each leg (Hirst and Robinson 1998). The endocytic function of clathrin is defined by the N-terminal domain (NTD) of clathrin heavy chain (CHC) that folds into a seven-bladed β-propeller, containing four interaction sites that are important for binding to different adaptor proteins (Fotin et al. 2004; Willox and Royle 2012). The NTD of CHC is located at the distal end of the leg, and is sometimes referred to as the 'foot'.

The clathrin triskelion is the basic assembly unit of the lattice-like structure that forms the vesicle coat. At the plasma membrane, this process is initiated by the adaptor protein, AP-2, that recognises the cargo and recruits clathrin, leading to a clathrin-coated pit. Recruitment of more clathrin to the pit leads to invagination, and the subsequent recruitment of dynamin leads to its scission from the plasma membrane, forming an internalised coated vesicle. Once inside the cell, the clathrin coat disassembles due to the recruitment of the uncoating

machinery (Robinson 2015).

Clathrin during mitosis

Separate from its role in membrane trafficking, clathrin also functions during mitosis, a time where endocytosis is significantly reduced, particularly during the early stages (Fielding and Royle 2013). Spindle staining observed with antibodies raised against clathrin via immunofluorescence (Okamoto et al. 2000), and its detection by mass spectrometry of purified spindles (Mack and Compton 2001), all hinted at a mitotic role, but a mechanism to describe its function was lacking. It was subsequently shown by antibody staining and expression of GFP-tagged clathrin fragments, that clathrin localises to the K-fibres (Royle et al. 2005). Furthermore, depletion of CHC by RNAi revealed defects in chromosome congression and a prolonged mitosis due to destabilisation of the K-fibres. Importantly, this phenotype was determined to be specific to loss of clathrin from the mitotic spindle, rather than an effect of inhibiting clathrin-mediated endocytosis (Royle et al. 2005). In a separate study, rescue experiments using mutants of CHC identified that the two functions of clathrin could be separated, as a mutant capable of rescuing mitotic defects was incapable of restoring clathrin-mediated endocytosis, and vice versa (Royle and Lagnado 2006; Hood and Royle 2009).

These studies also highlighted that the NTD on CHC is important for spindle localisation. Since clathrin exists as a triskelion in cells, with the NTDs positioned away from each other, this led to the hypothesis that clathrin may function to stabilise K-fibres by physically crosslinking the adjacent MTs within the fibre (Royle et al. 2005; Royle and Lagnado 2006). In the same way that clathrin requires adaptor proteins for its endocytic function, it also requires other proteins to function at the mitotic spindle. This was made clear by the observation that clathrin does not contain a well recognised MT-binding domain, nor does it bind MTs *in vitro* (Booth et al. 2011).

1.5.5 GTSE1

G2 and S phase expressed protein-1 (GTSE1) is a microtubule-associated protein found only in vertebrates (Rondelet et al. 2020). It is an intrinsically disordered protein, with a C-terminal region that represents a clathrin interaction domain (CID) containing five clathrin box-like motifs. An interaction between clathrin and GTSE1 has recently been characterised in human cells, where clathrin recruits GTSE1 to the mitotic spindle (Rondelet et al. 2020; Ryan et al. 2021). The details of this interaction will be described in section 1.5.6. Interestingly, clathrin and

GTSE1 have also been shown to interact during interphase, such that tethering the C-terminus of GTSE1 to the cell membrane can initiate clathrin-mediated endocytosis (Wood et al. 2017).

Investigation of GTSE1 was driven by the initial discovery that in mice, the gene encoding GTSE1 (originally named *B99*) is regulated by p53, and can be induced by DNA damage independently of p53 (Utrera et al. 1998). As its name suggests, the expression of human GTSE1 was found to occur specifically during the S/G2 phase of the cell cycle (Monte et al. 2000), with peak expression during mitosis (Scolz et al. 2012). It was initially observed that when overexpressed in cells, GTSE1 can bind the MT lattice during interphase (Monte et al. 2000). Indeed, we recently identified that the region 161-638 contains the site(s) responsible for this activity (Ryan et al. 2021).

A key function of GTSE1 is carried out at the MT plus-end via an interaction with EB1 through its SxIP motifs, where it has been shown to promote cell migration (Scolz et al. 2012). Using live-cell imaging, the authors showed that GTSE1 +TIP activity is lost following EB1 depletion, though its association with the MT lattice is retained (Scolz et al. 2012). More recently, it has been shown that GTSE1 is heavily phosphorylated during early mitosis by CDK1, which breaks the interaction with EB1 and +TIP activity is lost (Singh et al. 2020). The authors showed that CDK1 regulation of GTSE1 is necessary to destabilise long astral MTs and allow the mitotic spindle to reorient during early mitosis. In cells where CDK1 was inhibited, or a GTSE1 phosphorylation mutant was expressed, GTSE1 +TIP activity was observed during mitosis, leading to an increase in astral MT length and stability. Consequently, defects in spindle orientation were observed (Singh et al. 2020).

During mitosis, GTSE1 is localised to the mitotic spindle via clathrin, where it is proposed to have a role in regulating MT stability by inhibiting MCAK activity to promote chromosome alignment (Bendre et al. 2016). In this study, the authors showed that the N-terminal half of GTSE1 directly interacts with MCAK *in vitro*. Moreover, they found that GTSE1 can inhibit the MT depolymerase activity of MCAK *in vitro*, as observed by a reduction in MT depolymerisation rate when GTSE1 and MCAK were incubated with MTs, compared to MCAK alone (Bendre et al. 2016).

1.5.6 TACC3–ch-TOG–clathrin–GTSE1

Several early studies helped establish the composition of the TACC3–ch-TOG–clathrin–GTSE1 complex, and defined its role in stabilising the

K-fibres of the mitotic spindle to ensure accurate cell division. This section will outline the key findings from this work, and summarise the subsequent studies that have mapped the interactions, and contributed ideas towards a proposed MT-binding mechanism.

Lin and colleagues identified that the chromosome alignment defect, and delayed progression through mitosis observed in cells treated with RNAi targetting TACC3 or CHC, is observed to the same extent when both proteins are targeted simultaneously, illustrating that they function in the same pathway (Lin et al. 2010). The authors showed that ch-TOG was also part of this spindle complex, as knockdown of CHC or TACC3 by RNAi resulted in the loss of ch-TOG from the mitotic spindle, but not the centrosomes. Around the same time, Booth and colleagues detected by mass spectrometry, a complex containing clathrin, TACC3 and ch-TOG by immunoprecipitating clathrin from isolated mitotic spindle extract (Booth et al. 2011). Moreover, all three proteins were observed to colocalise at the metaphase spindle in fixed HeLa cells expressing fluorescently-tagged clathrin and ch-TOG proteins, with an antibody to visualise endogenous TACC3. To investigate the order of recruitment to the spindle MTs, the authors manipulated the expression levels of the individual complex proteins by RNAi or overexpression, and visualised the localisation of the remaining members by confocal microscopy. The results of these experiments suggested that TACC3 is the core member that recruits the other components (Booth et al. 2011). This finding was in direct contrast to previous reports that suggested the primary factor is clathrin (Lin et al. 2010; Fu et al. 2010; Hubner et al. 2010). Importantly, Booth and colleagues showed that recruitment of this complex to the mitotic spindle is regulated by phosphorylation at S558 on TACC3 by Aurora A, in line with previous suggestions that Aurora A is required for the localisation of TACC3 to spindle MTs (LeRoy et al. 2007; Kinoshita et al. 2005). Similarly, Fu and colleagues showed by an *in vitro* binding assay, that Aurora A phosphorylation of Maskin, the *Xenopus* homologue of TACC3, is required for the interaction with clathrin (Fu et al. 2010).

A key finding came from EM experiments that showed a reduction in the number of short inter-MT bridges in K-fibres of clathrin-depleted cells, and that this subset of bridges was composed of clathrin (Booth et al. 2011). Loss of TACC3 also resulted in the loss of short inter-MT bridges, which are described as those ranging between 14-17 nm in length. Medium and long bridges, ranging between 20-50 nm in length, were present in the K-fibres of cells depleted of TACC3 or clathrin, suggesting that these are comprised of other proteins (Booth et al. 2011).

More recently, electron tomography has revealed that although adjacent MTs

within K-fibres are connected by bridges in 2D, in 3D, the bridges are interconnected, forming a 'mesh' (Nixon et al. 2015). In this sense, the complex is a component of the mesh and is required to maintain the stability of the K-fibre. By overexpressing TACC3, the authors found that the mesh influences the position of MTs within the K-fibre, such that MTs connected in a chain were tightly packed together, whereas in control cells, MTs connected by the mesh were no more tightly packed than single MTs. To understand if the complex could bundle MTs within a K-fibre, the authors looked at taxol stabilised MTs formed *in vitro*. In the presence of the MT bundling protein PRC1, MT bundles were observed as expected. Interestingly, incubation of MTs with a mix of TACC3, clathrin, ch-TOG and GTSE1 proteins phosphorylated by Aurora A, resulted in the formation of bundled MTs *in vitro*. Together, this data suggests that the complex functions to bundle and stabilise MTs within a K-fibre (Nixon et al. 2015).

A significant milestone in our understanding of the complex was reached when Hood and colleagues mapped the interactions within it, and identified the mechanism by which it binds to MTs (Hood et al. 2013). To do this, the authors visualised truncated fragments of TACC3 in cells depleted of the endogenous protein, and identified that two regions, a clathrin interaction domain (CID) and the C-terminal TACC domain, are both required for spindle localisation. Truncations containing only one domain were not sufficiently recruited to the spindle when expressed in cells, and in both cases the spindle localisation of clathrin was also disrupted. The CID (aa 522-577) was identified to bind CHC by Lin and colleagues (Lin et al. 2010). In the study by Hood and colleagues, it was shown that mutation of a dileucine motif (LL[566,567]AA) within this region significantly disrupted TACC3 spindle localisation in cells (Hood et al. 2013). Importantly, this effect was specific to the dileucine motif, as S558 was still phosphorylated in the mutant protein. Via an *in vitro* binding assay using purified clathrin triskelia and purified TACC3 CID domain phosphorylated by Aurora A, the authors showed that the CID was sufficient to bind clathrin, and mutation of S558 or the dileucine motif broke this interaction (Hood et al. 2013).

Since previous studies had highlighted the NTD and ankle region of CHC as essential for spindle localisation (Royle and Lagnado 2006; Hood and Royle 2009), the authors set about to investigate the importance of these regions. By expressing CHC mutants in cells depleted of endogenous CHC, the authors identified that the clathrin box motif (CBM) within the NTD is required for spindle localisation, as fragments with mutations in this site failed to localise to the spindle. Using the same assay, they found that disruption of the ankle domain

also impaired spindle localisation. In both cases, TACC3 spindle localisation was disrupted, thus confirming the interdependent nature of these proteins at the mitotic spindle. An *in vitro* binding assay using CHC and TACC3 proteins revealed that deletion of the ankle domain on CHC abolished binding, while removal of the NTD containing the CBM-binding site had no effect, suggesting the ankle region mediates an interaction with TACC3. This finding led the authors to propose that the CHC ankle and TACC3 CID bind, which in turn allows the CHC NTD domain and TACC domain to form the MT binding surface. This idea was supported by the observation that a fusion protein consisting of the NTD and TACC domain, termed clACC, was enriched on the mitotic spindle in cells (Hood et al. 2013).

Within the CID of TACC3, there is the Aurora A phosphorylation site (S558), and a dileucine (L566,567) motif that interacts with the CHC ankle region. However, it has recently been established that within this region of TACC3 there is also an Aurora A binding site, in which a phenylalanine residue (F525) is critical (Burgess et al. 2018; Burgess et al. 2015). Moreover, the binding of TACC3 via this region enhances the kinase activity of phosphorylated Aurora A, and results in autophosphorylation of the catalytic domain of Aurora A *in vitro* (Burgess et al. 2015). Importantly, TACC3 and TPX2, a known activator of Aurora A, have distinct binding sites on Aurora A (Burgess et al. 2015). Thus, TACC3 could act as a local allosteric activator of Aurora A, for example along the K-fibres, whereas TPX2 is required for its global activity (Burgess et al. 2015). Collectively, the region of TACC3 (aa 519-570) that contains the dileucine motif, the Aurora A phosphorylation site, and the Aurora A docking site, is referred to as the Aurora A and CHC interaction domain (ACID). A structural study has recently shed light on how Aurora A phosphorylation regulates the TACC3–clathrin interaction (Burgess et al. 2018). In brief, Aurora A phosphorylation at S558 leads to stabilisation of an α-helix within TACC3, where this structural change is recognised by the ankle of CHC, leading to binding and the subsequent localisation of the complex to MTs (Burgess et al. 2018).

A quantitative proteomics study carried out by Hubner and colleagues, identified GTSE1 as an interaction partner of TACC3 and clathrin in mitotically arrested cells (Hubner et al. 2010). However, the involvement of GTSE1 in this context remained largely unsolved. Recently, a comprehensive study published by Rondelet and colleagues identified the mechanistic details about its recruitment to the mitotic spindle via clathrin (Rondelet et al. 2020). Here, the authors discovered that GTSE1 binds directly to sites 1 and 3 in the CHC NTD, both of which are established binding sites for adaptor proteins. This interaction

is mediated by five clathrin box-like motifs (LI[DQ][LF]), referred to as LIDL motifs, present in the C-terminal region of GTSE1. Importantly, the authors showed that in cells, a mutant of GTSE1 where the LIDL motifs are mutated to alanine residues, failed to localise to the mitotic spindle. However, the spindle localisation of clathrin and TACC3 was unaffected, suggesting that GTSE1 is recruited to the complex via its interaction with clathrin. Moreover, the GTSE1 LIDL mutant failed to rescue the chromosome alignment defect observed in cells depleted of endogenous GTSE1, and that a large proportion of misaligned chromosomes were in close proximity to the spindle pole. The authors showed that astral MTs are destabilised in cells expressing the GTSE1 mutant, and this was restored by depletion of MCAK, suggesting that GTSE1 is recruited by CHC to stabilise MTs by inhibiting MCAK activity (Rondelet et al. 2020). This is plausible given that GTSE1 has been shown to interact with MCAK in cells (Bendre et al. 2016). However, the authors also showed that the K-fibres in GTSE1-depleted cells are less resistant to cold-treatment than control cells (Rondelet et al. 2020). Thus, an alternative interpretation of this data is that GTSE1 is recruited to the complex on the K-fibres to provide K-fibre stability and enable timely chromosome congression.

We recently used CRISPR/Cas9-mediated gene editing to insert an FKBP-GFP tag at the endogenous loci of TACC3, clathrin, ch-TOG and GTSE1 in HeLa cells, generating four knock-in cell lines (Ryan et al. 2021). In brief, genome engineering using the CRISPR/Cas9 system relies on the targeting of a Cas9 nuclease to a specific region of genomic DNA by a guide RNA, enabling the Cas9 nuclease to introduce a double-strand break in the DNA and promote gene editing (Ran et al. 2013). In our study, homozygous cell lines were generated for TACC3, clathrin and GTSE1, where all alleles were edited (Ryan et al. 2021). Despite three independent attempts, no homozygous clones for ch-TOG were recovered, therefore a heterozygous cell line was used where an unedited allele remained. The generation of the CRISPR cell lines enabled us to utilise the knocksideways system and inducibly reroute each protein individually from the mitotic spindle to the mitochondria, and visualise the effect on the remaining complex components by microscopy. Using this method, we were able to establish that TACC3 and clathrin are the core components of the complex, such that removal of either protein from the mitotic spindle resulted in the mislocalisation of all complex members. In comparison, removal of GTSE1 or ch-TOG from the spindle did not significantly perturb TACC3 or clathrin. Moreover, we established that mutation of at least three LIDL motifs present at the C-terminal end of GTSE1, or removal of this region entirely, significantly reduced the spindle enrichment of GTSE1

but not clathrin. This is consistent with the idea that clathrin recruits GTSE1 to the spindle (Rondelet et al. 2020). Although an interaction with clathrin is required for the spindle recruitment of GTSE1, we determined that expression of this region alone is not sufficient, and that a region between aa 161-638 is also necessary. Finally, we showed that contrary to a previous report (Gulluni et al. 2017), PIK3C2A is not required to stabilise the complex, as knocking out this protein by CRISPR/Cas9-mediated gene editing had no effect on the other complex members. Furthermore, the antibody used in the initial study still stained the spindle in our knockout cell line, even after siRNA treatment, suggesting that the antibody is non-specific (Ryan et al. 2021).

Therefore based on these results, and the findings from previous studies, we propose that the complex interactions are as shown in Fig. 1.6. In this model, TACC3 and clathrin are the core components that interact in an Aurora A dependent manner, to form a MT binding surface. The spindle recruitment of ch-TOG and GTSE1 is via a direct interaction with TACC3 and clathrin, respectively. Due to the importance of this complex in mitotic spindle stability, it provides a potential target in an anti-cancer context. To achieve this, a complete understanding of the interactions that govern the complex, and an idea of the role that each protein contributes, is required. Traditional protein inactivation methods such as RNAi are ill-suited to this task, as the proteins described here have multiple roles, making it hard to assign a phenotype. For this reason, novel approaches that can block specific protein-protein interactions in living cells without perturbing the expression levels of target proteins are needed.

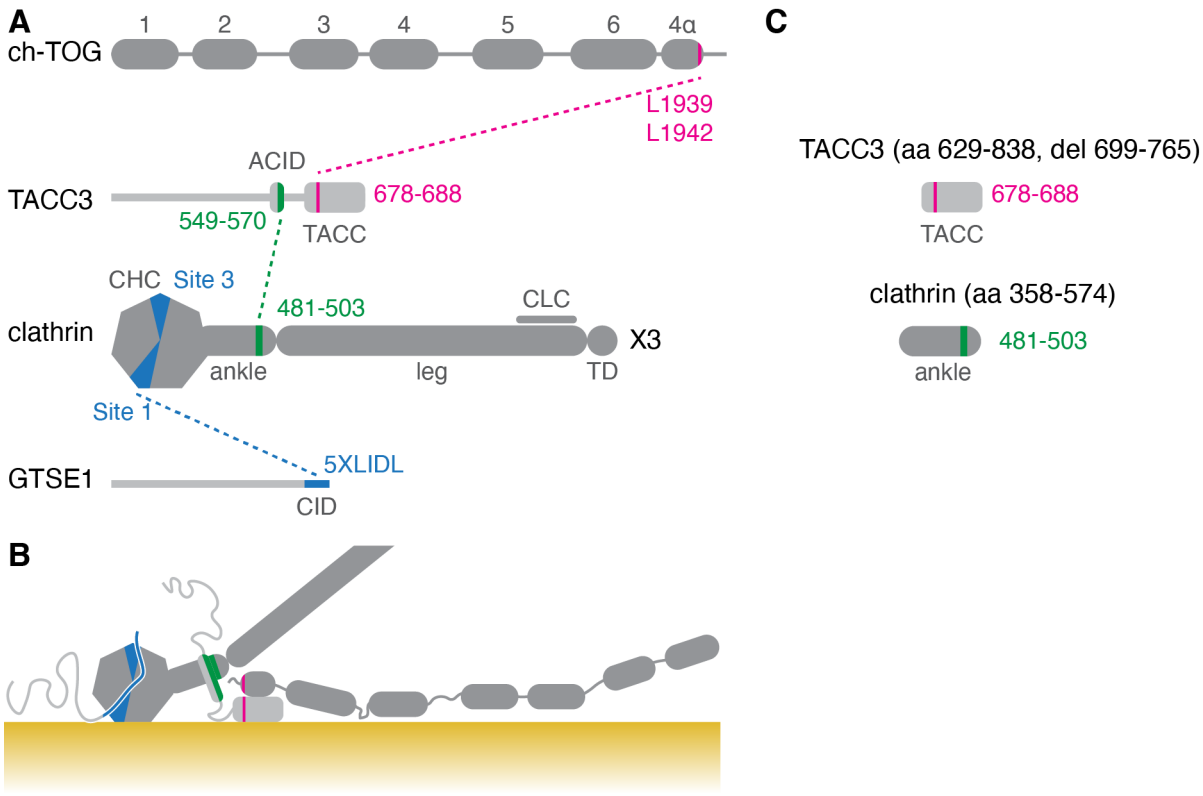

Figure 1.6. Cartoon to describe the interactions between TACC3–ch-TOG–clathrin–GTSE1 complex components and a proposed mechanism for microtubule binding. (**A**) Diagram to illustrate the interactions (dashed lines) between complex members, showing their primary structure. For ch-TOG, the TOG domains are numbered (1-6). For TACC3, the ACID (Aurora A and clathrin interaction domain) and TACC domains are shown. For clathrin, the heavy chain (CHC) and light chain (CLC) are shown, with the TD (trimerisation domain) at the C-terminus of CHC. For GTSE1, the CID (clathrin interaction domain) containing five LIDL (LI[DQ][LF]) is shown. (**B**) Proposed model for microtubule (shown in yellow) binding, where TACC3 and clathrin bind to form the microtubule binding surface and GTSE1 and ch-TOG bind clathrin and TACC3, respectively. (**C**) The fragments of TACC3 and clathrin used to screen for Affimers to block the TACC3–ch-TOG and TACC3–clathrin interactions, respectively. Figure adapted from (Ryan et al. 2021).

1.6 Protein inactivation methods

A major goal of cell biology is to understand the function(s) of individual proteins within a biological system. This is complicated by the fact that most proteins have more than one function, and often operate as part of a multiprotein complex. Understanding protein function is required to gain insight into cellular processes, and can shed light on how proteins could be targeted in a disease state. Over the last two decades, there has been a rapid increase in the number of available methods to study protein function in living cells. These methods can be grouped based on the mechanism in which they inactive protein function. For example, genetic methods seek to silence protein expression by targeting the genes that encode them, or the transcripts that are subsequently translated into protein.

There are also inducible protein inactivation methods, where upon addition of a stimulant, protein silencing can be achieved, typically by using the cell's proteolytic machinery. Inactivation of a protein via small molecule inhibitors, antibody-based reagents or non-immunoglobulin scaffolds are also popular ways to target protein function. Since the aim of the work presented in this thesis was to dissect a multiprotein complex during mitosis, the following sections will focus on describing current methods of protein inactivation in this context.

1.6.1 Genetic approaches

A popular method to assess protein function is to silence the expression of the gene encoding it using RNAi, resulting in a reduction or 'knockdown' of protein expression. Since its discovery in 1998 (Fire et al. 1998), it has been the method of choice for understanding the function of proteins associated with mitosis. Although this has proved successful in identifying important functions of mitotic spindle associated proteins, it also has several limitations. Firstly, the process is slow. To enable a strong reduction in protein expression, cells treated with RNAi are typically analysed 48-72 h post transfection, to allow time for existing protein to be degraded. During this time, other pathways may be upregulated to compensate for the loss of a protein, meaning a true phenotype may be masked by secondary effects. In the case of mitotic spindle proteins, studying phenotypes at specific stages of mitosis, for example metaphase, can be complicated by errors in earlier stages, e.g. spindle assembly.

Alternatively, CRISPR/Cas9-mediated gene editing can be used to generate 'knockout' cell lines to study protein function. In this context, a gene encoding a protein can be deleted or a frameshift introduced, meaning that only a small fragment of the protein is expressed rather than the full length version. In theory, this has an advantage over RNAi-mediated protein depletion, as clonal cells are generated that no longer express the functional protein of interest. However, there have been reports of incomplete loss of a target protein following CRISPR/Cas9-mediated gene deletion (Meraldi 2019). Moreover, it is possible that even in the complete absence of a protein, a cell can upregulate pathways to compensate.

1.6.2 Inducible protein inactivation

Another class of method to study protein function is inducible protein inactivation. In this case, the method relies on a signal provided by the researcher that will activate a certain process resulting in protein inactivation. Typically,

the response is quick, making it a useful tool to study protein function at specific points of the cell cycle.

Knocksideways

Knocksideways (KS) is a rapid and inducible method to inactivate proteins using a rapamycin-induced heterodimerisation system, originally developed by Margaret Robinson (Robinson et al. 2010). The method relies on the dimerisation of mammalian target of rapamycin (mTOR) and FKBP12, in the presence of rapamycin. To make use of this system in cells, the FK506-binding protein (FKBP) domain from FKBP12 can be fused to a protein of interest, and the FKBP and rapamycin-binding (FRB) domain from mTOR can be fused to a protein targeted to an organelle such as the mitochondria. Upon addition of rapamycin, a protein of interest can be relocated away from its site of function, and therefore inactivated.

The KS method has previously been used to remove the TACC3–ch-TOG–clathrin–GTSE1 complex from the mitotic spindle in human cells, showing that proteins in a complex with the target protein can also become mislocalised using this method (Cheeseman et al. 2013). Moreover, owing to the removal of proteins from the spindle in a timescale of minutes, this method was used to remove the complex at specific stages of mitosis, revealing that this complex is required at the metaphase spindle to maintain K-fibre tension and ensure timely progression to anaphase (Cheeseman et al. 2013). Importantly, the spindle localisation of HURP and Eg5 was intact following the removal of TACC3, suggesting that this method can be used to specifically study mitotic complexes. Surprisingly, removal of TACC3 at nuclear envelope breakdown resulted in a prolonged prometaphase that was more severe than that observed in TACC3-depleted cells. This study highlights the possibility that phenotypes observed with RNAi may be underestimated for a range of mitotic proteins. A downside of this study was the need to deplete endogenous TACC3 by RNAi and overexpress GFP-FKBP-TACC3 alongside MitoTrap, an FRB domain targeted to the mitochondria (Cheeseman et al. 2013).

More recently, we used CRISPR/Cas9-mediated gene editing to tag each member of the complex with FKBP and GFP at their endogenous locus in HeLa cells. This allowed us to study the interactions within the complex at the endogenous level, negating the need for overexpression and RNAi. Induced relocalisation of each complex member in mitotic cells enabled us to assess the effect on the localisation of the remaining proteins. Whilst removal of TACC3 or clathrin during metaphase resulted in removal of the entire complex, relocalisation of ch-TOG or GTSE1 had

no effect, suggesting that TACC3 and clathrin are core components (Ryan et al. 2021).

Therefore, KS is a powerful tool to study protein interactions within a multiprotein complex, and given the speed of removal, it can be used to assess interactions at different stages of mitosis. One disadvantage of this method is that it is irreversible. This is due to the strength of interaction between FKBP-rapamycin-FRB and the slow dissociation of rapamycin from FKBP (Robinson et al. 2010). A further limitation is that the kinetics of rerouting are dependent on the dynamics with which proteins cycle on and off their target, i.e. the mitotic spindle, therefore this method will not be applicable to all proteins. Moreover, KS is not an appropriate method to dissect the function of individual components within a multiprotein complex, as the removal of the target protein can lead to the mislocalisation of other members (Ryan et al. 2021). Similarly, proteins frequently have multiple functions and subcellular localisations that KS is not able to discriminate between.

The auxin-inducible degron system

The auxin-inducible degron (AID) system makes it possible to rapidly deplete a protein of interest to study protein function in living cells (Nishimura et al. 2009). This method exploits the auxin-dependent degradation pathway found in plants. It can be transferred to human cell lines by exogenously expressing an auxin receptor F-box protein (TIR1) and an AID-tagged protein of interest. The IAA17 protein found in Arabidopsis is used as the AID-tag, and the plant hormone auxin is used to induce the pathway. Upon addition of auxin, the AID-tagged protein is targeted for ubiquitination and is rapidly degraded by the proteasome.

Initially, use of this method in human cells was limited by the need for RNAi to repress the expression of the endogenous gene, and exogenous expression of an RNAi-resistant version of the target gene along with TIR1. However, the advent of CRISPR/Cas9-mediated gene editing has enabled the introduction of an AID-tag at the endogenous locus of a gene of interest. The timescale required to reach complete degradation varies between protein, however, it has been observed within 80 min for a variety of proteins, including PLK4 (Holland et al. 2012). The AID system has the advantage that it is reversible following auxin washout (Holland et al. 2012). Despite it being faster than RNAi-mediated protein inactivation, the time to achieve complete degradation is still not suitable for the study of proteins during transient periods of the cell cycle, such as metaphase.

1.6.3 Small molecule based inhibitors

An ideal way to inhibit protein function is through the use of small molecule inhibitors, that due to their size, can penetrate the cell membrane, negating the need for lengthy transfection. They function by targetting a ligand binding site present on proteins such as receptors and enzymes. However, since only a small proportion of the human proteome is deemed 'druggable' (Hopkins and Groom 2002), the use of small molecule inhibitors is inherently limited (Toure and Crews 2016). To circumvent this, novel ways of utilising the advantages of small molecules for the purpose of recognition are currently being investigated to induce protein degradation.

Aurora A inhibitors

MLN8237, also known as alisertib, is a well known small molecule inhibitor of Aurora A - a serine/threonine kinase that regulates key mitotic events including centrosome maturation and spindle assembly (Barr and Gergely 2007). Overexpression of Aurora A is associated with an array of human cancers, hence small molecule inhibitors including MLN8237, are currently in clinical trials (Novais et al. 2021).

However, small molecule inhibitors of Aurora A have also been used to study the cell biological function of TACC3, an established target of Aurora A phosphorylation (Kinoshita et al. 2005). For example, inhibition of Aurora A by MLN8054 revealed that phosphorylation at S558 on TACC3 is required for its mitotic spindle localisation (LeRoy et al. 2007). Moreover, inhibition of Aurora A by MLN8237, was shown to result in the loss of the TACC3–ch-TOG–clathrin–GTSE1 complex from the mitotic spindle in human cells (Booth et al. 2011; Cheeseman et al. 2011). MLN8237 treatment also results in a reduction of inter-MT bridges from K-fibres, indicating that inter-MT bridge formation via this complex is dependent on Aurora A kinase activity (Cheeseman et al. 2011).

While the use of small molecule inhibitors such as MLN8237 can be useful in elucidating protein function, there are limitations. First, kinases such as Aurora A have multiple substrates, meaning that any observed phenotype could be exaggerated as a result of global inhibition. In the case of MLN8237, it has been shown to also inhibit Aurora B, highlighting potential off-target effects (Asteriti et al. 2014).

TACC3 inhibitor

Small molecule inhibitors of mitotic proteins important for the assembly and or stability of the spindle, present attractive agents for cancer chemotherapy. A study carried out in TACC3 conditional knockout mice showed that loss of TACC3 in the thymic lymphoma led to tumour regression and apoptosis, with no effect observed in normal tissue (Yao et al. 2012). Moreover, the study highlighted that multipolar cells formed in thymic lymphoma cells following TACC3 depletion (Yao et al. 2012). Therefore, a chemical compound inhibitor of TACC3 termed spindlactone, was later developed, with a goal of perturbing spindle assembly in cancer cells (Yao et al. 2014). Using SKOV-3 cells, an ovarian cancer cell line where TACC3 expression is aberrant, the authors found that spindlactone induced the formation of multipolar spindles in a dose-dependent manner. Moreover, at high doses, spindlactone induced mitotic arrest in cancer cells, thus the authors concluded that TACC3 is indispensable for spindle assembly in this context. However, a pull-down experiment identified that along with TACC3, spindlactone also bound to ch-TOG and Aurora A (Yao et al. 2014), proteins that have a critical role in spindle assembly (Barr and Gergely 2007; Gergely et al. 2003). Therefore, more work is needed to determine if specific inhibition of TACC3 using spindlactone is responsible for the observed phenotype.

Neural progenitor cells (NPCs) are self-renewing cells found in the central nervous system that undergo neuronal differentiation in response to injury. Hence, small molecules that are able to induce differentiation of NPCs are attractive therapeutic agents to treat neurodegenerative disease. Conversely, small molecules that can negatively affect the proliferation of malignant progenitor-like cells are of interest in an anti-cancer setting. To this end, a recent phenotypic screen identified a small molecule called KHS101, that increased neuronal differentiation of rat NPCs (Wurdak et al. 2010). This was found to occur via a reduction in cell proliferation, leading to terminal differentiation. Interestingly, a crosslinking experiment revealed an interaction between KHS101 and TACC3 that was confirmed by mass spectrometry, implicating TACC3 in the NPC differentiation phenotype. In support of this, a similar neuronal differentiation phenotype was observed in cells depleted of TACC3 by RNAi. Treatment with KHS101 or depletion of TACC3 by RNAi, increased the nuclear localisation of the transcription factor ARNT2, a TACC3 interacting protein that is exclusively expressed in the nervous system. Thus, the authors concluded that induced differentiation of NPCs via KHS101 is attributed to TACC3/ARNT2 signalling (Wurdak et al. 2010). More recently, a study found that KHS101 does not block the TACC3–ARNT interaction, but rather leads to proteasomal degradation of

TACC3 (Guo et al. 2013).

Proteolysis-targeting chimeras

A novel way to achieve protein inactivation is through the use of proteolysis-targeting chimeras (PROTACs), that target specific proteins for degradation via the ubiquitin-proteasome system. In brief, PROTAC technology is based on a chimeric molecule that binds a protein of interest and an E3 ubiquitin ligase. The PROTAC essentially hijacks the E3 ligase and places the protein of interest within proximity to facilitate polyubiquitination, resulting in protein degradation via the proteasome. The idea was first tested using peptide ligands as a proof of concept, requiring transfection to enter the cell (Sakamoto et al. 2001). So-called small molecule PROTACs are now available owing to the development of small molecule ligands for a range of E3 ligases, which means transfection is no longer required. Moreover, the development of small molecules as ligands provides control over the concentration of the PROTAC, allowing for precise control of protein degradation. For these reasons, efforts are underway to develop PROTACs for therapeutic targets, with several currently in clinical trials (Burslem and Crews 2020; Mullard 2021).

In addition to their promising use in the clinic, PROTACs also have the potential to serve as useful tools in cell biology to study protein function. A recent example is the development of a PROTAC tool to degrade Aurora A, using the established small molecule inhibitor of this kinase, MLN8237, to generate the binding ligand (Wang et al. 2021). Here, the authors showed that the most efficient PROTAC tested, referred to as PROTAC-D, was effective at specifically degrading endogenous or overexpressed Aurora A in human cells, and resulted in loss of approximately 60% of endogenous Aurora A after 3 h. PROTAC-D was found to be less potent in inhibiting Aurora A than the original MLN8237 inhibitor, and that Aurora A at the centrosome remained functional in the presence of PROTAC-D. Moreover, while the mitotic spindle pool of Aurora A was degraded in the presence of PROTAC-D, the centrosome pool remained, suggesting that some pools may not be accessible to degradation (Wang et al. 2021). Therefore, it remains to be seen if PROTAC technology can be developed to efficiently degrade proteins found in multiprotein complexes.

The time required to develop PROTACs against a target protein, in addition to the need for synthetic chemistry expertise, somewhat limits the use of PROTACs as a research tool to study protein function. However, the development of tag-based methods to harness the potential of PROTAC technology may help make this tool more accessible to academic labs. One example is HaloPROTACs

(Buckley et al. 2015). In short, HaloPROTACs can inducibly degrade a protein of interest fused with a HaloTag - a modified bacterial dehalogenase that can covalently bind to synthetic ligands (Los et al. 2008). This works because HaloPROTACs contain a ligand capable of binding an E3 ligase that is also linked to a chloroalkane to bind a HaloTag, thus the protein of interest fused to a HaloTag is placed into proximity with the E3 ligase, leading to degradation (Buckley et al. 2015). HaloPROTACs combined with CRISPR/Cas9-mediated gene editing has recently been used to degrade endosomal proteins tagged with HaloTag at the endogenous locus (Tovell et al. 2019). It will be exciting to see if this technology can be applied to the study of mitotic proteins.

1.6.4 Antibody-based scaffolds

Antibodies or immunoglobulins, are the proteins produced by the immune system to recognise a target antigen with high specificity and bind it with high affinity, with the purpose of neutralising foreign material such as pathogenic bacteria and viruses. There are 5 classes of immunoglobulins in humans, IgG, IgM, IgA, IgE and IgD. However, IgG is the most abundant class and due to its high specificity towards antigens, it is the class of choice for use in research (Vincke and Muyldermans 2012).

Structurally, antibodies are a tetrameric protein composed of two pairs of identical heavy and light chains linked by disulphide bonds, forming a Y shape, with an approximate molecular weight of 150 kDa (Fig. 1.7 A). Each chain contains a variable domain at the N-terminal end followed by three constant domains in the case of the heavy chain, and a single constant domain in the light chain. Antibodies can bind two antigens simultaneously, through the action of two Fab regions, each consisting of variable and constant domains from the heavy and light chains. The two fab regions are linked by a hinge region between constant domains 1 and 2 on the heavy chain. The antigen-binding site is formed by the variable domain on the heavy and light chain, which each contain three antigen-binding loops, known as the complementarity determining regions (CDRs). Constant domains 2 and 3 on the heavy chain form the Fc region, which is the 'effector' region, responsible for the recruitment of immune cells (Vincke and Muyldermans 2012). As such, the smallest fragment of a conventional antibody that can retain antigen binding specificity is the combination of the variable domain on the heavy and light chain, connected by a synthetic linker, known as the single-chain variable fragment (scFv) (Vincke and Muyldermans 2012).

Antibodies are referred to as polyclonal or monoclonal, depending on their origin. Polyclonal antibodies are a heterogeneous mix of antibodies that can

bind different epitopes of a single antigen, and are purified from the serum of immunised animals. In contrast, monoclonal antibodies are derived from a single cell line and can bind a single epitope per antigen, meaning they have a higher specificity compared with polyclonal antibodies (Ruigrok et al. 2011). Large scale production of monoclonal antibodies via hybridoma technology has significantly transformed biomedical research (Köhler and Milstein 1975). Due to their high specificity and affinity, monoclonal antibodies are increasingly important in the treatment of disease, including cancer (Lu et al. 2020). However, they are also extensively used in basic research as affinity reagents to detect, purify, remove or inactivate target proteins. The following sections will describe ways in which antibodies and their derivatives are used as affinity reagents in academic research to study protein function.

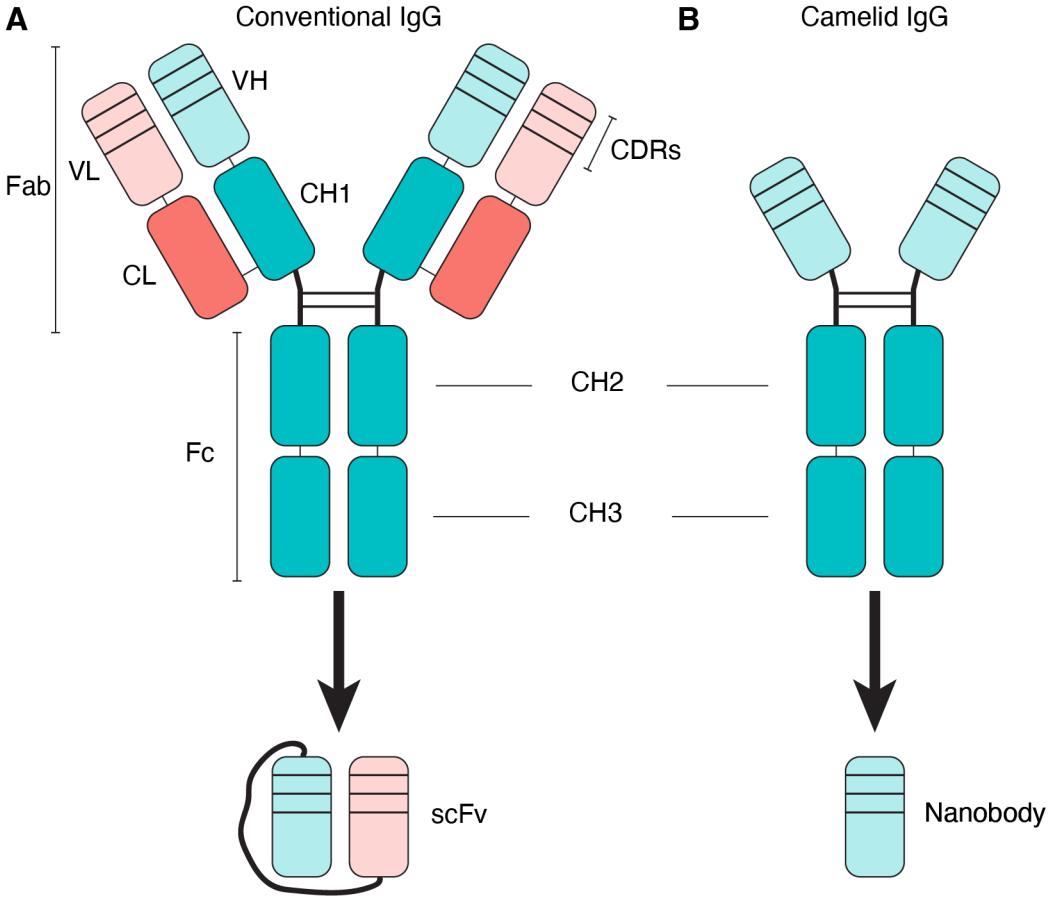

Figure 1.7. Structure of a conventional human immunoglobulin G (IgG) and a heavy chain only Ig found in Camelids. (**A**) Cartoon of a human IgG consisting of two pairs of identical heavy (blue) and light (red) chains, connected by disulphide bonds (black lines). Each heavy chain consists of three constant domains (CH1, CH2 and CH3; dark blue) and a variable domain (VH; light blue). Each light chain consists of a single constant domain (CL; dark red) and a single variable domain (VL; light red). The antigen-binding site is formed by the VL and VH domains, which each contain three complementary determining regions (CDRs). This is the smallest fragment that can retain antigen binding specificity, known as the single-chain variable fragment (scFv). (**B**) Cartoon of a heavy chain only Ig produced by Camelids. The antigen-binding site consists of a single variable domain containing three CDRs, collectively known as a nanobody.

Microinjection

Microinjection of antibodies into live cells to inactivate proteins is a direct way of studying protein function, and is particularly useful for the study of mitotic proteins (Day et al. 2018). The first example of this method is from the late 1970's where antibodies against myosin were injected into starfish eggs, resulting in inhibition of actin-activated ATPase activity of myosin and cytokinesis failure (Mabuchi and Okuno 1977). Microinjection of antibodies to inactivate PLK1 during different stages of the cell cycle, revealed an important function in centrosome maturation and bipolar spindle formation (Lane and Nigg 1996). Despite its advantages, microinjection does require specialist tools and expertise, meaning it is not easily accessible for all labs. Moreover, it is low throughput and is best suited to cell types that remain relatively flat during mitosis, further limiting its use (Day et al. 2018).

Nanobodies

In addition to conventional antibodies composed of two heavy and two light chains, mammals such as llamas and camels from the Camelidae family, also produce heavy chain only antibodies (Hamers-Casterman et al. 1993). Moreover, they lack the constant domain 1, meaning the antigen-binding site consists of a single variable domain containing three antigen-binding loops (Fig. 1.7 B). Importantly, recombinant expression of the single variable domain results in a soluble functional antibody with a molecular weight of 15 kDa, known as a nanobody (Vincke and Muyldermans 2012). Recombinant expression can be achieved in bacteria and yeast, and expression in eukaryotic cells is not typically affected by the reducing environment of the cytoplasm, which is not favourable for the formation of disulphide bridges. Furthermore, they can be expressed with a fluorescent tag, making them useful affinity reagents to track protein localisation and protein function (Beghein and Gettemans 2017).

Nanobodies can be expressed in cells to bind a target protein and block a specific function. Not only is this useful in gaining biological insight, it can also aid in drug development (Beghein and Gettemans 2017). This has been shown for the tumour suppressor p53, where nanobodies that interfere with the transcriptional functional of p53 were developed (Bethuyne et al. 2014). Importantly, the authors found that the nanobody did not perturb p53 DNA-binding, suggesting that nanobodies can be developed to intricately target protein function (Bethuyne et al. 2014).

Nanobodies have also been engineered for use as tools for protein degradation,

as a means to study protein function. An example of this is deGradFP, where a nanobody targeting GFP fused to the F-box domain of Slmb can be used to degrade a GFP-tagged protein of interest by utilising the ubiquitin-proteasome pathway of degradation in eukaryotic systems (Caussinus et al. 2011). The advantage of this system is that it is immediately accessible to researchers who already have cell lines expressing GFP-tagged proteins of interest. Furthermore, the GFP-targeting nanobody could be swapped with a nanobody to any protein of interest (Beghein and Gettemans 2017).

An inducible and reversible method is provided by the AID-nanobody, which makes use of the AID system described in section 1.6.2 to degrade GFP-tagged proteins of interest (Daniel et al. 2018). Here, expression of TIR1 and the AID-nanobody, which is an anti-GFP nanobody fused to the AID degron, can be used to degrade a GFP-tagged protein upon the addition of auxin (Daniel et al. 2018). Though a useful tool, nanobodies to target GFP-tagged proteins can also have unwanted effects that could hinder their use. This was shown through the unintended inhibition of dynamin-2 using a nanobody to study its removal via KS (Küey et al. 2019).

Trim-Away

Trim-Away is a novel method for studying protein function that uses antibodies to specifically target proteins for degradation (Clift et al. 2017). In brief, antibody-bound proteins are recognised by the E3 ubiquitin ligase TRIM21 and are subsequently targeted for degradation by the proteasome. Therefore, the method requires delivery of a specific antibody into a cell, either by microinjection or electroporation, and delivery of TRIM21, either by overexpression or electroporation of the purified protein. As already mentioned, microinjection is technically challenging and is low throughput. To circumvent this, electroporation was used to introduce anti-pericentrin antibodies into the cell, with depletion observed after 3 h (Clift et al. 2017). While it is possible to use Trim-Away to deplete a protein of interest in bulk cell populations, the timescale to achieve depletion is not suited to observing transient events such as mitosis. Furthermore, it may not be a useful tool to dissect multiprotein complexes, since it was found that degradation of mTOR also resulted in degradation of binding partners Raptor and Rictor (Clift et al. 2017).

Limitations

The high specificity and affinity in which intact monoclonal antibodies can bind a target antigen is highly advantageous, particularly in the context of protein

inhibition. However, they are large complex proteins that require disulphide bonds and glycosylation for stability, making their production in bacterial systems or the cytoplasm of eukaryotic cells difficult to achieve (Muyldermans 2021). Moreover, their production relies on the use of immunised animals, meaning the process is time consuming and expensive. Microinjection or electroporation are ways in which it is possible to deliver antibodies into live cells, however, this is technically challenging. Expression of small recombinant antibody fragments such as scFv (25 kDa), is seen as a possible strategy to use antibodies in live cells. However, there are still issues with aggregation and inefficient folding when expressed in human cells (Guglielmi and Martineau 2009).

Nanobodies offer an attractive solution for use as protein inhibitors in live cells, as they are soluble and demonstrate high stability when expressed in human cells (Rothbauer et al. 2006). However, they are limited by the requirement of immunised camelids for production. To circumvent this, the use of naïve or synthetic libraries to identify high affinity nanobodies to a target antigen is becoming more common (Muyldermans 2021). In the case of a naïve library, it is constructed using sequences obtained from the serum of camelids that have not been immunized against a specific antigen, and therefore contains a high diversity of variable domain regions (Woods 2019). Synthetic libraries can be generated by randomising the CDR sequences within a stable nanobody scaffold. Further work is still needed to improve this selection process as there are issues with reduced stability and affinity of nanobodies selected from these libraries compared with immune libraries (Woods 2019). In all cases, the libraries are typically screened using phage display (described in section 1.6.5) to select nanobodies with specificity towards a desired antigen.

1.6.5 Non-immunoglobulin scaffolds

To overcome the limitations of antibodies and their derivatives to study protein function in live cells, an array of alternative scaffolds have been developed that are not based on the structure of Igs, collectively referred to as non-Ig scaffolds. To date, there are at least 50 types of non-Ig scaffolds (Škrlec et al. 2015), based on the sequence or consensus sequence of proteins with various functions and origins. Although functionally diverse, they are typically small, monomeric proteins that are stable and easy to express in bacteria. In general, the introduction of randomised amino acids is required to form the binding site. This variation leads to the formation of a large library of affinity reagents that can be screened against a protein of interest. Affinity constants in the low nanomolar range is common for most non-Ig scaffolds (Škrlec et al. 2015), making them ideal candidates to

complement antibodies as therapeutic reagents but also as research tools to study protein function.

Affimers

Affimers, previously known as Adhirons, are a synthetic protein scaffold based on the consensus sequence (approximately 100 aa) of a phytocystatin cysteine protease inhibitor found in plants (Tiede et al. 2014). Owing to its small size (approximately 12 kDa), high solubility and stability, it is desirable for use as an affinity reagent. To display peptides for protein recognition, 18 randomised amino acids, excluding cysteine, are inserted across two loop regions (9 aa per loop) in place of the inhibitory sequence present in the consensus phytocystatin (Tiede et al. 2014). Structurally, the Affimer scaffold consists of a single α-helix and four anti-parallel β-strands connected by the variable loop regions (Fig. 1.8 A).

The following sections will describe how Affimer binding reagents are identified for a protein of interest, and examples of their use as tools to study cell biology.

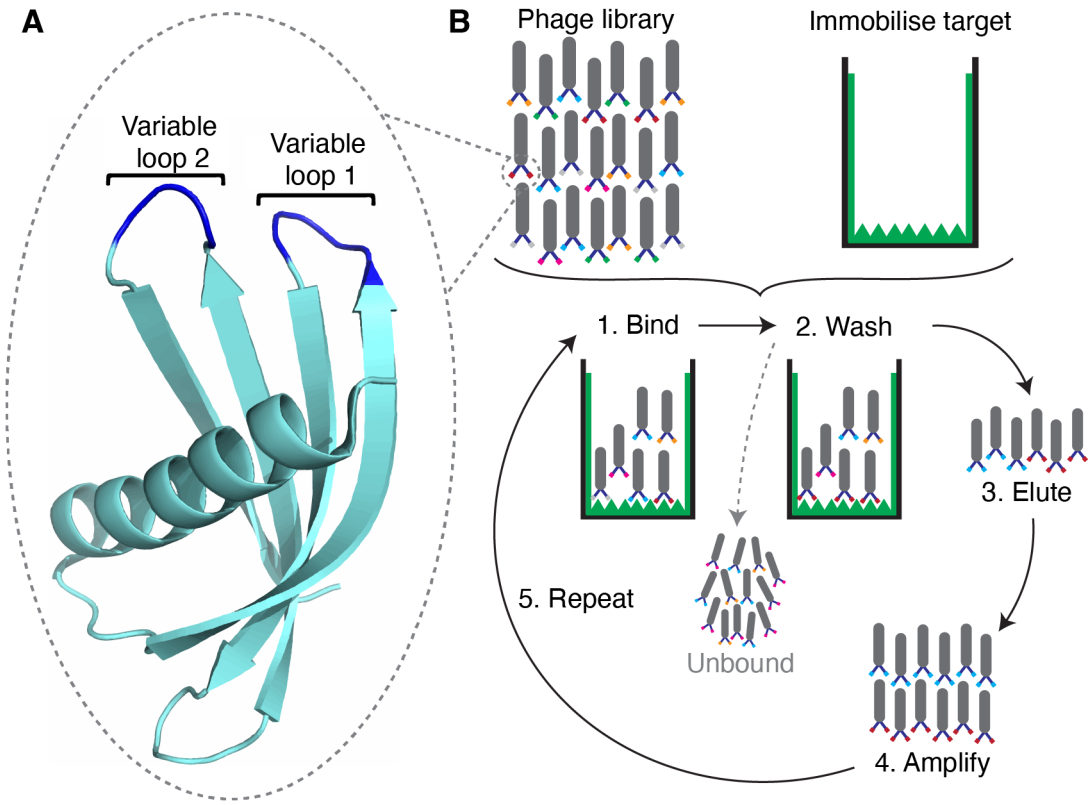

Figure 1.8. Biopanning of the Affimer-phage library. (**A**) Structure of the Affimer scaffold, as determined by X-ray crystallography. The scaffold is composed of a single α-helix and four antiparallel β-strands (both shown in light blue), joined by two loop regions (dark blue) that are responsible for molecular recognition. Adapted from (Tang et al. 2017). (**B**) Schematic to illustrate the biopanning process used to select high affinity Affimer reagents from the Affimer-phage library. A population of the Affimer-phage library is incubated with a purified protein of interest immobilised on a solid surface. Unbound phage is washed off while bound phage is eluted and amplified for further rounds of selection.

Screening by phage display

The Affimer library consists of 1.3×10^{10} clones, each containing randomised amino acids that make up the two loop regions (Tiede et al. 2014). One of the major advantages of Affimers over antibodies is that the library can be screened *in vitro* by phage display. Although developed almost 40 years ago with the intention of aiding antibody discovery (Smith 1985), phage display has since been modified for the purpose of screening Affimer proteins (Tang et al. 2017). In essence, this technique relies on the biology of a bacteriophage that displays a viral coat protein encoded by a gene present inside the phage. Therefore, a gene encoding a protein of interest, i.e. an Affimer, can be cloned into a plasmid alongside a capsid protein, meaning its expression will lead to an Affimer-displaying phage. Screening of the Affimer-phage library is performed by incubating a purified target protein immobilised on a solid surface with a population of Affimer-displaying phage (Fig. 1.8 B). This process is called biopanning, and involves several rounds of binding, wash and elution steps to

identify Affimers that can bind the target protein with high specificity and affinity. The entire screening process can be completed within two weeks, meaning it is significantly more efficient than identifying immunoglobulins from immunised animals (Tang et al. 2017). Furthermore, the coding sequence for positive Affimer clones can be cloned into an expression vector to produce recombinant protein using *E. coli* (Tiede et al. 2017). Due to the lack of disulphide bonds in the Affimer scaffold and no requirement for post-translational modifications, they can be expressed intracellularly in mammalian cells, making them ideal tools to study protein function.

A tool to study protein localisation

Affimers were developed by the BioScreening Technology Group set up by the University of Leeds and Leeds NHS Teaching Hospital Trust, with the goal of developing alternative affinity reagents against targets of clinical interest (Tiede et al. 2017). However, they have also been applied in basic research as microscopy tools to study protein localisation and as inhibitors to study protein function (Tiede et al. 2017).

For example, Affimers screened against tubulin were used to label microtubules in HeLa cells, exhibiting microtubule labelling to levels observed with an antibody (Tiede et al. 2017). Moreover, super-resolution imaging of microtubules labelled using the Affimer displayed increased localisation accuracy compared to antibodies, suggesting that Affimers could be advantageous in this context (Tiede et al. 2017). Similarly, Affimers screened against F-actin were recently shown to label the actin cytoskeleton in fixed and live cells (Lopata et al. 2018). For live cell imaging, Affimers labelled with GFP at the N-terminus were transfected into HeLa cells, where it was found that the pattern of actin localisation varied slightly between the Affimers tested. Differences in the rate of exchange from actin as observed by fluorescence recovery after photobleaching (FRAP), was also noted. Furthermore, filopodia labelling was not distinct in cells expressing Affimers, suggesting that the Affimers may recognise specific F-actin structures (Lopata et al. 2018). Application of the Affimers in fixed cells, using purified versions biotinylated at an engineered C-terminal cysteine and visualised by fluorescent streptavidin, revealed one Affimer that labelled actin in methanol and paraformaldehyde-fixed cells. This provides an advantage over phalloidin, a toxin used to label actin filaments in cells, as phalloidin is not compatible with methanol fixation (Lopata et al. 2018).

More recently, Affimers have been used as a tool to monitor the orientation of F-actin in live starfish embryos using fluorescence polarisation microscopy

(Sugizaki et al. 2021). Here, the authors developed a tool they call probe for orientation and localisation assessment, recognising specific intracellular structures of interest (POLArIS), where an Affimer and GFP are rigidly connected, enabling an Affimer to label a protein of interest with GFP in a rotationally constrained way. The high affinity of the Affimer for a protein of interest ensures the dipole of the GFP is sterically fixed to the target. Through this technique, the authors observed actin filaments radially extending towards the cell cortex in association with astral MTs (Sugizaki et al. 2021). Therefore, Affimers are suitable tools to visualise endogenous proteins in live mammalian cells, and owing to their small size, will likely have benefits over larger affinity reagents such as antibodies.

A tool to study protein function

Affimers can be screened against a purified fragment of a protein of interest, meaning that high affinity binding reagents can be generated to study the function of individual domains within a protein. In turn, Affimers can be used as a tool to study protein-protein interactions, with the advantage that they can be used without perturbing protein expression. By targeting individual domains, there is potential to inhibit specific functions, thus dissecting biological processes.

The specificity of Affimer reagents has previously been demonstrated by identifying binders to a defined region of a phosphoinositide 3-kinase, a heterodimeric complex composed of a regulatory p85 subunit and a catalytic p110 subunit (Tiede et al. 2017). Here, Affimers were screened against the N-terminal domain of p85 and were found to bind specifically, discriminating against the C-terminal domain *in vitro*. The Affimers were also found to bind endogenous p85 protein when expressed in mammalian cells, as determined by co-immunoprecipitation assays. Moreover, binding of the Affimers to the N-terminal domain of p85 led to an increase in phosphorylation activity, as would be expected if the interaction between this domain and p110 was blocked. Importantly, the Affimers did not inhibit the other domains of p85 that are required for p85–p110 complex formation (Tiede et al. 2017). Thus, Affimers can recognise specific protein domains and are an ideal tool to dissect protein function in cells.

1.7 Project motivation

The aim of this project was to take advantage of the recently developed Affimer library (Tiede et al. 2014; Tiede et al. 2017), to identify and screen affinity reagents to inhibit cell division, with the goal of achieving this in a cancer context. As has been described, TACC3–ch-TOG–clathrin–GTSE1 is a multiprotein complex that contributes to mitotic spindle stability in human cells to ensure timely mitosis. Moreover, TACC3 and clathrin have been identified as the core components of this complex (Ryan et al. 2021), which interact to form a MT binding surface (Hood et al. 2013). Thus, one aim of this thesis was to develop Affimer reagents to specifically target and inhibit this interaction in cells, as a means to break apart the complex without perturbing the expression levels of either protein.

In addition, we generated Affimers to disrupt the highly conserved interaction between TACC3 and ch-TOG, which outside of the complex, has been studied in the context of the centrosome and the MT plus-end. Based on studies performed in *Drosophila*, *Xenopus* and human cells, the cooperation of these proteins is important in promoting MT stability and regulating MT dynamics. Much of this work has utilised methods that manipulate the expression level of the proteins in question, potentially masking their true function. Thus, we used Affimers as a means to specifically inhibit the TACC3–ch-TOG interaction to decipher its contribution to MT dynamics and stability in human cells.

Chapter 2

Materials and methods

2.1 Molecular Biology

2.1.1 Reagents

Cloning reagents, including restriction enzymes, quick ligase kit and DNA gel extraction were purchased from New England Biolabs. Oligonucleotides were purchased from Sigma-Aldrich. Plasmid DNA miniprep and midiprep kits were purchased from Thermo Fisher Scientific and Sigma-Aldrich, respectively. Lysogeny broth (LB) media and plates were gratefully sourced from the Warwick Life Sciences media preparation service.

2.1.2 Cloning

The constructs made for this thesis were generated either by polymerase chain reaction (PCR) amplification of a gene of interest followed by digestion alongside the insert vector using the appropriate restriction enzymes, or by directly cutting the insert from an existing plasmid. In both cases, the digested vector and insert were ligated together with quick ligase and transformed into competent DH5α *E. coli* cells. Subsequent colonies were picked, amplified and their plasmid DNA extracted using a miniprep kit. Clones were sent to Source BioScience for Sanger sequencing to confirm correct identity of the insert. Correct constructs were transformed into DH5α cells and grown overnight in a 50 mL volume of LB media containing the appropriate antibiotic for subsequent DNA extraction using a midiprep kit for long term storage. Table 2.1 provides a list of constructs cloned for this study and table 2.2 lists the sequences of the respective oligos. Constructs used in this project but cloned by other lab members are listed in table 2.1.

Table 2.1. Constructs used in this study.

Construct	Vector	Method	Oligos	Source
FKBP-GFP-N1	pEGFP-N1	PCR, cut and ligate	-	Royle lab
FKBP-GFP-C1	pEGFP-C1	PCR, cut and ligate	-	Royle lab
pmCherry-N1	pEGFP-N1	PCR, cut and ligate	-	Royle lab
pmCherry-C1	pEGFP-C1	PCR, cut and ligate	-	Royle lab
pEGFP-C1	-	-	-	Royle lab
pIRES-EGFP-Puro	-	-	-	Royle lab
pMito-mCherry-FRB-K70N	pMito	PCR (SDM)	-	Royle lab
mNeonGreen-EB3	-	-	-	Royle lab
GFP-TACC3	pEGFP-C1	PCR, cut and ligate	-	Royle lab
pBrain-GFP-shch-TOG	pBrain	-	-	Royle lab
pBrain-ch-TOG-KDP (L1939,1942A)-GFP-shch-TOG	pBrain	-	-	Royle lab
pBrain-ch-TOG-KDP -GFP-shch-TOG	pBrain	-	-	Royle lab
mEmerald-γ-tubulin	mEmerald-C1	-	-	Addgene #54105
E4-His	pET11a	-	-	Bayliss lab
E7-His	pET11a	-	-	Bayliss lab
E8-His	pET11a	-	-	Bayliss lab
C3-His	pET11a	-	-	Bayliss lab
C4-His	pET11a	-	-	Bayliss lab
C5-His	pET11a	-	-	Bayliss lab
C6-His	pET11a	-	-	Bayliss lab
C7-His	pET11a	-	-	Bayliss lab
C8-His	pET11a	-	-	Bayliss lab
D1-His	pET11a	-	-	Bayliss lab
D2-His	pET11a	-	-	Bayliss lab
D3-His	pET11a	-	-	Bayliss lab
D4-His	pET11a	-	-	Bayliss lab
D5-His	pET11a	-	-	Bayliss lab
D6-His	pET11a	-	-	Bayliss lab
D7-His	pET11a	-	-	Bayliss lab
D8-His	pET11a	-	-	Bayliss lab
E4-mCherry	mCherry-N1	PCR, cut and ligate	JS034, JS035	Thesis
E7-mCherry	mCherry-N1	PCR, cut and ligate	JS034, JS035	Thesis
E8-mCherry	mCherry-N1	PCR, cut and ligate	JS034, JS035	Thesis
mCherry-E4	mCherry-C1	Cut and ligate	-	Thesis
mCherry-E7	mCherry-C1	Cut and ligate	-	Thesis
mCherry-E8	mCherry-C1	Cut and ligate	-	Thesis
mCherry-C3	mCherry-C1	Cut and ligate	-	Thesis
mCherry-C4	mCherry-C1	Cut and ligate	-	Thesis
mCherry-C5	mCherry-C1	Cut and ligate	-	Thesis
mCherry-C6	mCherry-C1	Cut and ligate	-	Thesis
mCherry-C7	mCherry-C1	Cut and ligate	-	Thesis
mCherry-C8	mCherry-C1	Cut and ligate	-	Thesis
mCherry-D1	mCherry-C1	Cut and ligate	-	Thesis
mCherry-D2	mCherry-C1	Cut and ligate	-	Thesis

Construct	Vector	Method	Oligos	Source
mCherry-D3	mCherry-C1	Cut and ligate	-	Thesis
mCherry-D4	mCherry-C1	Cut and ligate	-	Thesis
mCherry-D5	mCherry-C1	Cut and ligate	-	Thesis
mCherry-D6	mCherry-C1	Cut and ligate	-	Thesis
mCherry-D7	mCherry-C1	Cut and ligate	-	Thesis
mCherry-D8	mCherry-C1	Cut and ligate	-	Thesis
FKBP-GFP-E4	FKBP-GFP-C1	PCR, cut and ligate	JS036, JS037	Thesis
FKBP-GFP-E7	FKBP-GFP-C1	PCR, cut and ligate	JS036, JS037	Thesis
FKBP-GFP-E8	FKBP-GFP-C1	PCR, cut and ligate	JS036, JS037	Thesis
FKBP-GFP-C3	FKBP-GFP-C1	PCR, cut and ligate	JS036, JS037	Thesis
GFP-E4	GFP-C1	Cut and ligate	-	Thesis
GFP-E7	GFP-C1	Cut and ligate	-	Thesis
GFP-E8	GFP-C1	Cut and ligate	-	Thesis
E4-IRES-GFP	pIRES-GFP-Puro	PCR, cut and ligate	JS043, JS044	Thesis
E7-IRES-GFP	pIRES-GFP-Puro	PCR, cut and ligate	JS043, JS044	Thesis
E8-IRES-GFP	pIRES-GFP-Puro	PCR, cut and ligate	JS043, JS044	Thesis

Table 2.2. Oligonucleotides used to generate the plasmids listed in table 2.1.

Oligo name	Sequence (5' - 3')
JS034	TAAGCAAGCGCTGCCACCATGGCTAGCAACTCCCTGGAAATC
JS035	TGCTTAGTCGACGCAGCGTCACCAACCGGTTTG
JS036	TAAGCAGTCGACGCTAGCAACTCCCTGGAAATCG
JS037	TGCTTAGGATCCTTATGCAGCGTCACCAACCGGTTT
JS043	TGCTTAGAGCTCTTATGCAGCGTCACCAACC
JS044	TAAGCATCTAGAGCCACCATGGCTAGCAACTCCCTGGAAATC

2.2 Biochemistry

2.2.1 Reagents

Consumables for Western blotting, including Bradford reagent, 4× Laemmli sample buffer, mini-PROTEAN TGX precast protein gels, nitrocellulose membranes and Trans-Blot Turbo Transfer System were sourced from Bio-Rad Laboratories. Protease and phosphatase inhibitor cocktail tablets were purchased from Roche. Enhanced chemiluminescence detection reagent and Hyperfilms were purchased from GE Healthcare. Kits for the immunoprecipitation of RFP and GFP-tagged proteins were purchased from Chromotek. Phosphate buffered saline (PBS), tris buffered saline (TBS), tris buffered saline with tween 20 (TBS-T) and Tris/Glycine buffers were gratefully sourced from the Warwick Life Sciences media preparation service.

2.2.2 Western blotting

To check knockdown efficiency following small interfering RNA (siRNA) treatment, cell lysates were obtained by scraping the cells and incubating the resulting lysate on ice for 30 min in RIPA buffer (10 mM HEPES pH 7.4, 150 mM NaCl, 0.1% Triton X-100) containing a cOmplete EDTA-free protease inhibitor cocktail tablet. The lysate was centrifuged at 14,000 rpm for 15 min at 4 °C in an Eppendorf centrifuge 5417R. The protein concentration in the supernatant was quantified by performing a Bradford assay to ensure an equal amount of protein was used for subsequent analysis. Typically, 30 µg of protein lysate was prepared with 4× Laemmli sample buffer and 10% β-mercaptoethanol to reach a working concentration of 1×, and boiled at 95 °C for 5 min.

Samples were electrophoretically separated using a 4-15% mini-PROTEAN TGX precast protein gel at 110 V in 1× Tris/Glycine buffer, before being transferred to a nitrocellulose membrane using a Trans-Blot Turbo Transfer System. The resulting membrane was blocked for 1 h at room temperature in 5% milk in TBS-T before overnight incubation at 4 °C with primary antibodies diluted in 5% milk in TBS-T. The specific dilutions of primary antibodies used for Western blotting in this thesis are listed in table 2.3. Following overnight incubation with primary antibodies, the membrane was washed with TBS-T for 5 min and repeated twice. The membrane was incubated with HRP-conjugated secondary antibodies diluted 1:10,000 in 5% milk in TBS-T for 1 h at room temperature. The membrane was again washed 3 times in TBS-T before incubation with enhanced chemiluminescence detection reagent for 1 min. Membranes were positioned in a cassette and Hyperfilms were exposed to the membranes for varying lengths of time in a dark room. Hyperfilms were developed using a Xograph Compact X4 machine. Films were scanned and saved as an 8 bit image (greyscale) at 300dpi, Tiff.

Table 2.3. Primary antibodies used for Western blotting.

Antibody target	**Working concentration**	**Supplier**	**Cat No.**
∝-Tubulin (DM1A)	1:5,000	Abcam	ab7291
TACC3	1:1,000	Abcam	ab134154
clathrin heavy chain TD.1	1:1,000 (2% milk)	Hybridoma	CRL-2232
ch-TOG	1:1,000	QED Bioscience	34032
mCherry	1:1,000	Abcam	ab167453

Quantification

To quantify the intensities of protein bands in Western blots following the pull down of GFP-TACC3, a region of interest (ROI) was manually placed on each

band to be analysed and the mean intensity was measured using Fiji. To correct for background noise, a ROI was placed above each band and the mean intensity was measured. The same size ROI was used for all measurements in a single experiment, the smallest band to be measured was used to set the size of the ROI. Measurements were exported and read into R using a script where the mean pixel intensities were inverted and corrected for background noise. For each experiment, corrected values were normalised to the respective value from the mCherry control condition and plotted.

2.2.3 Immunoprecipitation (IP)

Commercial GFP and RFP-trap kits (Chromotek) were used to isolate GFP and mCherry-tagged proteins from cell lysates, respectively. To isolate GFP-TACC3, HeLa cells expressing GFP-TACC3 were first lysed on ice for 30 min using lysis buffer (10 mM Tris/HCl pH 7.5, 150 mM NaCl, 0.5 mM EDTA, 0.5% Nonidet™ P40 Substitute, 0.09% sodium azide, protease and phosphatase inhibitor tablets). To pull down TACC3, 1.5 mg of lysate was incubated with magnetic beads and the manufacturer's protocol followed. To elute the target protein and any binding partners, beads were resuspended in 80 µl 2× Laemmli buffer and 10% β-mercaptoethanol and boiled for 5 min at 95 °C. Co-immunoprecipitation of the target protein(s) was assessed by Western blotting as described in section 2.2.2, where 40 µl of the eluted sample was analysed and 50 µg of cell lysate was loaded as input.

Preparation of mitotic HeLa cell extract

To isolate transiently expressed mCherry-tagged Affimers from mitotic HeLa cell extract, cells were synchronised using thymidine and nocodazole as follows. A final concentration of 2 mM thymidine was added to cells 12 h post-transfection and incubated for 16 h. Media was changed and cells incubated for 8 h. A 330 nM concentration of nocodazole was added to cells for 16 h. To release mitotic cells, dishes were tapped firmly and the media used to wash down the dish several times before transferring to a falcon tube. In combination with further tapping, warm PBS was used to wash down residual cells and transferred to the same falcon tube. Cells were pelleted by centrifugation and resuspended in warm PBS, this was repeated twice. On the third wash, pelleted cells were resuspended in warm Dulbecco's Modified Eagle's Medium (DMEM) and transferred to a fresh plate containing warm DMEM. Cells were incubated for 40 min at 37 °C and 5% CO_2 before pelleting. Pelleted cells were lysed using RIPA buffer as described in section 2.2.2. To pull down mCherry-Affimers, 1 mg of lysate was

incubated with magnetic beads and the manufacturer's protocol followed. To elute the target protein and any binding partners, beads were resuspended in 80 µl 2× Laemmli buffer and 10% β-mercaptoethanol and boiled for 5 min at 95 °C. Co-immunoprecipitation of the target protein(s) was assessed by subsequent Western blotting as described in section 2.2.2, where 40 µl of the eluted sample was analysed and 30 µg of cell lysate was loaded as input.

2.3 Cell Biology

2.3.1 Reagents

Cell culture plasticware was sourced from Sarstedt Ltd, Scientific Laboratory Supplies Ltd or World Precision Instruments Ltd. All culture medium and chemicals were purchased from Fisher Scientific or Sigma-Aldrich. Aurora A inhibitor MLN8237 was obtained from Stratech Scientific Limited. For DNA transfections, GeneJuice and FuGENE HD were sourced from Novagen and Promega, respectively. For siRNA transfections, Lipofectamine 2000 was purchased from Invitrogen.

2.3.2 Cell maintenance

HeLa and U2OS cells were maintained in DMEM supplemented with 10% fetal bovine serum (FBS) and 1% antibiotics (100 U/mL penicillin, 100 µg/mL streptomycin) at 37 °C and 5% CO_2. RPE-1 EB3-tdTomato cells were maintained in DMEM/F-12 ham media supplemented with 10% FBS, 1% antibiotics (penicillin/streptomycin), 2.3 g/L sodium bicarbonate, 2 mM l-glutamine and 400 µg/mL Geneticin for selection of EB3-tdTomato. The GFP-FKBP-TACC3 and CLTA-FKBP-GFP homozygous clustered regularly interspaced short palindromic repeats (CRISPR) HeLa cell lines used in this thesis were generated in the lab (Ryan et al. 2021). Cells were maintained for a maximum of 25 passages following initial thawing.

2.3.3 DNA transfection

Cells were seeded on cover slips or in fluorodishes to reach a confluency of 70% prior to transfection. For HeLa cells, GeneJuice was used to transfect DNA plasmids as per the manufacturer's instructions. For RPE-1 cells, FuGENE HD was used to transfect DNA plasmids as per the manufacturer's instructions. In both instances, a 3:1 ratio of transfection reagent to DNA was used. Medium was changed 8 h following transfection or the next morning. Typically, cells were

processed 48 h post-transfection.

2.3.4 siRNA transfection

Cells were seeded on cover slips or in fluorodishes to reach a confluency of 70% prior to transfection. Lipofectamine 2000 was used to transfect siRNA as per the manufacturer's instructions. For experiments that required expression of plasmid DNA following knockdown, a transfection using GeneJuice was performed 24 h post siRNA transfection. For knockdown of ch-TOG, cells were transfected with 60 nM siRNA and processed 48 h post transfection. For knockdown of TACC3, cells were transfected with 100 nM siRNA and processed 48 h post transfection. The target DNA sequence used to generate the siRNA oligonucleotides used in this thesis are listed in table 2.4. All siRNA oligonucleotides were synthesised with deoxythymidine dinucleotide (dTdT) 3' overhangs.

Table 2.4. Target DNA sequence used to generate siRNA oligonucleotides.

Target protein	Target DNA sequence (5' - 3')
ch-TOG (3'UTR)	CACCCTGCAGCTTTAGTTTACTAAA
TACC3	GTTACCGGAAGATCGTCTG
GL2 (control)	CGTACGCGGAATACTTCGA

2.3.5 Immunofluorescence

Cells were fixed on glass cover slips 48 h post-transfection with PTEMF (20 mM PIPES, pH 6.8, 10 mM EGTA, 1 mM $MgCl_2$, 0.2% Triton X-100, and 4% paraformaldehyde) for 10 min at room temperature, with paraformaldehyde (PFA) solution (3% PFA, 4% sucrose in PBS) for 15 min at room temperature, or with ice-cold methanol for 10 min. Cells fixed in PTEMF or PFA were permeabilised in 0.5% Triton X-100 in PBS for 10 min. Following permeabilisation, cover slips were washed with PBS three times. For methanol fixation, cover slips were washed with PBS immediately following the removal of methanol. Following fixation and permeabilisation, cover slips were blocked at room temperature in 3% bovine serum albumin (BSA) in PBS for 1 h and incubated with primary antibodies diluted in blocking buffer for 1 h. Cover slips were washed with PBS three times, 5 min per wash, before incubation with Alexa-Fluor conjugated secondary antibodies in blocking buffer for 1 h at room temperature. In experiments where CRISPR GFP-FKBP/FKBP-GFP knock-in cell lines were used, anti-Rabbit GFP-boost (Invitrogen) or GFP-boost (Chromotek) antibodies were used to enhance the signal of GFP-tagged proteins. Cover slips were washed with PBS as before, dipped in dH_2O and left to dry completely before mounting. Dry cover slips were mounted on slides using mowiol containing DAPI (Sigma). Refer to table 2.5 for specific dilutions of the antibodies used in this thesis. Of note, an experiment to compare the specificity of commercial antibodies for the detection of ch-TOG in mitotic HeLa cells was performed and the results are displayed in Appendix 1 (Shelford and Royle 2020).

Table 2.5. Antibodies used for immunofluorescence.

Antibody name	Working concentration	Supplier	Cat No.
Mouse anti-α-tubulin	1:1,000	Sigma	T6074
Rabbit anti-α-tubulin	1:2,000	Invitrogen	PA5-19489
Rabbit anti-detyrosinated Tubulin	1:50	Abcam	ab48389
Mouse anti-acetylated Tubulin	1:100	Sigma	T6793
Rabbit anti-ch-TOG	1:5,000	QED Bioscience	34032
Rabbit anti-ch-TOG	1:800	Thermo	PA5-59150
Mouse anti-EB1	1:500	BD Transduction Laboratories	610534
Rabbit anti-Pericentrin	1:5,000	Abcam	ab4448

Antibody name	**Working concentration**	**Supplier**	**Cat No.**
Mouse anti-Centrin-1	1:500	Sigma	04-1624
Mouse anti-TACC3	1:1,000	Abcam	ab56595
Rabbit anti-GFP, Alexa-Fluor 488	1:200	Invitrogen	A-21311
GFP-boost	1:200	Chromotek	gba488
Alexa-Fluor 568 goat anti-mouse	1:500	Invitrogen	A-11031
Alexa-Fluor 568 goat anti-rabbit	1:500	Invitrogen	A-11036
Alexa-Fluor 488 goat anti-mouse	1:500	Invitrogen	A-11029
Alexa-Fluor 488 goat anti-rabbit	1:500	Invitrogen	A-11034
Alexa-Fluor 647 goat anti-rabbit	1:500	Invitrogen	A-27040
Alexa-Fluor 647 goat anti-mouse	1:500	Invitrogen	A-21235

2.3.6 Measuring transferrin uptake

Cells were rinsed twice in warm DMEM (containing no additions), serum starved (incubated in DMEM with no additions) for 30 min and incubated with DMEM containing 100 µg/mL Alexa Fluor 647-conjugated transferrin (Thermo) for 10 min, all at 37 °C and 5% CO_2. For the positive control, cells were treated with 0.45 M sucrose for the final 10 min of the serum starvation step. Cells were washed twice with warm PBS before fixing with PFA as described in section 2.3.5.

Quantification

Using an automated procedure in Fiji, single cells were manually outlined and a threshold applied to isolate vesicular structures in the transferrin channel. Puncta were counted using the *Analyze particles* procedure using a mask of 0.03 µm-0.8 µm and circularity of 0.3-1.0. Measurements were exported and read into R to generate plots displaying the number of puncta detected in each cell. All analysis was performed blind to the conditions of the experiment.

2.3.7 Knocksideways

KS is a rapid and inducible method used to inactivate proteins using a rapamycin-induced heterodimerisation system, originally developed by Margaret Robinson (Robinson et al. 2010). It has been used extensively in the lab to study the functions of proteins during various stages of mitosis, and can be used as a tool to study protein-protein interactions (Cheeseman et al. 2013). In brief, addition of rapamycin causes an FKBP domain fused to a target protein, to heterodimerise with an FRB domain fused to a protein with a localisation away from the target, such as the mitochondria. In experiments described in this thesis, a MitoTrap construct, consisting of the import signal of the yeast mitochondrial outer membrane protein Tom70p fused to an FRB domain was used. The target

proteins for KS were cloned into a vector containing FKBP fused to a fluorescent tag.
To perform KS in fixed cells, rapamycin (Alfa Aesar) was added to cells to a final concentration of 200 nM 30 min prior to fixation. Images of mitotic cells were acquired using a 60× oil objective on a Nikon CSU-W1 spinning disk inverted microscope.

Quantification of fixed cells

Analysis of knocksideways in fixed cells was performed by measuring the spindle localisation of the target protein and the protein of interest, as described in section 2.3.10, using a 1.4 µm^2 ROI for analysis.

2.3.8 Tracking and measuring the dynamics of microtubule plus-ends

Cells were seeded in 35 mm fluorodishes and transfected 24 h later with appropriate plasmids. Cells were imaged 48 h post-transfection. HeLa cells expressing NeonGreen-EB3 were imaged for 2 min at 2 s intervals in a single z position using a widefield Nikon Eclipse-Ti microscope. RPE-1 stably expressing EB3-tdTomato were imaged for 1 min at 1 s intervals in a single z position using a widefield Nikon Eclipse-Ti microscope. Immediately prior to imaging, cell media was changed to Leibovitz L-15 CO_2-independent medium supplemented with 10% FBS. Cells were kept at 37 °C in a temperature controlled chamber (Okolab) during acquisition.

Quantification

Movies were analysed using *u-track 2.2.0* (https://github.com/DanuserLab/u-track) in MATLAB R2018b (Applegate et al. 2011). The following parameters were used for all movies: Anisotropic Gaussian Detection method; maximum gap length, 4 frames; minimum track length, 3 frames; Brownian Search Radius, 2-10 pixels; maximum forward angle, 30°; maximum backward angle, 10°; maximum shrinkage factor relative to growth speed, 1.5; fluctuation radius, 1 pixel; time interval, 1 s or 2 s. Data from the analysis were exported and read into R where a script generated plots displaying growth speed (average velocity of each MT growth event), growth length (distance of MT growth in a track before a pause or catastrophe event) and growth lifetime (number of seconds of MT growth in a track before a pause or catastrophe event).

2.3.9 Measuring the microtubule plus-end intensity of TACC3

CRISPR GFP-FKBP-TACC3 HeLa cells were seeded in 35 mm fluorodishes and transfected 24 h later with plasmids to express free mCherry or mCherry-tagged Affimers. 48 h post-transfection, cells were imaged live for 1 min at 1 s intervals in a single z position using a Nikon CSU-W1 spinning disk microscope and 100× oil objective. Immediately prior to imaging, cell media was changed to Leibovitz L-15 CO_2-independent medium supplemented with 10% FBS. Cells were kept at 37 °C in a temperature controlled chamber (Okolab) during acquisition. To help improve the detection of TACC3 comets, cells in anaphase or telophase were imaged, as TACC3 +TIP activity is easier to distinguish during these stages of the cell cycle. To reduce the effects of phototoxicity, mCherry was acquired for the first frame only.

Quantification

Movies were analysed using *ComDet v.0.5.5* (https://github.com/ekatrukha/ComDet) in Fiji to detect TACC3 comets. The following parameters were used to detect TACC3 comets in all movies: particle size, 4 pixels; intensity threshold (in SD), 4. Data from the analysis were read into R to generate plots displaying the median number of TACC3 comets detected per cell and the median fluorescence intensity of the TACC3 comets detected per cell. All analysis was performed blind to the conditions of the experiment.

2.3.10 Measuring spindle recruitment

Cells were seeded onto glass cover slips in a 6-well plate and transfected 24 h later with appropriate plasmids. 48 h post-transfection, cells were processed for immunofluorescence as described in section 2.3.5. In experiments where ch-TOG was stained using the QED Bioscience antibody, cells were fixed in methanol. As a positive control to abolish spindle localisation, MLN8237 was added to cells at a final concentration of 0.3 µM 40 min prior to fixation. Images of mitotic cells were acquired using a 100× oil objective on a Nikon CSU-W1 spinning disk inverted microscope.

Quantification

Spindle recruitment analysis was performed as described in (Ryan et al. 2021). Using Fiji, a 11×11 ROI (1.455 µm^2) was manually placed to measure the average fluorescence intensities of three regions of the spindle (away from the poles), the

cytoplasm and one region outside of the cell as background. Measurements were exported and read into R using a script where, following background subtraction, the average spindle value was divided by the average cytoplasm value to generate a spindle enrichment ratio and plotted. All analysis was performed blind to the conditions of the experiment.

2.3.11 Quantification of mitotic spindle positioning

Cells were seeded onto glass cover slips in a 6-well plate and transfected 24 h later with plasmids to express free mCherry or mCherry-tagged Affimers. 48 h post-transfection, cells were fixed using PTEMF and stained with antibodies to detect α-tubulin and pericentrin, as described in section 2.3.5. Image stacks (17×0.3 µm) of mitotic cells were acquired using 100× or 60× oil objectives on a Nikon CSU-W1 spinning disk inverted microscope.

Quantification

Max intensity z projections of image stacks were analysed using a semi-automated procedure in Fiji. Analysis was performed blind to the conditions of the experiment. The centrosomes, cell outline and metaphase plate were manually outlined and the xy coordinates of each were measured and read into R for analysis. Spindle length is defined by the distance between the centrosomes. To allow for an accurate measurement of spindle length, only cells containing 2 distinct centrosomes were included in the analysis. Spindle position with respect to the outline of the cell was quantified by calculating the following parameters:

- d2-d1 is the absolute difference of d1 and d2, where d1 = distance from centrosome 1 to the cell outline and d2 = distance from centrosome 2 to the cell outline.
- D2-D1 is the absolute difference of D1 and D2, where D1 and D2 are the two distances from the metaphase plate to the cell outline. The position on the metaphase plate was calculated by finding the point of intersection of the centrosome line and the metaphase plate line.

2.3.12 Centrosome analysis

Cells were seeded onto glass cover slips in a 6-well plate and transfected 24 h later with appropriate plasmids to express Affimers or ch-TOG mutants. 48 h post-transfection, cells were fixed and stained with appropriate antibodies as described in section 2.3.5. In experiments where pericentrin or γ-tubulin antibodies were used, cells were fixed with PTEMF. In experiments where

centrin-1 staining was required, cells were fixed with methanol. Of note, the ch-TOG antibody used in these experiments was supplied by Thermo (Cat No. PA5-59150) as the antibody supplied by QED Bioscience (34032) used in the spindle recruitment assays was found to weakly stain the centrosome pool of ch-TOG and is only compatible with methanol fixation. Image stacks (17×0.3 µm) of mitotic cells were acquired using 100× or 60× oil objectives on a Nikon CSU-W1 spinning disk inverted microscope.

Quantification of pericentrin and γ-tubulin

For the quantification of pericentrin and γ-tubulin foci, image stacks were analysed using *3D Objects Counter*(https://imagej.nih.gov/ij/plugins/track/objects.html) in Fiji. Single cells were manually outlined to create a ROI that was used in the centrosome channel for object detection. Identical settings were used for all images in an experiment. Subsequent measurements were read into R to generate plots displaying the number of foci detected and the volume and fluorescence intensities of the foci.

In experiments where γ-tubulin was stained, the *subtract background* feature in Fiji was used in the γ-tubulin channel prior to launching *3D Objects Counter*, using the middle z position in the stack as the starting point for background subtraction. To measure the fluorescence intensity of ch-TOG at γ-tubulin foci, the mask of each γ-tubulin foci was redirected to the ch-TOG channel.

Quantification of centrin-1

Due to the small size of the centrin-1 foci and the tendency for them to overlap, *3D Objects Counter* was not suitable to quantify the number of centrin-1 foci present within pericentrin sites of mitotic cells. Instead, the foci of both proteins were manually counted using max intensity z projection images. The data was read into R to generate plots displaying the number of centrin-1 foci in each pericentrin site of individual cells. Analysis was performed blind to the conditions of the experiment.

2.3.13 Mitotic progression and centrosome analysis

HeLa cells were seeded in 35 mm fluorodishes with 4 compartments (Greiner) and transfected 24 h later with appropriate plasmids. 48 h post-transfection, cells were incubated in Leibovitz (Gibco) L-15 CO_2-independent media supplemented with 10% FBS containing 0.5 µM SiR-DNA (Spirochrome) for 30 min to visualise the DNA before imaging. Imaging was performed in a temperature controlled

chamber (Okolab) set to 37 °C. Image stacks (5×3 µm) were acquired using a 40× oil objective and widefield settings on a Nikon CSU-W1 spinning disk inverted microscope. To observe mitotic events, the DNA and centrosomes were imaged for 12 h-16 h at 3 min intervals. To reduce the effects of phototoxicity, mCherry was imaged every 7th frame (21 min intervals).

Quantification

Image stacks of transfected SiR-DNA labelled cells were analysed and the frame numbers for prometaphase, metaphase and anaphase were recorded in an Excel workbook. Alongside this, the frame numbers where > 2 γ-tubulin foci were observed were recorded and used to categorise the phenotype in relation to the stages of mitosis. For the timings of mitosis, prometaphase was recorded at the first sign of nuclear envelope rupture; metaphase when the majority of chromosomes were aligned at the metaphase plate; anaphase at the first sign of poleward movement of the sister chromatids. Only cells that displayed in-focus γ-tubulin foci and completed mitosis during acquisition were used in the analysis. For centrosome analysis, G2 was defined as the period 5 frames (15 min) prior to prometaphase. To visualise the centrosome results, data were read into R, where a Sankey diagram was produced using the networkD3 package (https://cran.r-project.org/web/packages/networkD3/index.html) to illustrate the flow of cells with two or > 2 γ-tubulin foci during the observed stages. To visualise mitotic progression, data were read into IgorPro, where a custom-written procedure was used to visualise the data.

2.3.14 Measuring microtubule regrowth

To investigate MT regrowth dynamics in HeLa cells expressing free mCherry or mCherry-tagged Affimers, an ice recovery assay was used (Grimaldi et al. 2013). Briefly, cells seeded onto glass cover slips in a 6-well plate were incubated on ice for 1 h and recovered at room temperature for 0, 5, 10 or 15 min before fixing immediately with PTEMF. The timings of the experiment were staggered such that all samples were fixed simultaneously. As a negative control, cells stored in an incubator set to 37 °C and 5% CO_2 were fixed alongside. Image stacks (11×0.2 µm) of interphase cells were acquired using a 100× oil objective on a Nikon CSU-W1 spinning disk inverted microscope.

Quantification

Max intensity z projection images were analysed using a semi-automated procedure in Fiji, whereby single cells were manually outlined using the mCherry

channel and the *auto threshold* method applied to isolate the MT network in the tubulin channel. An identical threshold method was applied to all images within a time point. The percentage area of the MT network within each cell was measured and read into R to generate plots. All analysis was performed blind to the conditions of the experiment.

2.4 Microscopy

2.4.1 Widefield microscopy

Widefield images were acquired with a Nikon Eclipse-Ti microscope and a Photometrics CoolSNAP MYO cooled CCD camera using a 100× oil objective (1.40 NA, pixel size = 0.0453 µm). Images were captured with NIS Element acquisition software using standard filter sets for DAPI, GFP and mCherry. For live cell imaging, cells were seeded in 35 mm glass bottom fluorodishes. Immediately prior to imaging, media was changed to Leibovitz L-15 CO_2-independent medium supplemented with 10% FBS and cells were kept at 37 °C in a temperature controlled chamber (Okolab).

2.4.2 Confocal microscopy

Confocal imaging of fixed and live cells was performed using a Nikon CSU-W1 spinning disk inverted microscope equipped with a 2x Photometrics 95B Prime sCMOS camera using either a 100× oil (1.49 NA, pixel size = 0.110 µm) or 60× oil objective (1.40 NA, pixel size = 0.182 µm). In all experiments, imaging was performed sequentially. Excitation was via 405 nm, 488 nm, 561 nm and 638 nm lasers, with 405/488/561/640 nm dichroic mirrors and Blue, 446/60; Green, 525/50; Red, 600/52; FRed, 708/75 emission filters. The system also contains an Okolab microscope incubator, Nikon motorised xy stage and a Nikon 200 µm z-piezo. Images were acquired with Nikon NIS-Elements software.

For mitotic progression experiments, the system described above was used with widefield settings. A 40× oil (1.30 NA, pixel size = 0.28 µm) objective was used. Excitation was via a CoolLED (pE-300) light source, with Chroma ZET561/10× (mCherry), Chroma ZET488/10× (GFP) and Chroma ZT647rdc (FRed) excitation filters. Chroma ET575lp (mCherry), Chroma ET500lp (GFP) and Chroma ET665lp and Chroma ZT647rdc (FRed) dichroic mirrors were used with Chroma ET600/50m (mCherry), Chroma ET525/50m (GFP) and Chroma ET705/72m (FRed) emission filters.

2.5 Data analysis

2.5.1 Figure preparation and code

All figures were made in Fiji (Schindelin et al. 2012) (https://imagej.net/software/fiji/), IgorPro (WaveMetrics; https://www.wavemetrics.com/products/igorpro) or R (https://www.r-project.org/) and assembled in Adobe Illustrator. Custom-written procedures to analyse, process and plot data for the fixed centrosome experiments, transferrin uptake assay and live MT tracking experiments are available at:

- https://github.com/james-shelford/Image_Analysis_Projects.

Code for the spindle position experiment is available at:

- https://github.com/james-shelford/SpindleAnalytics.

The code for analysis of mitotic progression was written by Stephen Royle and is available at:

- https://github.com/quantixed/MitoticTiming.

2.5.2 Statistical analysis

To compare the means of two groups, an independent two-sample t-test was used. To compare among three or more groups, a one-way analysis of variance (ANOVA) was used with Tukey's post hoc test. A Kruskal-Wallis test with Dunn's post hoc test was used for data that did not follow a normal distribution. To assess normality, a Shapiro-Wilk test was used. Fisher's exact test was used to test for an association between Affimer expression and PCM fragmentation. The Bonferroni correction method was used to adjust p values to account for multiple comparisons.

Chapter 3

Generation and screening of Affimers

3.1 Background

The mitotic spindle, consisting of a dynamic array of MTs that are organised and stabilised by a variety of motor and non-motor proteins, is responsible for the alignment and segregation of the genetic material during mitosis. A complex containing TACC3, clathrin, ch-TOG and GTSE1 (TACC3–ch-TOG–clathrin–GTSE1), has been identified as important in the stabilisation of K-fibres, and in turn maintaining overall spindle stability (Booth et al. 2011; Hood et al. 2013; Nixon et al. 2015; Cheeseman et al. 2013; Ryan et al. 2021). Recent work has highlighted TACC3 and clathrin as core components of this complex, acting as a scaffold to recruit ch-TOG and GTSE1, respectively (Ryan et al. 2021; Rondelet et al. 2020). Studies involving siRNA-mediated depletion of TACC3 and clathrin, or expression of mutant proteins deficient in binding one another, have demonstrated that these proteins are interdependent for their spindle localisation (Hood et al. 2013; Hubner et al. 2010; Booth et al. 2011; Lin et al. 2010). This interaction has been mapped to the CID of TACC3, where a dileucine motif (L566, 567), and a S558 residue that undergoes phosphorylation by Aurora A, are required to mediate an interaction with the ankle region of CHC. This allows the N-terminal domain of clathrin and the C-terminal TACC domain of TACC3 to form a MT binding surface required for spindle localisation (Hood et al. 2013; Burgess et al. 2018). Extensive work has been carried out to identify the components of this complex and map the interactions within it, however, the roles of specific interactions remain unclear. Additionally, since TACC3 and clathrin form the MT binding surface required

for the formation of the inter-MT bridge complex, they provide an interesting target to disrupt spindle stability in an anti-cancer context.

The work in this chapter aims to tackle these questions by screening candidate Affimer proteins to identify high affinity binding reagents that can be used to dissect protein-protein interactions in living cells. Secondly, this work will determine if the Affimer reagents can be used to label and track target proteins in fixed and live cells. In collaboration with Richard Bayliss' group, 14 Affimers raised against the ankle region of CHC (aa 358-574) to disrupt an interaction with the CID of TACC3, were isolated and screened in HeLa cells. In addition, 3 Affimers raised against the C-terminal TACC domain of TACC3 (aa 629-838 Δ699-765), thought to be responsible for the interaction with ch-TOG, were isolated and screened *in vitro* before screening in HeLa cells. The first half of this chapter describes experiments carried out in human cells to screen Affimers designed to bind clathrin, whilst the second half describes *in vitro* experiments and experiments in HeLa cells to screen Affimers designed to bind TACC3.

3.2 Preparation of Affimers for expression in human cell lines

To prepare plasmids that express fluorescently-tagged Affimers in human cells, the sequence of each His-tagged Affimer was amplified, removing a C-terminal His-tag and two alanine residues, and ligated into pmCherry-N1 and pmCherry-C1 vectors. To determine if the orientation of the fluorescent tag is important, GFP-TACC3 and Affimers tagged with mCherry at either the N or C-terminus were transfected into HeLa cells and viewed live by widefield microscopy. Interestingly, all of the N-terminally tagged Affimers colocalised with TACC3 in mitotic cells, whilst C-terminally tagged Affimers were localised throughout the cell and did not display the same level of colocalisation (Fig. 3.1). This suggests that the orientation of the fluorescent tag does indeed affect the localisation of the Affimer in human cells. Thus, Affimers tagged at the N-terminus were used in subsequent experiments and are referred to as mCherry-Affimer throughout the thesis. Of note, some aggregation of the N-terminally tagged Affimers but not the C-terminally tagged versions was observed.

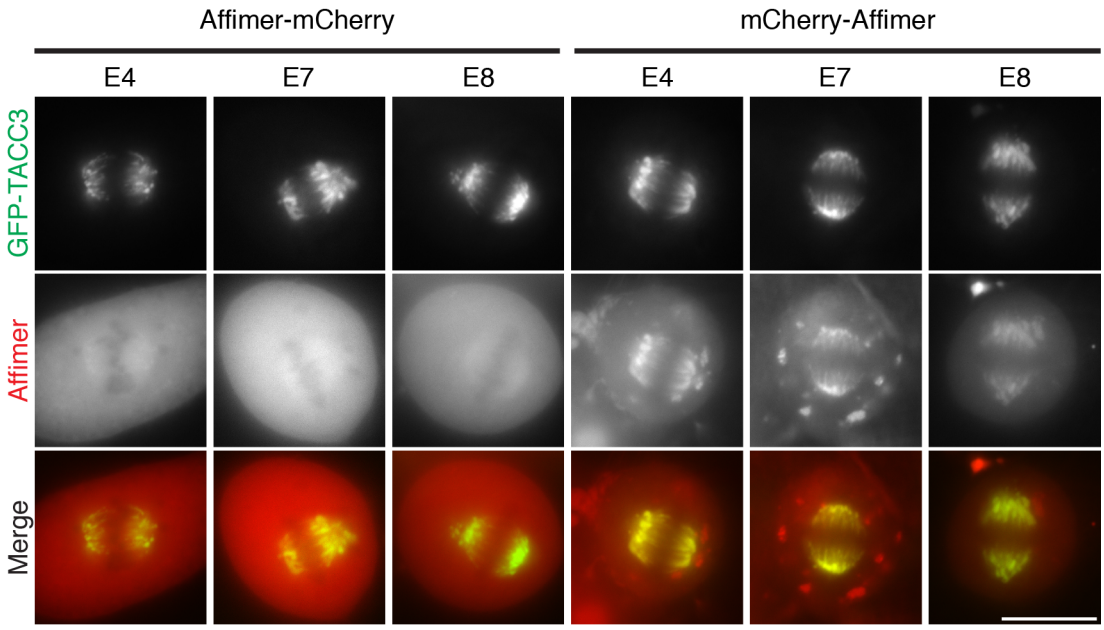

Figure 3.1. The orientation of the fluorescent tag affects the localisation of TACC3 Affimers in HeLa cells. Widefield micrographs of live HeLa cells in metaphase expressing GFP-TACC3 (green) and TACC3 Affimers (red) labelled with mCherry at either the C or N-terminus as indicated. Scale bar = 10 µm.

3.3 Screening clathrin Affimers

Using the ankle region of CHC (aa 358-574), a screen against an Affimer library via phage display identified 14 candidate Affimer proteins suitable for further screening. Based on results in Fig. 3.1, the Affimer sequences were subcloned into the pmCherry-C1 vector and screened in HeLa cells. To identify binders to CHC and determine if this binding can block an interaction with TACC3, a pull-down assay using lysate from HeLa cells expressing each of the mCherry-Affimers was performed.

As an interaction between TACC3 and clathrin is required for the formation of inter-MT bridges during mitosis, HeLa cells were synchronised to collect lysate from predominantly mitotic cells (see 2.2.3 for details). A commercial RFP-trap system was used to isolate mCherry-Affimers and any binding partners. The immunoprecipitates were assessed by Western blot, using antibodies to detect mCherry (Affimer), CHC and TACC3 (Fig. 3.2). The blot revealed a strong band at the predicted molecular weight of CHC (180 kDa) in the immunoprecipitate of 6 Affimers: C4, C8, D2, D5, D6 and D8. In contrast, no band for CHC was detected in the immunoprecipitate of 8 Affimers: C3, C5, C6, C7, D1, D3, D4 and D7. Furthermore, with the exception of D3, no band for CHC was observed in the unbound fraction of these samples, suggesting that CHC may have been lost during the subsequent wash steps of the experiment. Interestingly, no band at

the molecular weight of TACC3 (140 kDa) was observed in the immunoprecipitate from cells expressing CHC binding Affimers, suggesting that the Affimer may be interfering with the TACC3–clathrin interaction in these cells. However, it should be noted that a negative control was not included in the experiment for comparison. Nevertheless, this result demonstrates that Affimers: C4, C8, D2, D5, D6 and D8 all bind to CHC in HeLa cells. Since CHC was only observed in the unbound sample of Affimer D3, this Affimer could serve as a negative control, where no binding to CHC is observed in HeLa cells.

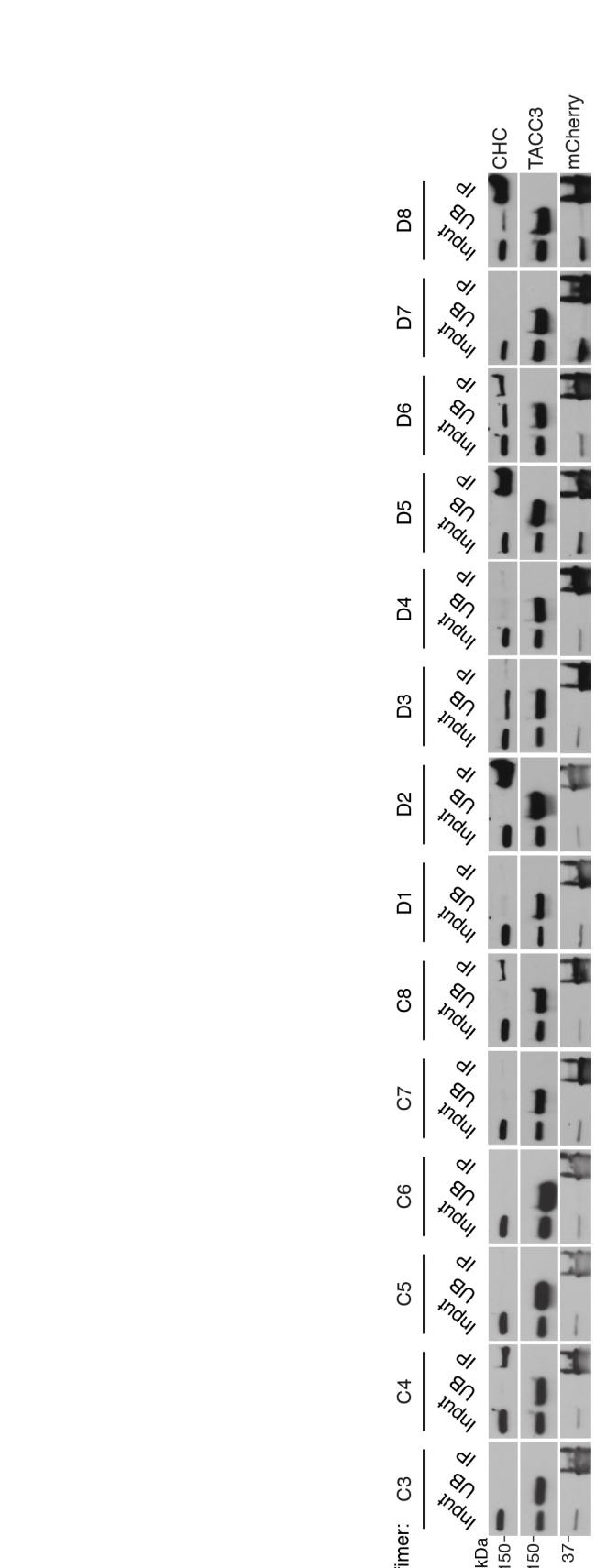

Figure 3.2. Pull down of mCherry-Affimers in HeLa cells to identify high affinity binders to clathrin heavy chain. Pull-down assay using extracts of mitotic HeLa cells overexpressing the indicated mCherry-Affimers designed to bind clathrin heavy chain (CHC). The RFP-trap system was used to isolate Affimers and their binding partners using 1 mg of HeLa cell lysate. The immunoprecipitates (IP) were analysed by Western blot, using antibodies against: mCherry to detect successful pull down of the bait (Affimer); CHC to detect an interaction with the target protein; TACC3 to observe the TACC3–clathrin interaction. Input represents 30 µg of HeLa cell lysate. Unbound (UB) represents the unbound sample of protein following 1 h incubation with RFP-trap beads.

Previous studies have demonstrated that the spindle localisation of TACC3 and clathrin is interdependent (Hood et al. 2013; Hubner et al. 2010; Booth et al. 2011; Lin et al. 2010). Therefore, we rationalised that perturbing this interaction via the expression of an Affimer should result in the mislocalisation of both proteins during mitosis. To test this, four mCherry-Affimers (D2, D5, C4 and C8) found to bind CHC in HeLa cells, along with Affimer D3 that was determined unable to bind CHC (Fig. 3.2), were expressed in CRISPR CLTA-FKBP-GFP HeLa cells and prepared for immunofluorescence (IF) using an antibody to label endogenous TACC3. As a positive control, cells were treated with the Aurora A inhibitor MLN8237 (0.3 µM) 40 minutes prior to fixation, to inhibit TACC3 and clathrin spindle localisation as described previously (Booth et al. 2011; Hood et al. 2013). The spindle localisation of clathrin and TACC3 in cells fixed at metaphase was observed by confocal microscopy. As expected, cells treated with MLN8237 displayed clear mislocalisation of TACC3 and clathrin, whereas untreated control cells displayed spindles decorated with clathrin and TACC3 (Fig. 3.3 A). Disappointingly, in cells expressing mCherry-tagged Affimers, no effect on TACC3 or clathrin spindle localisation was observed.

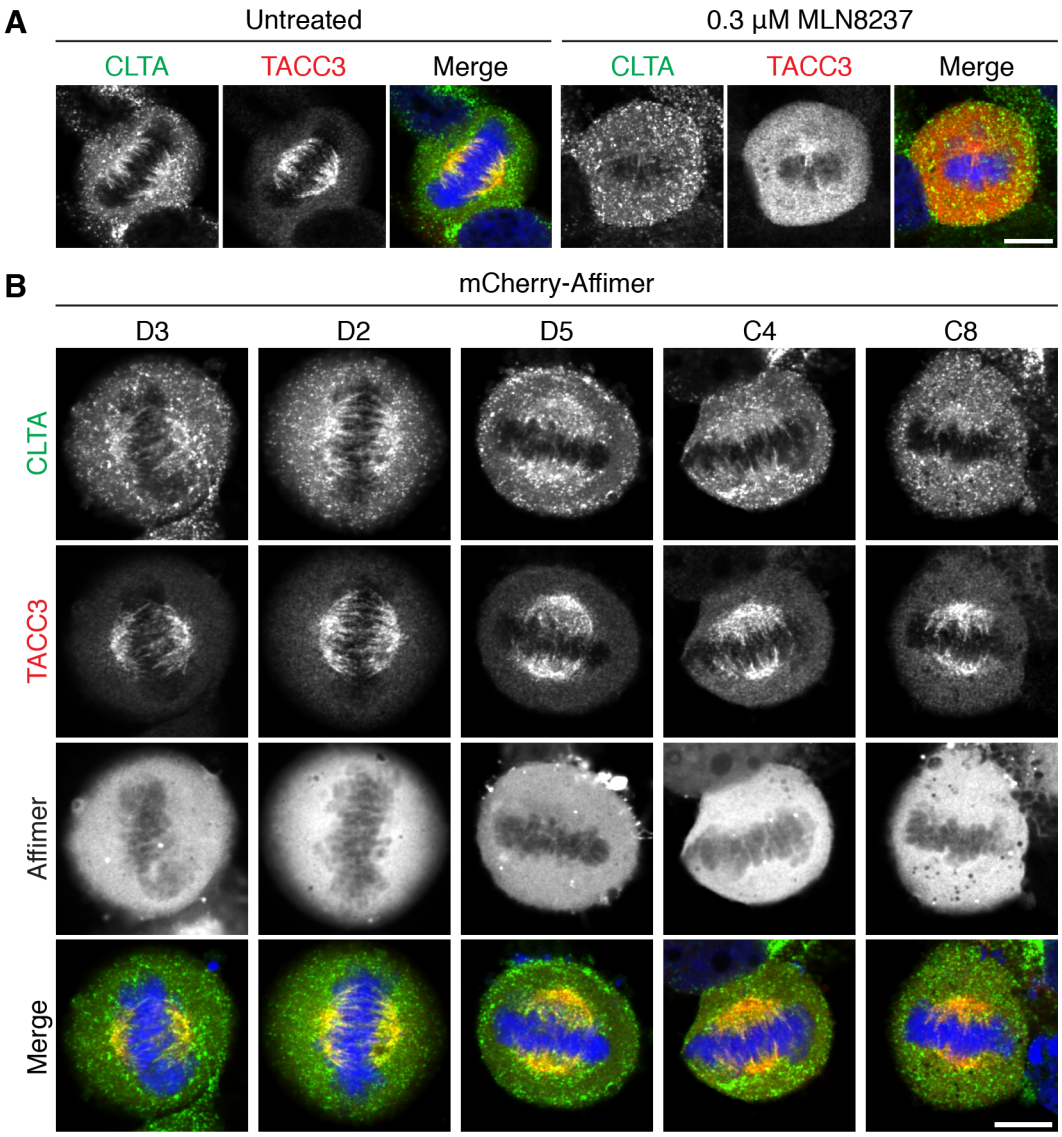

Figure 3.3. Clathrin Affimers do not affect the spindle localisation of clathrin or TACC3 in HeLa cells. Representative confocal micrographs of untransfected CLTA-FKBP-GFP HeLa cells (**A**), or cells expressing mCherry-tagged Affimers (**B**) at metaphase to observe the spindle localisation of clathrin and TACC3. Aurora A kinase was inhibited with MLN8237 (0.3 µM, 40 min) in untransfected cells (as indicated in panel A) as a positive control. Cells were stained for TACC3 (red) and DNA (blue). A GFP-boost antibody was used to enhance the signal of CLTA-FKBP-GFP (green). Scale bar = 10 µm.

Independent of its role in mitosis, clathrin is required for the trafficking of endocytic vesicles during interphase (Pearse 1976). Although the Affimers were raised against the ankle domain of CHC (aa 358-574) with the aim of blocking an interaction with the CID of TACC3, this region also interacts with the β2 subunit of AP-2 to mediate the formation of clathrin-coated endocytic vesicles (Hood et al. 2013; Edeling et al. 2006). Therefore, it is possible that the Affimer may affect the endocytic function of clathrin. To test this, a transferrin-uptake experiment, a gold standard for measuring clathrin-mediated endocytosis, was performed. Four mCherry-Affimers found to bind CHC via the pull-down assay

(D2, D5, C4 and C8), and an Affimer unable to bind CHC (D3), were expressed in HeLa cells. To visualise transferrin, cells were serum starved and incubated in media containing Alexa Fluor 647-conjugated transferrin before being fixed in PFA (see 2.3.6 for details). As a positive control, cells were treated with 0.45 M sucrose prior to fixing to inhibit transferrin uptake. Untransfected cells were included as a further control. Transferrin uptake in control interphase cells and those expressing the indicated mCherry-Affimers was visualised by confocal microscopy. As expected, transferrin uptake was severely inhibited in sucrose treated cells compared to untreated cells (Fig. 3.4 A). Conversely, transferrin uptake was unaffected in cells expressing mCherry-Affimers (Fig. 3.4 B). To confirm this, an automated method in Fiji (see 2.3.6 for details) was used to count the number of transferrin puncta per cell and the results were plotted (Fig. 3.4 C). An ANOVA test to compare the mean puncta between each group was performed. Using the untransfected and untreated cells as the reference group, the results from Tukey's post hoc analysis revealed a significant reduction in transferrin uptake in sucrose treated cells ($p < 0.001$) and no significant effect in Affimer expressing cells ($p > 0.05$).

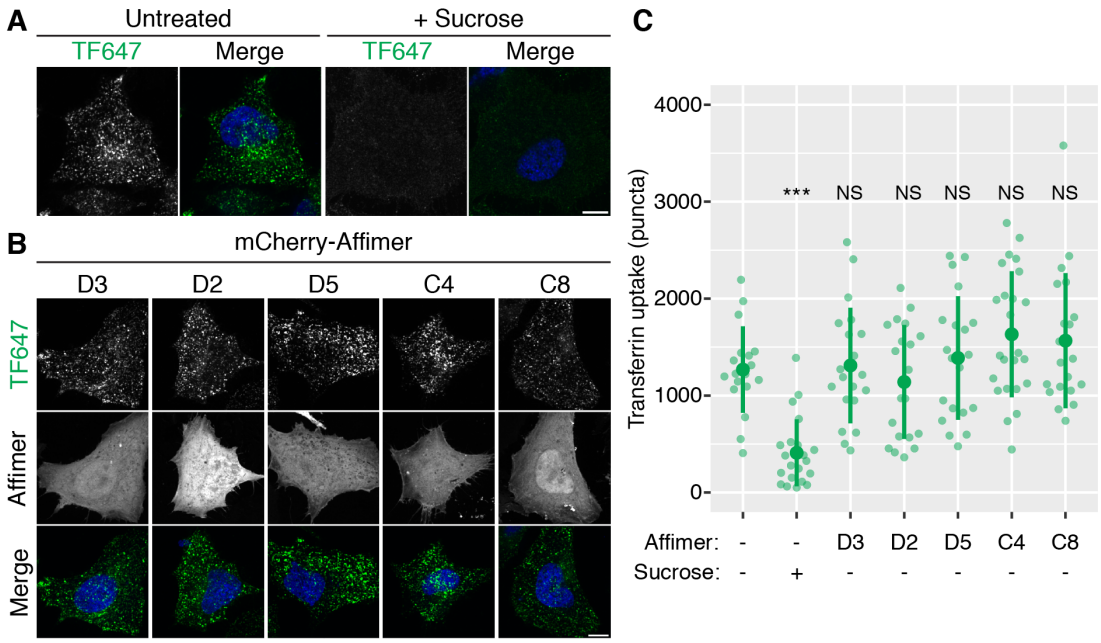

Figure 3.4. Clathrin Affimers do not interfere with clathrin-mediated endocytosis. (**A**) Representative confocal micrographs of untransfected HeLa cells and (**B**) cells transfected with mCherry-Affimers (colour not shown on merge) treated with transferrin-Alexa Fluor 647 (TF647, green in merge). Untransfected cells treated with 0.45 M sucrose (as indicated) served as a positive control. All images were acquired using the same settings and are displayed using the same minimum and maximum values per channel. Scale bar = 10 µm. (**C**) Dot plot to show quantification of transferrin uptake. Dots represent individual cells from a single experiment, n = 18-24 cells per condition. The large dot represents the mean and the error bars show the mean ± one standard deviation. Analysis of variance (ANOVA) was used to compare the means between each group. The significance from Tukey's post hoc test are shown above each plot, using the untransfected/untreated group for comparison. ***, $p < 0.001$; NS (not significant), $p > 0.05$.

Despite D2, D5, C4 and C8 Affimers displaying an interaction with CHC in HeLa cells via the pull-down assay (Fig. 3.2), this interaction is not sufficient to interfere with the TACC3–clathrin interaction, as demonstrated by the intact spindle localisation of both proteins (Fig. 3.3). Moreover, binding of the Affimers to the ankle domain of CHC does not affect clathrin-mediated endocytosis, as demonstrated by the lack of effect on the uptake of transferrin (Fig. 3.4). Therefore, no further experiments were performed with Affimers targeting clathrin.

3.4 Generating and screening recombinant TACC3 Affimers

Biopanning of the Affimer library was performed by Christian Tiede using the C-terminal TACC domain of TACC3 (aa 629-838 Δ699-765) to identify antigen-specific clones. The subsequent clones were confirmed by phage

enzyme-linked immunosorbent assay (ELISA) and subject to DNA sequencing, where they were grouped into 6 unique sequence families. A representative of each family was recombinantly expressed and purified for *in vitro* screening. Of the 6 Affimers, 2 displayed significant precipitation during the purification procedure and were not taken forward. Therefore, Affimers E4, E7, E8 and E5 were selected for further characterisation.

In contrast to Affimers targeting clathrin, those designed to bind TACC3 were screened using recombinant protein prior to screening experiments in human cells. *In vitro* co-precipitation assays using purified recombinant proteins, confirmed binding of Affimers E4, E7, E8 and E5 to the TACC domain (Fig. 3.5). Upon addition of ch-TOG, formation of a triple complex could only be observed for Affimer E5, indicating that Affimers E4, E7 and E8 bind at a site on the TACC domain that is required for ch-TOG association (Fig. 3.5).

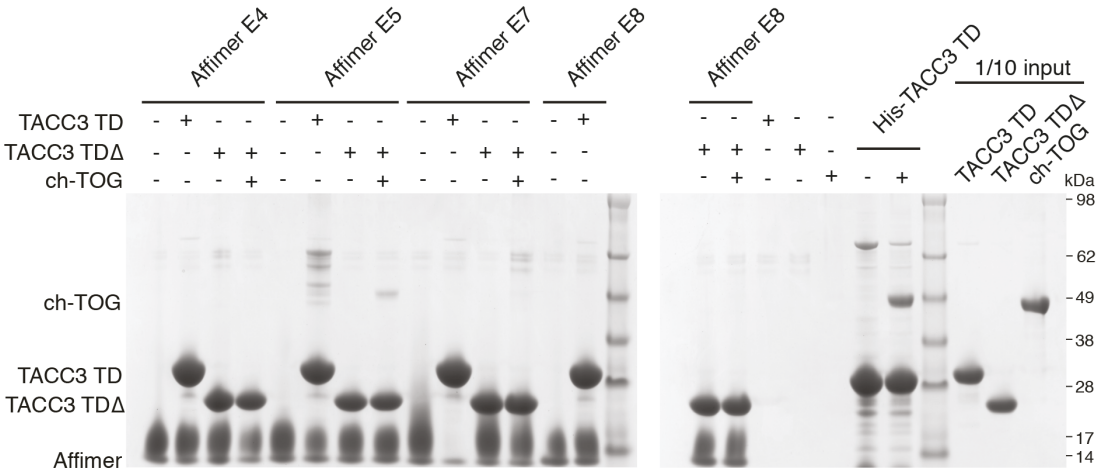

Figure 3.5. *In vitro* co-precipitation assay between TACC3 Affimers, TACC3 and ch-TOG. C-terminal His-tagged Affimers were immobilised on Nickel Sepharose resin and incubated with TACC3 aa 629-838 (TACC3 TD) or TACC3 aa 629-838 Δ699-765 (TACC3 TDΔ). Binding of ch-TOG in the presence of the Affimer was assessed by the addition of ch-TOG (aa 1517-1957) to TACC3 TDΔ reactions. Data and figure provided by Selena Burgess.

To investigate the binding specificity of the Affimers to TACC3, ELISA experiments were performed using immobilised TACC3 (aa 629-838 Δ699-765) and purified Affimer protein. For Affimers E4, E7 and E8, clear binding over the background control reactions where no antigen had been immobilised was observed (Fig. 3.6). In contrast, Affimer E5 displayed high background binding to the plate indicating significant non-specific binding (Fig. 3.6). Taken together, data from the *in vitro* co-precipitation assay and ELISA experiment indicate that Affimers E4, E7 and E8 bind to TACC3 with specificity to block an interaction with ch-TOG and were taken forward for analysis in human cells.

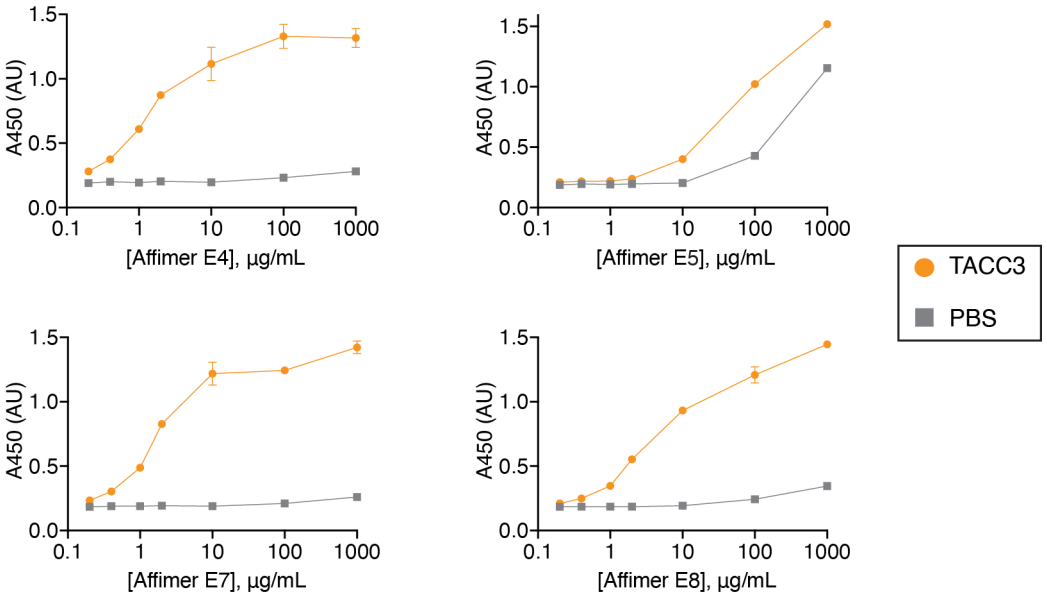

Figure 3.6. Enzyme-linked immunosorbent assay to assess binding between TACC3 Affimers and TACC3. Biotinylated TACC3 (aa 629-838 Δ699-765) was immobilised on Streptavidin coated plates and incubated with an Affimer dilution series (orange circles). Background binding of Affimers to the plate was measured by incubating the proteins in wells coated with PBS (grey squares). Data points are the mean of two experiments. Error bars represent standard error. Data and figure provided by Selena Burgess.

3.5 Screening TACC3 Affimers in HeLa cells

Since recombinantly expressed Affimers bind to the TACC domain of TACC3 and block association with ch-TOG (Fig. 3.5), we sought to investigate whether this is true when fluorescently-tagged Affimers are transiently expressed in human cells. To do this, HeLa cells were transfected with plasmids to express GFP-TACC3 and mCherry-Affimers/free mCherry. Cells expressing free mCherry served as a negative control. Cell lysate was prepared and a commercial GFP-trap system was used to isolate GFP-TACC3 and its binding partners (see 2.2.3 for details). The immunoprecipitates were analysed by Western blot, using antibodies to probe for TACC3, mCherry (Affimer) and ch-TOG. Three independent experiments were performed and the mean intensities of the mCherry and ch-TOG bands in each of the Affimer lanes were measured and normalised to the mCherry control value (see 2.2.2 for details). The Western blot shows a striking band at the predicted molecular weight of mCherry-E8 in the immunoprecipitate (Fig. 3.7 A), and corresponds to an almost complete loss of ch-TOG from this complex relative to the control (Fig. 3.7 B). In comparison, a weak interaction between TACC3 and the Affimers E4 and E7 was observed. In the case of E4, the intensity of ch-TOG is slightly increased with respect to the control and for E7, there is a minor reduction in ch-TOG intensity (Fig. 3.7 B). Together, this data suggest

that in HeLa cells, Affimer E8 binds to TACC3 and inhibits an interaction with ch-TOG, whilst a smaller effect is observed with E7 and no effect is detected with E4, relative to the mCherry control.

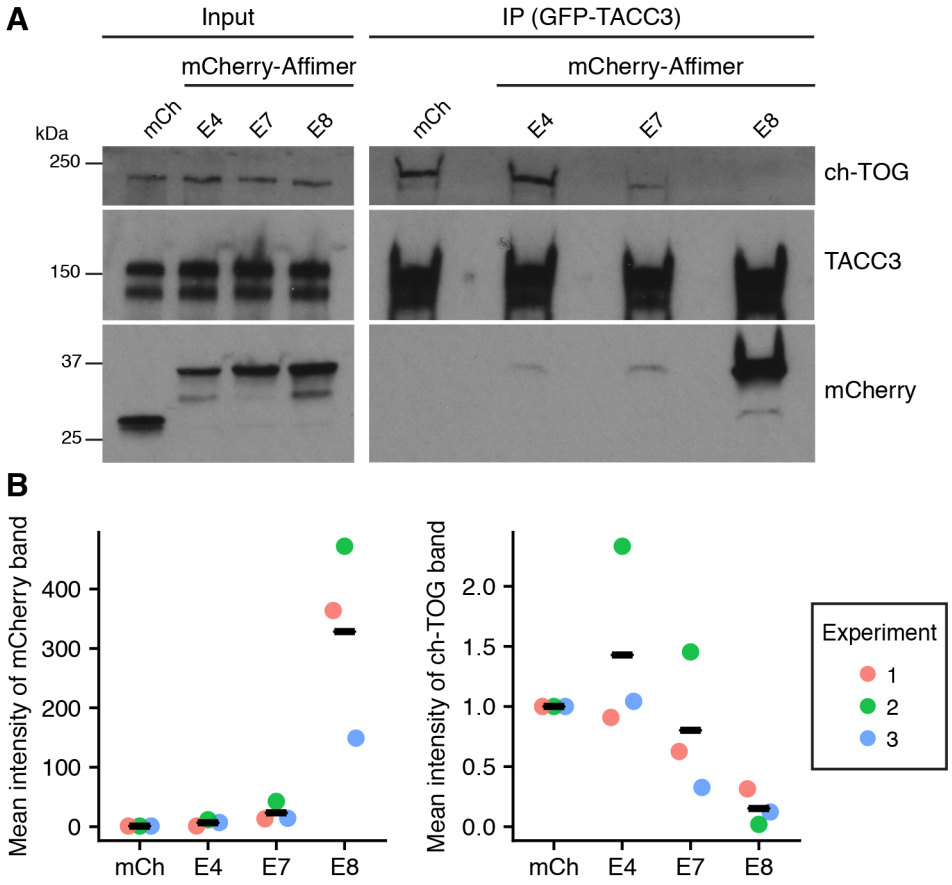

Figure 3.7. Pull down of GFP-TACC3 in HeLa cells to screen TACC3 Affimers. **(A)** Pull-down assay using asynchronous HeLa cell extract overexpressing GFP-TACC3 and the indicated mCherry-Affimers. HeLa cells expressing GFP-TACC3 and free mCherry was included as a negative control. The GFP-trap system was used to isolate GFP-TACC3 using 1.5 mg of HeLa cell lysate. The resulting immunoprecipitate (IP) was analysed by Western blot, using antibodies to probe for TACC3, mCherry and ch-TOG. Input represents 50 µg of HeLa cell lysate. A representative blot from three independent experiments is shown. **(B)** Quantification of the mCherry and ch-TOG bands from three independent pull-down assays. Each dot represents the mean intensity of the indicated protein band normalised to the mCherry condition, coloured by experiment. The crossbar represents the mean from three experiments.

3.6 Localisation of TACC3 Affimers in HeLa cells

We sought to visualise the localisation of mCherry-Affimers in cells to determine whether they can be used as imaging tools, as has been reported for Affimers targeting actin (Lopata et al. 2018). To do this, parental HeLa cells or CRISPR GFP-FKBP-TACC3 HeLa cells expressing mCherry-Affimers were processed for

IF. To investigate whether the method of fixation may affect the localisation of the Affimers, cells fixed with PTEMF or ice-cold methanol were compared. To assess colocalisation of the Affimer with TACC3, endogenous TACC3 was visualised by antibody staining in parental HeLa cells, whilst endogenous TACC3 was visualised by virtue of the GFP-FKBP tag in the CRISPR knock-in cell line. Visualisation of fixed cells at metaphase by confocal microscopy revealed that in all cases, the Affimers were localised throughout the cell and were not enriched on the spindle like TACC3 (Fig. 3.8). Moreover, the imaging revealed no significant difference in the localisation of the Affimers in PTEMF and methanol fixed cells (Fig. 3.8). This experiment demonstrates that using the conditions tested here, Affimers targeting TACC3 are not suitable for use as imaging tools to study the intracellular localisation of TACC3.

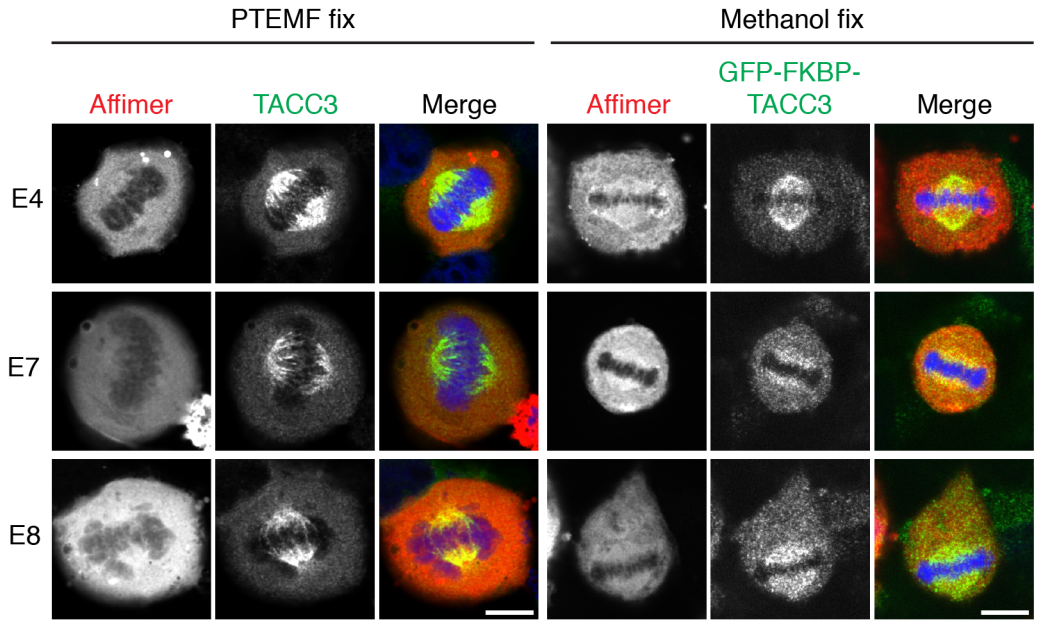

Figure 3.8. Localisation of mCherry-TACC3 Affimers in fixed HeLa cells. Representative confocal micrographs of metaphase parental HeLa cells (left) and CRISPR GFP-FKBP-TACC3 HeLa cells (right) expressing the indicated mCherry-Affimers (red). Cells were fixed with PTEMF or ice-cold methanol, as indicated. Where parental HeLa cells were used, an antibody to stain endogenous TACC3 (green) was used. To enhance the fluorescence of TACC3 in the CRISPR cells (green), a GFP-boost antibody was used. DNA (blue) is shown in the merge. Scale bar = 10 µm.

Next, we wanted to determine if the Affimers could be used to inducibly relocalise endogenous TACC3 by the KS method. This method was originally developed by Margaret Robinson to rapidly inactivate proteins (Robinson et al. 2010), but has been used in the lab to study protein-protein interactions at the mitotic spindle (Ryan et al. 2021; Cheeseman et al. 2013). Here, FKBP-GFP-tagged Affimers were expressed in HeLa cells and rerouted to the mitochondria upon the addition of rapamycin (200 nM, 30 min) prior to fixation (see 2.3.7 for details). Cells

were stained for tubulin to visualise the mitotic spindle, and TACC3 to visualise any change in localisation following Affimer rerouting by KS. Confocal images of mitotic cells from untreated and rapamycin treated samples were acquired and analysed to quantify the spindle localisation of the Affimer and TACC3. In cells treated with rapamycin, Affimers were successfully rerouted to the mitochondria (Fig. 3.9 A). The localisation of TACC3 and tubulin appeared unaffected in rerouted cells compared with the untreated cells, with both proteins decorating the mitotic spindle as expected (Fig. 3.9 A). To quantify this observation, the spindle localisation of Affimer and TACC3 was measured, using tubulin as a reference for the spindle (see 2.3.7 for details). As expected, the analysis revealed a reduction in spindle localisation of the Affimer (x-axis) in cells treated with rapamycin (turquoise dots) compared with the untreated control cells (red dots). In comparison, no shift in TACC3 spindle localisation (y-axis) was observed (Fig. 3.9 B). In conclusion, rerouting TACC3 Affimers by KS does not affect the localisation of TACC3, thus they cannot be used as a method for inducible relocalisation.

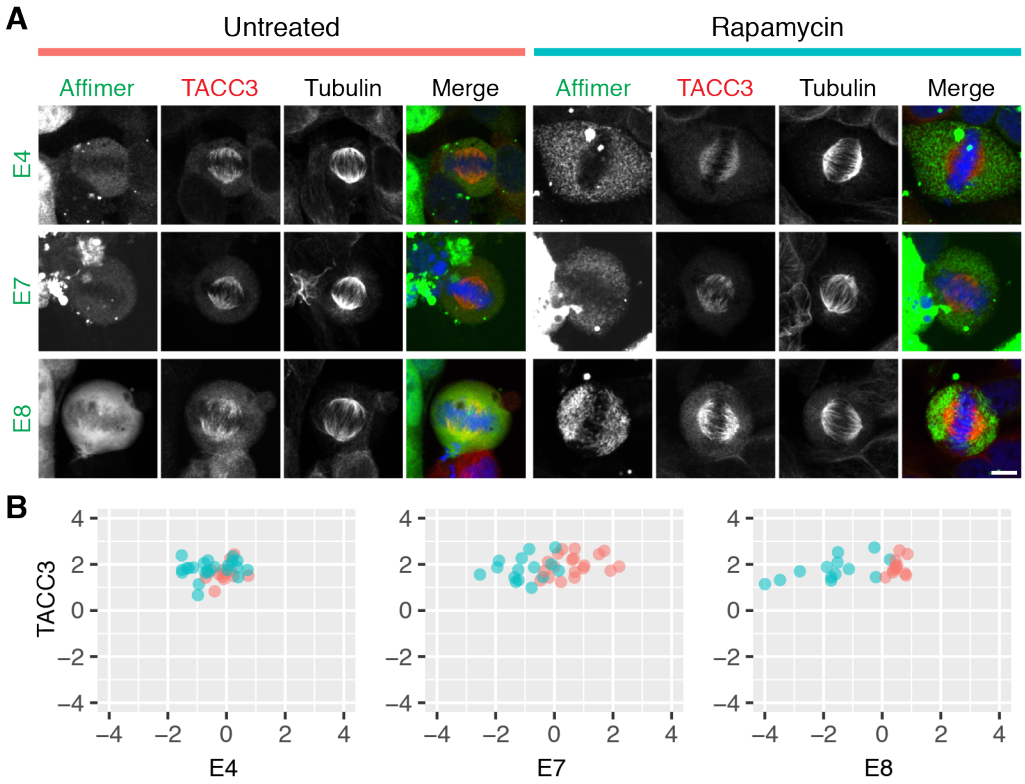

Figure 3.9. Induced rerouting of TACC3 Affimers by knocksideways. (**A**) Representative confocal micrographs of HeLa cells at metaphase expressing the indicated FKBP-GFP-Affimers (green) that were either untreated or treated with rapamycin (200 nM, 30 min) prior to fixation. Cells were stained for tubulin (not shown in merge) and TACC3 (red). DNA (blue) is shown in the merge. Scale bar = 10 µm. (**B**) Quantification of Affimer (x-axis) and TACC3 (y-axis) spindle localisation in untreated cells (red) and rapamycin treated cells (turquoise). Spindle localisation was calculated as the ratio of spindle to cytoplasmic fluorescence shown on a $\log_2$ scale. A value of 1 indicates twice the amount of fluorescence at the spindle compared to the cytoplasm. A value of −1 indicates half the amount of fluorescence at the spindle versus the cytoplasm. Dots represent single cells from one experiment, n = 11-22 cells per condition.

3.7 Chapter summary

The primary goal of the work described in this chapter was to generate and screen novel Affimer binding proteins, to dissect the TACC3–ch-TOG–clathrin–GTSE1 complex in human cells and potentially develop anti-cancer therapeutic strategies. Since TACC3 and clathrin are thought to be the core components of this complex (Ryan et al. 2021), with their interaction required to form the MT binding surface (Hood et al. 2013), we generated Affimers to target clathrin and block the interaction with TACC3. Despite identifying several Affimers that bind CHC in cells, we observed no effect on the mitotic spindle localisation of clathrin or TACC3, as would be expected if this interaction was abolished. Furthermore, no phenotype was observed in a transferrin-uptake experiment that aimed to assay clathrin-mediated endocytosis.

It is possible that the Affimers identified to bind CHC, may not bind at the exact site required for the TACC3 interaction, or at an affinity strong enough to abolish an interaction with TACC3. Developing a TACC3–clathrin inhibitor to disrupt mitotic spindle stability offers a therapeutic approach to target proliferating cells in an anti-cancer context. However, specifically targeting the mitotic function of clathrin without altering its endocytic role may be challenging, especially considering that TACC3 and auxilin are thought to bind in close proximity (Burgess et al. 2018). For this reason, targeting the CID of TACC3 may provide a better alternative in developing a mitosis-specific inhibitor.

To dissect the TACC3–ch-TOG interaction, Affimers were raised against the C-terminal TACC domain of TACC3 (aa 629-838 Δ699-765), which has previously been mapped to interact with ch-TOG (Hood et al. 2013). *In vitro* screening of purified Affimers with recombinant fragments of TACC3 and ch-TOG, revealed three candidates for screening experiments in human cells. Of these, Affimers E7 and E8 were identified to bind TACC3 and reduce the interaction with ch-TOG via a pull-down experiment using HeLa cell lysate.

When viewed by IF, the TACC3 Affimers displayed some spindle localisation but high background signal was also detected in the cytoplasm. The high background signal is likely attributed to overexpression of the Affimer in a cell containing endogenous levels of TACC3. This is supported by the observation that Affimers tagged with mCherry at the N-terminus colocalised with TACC3 at the mitotic spindle in HeLa cells when GFP-TACC3 was overexpressed. The reason why Affimer E4 appeared to colocalise with GFP-TACC3 at the mitotic spindle in these cells, despite only a weak band for mCherry-E4 present in the immunoprecipitate of TACC3, is unclear. One possibility is that even weakly associated protein can be loaded onto the spindle when TACC3 is overexpressed. For example, an increased spindle localisation of the complex members clathrin, GTSE1 and ch-TOG has been observed in HeLa cells overexpressing mCherry-TACC3 (Ryan et al. 2021). Of note, Affimers tagged at the C-terminus failed to colocalise with GFP-TACC3, suggesting that the orientation of the fluorescent tag is important. Methods to optimise the labelling of endogenous TACC3 or clathrin using Affimers could be carried out in the future. For example, purified Affimers could be used to label fixed cells, as has been described previously with Affimers to label actin (Lopata et al. 2018). Furthermore, a control Affimer that cannot bind to the target protein in cells but maintains the scaffold structure should be sought for future experiments.

Similarly, KS of the FKBP-GFP-Affimers failed to remove TACC3 from the mitotic spindle. In this experiment, the Affimer was successfully rerouted to

the mitochondria, however, TACC3 remained localised at the spindle. Moreover, Affimer on the mitochondria was not sufficient to detectably mislocalise TACC3. One explanation for the lack of removal is that TACC3 is bound too tightly to the spindle. However, we have seen that relocalisation of endogenous clathrin causes the removal of TACC3 from the spindle (Ryan et al. 2021). Furthermore, FRAP experiments have showed that TACC3 exchange with the cytoplasm is quick (Nixon et al. 2015), suggesting that high affinity to the spindle is an unlikely reason for a lack of rerouting seen with the Affimer. A more likely reason is that the affinity of the Affimer towards TACC3 is too weak to cause rerouting. To overcome this, future work should aim to identify higher affinity binding reagents through consecutive biopanning rounds. Moreover, determining the kinetics of binding between Affimers and TACC3 using surface plasmon resonance (SPR) may help in isolating high affinity Affimers (Shamsuddin et al. 2021), ideally with affinities in the nM range as has been reported previously (Tiede et al. 2017). Taken together, the Affimers described here are not suitable to study the intracellular localisation of endogenous TACC3, or to inducibly relocalise it to different locations within the cell. In the next chapter, the TACC3 Affimers will be used as a tool to inhibit the TACC3–ch-TOG interaction and investigate its biological function in human cells.

Chapter 4

Investigating the function of TACC3–ch-TOG in human cells

4.1 Background

Understanding the function of TACC3–ch-TOG has been a topic of research for over 20 years, driven in part by their association with human cancers (Gergely et al. 2003; Still et al. 1999b; Charrasse et al. 1995). During mitosis, TACC3 and ch-TOG are part of a multiprotein complex with clathrin and GTSE1 (TACC3–ch-TOG–clathrin–GTSE1), that functions to crosslink MTs within the K-fibres of the mitotic spindle to ensure stability during cell division (Booth et al. 2011; Hood et al. 2013). Independent of the complex, TACC3 and ch-TOG have been proposed to interact at the growing ends of MTs in human cells during interphase and mitosis (Gutierrez-Caballero et al. 2015). Despite this, the precise role of TACC3–ch-TOG in this context is unclear and there are conflicting reports regarding their role in regulating MT plus-end dynamics in human cells (Gutierrez-Caballero et al. 2015; Furey et al. 2020; Nwagbara et al. 2014). Early work carried out in *Drosophila* investigating D-TACC and Msps, homologues of TACC3 and ch-TOG, identified D-TACC to be important in localising Msps to mitotic centrosomes to stabilise centrosomal MTs (Lee et al. 2001; Cullen and Ohkura 2001). In HeLa cells, TACC3 is localised in a diffuse region around the centrosome and its depletion does not affect the centrosomal localisation of ch-TOG (Booth et al. 2011; Gergely et al. 2003; Lin et al. 2010), suggesting that this function of TACC3–ch-TOG is different in human cells. Despite this, a model to describe the role of TACC3–ch-TOG at the centrosome in human cells is lacking.

To date, studies investigating the roles of these proteins have relied on

RNAi-mediated depletion and/or overexpression of mutant proteins, both of which have limitations. For example, ch-TOG has an established role in bipolar spindle formation and its depletion by siRNA results in cells containing highly disorganised multipolar spindles (Gergely et al. 2003), making it difficult to distinguish the role of ch-TOG in spindle assembly versus its function during later stages of mitosis. Moreover, overexpression of TACC3 can result in the formation of aggregates (Gergely et al. 2000a). Technologies that modulate expression levels of proteins of interest are useful tools, however, they do not provide conclusive information regarding the relationship between proteins and an observed phenotype. For this, tools that can block specific protein-protein interactions in living cells without perturbing the expression levels of target proteins are needed. In the previous chapter, Affimers designed to bind TACC3 and inhibit its interaction with ch-TOG, were screened in HeLa cells. This work identified two Affimers, E7 and E8, that could be used to investigate the role of TACC3–ch-TOG at different subcellular locations in HeLa cells.

4.2 Dissecting TACC3–ch-TOG microtubule plus-end activity

A role for TACC3–ch-TOG in regulating MT plus-end dynamics was previously identified in embryonic cell types of the *Xenopus* system, where manipulation of TACC3 levels was found to affect MT dynamics and axon outgrowth (Erdogan et al. 2017; Nwagbara et al. 2014). Similar experiments performed in human cells uncovered that TACC3 +TIP behaviour depends on an interaction with ch-TOG, though no major role in regulating MT plus-end dynamics was identified (Gutierrez-Caballero et al. 2015). Since these studies relied on the use of methods to modulate levels of TACC3 expression, we sought to use the TACC3 Affimers identified in the previous chapter, to selectively disrupt TACC3–ch-TOG in human cells and decipher the dependency on one another in regulating MT plus-end dynamics.

4.2.1 Effect of TACC3 Affimers on the microtubule plus-end dynamics during interphase

To measure MT plus-end dynamics, HeLa cells co-expressing NeonGreen-EB3, a marker for growing MT ends, and mCherry-tagged Affimers, were imaged live. As a negative control, cells expressing an Affimer targeting clathrin (Fig. 3.2) were included to ensure that any effect on MT dynamics was specific to disruption

of the TACC3–ch-TOG interaction, and not a consequence of expressing an alien protein in the cell. Interphase cells were imaged in a single z plane for 2 min at 2 s intervals using a widefield microscope. Parameters of MT dynamics were quantified using automated particle tracking analysis (see 2.3.8 for details). Quantification revealed no change in the mean speed, lifetime or length of growing MT tracks outlined by NeonGreen-EB3 comets in cells expressing any of the Affimers when compared with untransfected cells (Fig. 4.1).

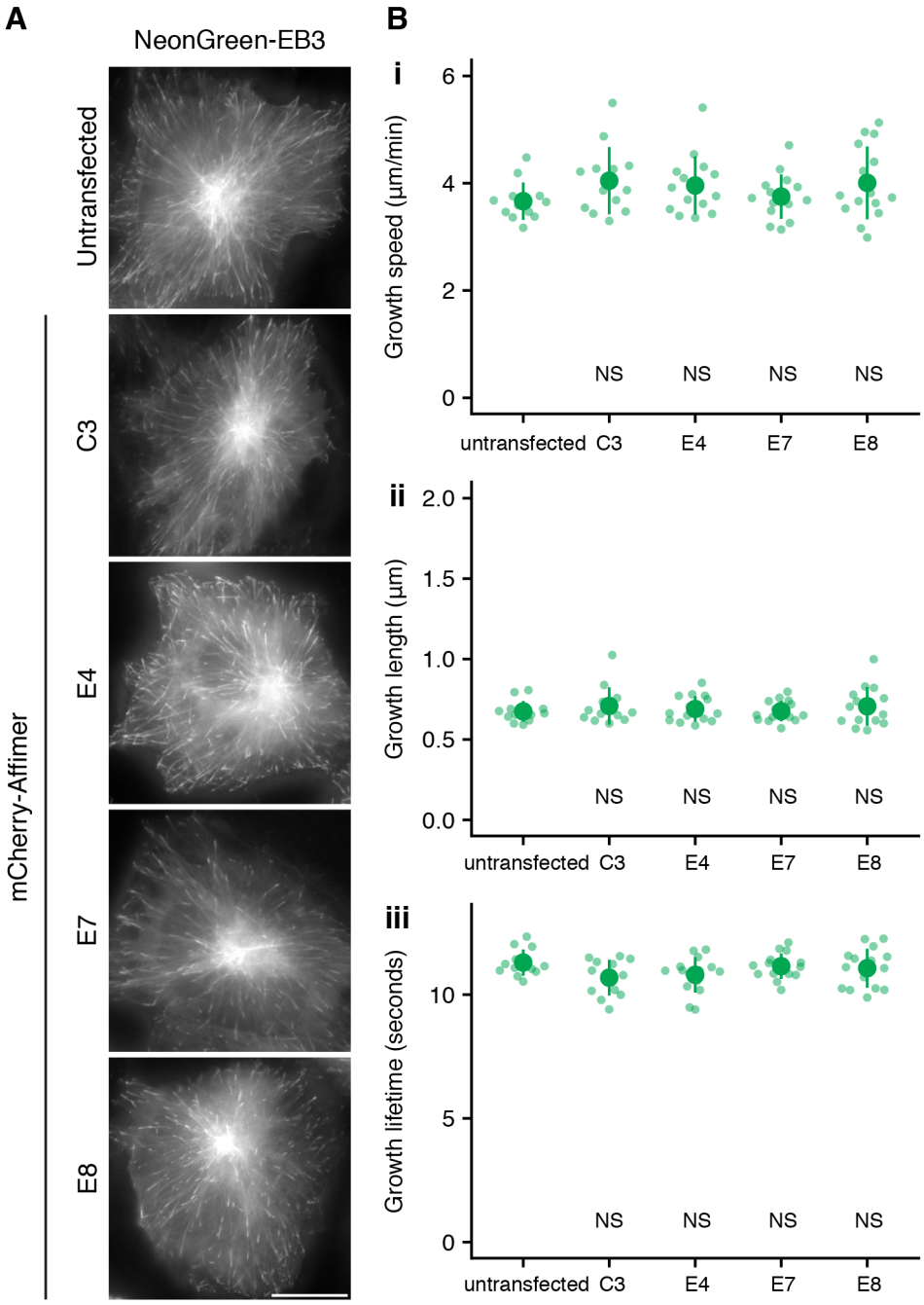

Figure 4.1. TACC3 Affimers do not detectably influence microtubule plus-end dynamics in HeLa cells. (**A**) Representative stills from movies of NeonGreen-EB3 comets in untransfected HeLa cells and cells expressing the indicated mCherry-tagged Affimers. An Affimer targeting clathrin (C3) was included as a negative control. Scale bar = 10 µm. (**B**) Dot plots to show the mean speed (**i**), length (**ii**) and lifetime (**iii**) of growing microtubule tracks, determined by the automated tracking of NeonGreen-EB3 comets in interphase HeLa cells. Each dot represents the mean value for a single cell, n = 13-15 cells per condition over 2 separate experiments. The large dot represents the mean and the error bars show the mean ± one standard deviation. A Kruskal-Wallis test was used to compare the means between each group. The significance from Dunn's post hoc test is shown above each group, using the untransfected group for comparison. NS (not significant), $p > 0.05$.

To ensure that a change to the dynamics of MT plus-ends could be detected using this assay, we sought to include a positive control. As ch-TOG is a MT

polymerase that catalyses the addition of tubulin to the growing plus-end of MTs (Brouhard et al. 2008), we hypothesised that depletion of ch-TOG should result in a measurable change to MT growth dynamics. To test this, HeLa cells were treated with siRNA to deplete ch-TOG and imaged alongside control GL2 treated cells. Disappointingly, only a minor decease in growth parameters was observed in cells depleted of ch-TOG compared to control-treated cells (Fig. 4.2 B). However, it should be noted that the level of ch-TOG knockdown was incomplete (Fig. 4.2 C), and attempts to increase knockdown efficiency resulted in cell death.

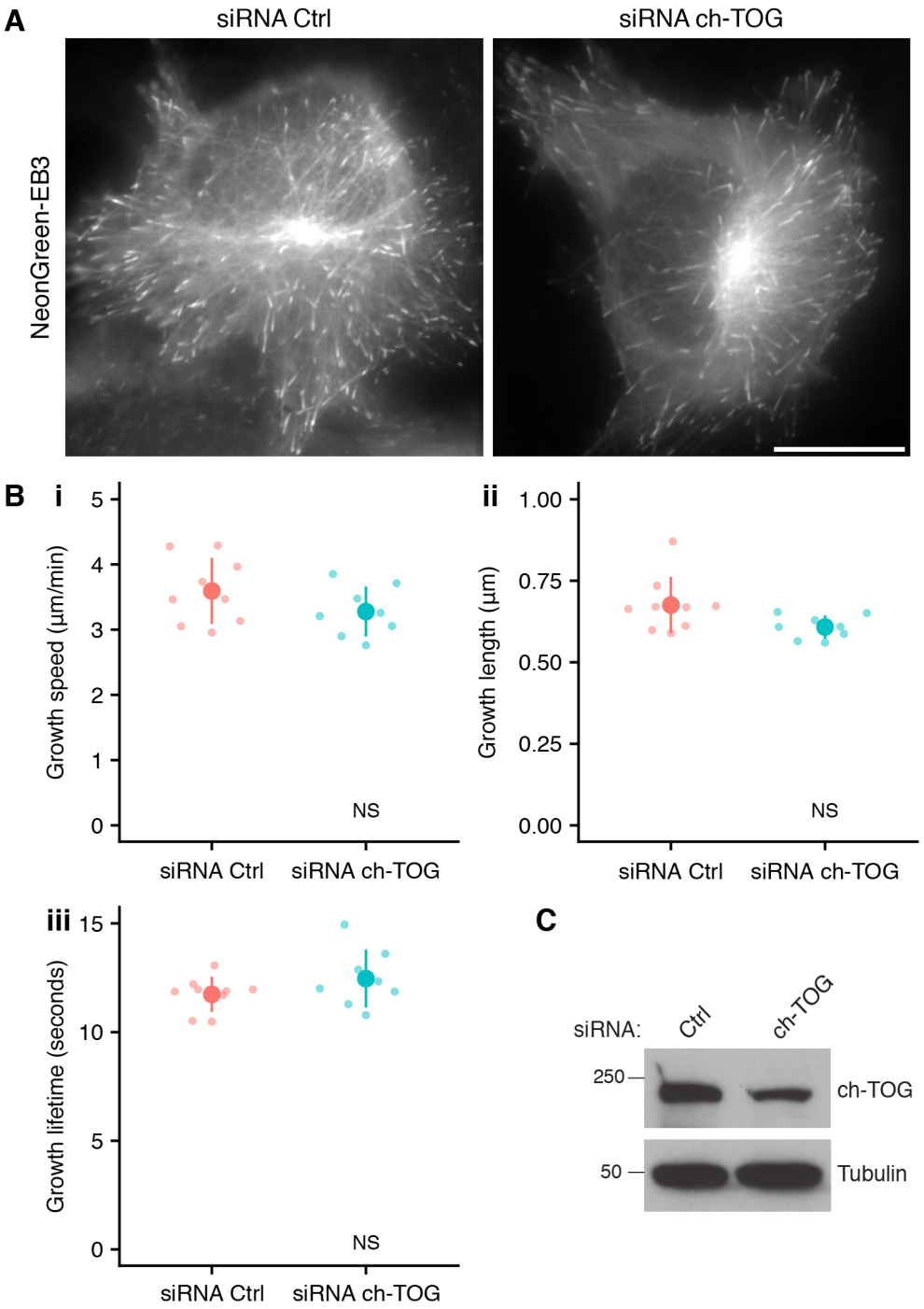

Figure 4.2. Measuring the effect of ch-TOG depletion on microtubule plus-end dynamics in HeLa cells. (**A**) Representative stills from videos of NeonGreen-EB3 comets in HeLa cells treated with control siRNA (Ctrl) or siRNA targeting ch-TOG. Scale bar = 10 µm. (**B**) Dot plots to show the mean speed (**i**), length (**ii**) and lifetime (**iii**) of growing microtubule tracks, determined by the automated tracking of NeonGreen-EB3 comets in interphase HeLa cells. Each dot represents the mean value for a single cell, $n = 9$ cells per condition imaged in a single experiment. The large dot represents the mean and the error bars show the mean ± one standard deviation. An independent two-samples t-test was used to compare the means. The significance is shown on each plot, using the Ctrl group as the reference. NS (not significant), $p > 0.05$. (**C**) Western blot to show the depletion of ch-TOG following siRNA treatment of HeLa cells used for imaging. Tubulin was used as a loading control.

Although best efforts were made to image cells expressing similar levels of EB3, it is possible that high expression levels of EB proteins may alter MT polymerisation rates (Herman et al. 2020). A further possibility is that the mCherry tag may impede the ability of the Affimer to bind TACC3 when expressed in cells. This is plausible since the molecular weight of mCherry is approximately 27 kDa, compared to approximately 12 kDa for the Affimer. To test this, the sequence for each Affimer was cloned into a bicistronic vector containing an internal ribosome entry site (IRES) to enable expression of the Affimer, and free GFP as a marker for expression. To circumvent a potential difference in EB3 expression, RPE1 cells stably expressing EB3-tdTomato were transfected with plasmids to express GFP-Affimers or the untagged versions. In an attempt to capture the dynamics of MT plus-ends in more detail, cells were imaged for 1 min at 1 s intervals. In accordance with experiments performed in HeLa cells, no significant change in any of the MT growth parameters was observed in cells expressing E4 or E7 Affimers compared with untransfected cells (Fig. 4.3). A statistically significant decrease in growth speed was observed in cells expressing GFP-E8 compared to untransfected cells, however, this decrease was not significant when compared to the untagged version. This suggests that GFP-E8 may be a better inhibitor of TACC3–ch-TOG than untagged E8, however, this experiment should be repeated to further test the significance of this result.

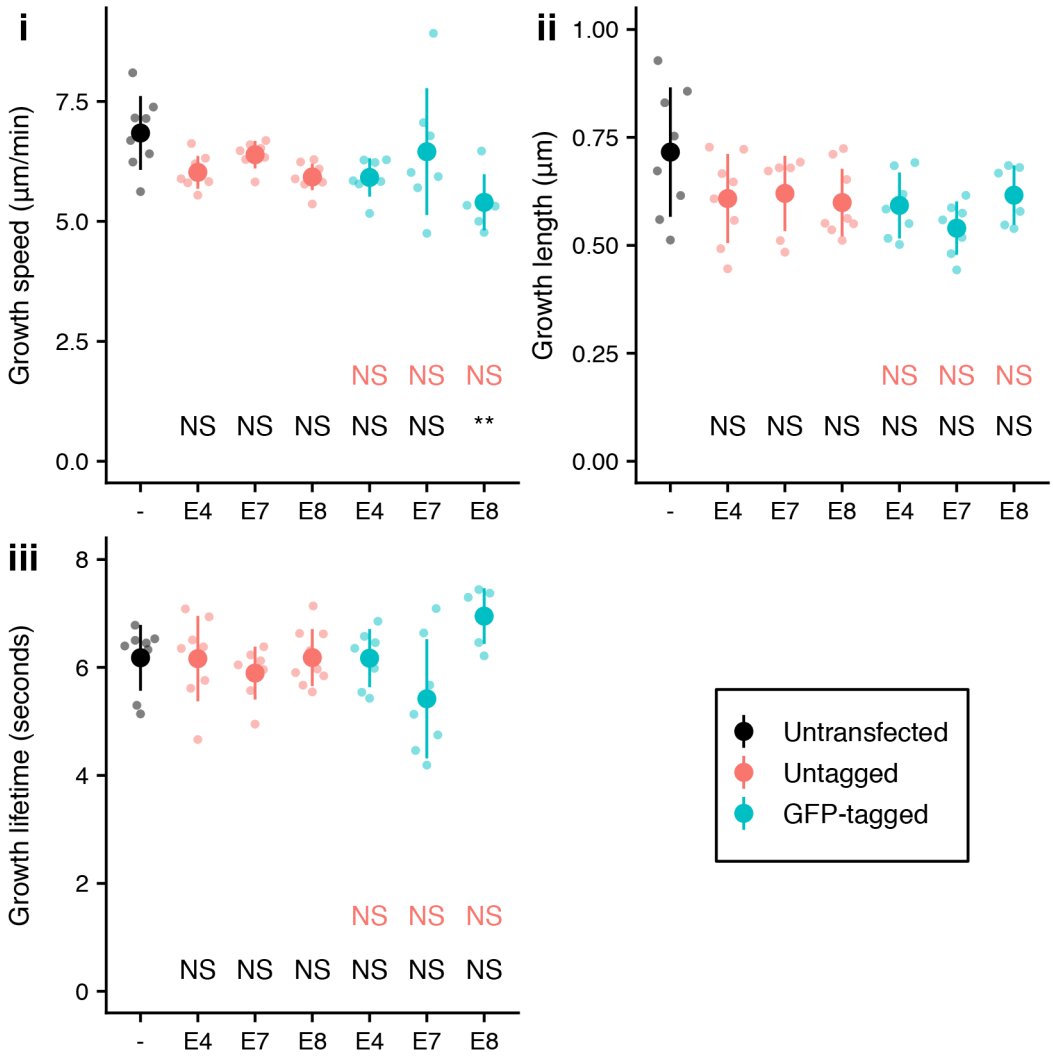

Figure 4.3. TACC3 Affimers do not detectably influence microtubule plus-end dynamics in RPE1 cells. Quantification of microtubule plus-end growth parameters from the automated tracking of EB3 comets in untransfected RPE1 EB3-tdTomato cells (black dots) and cells expressing untagged Affimers (red dots) and GFP-Affimers (turquoise dots), as indicated. Untagged Affimers were expressed using a bicistronic vector to express the Affimer, and free GFP as a marker for expression. Dot plots show the average speed (**i**), length (**ii**) and lifetime (**iii**) of growing microtubule tracks. Each dot represents the mean value for a single cell, n = 6-9 cells per condition imaged in a single experiment. The large dot represents the mean and the error bars show the mean ± one standard deviation. A Kruskal-Wallis test was used to compare the means between each group. The significance from Dunn's post hoc test is shown above each group, using the untransfected group (shown in black) or the respective untagged Affimer (shown in red) for comparison. **, $p < 0.01$; NS (not significant), $p > 0.05$.

4.2.2 Does TACC3 regulate interphase microtubule networks?

A recent study investigating the role of +TIPs during virus infection unexpectedly identified that TACC3 influences MT plus-end dynamics in interphase SK-N-SH cells, a human neuroblastoma cell line predominantly used to model neuronal infection (Furey et al. 2020). Using siRNA to deplete TACC3, the authors

showed that loss of TACC3 leads to a decrease in EB1 comet number and an increase in disorganised networks of stable MTs, as demonstrated by staining detyrosinated MTs. Interestingly, they show that in TACC3-depleted cells, ch-TOG accumulates in the nucleus, suggesting that TACC3 regulates the cytoplasmic localisation of ch-TOG. The authors conclude that an important function of TACC3 is to regulate MT dynamics by modulating the balance of dynamic and stable MTs during interphase.

In light of this study, we wondered if this model was applicable to other human cell lines and if inhibition of TACC3–ch-TOG via expression of the Affimers, would result in a similar phenotype. We first sought to confirm whether the reported phenotypes are observed in HeLa or U2OS cell lines. Following TACC3 depletion using siRNA, cells were fixed with ice-cold methanol and counterstained with antibodies to visualise detyrosinated or acetylated MT networks, EB1 comet number or ch-TOG localisation (Fig.4.4 A, B, C & D). Despite good depletion of TACC3 (Fig. 4.4 E), imaging of interphase cells by confocal microscopy revealed no detectable change in the organisation of the MT network, EB1 comet number or ch-TOG localisation in TACC3-depleted cells compared to control-treated cells. However, the possibility that other siRNA-insensitive isoforms of TACC3 are expressed was not tested.

In line with data from the live EB3 tracking experiments (Fig 4.1 and 4.3), the data from this experiment suggest that in HeLa or U2OS cells, TACC3 does not have a major role in regulating MT plus-end dynamics, or MT lattice stability. A separate study carried out using the *Xenopus* system also found no significant change in detyrosinated MTs in TACC3-depleted growth cones (Erdogan et al. 2017), highlighting potential cell-type specific differences in this function of TACC3.

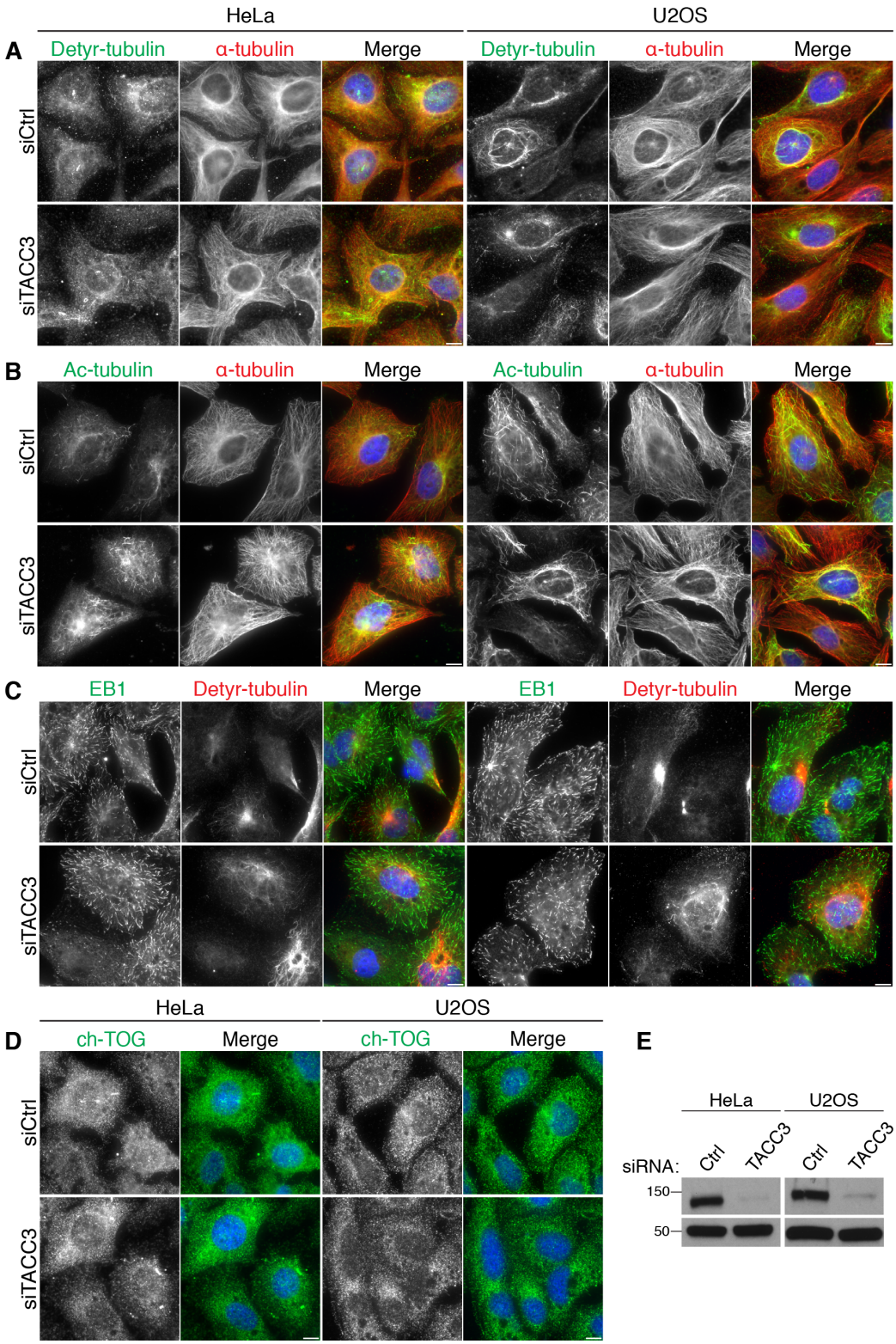

Figure 4.4. TACC3 does not regulate the stability of the microtubule lattice in HeLa or U2OS cells. HeLa and U2OS cells treated with either control siRNA (siCtrl) or siRNA targeting TACC3 (siTACC3) were fixed in ice-cold methanol and stained for detyrosinated tubulin (Detyr, green) and α-tubulin (red) (**A**), acetylated tubulin (Ac, green) and α-tubulin (red) (**B**), EB1 (green) and detyrosinated tubulin (red) (**C**), or ch-TOG (green) (**D**). In all cases DNA was stained using DAPI. Representative confocal micrographs of interphase cells from one experiment are shown. Scale bar = 10 µm. (**E**) Western blot to show the depletion of TACC3 in the indicated cell line following treatment with control or TACC3 siRNA. Tubulin was used as a loading control.

4.2.3 Measuring TACC3 microtubule plus-end localisation during mitosis

Although the experiments described above found no evidence for a functional role of TACC3–ch-TOG in regulating the dynamics of growing MTs, we sought to determine the dependency of these two proteins for their plus-end localisation. Previous work has suggested that TACC3–ch-TOG tracks the growing ends of MTs via an interaction between ch-TOG and the distal end of the growing MT, independently of EB proteins (Gutierrez-Caballero et al. 2015). Since an interaction with ch-TOG is required for TACC3 +TIP activity, we hypothesised that inhibition of TACC3–ch-TOG through expression of the Affimer should result in a reduction of TACC3 at the MT plus-end. To test this, CRISPR GFP-FKBP-TACC3 HeLa cells transfected with free mCherry or mCherry-Affimers, were imaged for 1 min at 1 s intervals by confocal microscopy to observe TACC3 comets tracking the growth of MT plus-ends. To accurately measure the localisation of TACC3 at the MT plus-end, cells in anaphase or telophase were imaged, as TACC3 comets are easier to distinguish during these stages of the cell cycle. The resulting movies were analysed using *ComDet* in Fiji, where each time point was used to quantify the number of comets and the fluorescence intensity of each comet (see 2.3.9 for details). For both parameters, the median value was calculated for each cell and plotted (Fig. 4.5 B). Surprisingly, the number and fluorescence intensity of TACC3 comets at the MT plus-end was comparable between Affimer expressing cells and mCherry control cells. In all cases, TACC3 tracked the growth at MT plus-ends in a comet-like manner, as can be seen by a colour projection of consecutive time frames (Fig. 4.5 A). Therefore, this experiment demonstrates that TACC3 MT plus-end localisation is not detectably altered when the TACC3 Affimers are expressed in cells.

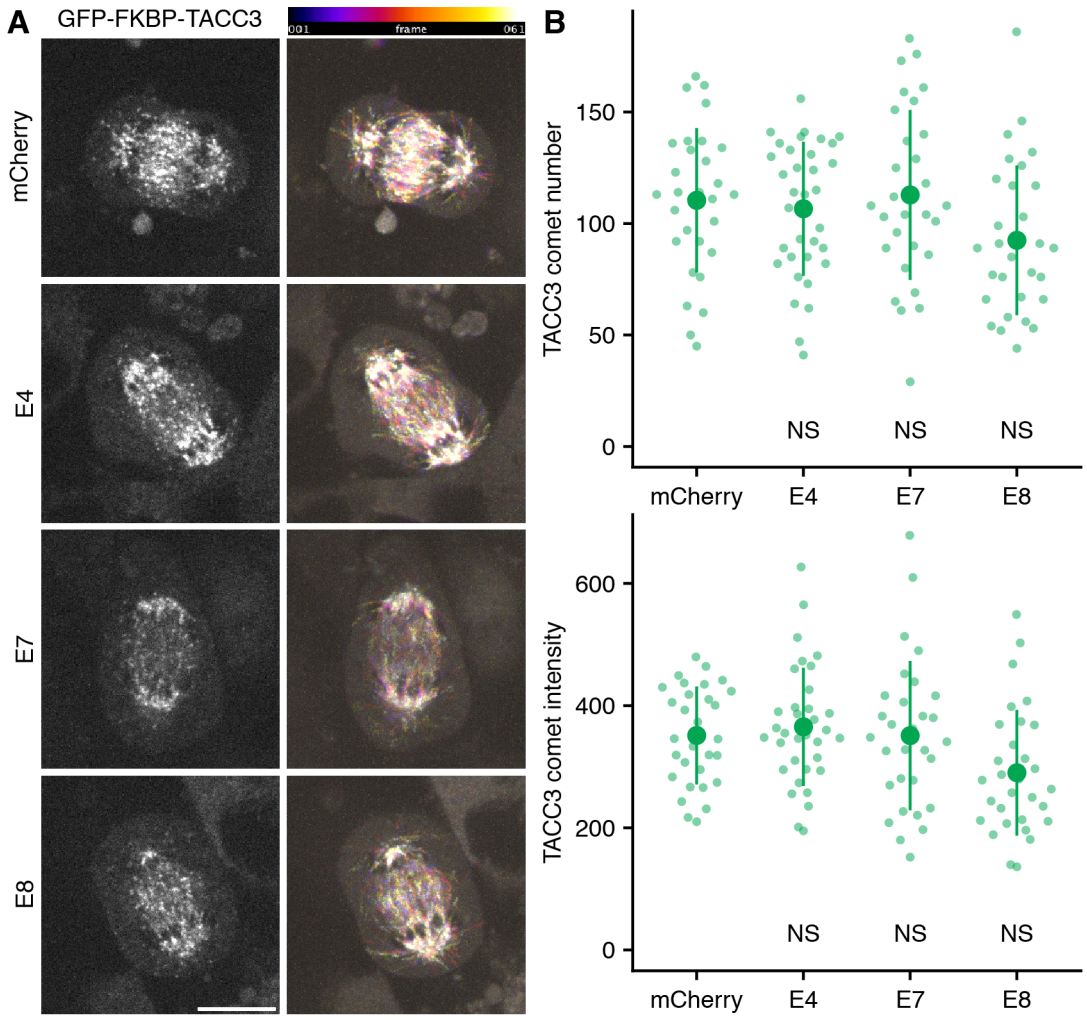

Figure 4.5. TACC3 Affimers do not detectably influence TACC3 microtubule plus-end localisation. (**A**) Representative single frame stills (left) and colour projections (right) from live cell imaging of CRISPR GFP-FKBP-TACC3 HeLa cells expressing free mCherry or mCherry-Affimers (not shown), as indicated. Late anaphase cells were imaged for 1 min at 1 s intervals and the resulting frames were projected using different colours as indicated by the time colour scale bar. Identical brightness and contrast settings were applied to all images shown in the figure. Scale bar = 10 µm. (**B**) Dot plots show the median number of TACC3 comets (top) and the median fluorescence intensity (bottom). Each dot represents a single cell, n = 30-34 cells per condition over 3 independent experiments. The large dot represents the mean and the error bars show the mean ± one standard deviation. Analysis of variance (ANOVA) was used to compare the means between each group. The significance from Tukey's post hoc test are shown above each group, using the mCherry control group for comparison. NS (not significant), $p > 0.05$.

4.2.4 Investigating ch-TOG microtubule plus-end localisation during interphase

To rule out the possibility that TACC3 Affimers may be interfering with ch-TOG MT plus-end localisation, a live cell imaging experiment was carried out to observe ch-TOG comets. To visualise ch-TOG, a plasmid to co-express RNAi-resistant ch-TOG-GFP and a short hairpin RNA to silence the expression

of endogenous ch-TOG, was expressed in HeLa cells along with free mCherry or mCherry-Affimers. Interphase cells were imaged for 1 min at 1 s intervals by confocal microscopy. In all cases, ch-TOG tracked the growth at MT plus-ends in a comet-like manner (Fig. 4.6), suggesting that ch-TOG plus-end localisation is not detectably altered in cells where the TACC3–ch-TOG interaction is disrupted. This is in agreement with a model where ch-TOG can track MT plus-ends independently of its interaction with TACC3 (Gutierrez-Caballero et al. 2015).

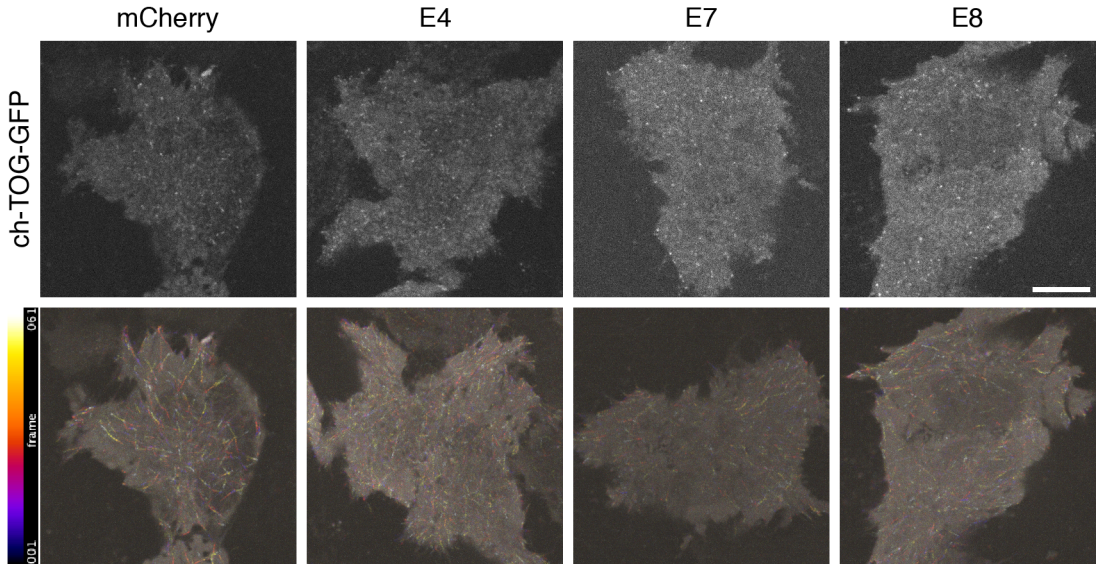

Figure 4.6. TACC3 Affimers do not detectably influence ch-TOG microtubule plus-end localisation. Representative single frame stills (top) and colour projections (bottom) from live cell imaging of ch-TOG depleted HeLa cells in interphase expressing knockdown proof ch-TOG-GFP and free mCherry or mCherry-Affimers (not shown), as indicated. Interphase cells were imaged for 1 min at 1 s intervals and the resulting frames were projected using different colours as indicated by the time colour scale bar. Identical brightness and contrast settings were applied to all images shown in the figure. Scale bar = 10 µm.

In summary, the experiments described in this section aimed to explore the role of TACC3–ch-TOG in regulating MT plus-end growth dynamics, by using Affimers to specifically perturb this interaction. Data from the automated tracking of EB3 comets in HeLa and RPE-1 cells, showed no detectable effect on MT growth parameters (Fig. 4.1 & 4.3), suggesting that the role of TACC3–ch-TOG is minimal in these cell lines using the methods described here. Furthermore, the MT plus-end localisation of TACC3 and ch-TOG was unaffected in cells expressing Affimers. It is possible that the Affimer is unable to outcompete ch-TOG for TACC3 binding at the MT plus-end. Taken together, the experiments indicate that the Affimers developed in this study, are not an appropriate tool to dissect the TACC3–ch-TOG interaction at the MT plus-end.

4.3 Disrupting the TACC3–ch-TOG interaction during mitosis

Independent of their MT plus-end localisation, TACC3 and ch-TOG localise to the mitotic spindle in an Aurora A dependent manner, where they are part of a multiprotein complex with clathrin and GTSE1 (TACC3–ch-TOG–clathrin–GTSE1) (Booth et al. 2011; Ryan et al. 2021). Experiments involving the manipulation of TACC3 protein levels by siRNA-mediated depletion or overexpression of mutant constructs deficient in binding ch-TOG, have demonstrated that ch-TOG is recruited to the spindle MTs via an interaction with TACC3 (Gergely et al. 2003; Lin et al. 2010; Booth et al. 2011; Hood et al. 2013).

4.3.1 Effect of TACC3 Affimers on the mitotic spindle localisation of TACC3 and ch-TOG

We hypothesised that Affimers designed to inhibit the TACC3–ch-TOG interaction should result in a reduction of ch-TOG spindle recruitment. To test this, CRISPR GFP-FKBP-TACC3 HeLa cells expressing free mCherry or mCherry-Affimers, were fixed in ice-cold methanol and stained with an antibody to visualise endogenous ch-TOG. As a positive control, cells were treated with the Aurora A kinase inhibitor MLN8237, to abolish TACC3 and ch-TOG spindle localisation, as described previously (Booth et al. 2011; Hood et al. 2013). Metaphase cells were imaged by confocal microscopy and analysed to quantify the spindle localisation of TACC3 and ch-TOG (see 2.3.10 for details). As expected, TACC3 and ch-TOG spindle localisation was abolished in MLN8237-treated cells compared to untreated cells (Fig. 4.7 A & C). Surprisingly, TACC3 spindle localisation was significantly reduced in cells expressing E4, E7 and E8 Affimers with respect to untransfected cells (Fig. 4.7 B & C). However, the level of spindle localisation in these cells was significantly higher than MLN8237-treated cells, suggesting that although there is a slight reduction, TACC3 remained enriched on the spindle. Similarly, the spindle localisation of ch-TOG was significantly reduced in cells expressing E4, E7 and E8 Affimers with respect to untransfected cells. In the case of E4, ch-TOG spindle localisation was significantly higher than that of MLN8237-treated cells, and remained visibly enriched on the spindle (Fig. 4.7 B). In comparison, ch-TOG spindle localisation was abolished in cells expressing E7 and E8 Affimers, similar to the effect of MLN8237 treatment. Importantly, ch-TOG spindle localisation was not affected in cells expressing free mCherry, suggesting that mislocalisation of ch-TOG is attributed to the

Affimer. Overall, this result is consistent with a model where ch-TOG requires an intact interaction with TACC3 for its mitotic spindle localisation (Hood et al. 2013). Moreover, it suggests that Affimers E7 and E8 can be used to dissect the TACC3–ch-TOG interaction during mitosis in living cells.

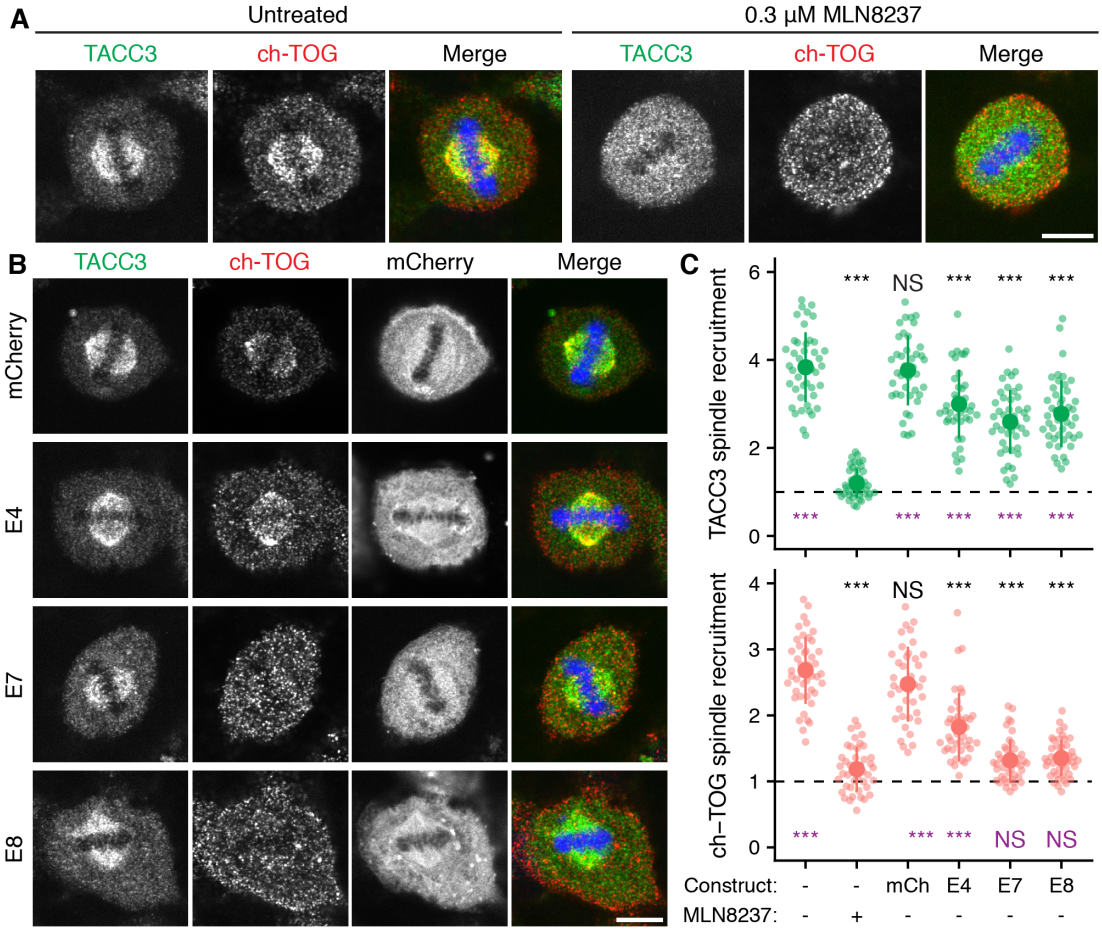

Figure 4.7. The mitotic spindle localisation of ch-TOG is severely reduced in the presence of E7 and E8 Affimers. (**A**) Representative confocal micrographs of untreated or MLN8237-treated (0.3 µM, 40 min) CRISPR GFP-FKBP-TACC3 HeLa cells in metaphase. Cells were fixed in ice-cold methanol and stained for ch-TOG (red) and DNA (blue). A GFP-boost antibody was used to enhance the signal of GFP-FKBP-TACC3 (green). (**B**) Cells expressing free mCherry or mCherry-Affimers, as labelled. Scale bar = 10 µm. (**C**) Quantification of spindle recruitment of TACC3 (green) and ch-TOG (red). Each dot represents a single cell, n = 40-45 cells per condition over 3 independent experiments. The dashed horizontal line ($y = 1$) represents no enrichment on the spindle. The large dot and error bars show the mean ± one standard deviation, respectively. Analysis of variance (ANOVA) was used to compare the means between each group. The significance level from Tukey's post hoc test is shown above each group, using the untransfected and untreated cells (black) and untransfected MLN8237-treated cells (purple) for comparison. ***, $p < 0.001$; NS, $p > 0.05$.

To ensure that the E7 and E8 Affimers are specifically blocking the TACC3–ch-TOG interaction, we sought an experiment to visualise the mitotic spindle localisation of another member of this complex, clathrin. Since the mitotic spindle localisation of TACC3 and clathrin is interdependent (Hood et

al. 2013), any inhibition of the TACC3–clathrin interaction via the Affimer will be observed by mislocalisation of clathrin or TACC3 during mitosis. To test this, CRISPR CLTA-FKBP-GFP HeLa cells expressing mCherry-Affimers were fixed in PTEMF and stained with an antibody to visualise endogenous TACC3. To provide a reference for spindle mislocalisation, cells were treated with the Aurora A inhibitor MLN8237. As expected, inhibition of Aurora A by MLN8237 resulted in the mislocalisation of TACC3 and clathrin, with no spindle enrichment of either protein observed in metaphase cells (Fig. 4.8 A). In contrast, cells expressing mCherry-Affimers displayed distinct spindle staining of TACC3 and clathrin, comparable to untreated control cells (Fig. 4.8 B). Therefore, inhibition of TACC3–ch-TOG by E7 and E8 Affimers is specific and does not interfere with the other interactions within the complex.

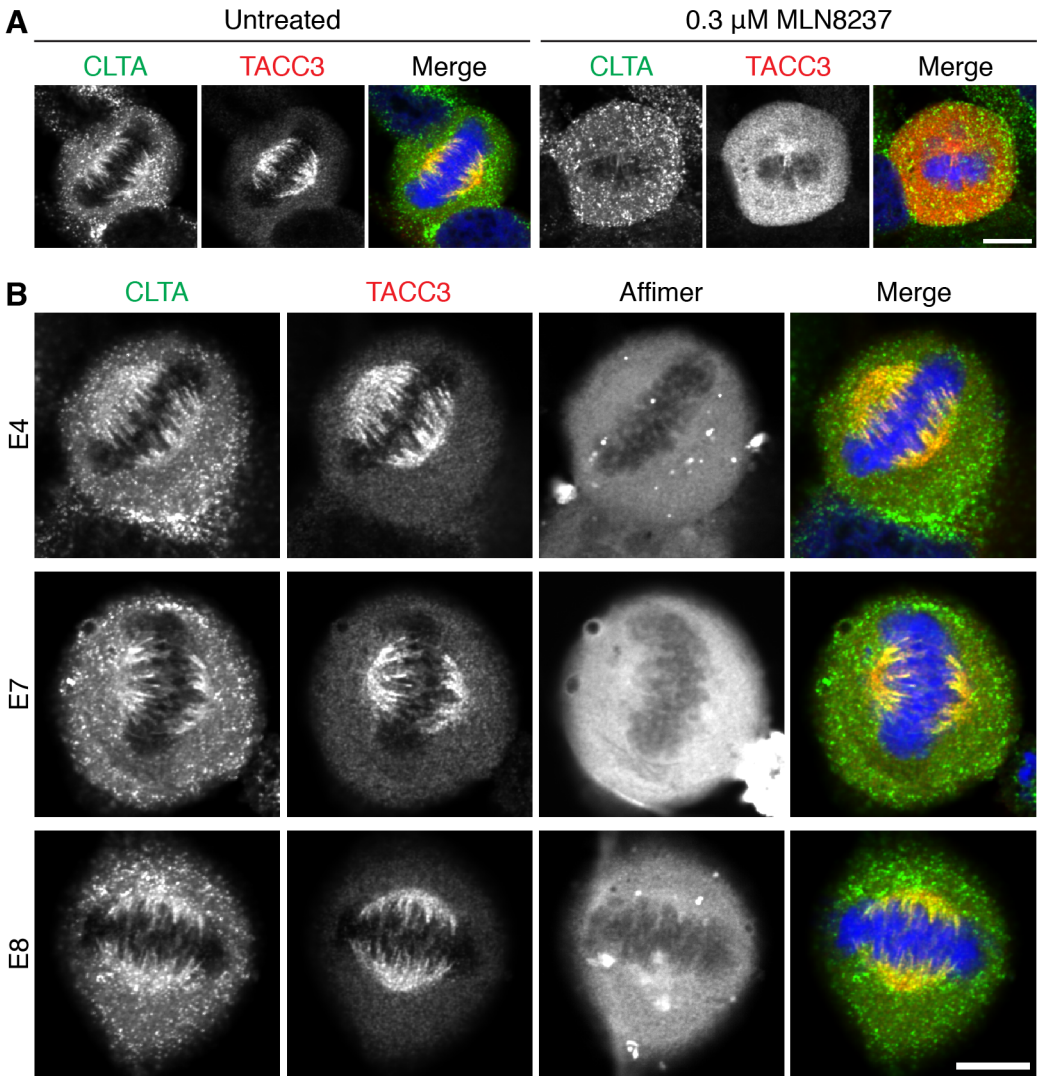

Figure 4.8. TACC3 Affimers do not affect the mitotic spindle localisation of clathrin or TACC3 in HeLa cells. (**A**) Representative confocal micrographs of untreated or MLN8237-treated (0.3 µM, 40 min) CRISPR CLTA-FKBP-GFP HeLa cells in metaphase. Cells were fixed in PTEMF and stained for TACC3 (red) and DNA (blue). A GFP-boost antibody was used to enhance the signal of CLTA-FKBP-GFP (green). (**B**) Cells expressing the indicated mCherry-Affimers (not shown in merge). Scale bar = 10 µm.

4.3.2 Effect of TACC3 Affimers on mitotic spindle positioning

During the quantification of TACC3 and ch-TOG mitotic spindle localisation in Fig. 4.7, it was noted that in some cells, particularly those expressing E7 and E8 Affimers, the position of the mitotic spindle appeared offset. This is plausible since TACC3 has been suggested to play a role in regulating the formation of astral MTs, which aid in positioning the mitotic spindle during mitosis (Singh et al. 2014; Rajeev et al. 2019). To investigate if the TACC3–ch-TOG interaction is important in mitotic spindle positioning, HeLa cells expressing free mCherry or mCherry-Affimers were fixed and stained to visualise α-tubulin and pericentrin

as markers for the mitotic spindle and centrosomes, respectively. Image stacks of mitotic cells were acquired using a confocal microscope and the max intensity z projections were used for analysis. To quantitatively assess mitotic spindle positioning, I developed a semi-automated pipeline in Fiji and R to measure the length of the mitotic spindle, defined as the length between the two centrosomes, and the spindle position, defined as the absolute difference in the cortex to centrosome distance (d1 and d2) and the cortex to metaphase plate distance (D1 and D2; see 2.3.11 and Fig. 4.9 D for details). Visualisation of the data revealed that the average spindle length was comparable between all conditions (Fig. 4.9 A). Although spindle shift was slightly increased in cells expressing Affimers relative to the mCherry control, this effect was not statistically significant (Fig. 4.9 B & C). Therefore, disruption of the TACC3–ch-TOG interaction using the Affimers developed here, does not significantly affect the length or position of the mitotic spindle in HeLa cells. Despite this, the image analysis pipeline was released and will be a useful tool for future studies, enabling researchers to quantitatively assess mitotic spindle parameters.

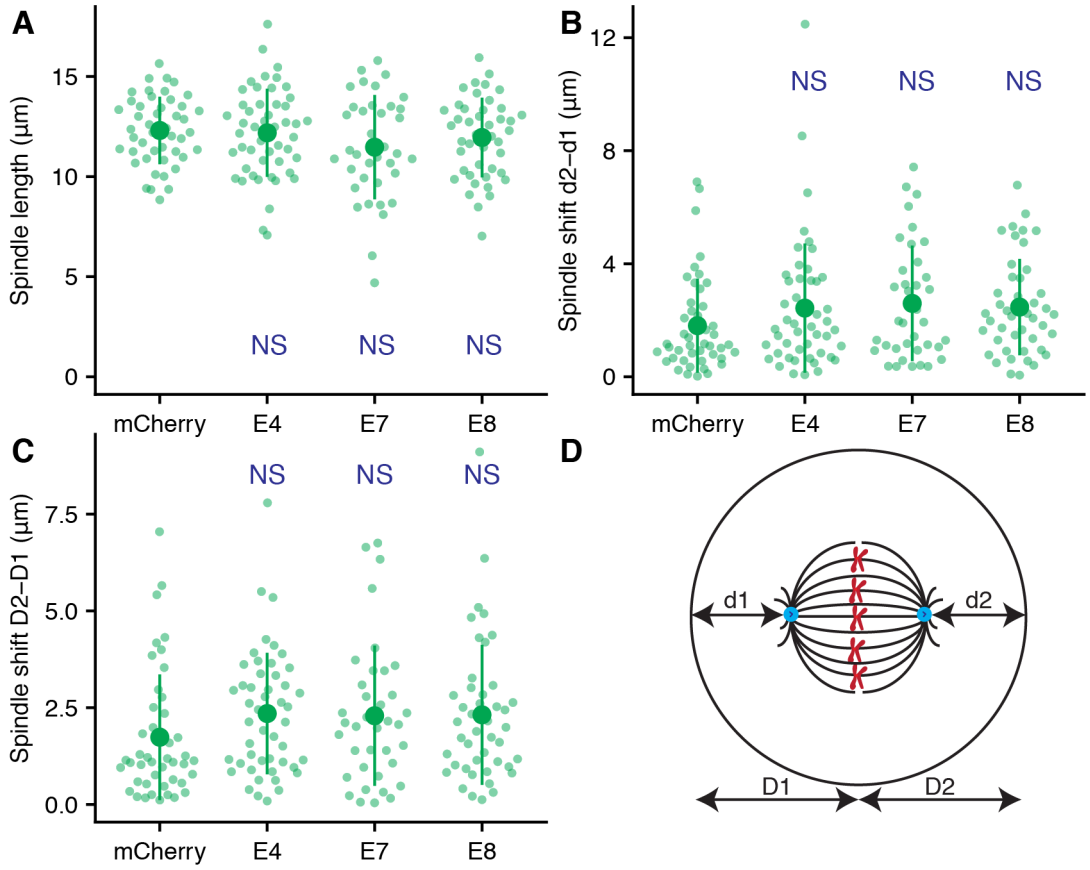

Figure 4.9. TACC3 Affimers do not affect mitotic spindle positioning in HeLa cells. Quantification of mitotic spindle parameters in HeLa cells expressing free mCherry or mCherry-Affimers. Cells were fixed in PTEMF and stained to visualise α-tubulin, pericentrin and DNA as markers for the mitotic spindle, centrosomes and metaphase plate, respectively. Dot plots show the spindle length (**A**) and measurements of spindle positioning (**B & C**). The schematic (**D**) describes the measurements plotted. The metaphase plate is depicted by the alignment of chromosomes (red), the mitotic spindle is shown in black and the centrosomes are in blue. Each dot represents a single cell, n = 37-49 cells per condition pooled from 3 independent experiments. The large dot represents the mean and the error bars show the mean ± one standard deviation. A Kruskal-Wallis test was used to compare the means between each group. Dunn's post hoc test with Bonferroni adjustment was used to calculate p values. The significance level is shown above each group, using the mCherry group for comparison. NS (not significant), $p > 0.05$.

4.3.3 Dissecting the role of TACC3–ch-TOG at the mitotic centrosome

To allow for an accurate measure of spindle length, only cells containing 2 distinct centrosomes were included in the analysis of the previous experiment (Fig. 4.9). During the analysis, it was noted that a large number of cells contained more than 2 distinct pericentrin foci, and that these additional foci were associated with small MT asters (Fig. 4.10 A). To investigate this, the dataset was analysed using *3D Objects Counter* in Fiji (see 2.3.12 for details) to detect and count pericentrin foci within the image stacks. Interestingly, a higher proportion of

cells containing more than 2 pericentrin foci was observed in cells expressing the E7 (30.4%) or E8 (33.3%) Affimer, compared to E4 (8.2%) or mCherry (2.2%) (Fig. 4.10 B). Moreover, the additional pericentrin foci appeared smaller in size compared to the 2 foci that formed the bipolar spindle. Quantification of the total volume of pericentrin foci present in each cell revealed no significant change in E7 or E8 cells compared to the mCherry control (Fig. 4.10 B), suggesting that it is not likely that the additional foci represent amplified centrosomes, or arise due to cytokinesis failure. Fisher's exact test was used to test for an association between the type of Affimer expressed and the PCM foci category, i.e. 2 or > 2. A 2×2 contingency table comparing the observed frequencies of the PCM foci categories in the mCherry control group and each of the Affimer groups was used for analysis. The Bonferroni corrected p values from this analysis confirmed that the groups are independent in the case of E4 ($p = 1$), but are associated in E7 ($p = 0.001$) and E8 ($p = 0.0002$). Based on this finding, we hypothesised that the TACC3–ch-TOG interaction could be involved in maintaining the structure of the PCM during mitosis.

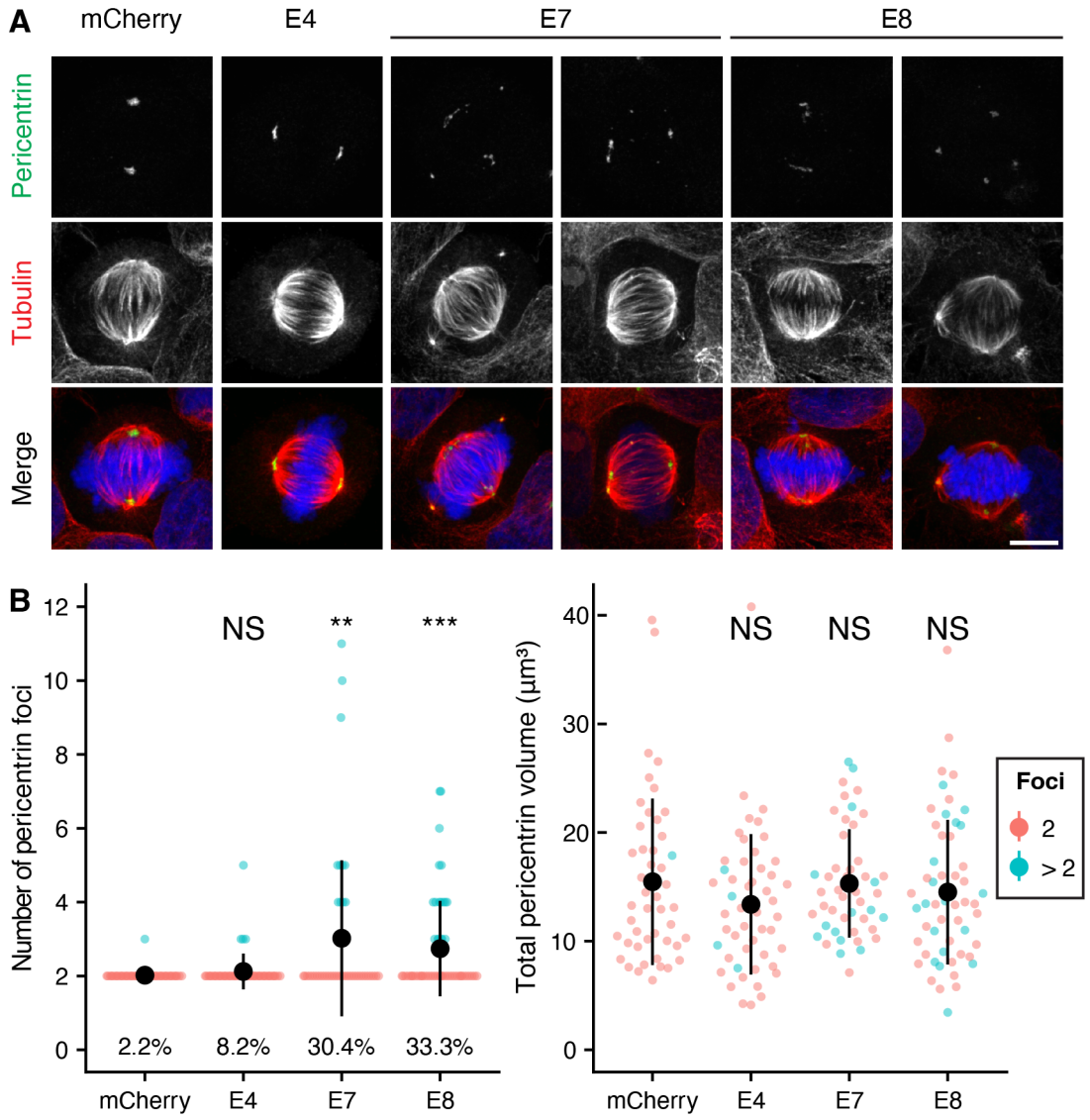

Figure 4.10. Expression of E7 and E8 Affimers leads to additional pericentrin foci in mitotic HeLa cells. (**A**) Representative max intensity z projection images of HeLa cells in metaphase expressing free mCherry or mCherry-Affimers, as indicated. Cells were fixed in PTEMF and stained for pericentrin (green), α-tubulin (red) and DNA (blue). Scale bar = 10 µm. (**B**) Quantification of pericentrin in the images shown in A using *3D Objects Counter* in Fiji. Dot plots show the number (left) and the total volume (right) of detected pericentrin foci. Each dot represents a single cell, n = 46-54 cells per condition over 3 independent experiments. The large dot and error bars show the mean ± one standard deviation, respectively. Cells containing exactly 2 pericentrin foci are shown in red and those with > 2 are shown in turquoise. Fisher's exact test was used to test for association between the type of Affimer expressed and the PCM foci category. Bonferroni adjustment was used to calculate p values. A Kruskal-Wallis test was used to compare the means between each group for the total pericentrin volume data. Dunn's post hoc test with Bonferroni adjustment was used to calculate p values. The significance level is shown above each group, using the mCherry group for comparison. NS (not significant), $p > 0.05$; **, $p < 0.01$; ***, $p < 0.001$.

To test whether the additional sites of pericentrin are fragments of PCM, and not centriole-containing centrosomes as a result of centrosome amplification or cytokinesis failure, an experiment to visualise the PCM and the centrioles together

was necessary. We hypothesised that if the additional pericentrin foci represent true centrosomes as a result of centrosome amplification, centrioles should be present in the additional sites (Fig. 4.11 A). To test this, HeLa cells expressing free mCherry or mCherry-Affimers were fixed and stained to visualise pericentrin and centrin-1, as markers for the PCM and centrioles, respectively. As before, image stacks of mitotic cells were acquired using a confocal microscope and the resulting max intensity z projections were analysed. Due to difficulties in detecting individual centrin-1 foci using automated image analysis methods, the number of centrin-1 foci associated with each pericentrin foci was manually counted and recorded (see 2.3.12 for details). Data from this analysis revealed that in the majority of cells containing > 2 pericentrin foci, centrin-1 is absent from the additional sites (Fig. 4.11 B), confirming that the additional sites are likely fragments of the PCM.

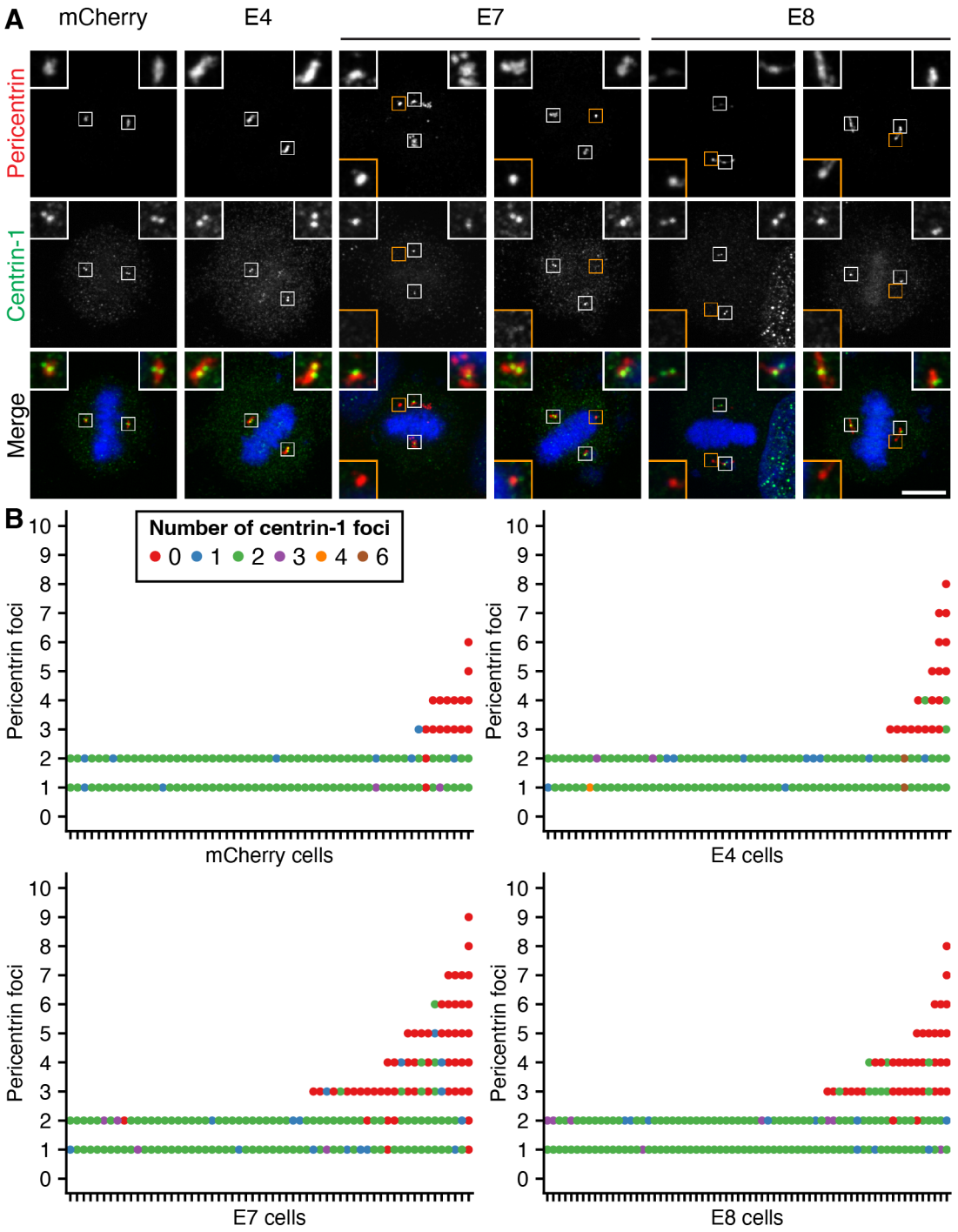

Figure 4.11. Additional pericentrin foci are not a result of centrosome amplification or cytokinesis failure. (**A**) Representative max intensity z projection images of HeLa cells in metaphase expressing free mCherry or mCherry-Affimers, as indicated. Cells were fixed in ice-cold methanol and stained for pericentrin (red), centrin-1 (green) and DNA (blue). Insets show a 2.5× zoom of pericentrin at the spindle poles, orange insets show sites of fragmentation. Scale bar = 10 µm. (**B**) Quantification of the pericentrin foci and the corresponding number of centrin-1 foci. Each tick on the x-axis represents a single cell. The number of pericentrin foci present in each cell is indicated on the y-axis. Each dot represents a single pericentrin foci, with the colour of the dot indicating the number of centrin-1 foci present, as described in the legend. Data is shown for n = 57-68 cells per condition over 3 independent experiments.

We next sought to confirm that the PCM fragmentation phenotype described above, is due to the specific disruption of the TACC3–ch-TOG interaction and not via an off-target effect. To test this, a plasmid to co-express a GFP-tagged construct and a short hairpin RNA to silence expression of endogenous ch-TOG, was used to express a mutant of ch-TOG deficient in binding TACC3, full-length ch-TOG or free GFP in HeLa cells. The ch-TOG mutant, hereafter referred to as LLAA, is a full-length construct of ch-TOG containing mutations to a pair of conserved leucine residues (LL1939, 1942AA) within the C-terminal region that are required for binding the C-terminal TACC domain of TACC3, as demonstrated in a previous study (Gutierrez-Caballero et al. 2015). Transfected cells were prepared for IF and analysed as before (Fig. 4.10). As expected, in ch-TOG depleted cells expressing free GFP, approximately 50% of mitotic cells contained multipolar spindles (Fig. 4.12 A & B). This is consistent with previous reports of ch-TOG depletion, highlighting its role in spindle pole organisation (Gergely et al. 2003; Cassimeris and Morabito 2004). Expression of full-length ch-TOG rescued the multipolar phenotype, with only 14.2% of cells containing > 2 pericentrin foci (Fig. 4.12 A & B). In contrast, expression of the LLAA mutant led to a pericentrin fragmentation phenotype in 36% of cells (Fig. 4.12 A & B), similar to the result observed with Affimers E7 and E8 (Fig. 4.10). Taken together, this result suggests that the phenotype observed with the E7 and E8 Affimers in Fig. 4.10, is specific to the TACC3–ch-TOG interaction.

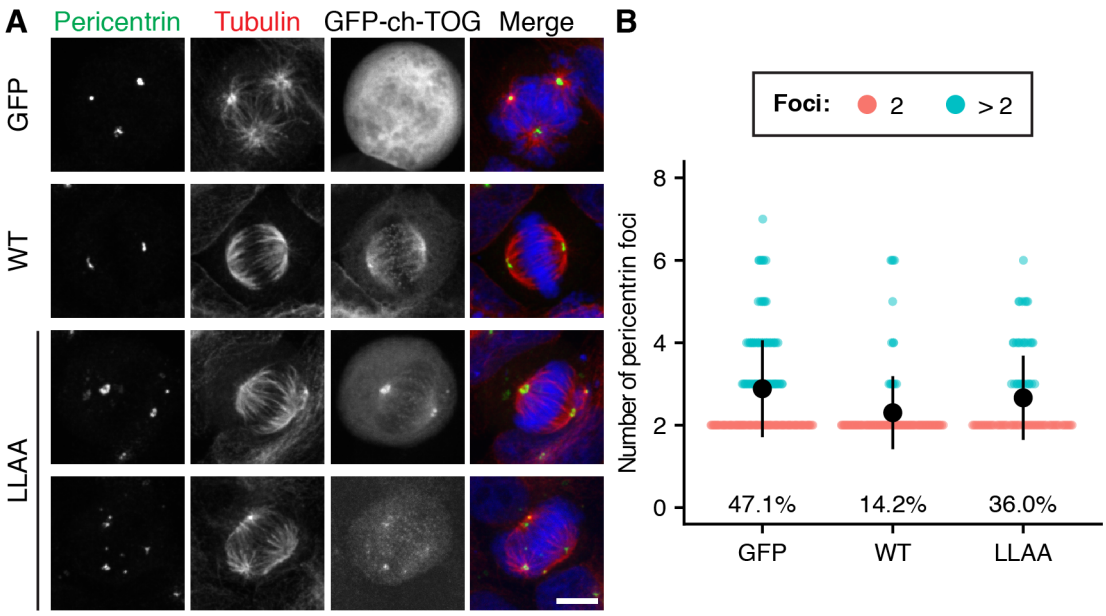

Figure 4.12. Expression of a ch-TOG mutant deficient in binding TACC3 leads to fragmentation of pericentrin in mitotic HeLa cells. (**A**) Representative max intensity *z* projection images of HeLa cells co-expressing sh ch-TOG, to knockdown endogenous ch-TOG, and knockdown proof GFP, ch-TOG-GFP (WT) or ch-TOG (L1939,1942A)-GFP (LLAA; colour not shown in the merge). Cells were fixed in PTEMF and stained for pericentrin (green), α-tubulin (red) and DNA (blue). Scale bar = 10 µm. (**B**) Quantification of pericentrin in the images shown in A using *3D Objects Counter* in Fiji. The dot plot shows the number of pericentrin foci detected. Each dot represents a single cell, n = 89-155 cells per condition over 3 independent experiments. The large dot and error bars show the mean ± one standard deviation, respectively. Cells containing exactly 2 pericentrin foci are shown in red and those with > 2 are shown in turquoise.

The experiments described so far have used pericentrin as a marker for the PCM. We wondered if the fragments observed in the previous experiments also contain other components of the PCM, and whether ch-TOG, which is enriched at the mitotic centrosome under normal conditions, is localised at the additional sites.

To answer these questions, HeLa cells expressing free mCherry or mCherry-Affimers were processed for IF. To visualise endogenous ch-TOG, a new antibody was purchased (Thermo, Cat No. PA5-59150), as an experiment comparing a range of commercial antibodies revealed clear staining of the centrosome pool of ch-TOG using this antibody (see appendix 1, p146). As a marker of a core component of the PCM, an antibody to detect γ-tubulin was used. We hypothesised that this would also shed light on the MT nucleation status of PCM fragments, as γ-tubulin is recruited to the PCM to carry out this function (Khodjakov and Rieder 1999). Image stacks of mitotic cells were acquired using a confocal microscope and the resulting images were analysed using *3D Objects Counter* in Fiji to detect and count γ-tubulin foci. To quantify the fluorescence intensity of ch-TOG at the centrosome, the mask of each γ-tubulin foci was passed to the ch-TOG channel for measurement (see 2.3.12 for details).

As before, fragmentation of the PCM was observed in cells expressing E7 and E8 Affimers, indicated by the presence of > 2 γ-tubulin foci in 25.4% and 24.2% of cells, respectively. In comparison, fragmentation was observed in 12.9% and 12.7% of mCherry and E4 expressing cells, respectively (Fig. 4.13 A & B). Despite a higher proportion of E7 and E8 cells displaying > 2 γ-tubulin foci relative to mCherry control, Fisher's exact test revealed no significant association between the type of Affimer expressed and the PCM foci category (E4, $p = 1.00$; E7, $p = 0.181$; E8, $p = 0.208$). Interestingly, ch-TOG was observed at sites of fragmented PCM (see E7 and E8 cells in Fig. 4.13 A), suggesting that inhibition of the TACC3–ch-TOG interaction does not affect recruitment of ch-TOG to the mitotic centrosome. Moreover, the sum fluorescence intensity of ch-TOG present at the sites of γ-tubulin was not significantly different in cells expressing the Affimers relative to the mCherry control (Fig. 4.13 A & B). This is consistent with studies that found no change in the level of ch-TOG at the mitotic centrosome following TACC3 knockdown (Gergely et al. 2003; Lin et al. 2010; Booth et al. 2011). Of note, a striking reduction in the mitotic spindle localisation of ch-TOG was observed in E7 and E8 cells (Fig. 4.13 A), confirming the result in Fig. 4.7 that inhibition of the TACC3–ch-TOG interaction blocks ch-TOG spindle recruitment.

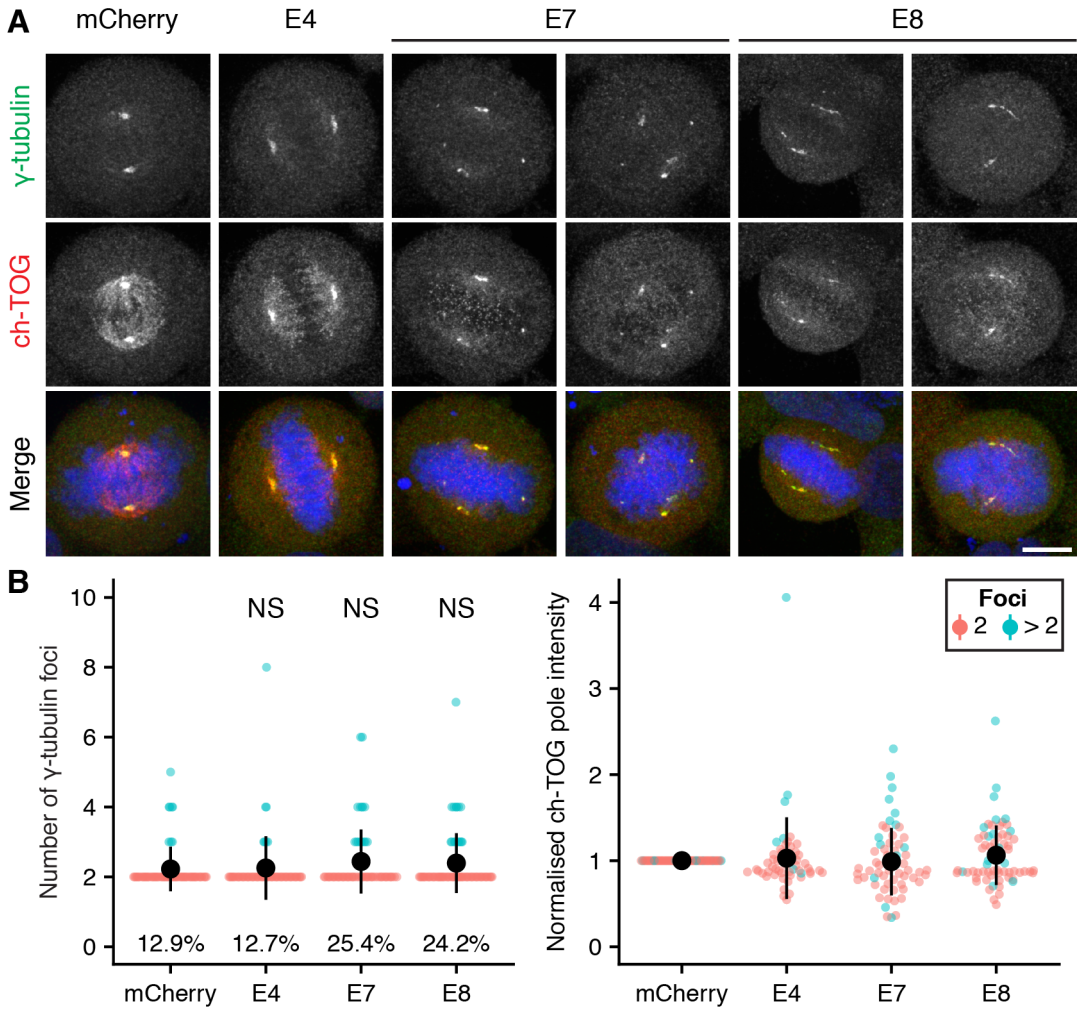

Figure 4.13. Expression of E7 and E8 Affimers leads to fragmentation of γ-tubulin in mitotic HeLa cells. (**A**) Representative max intensity z projection images of HeLa cells in metaphase expressing free mCherry or mCherry-Affimers, as indicated. Cells were fixed in PTEMF and stained for γ-tubulin (green), ch-TOG (red) and DNA (blue). Scale bar = 10 µm. (**B**) Quantification of the images shown in A using *3D Objects Counter* in Fiji. Dot plots show the number of detected γ-tubulin foci (left) and the total fluorescence intensity of ch-TOG at the detected sites normalised to the mCherry condition (right). Each dot represents a single cell, n = 54-66 cells per condition over 3 independent experiments. The large dot and error bars show the mean ± one standard deviation, respectively. Cells containing two pericentrin foci are shown in red and those with > 2 are shown in turquoise. Fisher's exact test was used to test for association between the type of Affimer expressed and the PCM foci category. Bonferroni adjustment was used to calculate p values. The significance level is shown above each group, using the mCherry group for comparison. NS (not significant), $p > 0.05$.

My experiments so far have revealed that disruption of the TACC3–ch-TOG interaction through expression of the E7 or E8 Affimer, leads to fragmentation of the PCM in 25-30% mitotic HeLa cells, as observed using pericentrin or γ-tubulin antibodies. Importantly, centrioles are absent from these additional sites, suggesting they are not amplified centrosomes. Furthermore, whilst spindle staining of ch-TOG is reduced, the levels of ch-TOG at the centrosome are unaffected and ch-TOG staining is observed in the PCM fragments. All of these

experiments have focussed on mitotic centrosomes in fixed samples, and therefore do not reveal information regarding the dynamics of the PCM fragmentation. For example, we wondered if this fragmentation occurs prior to the cell entering mitosis, during spindle assembly, or once the spindle has formed.

To answer this point, a live-imaging approach to visualise the PCM and DNA was needed. For this, HeLa cells were co-transfected with a plasmid to express free mCherry or mCherry-Affimers, and a plasmid to express mEmerald-γ-tubulin, as a marker for the PCM. Live-imaging of transfected cells was performed overnight, using SiR-DNA to label the DNA and enable tracking of the PCM during defined stages of the cell cycle (see 2.3.13 for details). To quantify progression through mitosis, the frame numbers for prometaphase, metaphase and anaphase of transfected cells was recorded using image stacks from the overnight movies. To assess PCM fragmentation, frame numbers where > 2 γ-tubulin foci were observed were recorded. G2 was defined as the period 5 frames (15 min) prior to prometaphase, and was used as a window to observe the PCM before entry into mitosis. Together, this information was used to track the PCM during 3 stages, G2-prometaphase, prometaphase-metaphase and metaphase-anaphase. To visualise the frequency of fragmentation at each stage, the data for each construct was plotted using a Sankey diagram (Fig. 4.14).

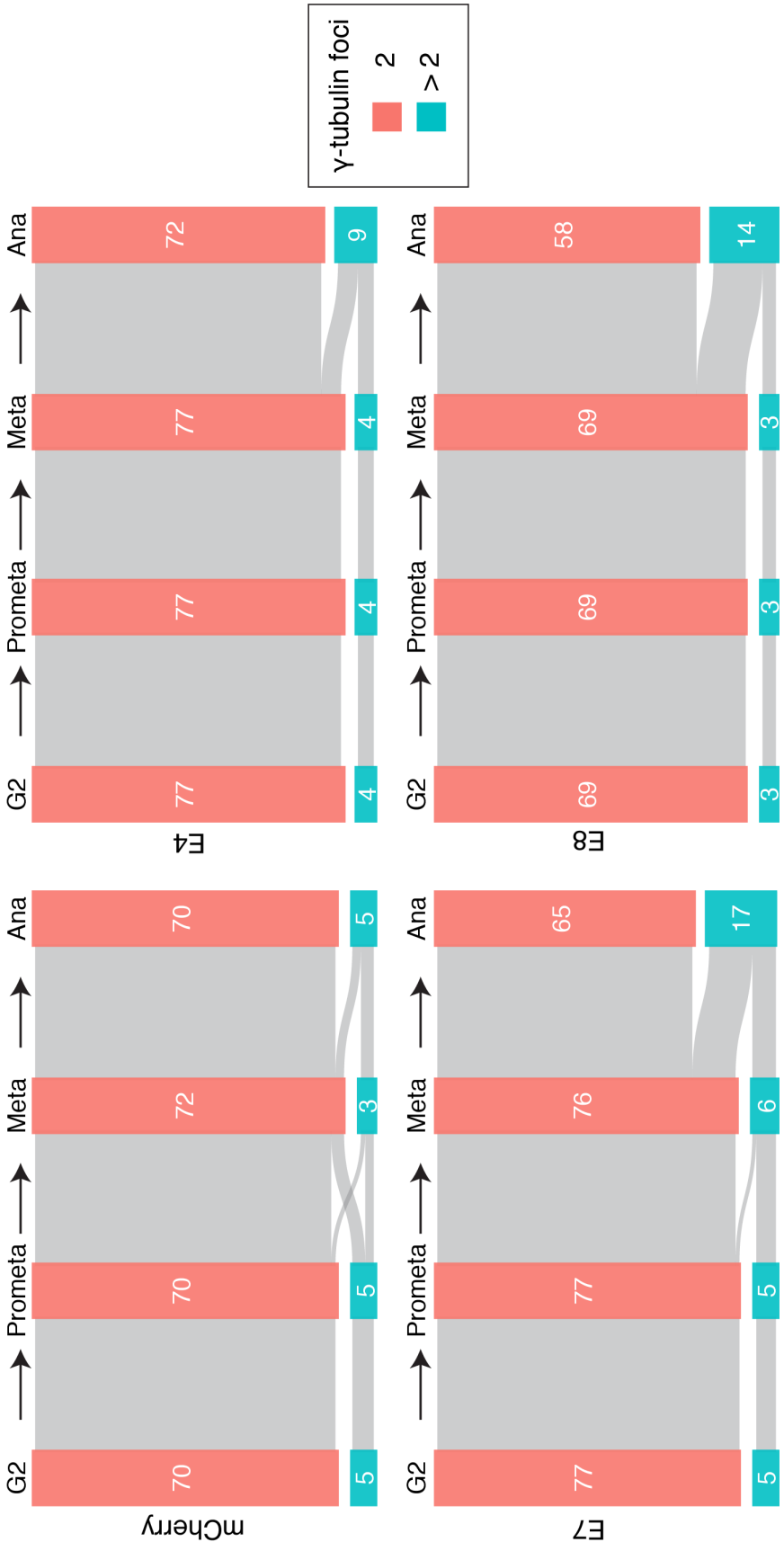

Figure 4.14. Expression of E7 and E8 Affimers leads to fragmentation of γ-tubulin foci during metaphase in HeLa cells. Sankey diagrams to show the number of γ-tubulin foci present in HeLa cells co-expressing mEmerald-γ-tubulin and free mCherry or mCherry-Affimers, at the indicated stages of cell division. The number of γ-tubulin foci was tracked across 3 stages, G2-prometaphase, prometaphase-metaphase and metaphase-anaphase. G2 was defined as the period 5 frames (15 min) prior to prometaphase. The numbers in each node represent the number of cells observed at each stage, as labelled. The colour of the node represents the number of γ-tubulin foci in the cell, those containing 2 are shown in red and those with > 2 are shown in turquoise. Data is pooled from four independent overnight experiments where all conditions were included in each experiment.

Consistent with the fixed experiments, the proportion of cells with > 2 γ-tubulin foci during metaphase, defined as the number of cells with > 2 foci before the onset of anaphase, was higher in E7 (20.7%) and E8 (19.4%) expressing cells, compared to mCherry (6.7%) and E4 (11.1%). Interestingly, in E7 and E8 cells, the metaphase-anaphase transition was when the majority of cells displayed > 2 γ-tubulin foci for the first time, with 13.4% and 15.3% of cells displaying this phenotype, respectively. In these cells, the γ-tubulin foci underwent fragmentation to form smaller foci that remained in close proximity to the bipolar spindle before dividing into two daughter cells (Fig. 4.15 B). Moreover, a prolonged metaphase-anaphase transition was observed in cells with this phenotype. In comparison, control cells maintained two distinct γ-tubulin foci throughout the observed stages and divided without a delay (Fig. 4.15 A). Across all conditions, a very small number of cells contained > 2 γ-tubulin foci in G2 prior to prometaphase, and continued to display the additional foci in the subsequent stages of mitosis, before dividing with a multipolar spindle. This population of cells likely represents the basal level of centrosome amplification in HeLa cells (Wong et al. 2015), irrespective of mCherry/Affimer expression.

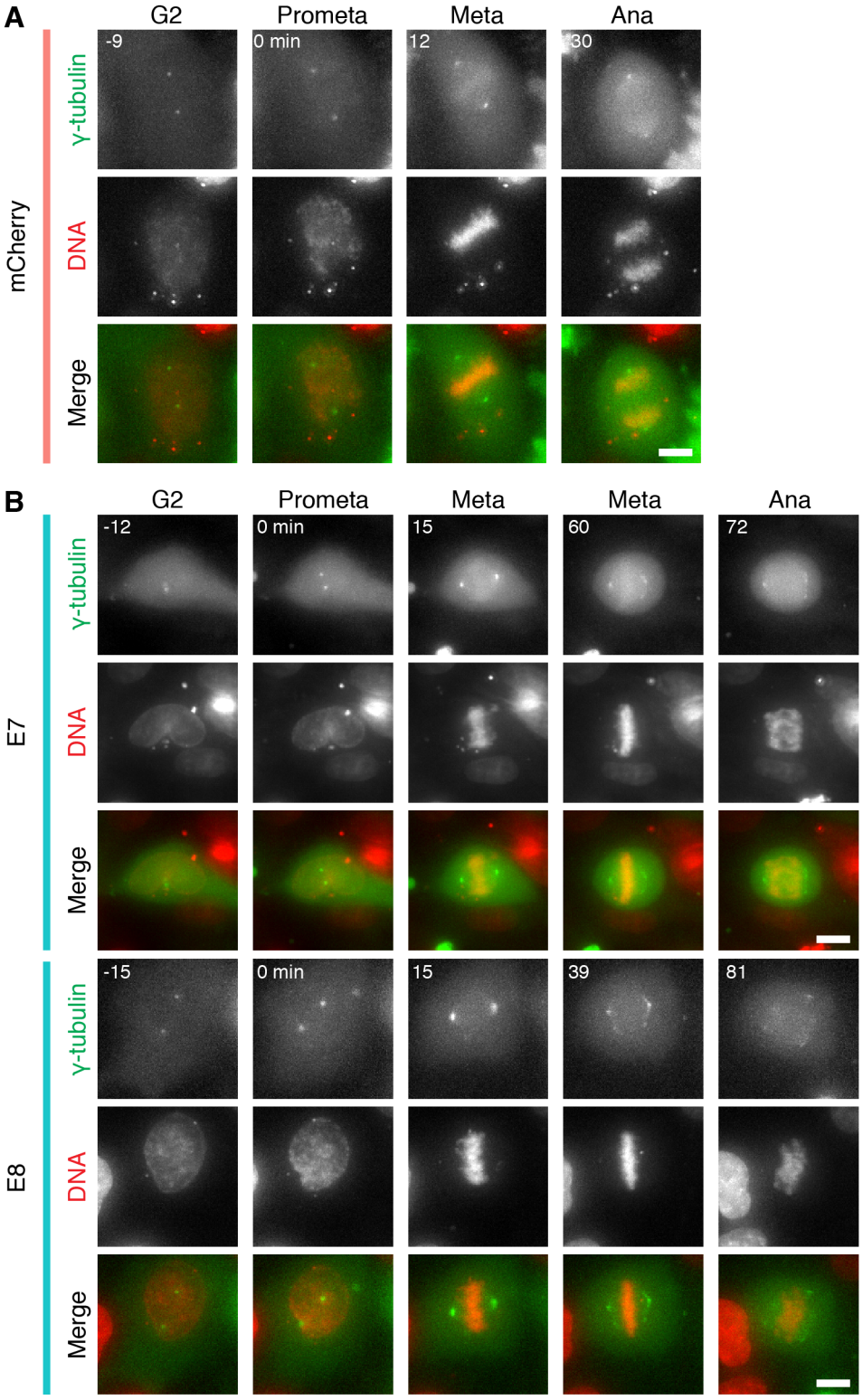

Figure 4.15. Stills from live cell imaging experiments to track the number of γ-tubulin foci. Max intensity z projection images of HeLa cells expressing mEmerald-γ-tubulin (green) and the indicated free mCherry or mCherry-Affimers constructs (not shown) during different stages of mitosis as indicated by the labelling of the DNA (red) using SiR-DNA. (**A**) Representative control HeLa cell expressing free mCherry containing two γ-tubulin foci throughout the observed stages. (**B**) Representative HeLa cells expressing mCherry-E7 or mCherry-E8 Affimers undergoing fragmentation of γ-tubulin during metaphase-anaphase. The timings (minutes) at each stage are shown in white. Scale bar = 10 µm.

To determine the impact of TACC3–ch-TOG inhibition on the progression of mitosis, the mitotic timings of all cells displayed in Fig. 4.14, irrespective of their centrosome status, were plotted (Fig. 4.16 A). This data revealed no significant change in the timings of prometaphase to metaphase or prometaphase to anaphase in cells expressing the Affimers relative to the mCherry control (Fig. 4.16 A). To determine the impact of PCM fragmentation as a result of TACC3–ch-TOG inhibition on cell division, the mitotic timings of E7 and E8 expressing cells containing 2 or > 2 γ-tubulin foci during metaphase were plotted (Fig. 4.16 B). To specifically look at the effect of PCM fragmentation during metaphase, cells containing > 2 foci prior to metaphase were excluded from the analysis. The plots revealed no change in the time taken to align the majority of chromosomes (prometaphase-metaphase), however, a significantly prolonged metaphase in cells with > 2 foci was observed (Fig. 4.16 B). E7 and E8 expressing cells that underwent PCM fragmentation during metaphase displayed a median metaphase-anaphase timing of 60 min and 102 min, respectively. In comparison, a median metaphase-anaphase timing of 30 min was observed in E7 and E8 expressing cells containing two foci throughout metaphase. Taken together, this data shows that inhibition of TACC3–ch-TOG in HeLa cells through the expression of Affimer E7 or E8, leads to fragmentation of the PCM in metaphase and a prolonged metaphase-anaphase, following the timely formation of a bipolar spindle. Although this experiment shows a correlation between PCM fragmentation and prolonged metaphase-anaphase, it does not show causality between the two defects, since it is possible that there is another unknown defect that is the common cause.

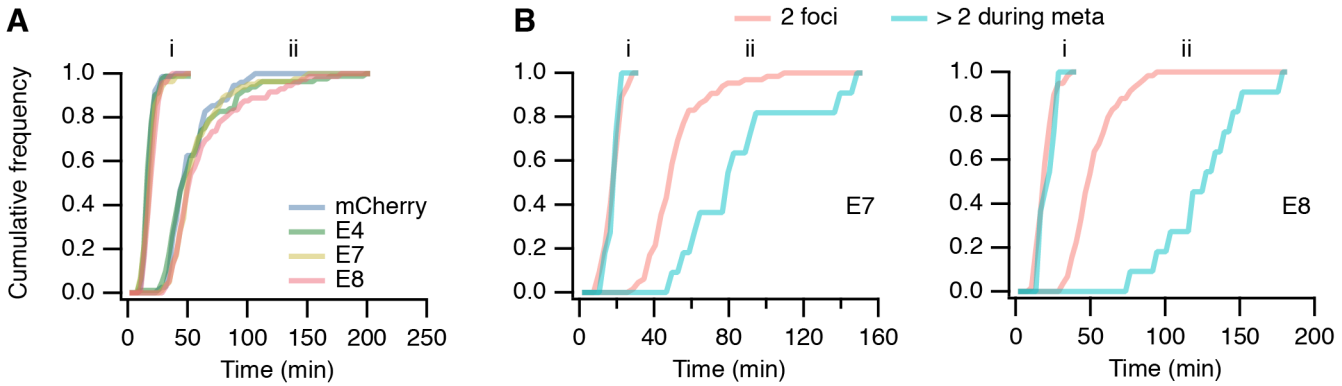

Figure 4.16. Mitotic progression of HeLa cells expressing free mCherry or mCherry-Affimers. Cumulative histograms of timings for prometaphase to metaphase (i) and prometaphase to anaphase (ii). (**A**) Frequencies of HeLa cells co-expressing mEmerald-γ-tubulin and the indicated construct, irrespective of centrosome status. (**B**) Frequencies of E7 and E8 expressing cells shown in A, comparing timings of cells with two γ-tubulin foci (2; red line) during metaphase with cells that undergo PCM fragmentation during metaphase (> 2; blue line). Number of cells analysed in A: mCherry, 75; E4, 81; E7, 82; E8, 72. Number of cells displayed in B (2 and > 2 foci, respectively): E7, 65 and 11; E8, 58 and 11.

4.4 Effect of TACC3 Affimers on MT regrowth

It has previously been reported that TACC3 regulates centrosomal MT nucleation by stabilising the γ-TuRC at the centrosome (Singh et al. 2014), however, the mechanism behind this function is unclear. We wondered if this described function of TACC3 requires an interaction with ch-TOG and could therefore be inhibited using the Affimers. To test this, an ice recovery assay was used to depolymerise the MT network and study MT regrowth following different periods of recovery at room temperature (see 2.3.14 for details). HeLa cells expressing free mCherry or mCherry-Affimers were processed for IF immediately after recovery, using antibodies against α-tubulin and γ-tubulin as markers for the MTs and centrosomes, respectively. Image stacks of interphase cells were acquired by a confocal microscope and the resulting max intensity z projection images were analysed to measure the area of the cell occupied by the MT network, as a read out for MT regrowth. As expected, in all conditions, the MT network was completely disassembled following a 1 h ice incubation (Fig. 4.17). In cells expressing free mCherry, the average area of the cell occupied by MTs increased with recovery time. Interestingly, MT regrowth in Affimer expressing cells was identical to that of the mCherry control at all time points tested. This suggests that the previously described function of TACC3 in regulating MT nucleation is independent of ch-TOG, and therefore defective MT nucleation is not likely to be responsible for the PCM fragmentation phenotype observed in previous experiments.

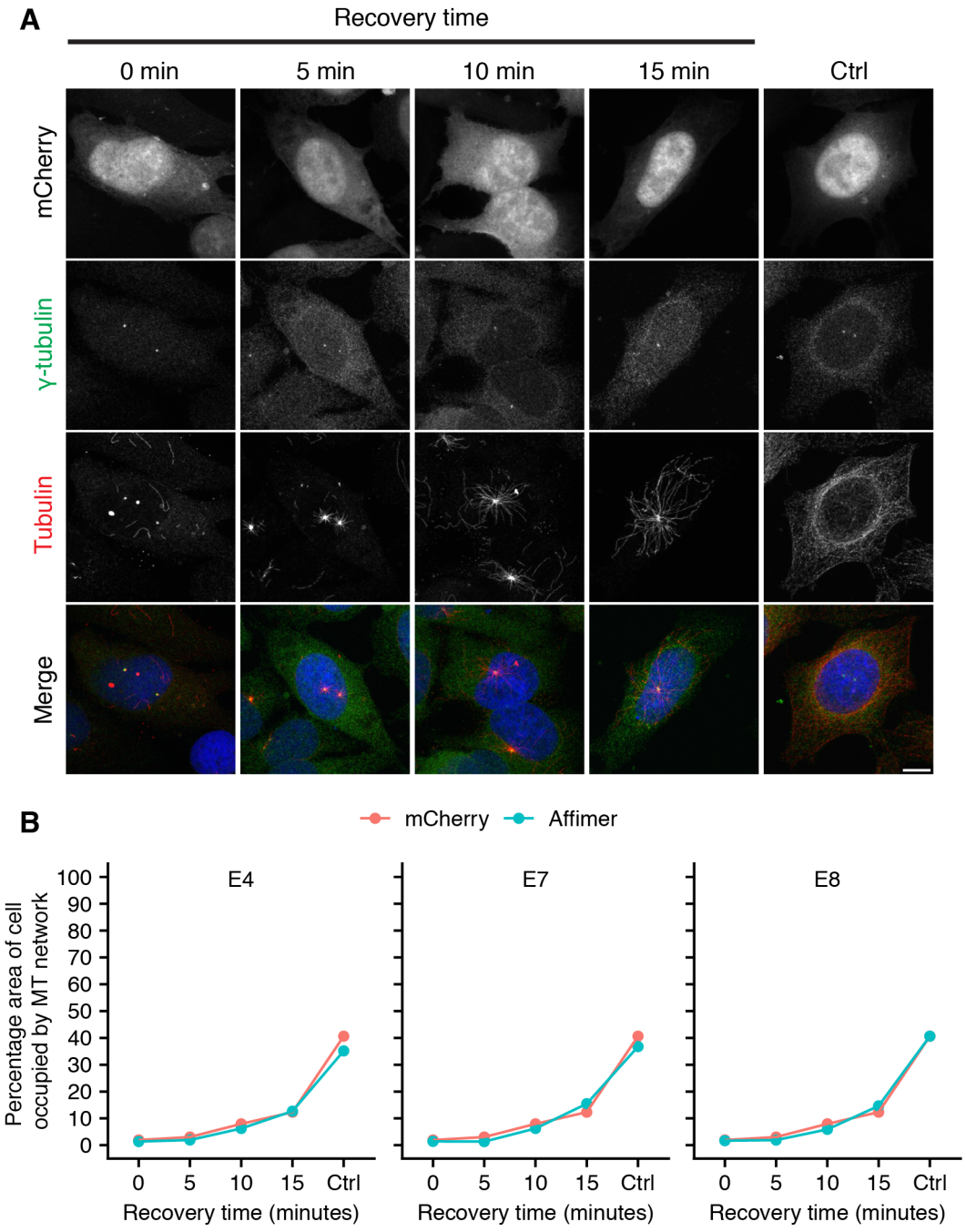

Figure 4.17. Microtubule regrowth is unaffected in interphase HeLa cells expressing TACC3 Affimers. (**A**) Representative max intensity z projection images of interphase HeLa cells expressing free mCherry fixed after different lengths of recovery at room temperature following 1 h ice treatment, as indicated. Untreated cells (Ctrl) with an intact microtubule (MT) network were included as a control. Cells were fixed in PTEMF and stained for γ-tubulin (green), α-tubulin (red) and DNA (blue). Scale bar = 10 µm. (**B**) Quantification of the images shown in A. The *auto threshold* method in Fiji was used to isolate the MT network. Plots show the average area of the cell occupied by the isolated MT network at the indicated recovery points in cells expressing free mCherry (red) or the indicated Affimer (turquoise). Each dot represents the mean area using cell measurements from 3 independent experiments. Data is shown for 1031 cells.

4.5 Chapter summary

The aim of this chapter was to investigate cell biological consequences of interfering with the TACC3–ch-TOG interaction. The first section describes work carried out to investigate the role of TACC3–ch-TOG in regulating MT dynamics at the plus-end of MTs in HeLa and RPE-1 cell lines. The data from the MT plus-end tracking experiments revealed no detectable change in MT growth speed in cells expressing the Affimers, suggesting that the TACC3–ch-TOG interaction may not have a significant function in regulating dynamics at the MT plus-end. This is in line with the finding that TACC3 depletion does not affect MT dynamics in RPE-1 cells (Gutierrez-Caballero et al. 2015). Other studies have identified a role for TACC3–ch-TOG in regulating MT dynamics to promote axon outgrowth using *Xenopus* embryonic cell types (Erdogan et al. 2017; Nwagbara et al. 2014). It is possible that the function of TACC3 at the MT plus-end is more critical during development, hence why differences are observed between embryonic and somatic cell types.

The second section of this chapter focussed on dissecting the role of TACC3–ch-TOG during mitosis, where I found that Affimers which disrupted this interaction displaced ch-TOG from K-fibres, in agreement with previous published reports that TACC3 is required to recruit ch-TOG to the mitotic spindle (Gergely et al. 2003; Lin et al. 2010; Booth et al. 2011; Hood et al. 2013). Moreover, this experiment validates the result from the pull-down assay in Chapter 3, where a reduction in ch-TOG was seen in the immunoprecipitate of cells expressing Affimers E7 and E8, but not E4. Importantly, I showed that this inhibition was specific, leaving the TACC3–clathrin interaction intact, as observed by an enrichment of clathrin on the spindle. Although the localisation of GTSE1 was not examined in cells expressing TACC3 Affimers, it is assumed that it remains enriched on the spindle given that the localisation of clathrin is not altered and that clathrin recruits GTSE1 to the spindle (Rondelet et al. 2020; Ryan et al. 2021). Nonetheless, a future experiment could be carried out to observe GTSE1 in mitotic cells expressing TACC3 Affimers to formally address this.

Experiments investigating the role of TACC3–ch-TOG in mitotic spindle positioning unexpectedly revealed a PCM fragmentation phenotype that was more frequently observed in E7 and E8 expressing cells compared to E4 or free mCherry cells. Based on the observation that the total volume of pericentrin was unchanged in cells expressing E7 and E8 Affimers compared to the mCherry control, and that centrin-1 was absent from the additional foci, we conclude that

the additional sites likely arise via fragmentation of the PCM, rather than a consequence of centriole overduplication, centriole disengagement or cytokinesis failure. Therefore, this work has uncovered a novel role for TACC3–ch-TOG in maintaining the integrity of mitotic centrosomes.

Chapter 5

Discussion

5.1 Using Affimers to dissect the TACC3–ch-TOG–clathrin–GTSE1 complex

The work presented in this thesis demonstrates that Affimers are a useful research tool to dissect the functions of members of the TACC3–ch-TOG–clathrin–GTSE1 complex in human cells. In the case of the TACC3 Affimers, their expression in HeLa cells led to specific disruption of the TACC3–ch-TOG interaction at the spindle, displacing ch-TOG while leaving the localisation of the other complex components intact. Specific inhibition of TACC3–ch-TOG led to unexpected fragmentation of the PCM in metaphase cells following the formation of a bipolar spindle, coupled with a delayed transition to anaphase. Thus, this work provides novel insight into the function of TACC3–ch-TOG in human cells, highlighting an important role in maintaining PCM integrity during mitosis. More broadly, this work demonstrates the potential of Affimers for dissecting other multiprotein complexes, with the possibility to discretely inhibit functions of multifunctional proteins.

5.1.1 The function of TACC3–ch-TOG at the microtubule plus-end

Given that my experiments revealed no detectable change in MT plus-end growth speed in cells expressing the Affimers, and that previous work found TACC3 depletion does not affect MT dynamics in RPE-1 cells (Gutierrez-Caballero et al. 2015), it is likely that the TACC3–ch-TOG interaction may not have a significant function in regulating dynamics at the MT plus-end. However, a study involving depletion of TACC3 in normal human dermal fibroblasts and

SK-N-SH cells, a human neuroblastoma cell line, reported a dose-dependent effect of TACC3 depletion on EB3 comet number in fixed cells (Furey et al. 2020). Similarly, they performed a live cell experiment tracking the movement of CLIP170, a +TIP, and saw reduced comet numbers and growth speeds in cells depleted of TACC3 compared with control cells. In this thesis, TACC3 depletion experiments carried out in HeLa and U2OS cells failed to show similar results. Moreover, no change in the organisation or stability of the MT network was observed in my experiments, illustrating potential cell-specific functions of TACC3. Nonetheless, a role for TACC3–ch-TOG in regulating MT dynamics during mitosis cannot be ruled out, since the experiments performed here were done so using interphase cells. It is possible that the role of TACC3–ch-TOG is less critical during interphase and becomes more important during mitosis, especially considering that phosphorylation of SLAIN2 during mitosis inhibits its interaction with ch-TOG (van der Vaart et al. 2011). Future experiments investigating the role of TACC3–ch-TOG in regulating plus-end dynamics during mitosis could shed light on this possibility.

To investigate the dependency of TACC3 and ch-TOG for their MT plus-end localisation, live cell experiments to visualise the localisation of each protein independently were performed. Surprisingly, both proteins tracked plus-ends in a comet-like manner in cells expressing Affimers. One interpretation of this data is that TACC3 plus-end localisation is not dependent on its interaction with ch-TOG as described previously (Gutierrez-Caballero et al. 2015). Another possibility is that the protein turnover of TACC3 and ch-TOG is slow at the MT plus-ends, meaning that the Affimer is unable to efficiently inhibit this interaction at the point of protein synthesis. This could explain why only a minor reduction in TACC3 fluorescence at the MT plus-end was observed in cells expressing Affimer E8 relative to the control. Since the function of TACC3–ch-TOG at the MT plus-end appears to be more critical in *Xenopus* embryonic cell types (Erdogan et al. 2017; Nwagbara et al. 2014), Affimers could be expressed in these cell lines to determine the dependency of TACC3 and ch-TOG in this context.

5.1.2 TACC3–ch-TOG is required to maintain centrosome integrity during mitosis

Fixed experiments using pericentrin as a marker for the PCM unexpectedly revealed a fragmentation phenotype that was more frequently observed in E7 and E8 expressing cells compared to E4 or free mCherry cells. A similar result was observed in cells stained with an antibody to detect γ-tubulin, a major component of the PCM. Interestingly, live imaging of γ-tubulin showed that fragmentation

of the PCM occurred almost exclusively during metaphase. Taken together, our data suggests a role for TACC3–ch-TOG in maintaining the integrity of the PCM during metaphase, where disruption of this interaction makes cells more susceptible to fragmentation. Given that PCM fragmentation was observed with two independent Affimers, E7 and E8, and the same phenotype was observed in cells expressing a mutant of ch-TOG deficient in binding TACC3, it is unlikely that the phenotype observed with the Affimers is a result of an off-target effect.

Live imaging of DNA and γ-tubulin revealed a delay in metaphase-anaphase in cells that undergo fragmentation of their PCM during metaphase, while the time taken to align the DNA at the metaphase plate was unaffected. What is the reason for the delayed metaphase in these cells? One possibility is that a reduction in ch-TOG at the spindle, or a minor reduction in TACC3 at the spindle, could lead to a decrease in K-fibre tension or an unattached kinetochore, that is recognised by the SAC. This has previously been demonstrated in KS experiments, where TACC3 was inducibly relocalised to the mitochondria during metaphase, which in turn led to decreased K-fibre tension and a delayed transition to anaphase (Cheeseman et al. 2013). Future experiments should therefore assess the activity of the SAC in metaphase cells expressing TACC3 Affimers, and assay the stability and MT occupancy of K-fibres. In particular, electron tomography could be used to investigate the ultrastructural organisation of K-fibres in Affimer expressing cells where ch-TOG is specifically excluded from the 'mesh' (Nixon et al. 2015).

It is puzzling why a reduction in spindle ch-TOG was observed in almost all E7 and E8 cells, while PCM fragmentation and a metaphase delay was observed in only a population of cells. This would suggest that in the absence of spindle ch-TOG, other proteins are able to compensate for its loss. Alternatively, it could mean that the affinity of the Affimers used here is suboptimal. In other words, they do not fully disrupt the TACC3–ch-TOG interaction in living cells and a more severe phenotype could be observed with higher affinity reagents. However, only a small increase in the number of cells containing fragmented PCM was observed in cells expressing a mutant of ch-TOG deficient in binding TACC3 (36%) compared to cells expressing E7 (30.4%) or E8 (33.3%) Affimers. It is therefore more likely that in HeLa cells, disruption of TACC3–ch-TOG makes cells more susceptible to this phenotype.

An interesting possibility is that in cells where TACC3–ch-TOG is compromised, TACC1 and TACC2, the other members of the TACC family that all share the conserved C-terminal coiled-coil TACC domain, could compensate for the lack of TACC3 function. This is plausible given that the transcripts encoding both proteins are expressed in HeLa cells (TACC1: https://www.proteinatlas.org/

ENSG00000147526-TACC1/cell+line; TACC2: https://www.proteinatlas.org/ENSG00000138162-TACC2/cell+line). Moreover, early work found that TACC1 and TACC2 show a similar localisation to TACC3 in mitotic HeLa cells, though TACC3 is more strongly expressed on the spindle MTs (Gergely et al. 2000a). To determine if a more severe phenotype is observed in cells lacking TACC1 and TACC2, future experiments could use siRNA to deplete endogenous TACC1 and TACC2 and express Affimers targetting TACC3.

Does the PCM fragmentation phenotype lead to a mitotic delay, or is it a consequence of one? Future work is needed to formally address this point, however, it is unlikely that a mitotic delay is the cause of PCM fragmentation, as metaphase delay induced by the proteasome inhibitor MG132, does not cause PCM fragmentation in HeLa cells (Sapkota et al. 2020). It is therefore more likely that disruption of TACC3–ch-TOG via the Affimer, leads to compromised PCM integrity that is susceptible to fragmentation during mitotic delay. Mechanistic details to explain the PCM fragmentation observed in this study, and indeed the literature, are currently lacking (Maiato and Logarinho 2014). However, it is reasonable to suggest that an imbalance of MT-generated forces is a contributing factor. To formally test this, future experiments should investigate the effect of inactivating centrosome-directed forces, for example via inhibition of Eg5, as has been performed in similar studies (Asteriti et al. 2014). Moreover, previous work has described a PCM fragmentation phenotype in Augmin defective cells, that was explained by a concomitant loss of kinetochore MTs and a suspected imbalance of forces within the spindle (Lawo et al. 2009). Given that the TACC3 Affimers were found to exclude ch-TOG from the spindle MTs in my experiments, it is possible that there is a decrease in K-fibre stability in these cells that could also lead to an imbalance of forces causing PCM fragmentation.

Based on the data generated in this thesis and what is currently known, we propose that TACC3 is required to 'activate' ch-TOG activity to stabilise centrosome MTs. In absence of the TACC3–ch-TOG interaction, ch-TOG is still localised to the mitotic centrosome, but is not 'activated' by TACC3. In turn, cells are more susceptible to PCM fragmentation during metaphase. This is in line with a previous finding that *in vitro*, the presence of Maskin (TACC3) enhanced the pelleting of XMAP215 (ch-TOG) with MTs (Peset et al. 2005). Of note, a similar PCM fragmentation phenotype to the one observed in my experiments was previously reported by De Luca and colleagues (De Luca et al. 2008). Here they showed that PCM fragmentation occurs in Aurora A-depleted mitotic cells and correlates with an increase in ch-TOG and a decrease in MCAK at the spindle poles. Given that previous work has identified that TACC3 binds

Aurora A and enhances its kinase activity (Burgess et al. 2015), it is plausible that the Affimers could be blocking or weakening this event. Therefore, the PCM fragmentation phenotype observed in my experiments could also be explained by a reduction in Aurora A activity. Although my experiments found no change in the localisation of ch-TOG at the spindle poles of cells expressing TACC3 Affimers, a future experiment to investigate the localisation of its functional antagonist, MCAK, should be performed.

Alternatively, TACC3–ch-TOG could form a structural lattice at the centrosome that functions to maintain the integrity of spindle poles, as was suggested following early work in HeLa cells (Gergely et al. 2003). In this sense, it is likely that TACC3–ch-TOG are part of a larger complex that functions to support spindle pole integrity, where TACC3–ch-TOG act as a scaffold to recruit other PCM proteins. To investigate this, protein-protein interactions of TACC3 and/or ch-TOG could be determined in cells expressing Affimers and compared to control cells, for example by BioID and subsequent analysis by mass spectrometry (Roux et al. 2018). In this regard, it is tempting to speculate that TACC3–ch-TOG could contribute to the suggested liquid-like nature of the mitotic PCM (Woodruff et al. 2017; Woodruff 2021). This is plausible, since TACC3 has been described to be a core component of the recently identified liquid-like meiotic spindle domain in mammalian oocytes, that forms by phase separation (So et al. 2019). Moreover, TACC3 has been shown to self-assemble into liquid-like droplets in the presence of polyethylene glycol *in vitro* (So et al. 2019).

5.1.3 Affimers targeting TACC3–clathrin

Given that a handful of the clathrin Affimers screened in this thesis were found to bind clathrin in cells, it was disappointing that no phenotype was observed during mitosis or interphase. Nonetheless, the TACC3–clathrin interaction site, or the subsequent MT binding surface, remains an attractive site to target in a cancer context. However, developing mitosis-specific inhibitors of clathrin is not without its challenges, especially given that auxilin is predicted to bind at the same site on the ankle as TACC3 (Burgess et al. 2018). For this reason, developing inhibitors against TACC3 to block an interaction with clathrin may be more appropriate. Alternatively, inhibitors could be developed to disrupt the interaction between TACC3–clathrin and the MTs. For this, an ultrastructural understanding of the MT interface formed by TACC3–clathrin is required.

5.2 The use of Affimers as a tool to study cell biology

The work in this thesis, and previous published works, has demonstrated the use of Affimers to study protein function. However, a current limitation is the lack of temporal control over their use. To circumvent this, a tether-and-release system could be employed, such as the rapamycin activated protease through induced dimerisation and release of tethered cargo (RAPID-release) method, that has previously been developed to study the nuclear import dynamics of newly synthesised histones (Apta-Smith et al. 2018). With this system, Affimers could be tethered to the mitochondria and upon the addition of rapamycin, the auto-inhibited TVMV protease would be recruited to the mitochondria and activated, thus releasing the Affimers to inhibit the desired protein-protein interaction. If release of the tethered Affimers could be achieved in the timescale of minutes as previously described for histones (Apta-Smith et al. 2018), it would enable temporal inhibition of protein complexes during defined stages of mitosis.

As observed with the clathrin Affimers in this thesis, they may bind the protein of interest but may not sufficiently inhibit the intended interaction. Though not determined in this thesis, a likely reason for the lack of effect is a low binding affinity. Therefore, a key challenge is the identification of high-affinity Affimer reagents that will abolish the interaction of strong protein-protein interactions. Similarly, although Affimers have previously been reported as tools to visualise endogenous proteins (Tiede et al. 2017; Lopata et al. 2018), the Affimers developed in this thesis were not suitable for this purpose, suggesting that this could be dependent on the target protein.

The work with TACC3 Affimers presented in this thesis has demonstrated that Affimers can be used as tools to dissect a multiprotein complex in living cells, achieving specific inhibition of TACC3–ch-TOG while leaving the other interactions within the TACC3–ch-TOG–clathrin–GTSE1 complex intact. Moreover, given the short time required to screen and identify Affimer reagents to a protein of interest, they provide an attractive alternative to antibody-based scaffolds to gain biological insight into protein-protein interactions in cells. To further increase the functionality of Affimers as research tools, future work could investigate the option to fuse them with E3 ligase ligands for use as specific protein degraders, in the same way as PROTACs (Burslem and Crews 2020). Finally, given that Affimers are genetically encoded, small proteins (12 kDa) with high stability, they may serve as a useful tool in therapeutic applications of the future.

Bibliography

Akhmanova, A. and M. O. Steinmetz (2015). 'Control of Microtubule Organization and Dynamics: Two Ends in the Limelight'. *Nat Rev Mol Cell Biol* 16.12, pp. 711–726. DOI: 10.1038/nrm4084.

Applegate, K. T., S. Besson, A. Matov, M. H. Bagonis, K. Jaqaman and G. Danuser (2011). 'PlusTipTracker: Quantitative Image Analysis Software for the Measurement of Microtubule Dynamics'. *Journal of Structural Biology* 176.2, pp. 168–184. DOI: 10.1016/j.jsb.2011.07.009.

Apta-Smith, M. J., J. R. Hernandez-Fernaud and A. J. Bowman (2018). 'Evidence for the Nuclear Import of Histones H3.1 and H4 as Monomers'. *EMBO J* 37.19, e98714. DOI: 10.15252/embj.201798714.

Asbury, C. L. (2017). 'Anaphase A: Disassembling Microtubules Move Chromosomes toward Spindle Poles'. *Biology (Basel)* 6.1, p. 15. DOI: 10.3390/biology6010015.

Asteriti, I. A., E. Di Cesare, F. De Mattia, V. Hilsenstein, B. Neumann, E. Cundari, P. Lavia and G. Guarguaglini (2014). 'The Aurora-A Inhibitor MLN8237 Affects Multiple Mitotic Processes and Induces Dose-Dependent Mitotic Abnormalities and Aneuploidy'. *Oncotarget* 5.15, pp. 6229–6242. DOI: 10.18632/oncotarget.2190.

Ayaz, P., S. Munyoki, E. A. Geyer, F.-A. Piedra, E. S. Vu, R. Bromberg, Z. Otwinowski, N. V. Grishin, C. A. Brautigam and L. M. Rice (2014). 'A Tethered Delivery Mechanism Explains the Catalytic Action of a Microtubule Polymerase'. *Elife* 3, e03069. DOI: 10.7554/eLife.03069.

Banani, S. F., H. O. Lee, A. A. Hyman and M. K. Rosen (2017). 'Biomolecular Condensates: Organizers of Cellular Biochemistry'. *Nat Rev Mol Cell Biol* 18.5, pp. 285–298. DOI: 10.1038/nrm.2017.7.

Barr, A. R. and C. Bakal (2015). 'A Sensitised RNAi Screen Reveals a Ch-TOG Genetic Interaction Network Required for Spindle Assembly'. *Sci Rep* 5.1, p. 10564. DOI: 10.1038/srep10564.

Barr, A. R. and F. Gergely (2007). 'Aurora-A: The Maker and Breaker of Spindle Poles'. *J Cell Sci* 120.Pt 17, pp. 2987–2996. DOI: 10.1242/jcs.013136.

Barros, T. P., K. Kinoshita, A. A. Hyman and J. W. Raff (2005). 'Aurora A Activates D-TACC–Msps Complexes Exclusively at Centrosomes to Stabilize Centrosomal Microtubules'. *Journal of Cell Biology* 170.7, pp. 1039–1046. DOI: 10.1083/jcb.200504097.

Beghein, E. and J. Gettemans (2017). 'Nanobody Technology: A Versatile Toolkit for Microscopic Imaging, Protein-Protein Interaction Analysis, and Protein Function Exploration'. *Front Immunol* 8, p. 771. DOI: 10.3389/fimmu.2017.00771.

Bendre, S., A. Rondelet, C. Hall, N. Schmidt, Y. C. Lin, G. J. Brouhard and A. W. Bird (2016). 'GTSE1 Tunes Microtubule Stability for Chromosome Alignment and Segregation by Inhibiting the Microtubule Depolymerase MCAK'. *Journal of Cell Biology* 215.5, pp. 631–647. DOI: 10.1083/jcb.201606081.

Bethuyne, J., S. De Gieter, O. Zwaenepoel, A. Garcia-Pino, K. Durinck, A. Verhelle, G. Hassanzadeh-Ghassabeh, F. Speleman, R. Loris and J. Gettemans (2014). 'A Nanobody Modulates the P53 Transcriptional Program without Perturbing Its Functional Architecture'. *Nucleic Acids Res* 42.20, pp. 12928–12938. DOI: 10.1093/nar/gku962.

Booth, D. G., F. E. Hood, I. A. Prior and S. J. Royle (2011). 'A TACC3/Ch-TOG/Clathrin Complex Stabilises Kinetochore Fibres by Inter-Microtubule Bridging'. *EMBO Journal* 30.5, pp. 906–919. DOI: 10.1038/emboj.2011.15.

Borisy, G. G. and E. W. Taylor (1967). 'The Mechanism of Action of Colchicine. Colchicine Binding to Sea Urchin Eggs and the Mitotic Apparatus'. *J Cell Biol* 34.2, pp. 535–548. DOI: 10.1083/jcb.34.2.535.

Brouhard, G. J., J. H. Stear, T. L. Noetzel, J. Al-Bassam, K. Kinoshita, S. C. Harrison, J. Howard and A. A. Hyman (2008). 'XMAP215 Is a Processive Microtubule Polymerase.' *Cell* 132.1, pp. 79–88. DOI: 10.1016/j.cell.2007.11.043.

Buckley, D. L., K. Raina, N. Darricarrere, J. Hines, J. L. Gustafson, I. E. Smith, A. H. Miah, J. D. Harling and C. M. Crews (2015). 'HaloPROTACS: Use of Small Molecule PROTACs to Induce Degradation of HaloTag Fusion Proteins'. *ACS Chem Biol* 10.8, pp. 1831–1837. DOI: 10.1021/acschembio.5b00442.

Burgess, S. G., I. Peset, N. Joseph, T. Cavazza, I. Vernos, M. Pfuhl, F. Gergely and R. Bayliss (2015). 'Aurora-A-Dependent Control of TACC3 Influences the Rate of Mitotic Spindle Assembly'. *PLoS Genetics* 11.7. DOI: 10.1371/journal.pgen.1005345.

Burgess, S. G., M. Mukherjee, S. Sabir, N. Joseph, C. Gutiérrez-Caballero, M. W. Richards, N. Huguenin-Dezot, J. W. Chin, E. J. Kennedy, M. Pfuhl, S. J. Royle, F. Gergely and R. Bayliss (2018). 'Mitotic Spindle Association of TACC3

Requires Aurora-A-dependent Stabilization of a Cryptic *A*-helix'. *The EMBO Journal*, e97902–e97902. DOI: 10.15252/embj.201797902.

Burslem, G. M. and C. M. Crews (2020). 'Proteolysis-Targeting Chimeras as Therapeutics and Tools for Biological Discovery'. *Cell* 181.1, pp. 102–114. DOI: 10.1016/j.cell.2019.11.031.

Carlier, M. F. and D. Pantaloni (1981). 'Kinetic Analysis of Guanosine 5'-Triphosphate Hydrolysis Associated with Tubulin Polymerization'. *Biochemistry* 20.7, pp. 1918–1924. DOI: 10.1021/bi00510a030.

Carlton, J. G. and J. Martin-Serrano (2007). 'Parallels between Cytokinesis and Retroviral Budding: A Role for the ESCRT Machinery'. *Science* 316.5833, pp. 1908–1912. DOI: 10.1126/science.1143422.

Cassimeris, L. and J. Morabito (2004). 'TOGp, the Human Homolog of XMAP215/Dis1, Is Required for Centrosome Integrity, Spindle Pole Organization, and Bipolar Spindle Assembly'. *MBoC* 15.4, pp. 1580–1590. DOI: 10.1091/mbc.e03-07-0544.

Caussinus, E., O. Kanca and M. Affolter (2011). 'Fluorescent Fusion Protein Knockout Mediated by Anti-GFP Nanobody'. *Nat Struct Mol Biol* 19.1, pp. 117–121. DOI: 10.1038/nsmb.2180.

Charrasse, S., M. Mazel, S. Taviaux, P. Berta, T. Chow and C. Larroque (1995). 'Characterization of the cDNA and Pattern of Expression of a New Gene Over-Expressed in Human Hepatomas and Colonic Tumors'. *Eur J Biochem* 234.2, pp. 406–413. DOI: 10.1111/j.1432-1033.1995.406_b.x.

Cheeseman, I. M. (2014). 'The Kinetochore'. *Cold Spring Harb Perspect Biol* 6.7, a015826. DOI: 10.1101/cshperspect.a015826.

Cheeseman, L. P., E. F. Harry, A. D. McAinsh, I. A. Prior and S. J. Royle (2013). 'Specific Removal of TACC3-ch-TOG-clathrin at Metaphase Deregulates Kinetochore Fiber Tension'. *Journal of Cell Science* 126.9, pp. 2102–2113. DOI: 10.1242/jcs.124834.

Cheeseman, L. P., D. G. Booth, F. E. Hood, I. A. Prior and S. J. Royle (2011). 'Aurora A Kinase Activity Is Required for Localization of TACC3/Ch-TOG/Clathrin Inter-Microtubule Bridges.' *Communicative & integrative biology* 4.4, pp. 409–12. DOI: 10.4161/cib.4.4.15250.

Choi, Y.-K., P. Liu, S. K. Sze, C. Dai and R. Z. Qi (2010). 'CDK5RAP2 Stimulates Microtubule Nucleation by the Gamma-Tubulin Ring Complex'. *J Cell Biol* 191.6, pp. 1089–1095. DOI: 10.1083/jcb.201007030.

Clift, D., W. A. McEwan, L. I. Labzin, V. Konieczny, B. Mogessie, L. C. James and M. Schuh (2017). 'A Method for the Acute and Rapid Degradation of Endogenous Proteins'. *Cell* 171.7, 1692–1706.e18. DOI: 10.1016/j.cell.2017.10.033.

Conduit, P. T., A. Wainman and J. W. Raff (2015). 'Centrosome Function and Assembly in Animal Cells'. *Nat Rev Mol Cell Biol* 16.10, pp. 611–624. DOI: 10.1038/nrm4062.

Cullen, C. F. and H. Ohkura (2001). 'Msps Protein Is Localized to Acentrosomal Poles to Ensure Bipolarity of Drosophila Meiotic Spindles'. *Nat Cell Biol* 3.7, pp. 637–642. DOI: 10.1038/35083025.

Daniel, K., J. Icha, C. Horenburg, D. Müller, C. Norden and J. Mansfeld (2018). 'Conditional Control of Fluorescent Protein Degradation by an Auxin-Dependent Nanobody'. *Nat Commun* 9.1, p. 3297. DOI: 10.1038/s41467-018-05855-5.

Day, C. A., J. Hornick, A. Langfald, C. Mader and E. H. Hinchcliffe (2018). 'Microsurgery and Microinjection Techniques in Mitosis Research'. *Methods Cell Biol* 145, pp. 159–172. DOI: 10.1016/bs.mcb.2018.03.020.

De Luca, M., L. Brunetto, I. A. Asteriti, M. Giubettini, P. Lavia and G. Guarguaglini (2008). 'Aurora-A and Ch-TOG Act in a Common Pathway in Control of Spindle Pole Integrity'. *Oncogene* 27.51, pp. 6539–6549. DOI: 10.1038/onc.2008.252.

Edeling, M. A., S. K. Mishra, P. A. Keyel, A. L. Steinhauser, B. M. Collins, R. Roth, J. E. Heuser, D. J. Owen and L. M. Traub (2006). 'Molecular Switches Involving the AP-2 Beta2 Appendage Regulate Endocytic Cargo Selection and Clathrin Coat Assembly'. *Dev Cell* 10.3, pp. 329–342. DOI: 10.1016/j.devcel.2006.01.016.

Enos, S. J., M. Dressler, B. F. Gomes, A. A. Hyman and J. B. Woodruff (2018). 'Phosphatase PP2A and Microtubule-Mediated Pulling Forces Disassemble Centrosomes during Mitotic Exit'. *Biol Open* 7.1, bio029777. DOI: 10.1242/bio.029777.

Erdogan, B., G. M. Cammarata, E. J. Lee, B. C. Pratt, A. F. Francl, E. L. Rutherford and L. A. Lowery (2017). 'The Microtubule Plus-End-Tracking Protein TACC3 Promotes Persistent Axon Outgrowth and Mediates Responses to Axon Guidance Signals during Development'. *Neural Dev* 12. DOI: 10.1186/s13064-017-0080-7.

Evans, T., E. T. Rosenthal, J. Youngblom, D. Distel and T. Hunt (1983). 'Cyclin: A Protein Specified by Maternal mRNA in Sea Urchin Eggs That Is Destroyed at Each Cleavage Division'. *Cell* 33.2, pp. 389–396. DOI: 10.1016/0092-8674(83)90420-8.

Farache, D., L. Emorine, L. Haren and A. Merdes (2018). 'Assembly and Regulation of γ-Tubulin Complexes'. *Open Biol* 8.3, p. 170266. DOI: 10.1098/rsob.170266.

Fielding, A. B., S. Lim, K. Montgomery, I. Dobreva and S. Dedhar (2011). 'A Critical Role of Integrin-Linked Kinase, Ch-TOG and TACC3 in Centrosome Clustering in Cancer Cells'. *Oncogene* 30.5, pp. 521–534. DOI: 10.1038/onc.2010.431.

Fielding, A. B. and S. J. Royle (2013). 'Mitotic Inhibition of Clathrin-Mediated Endocytosis'. *Cell Mol Life Sci* 70.18, pp. 3423–3433. DOI: 10.1007/s00018-012-1250-8.

Fire, A., S. Xu, M. K. Montgomery, S. A. Kostas, S. E. Driver and C. C. Mello (1998). 'Potent and Specific Genetic Interference by Double-Stranded RNA in Caenorhabditis Elegans'. *Nature* 391.6669, pp. 806–811. DOI: 10.1038/35888.

Fotin, A., Y. Cheng, N. Grigorieff, T. Walz, S. C. Harrison and T. Kirchhausen (2004). 'Structure of an Auxilin-Bound Clathrin Coat and Its Implications for the Mechanism of Uncoating'. *Nature* 432.7017, pp. 649–653. DOI: 10.1038/nature03078.

Fry, A. M., J. Sampson, C. Shak and S. Shackleton (2017). 'Recent Advances in Pericentriolar Material Organization: Ordered Layers and Scaffolding Gels'. *F1000Res* 6, p. 1622. DOI: 10.12688/f1000research.11652.1.

Fu, W., W. Tao, P. Zheng, J. Fu, M. Bian, Q. Jiang, P. R. Clarke and C. Zhang (2010). 'Clathrin Recruits Phosphorylated TACC3 to Spindle Poles for Bipolar Spindle Assembly and Chromosome Alignment'. *J Cell Sci* 123.Pt 21, pp. 3645–3651. DOI: 10.1242/jcs.075911.

Furey, C., V. Jovasevic and D. Walsh (2020). 'TACC3 Regulates Microtubule Plus-End Dynamics and Cargo Transport in Interphase Cells'. *Cell Reports* 30.1, 269–283.e6. DOI: 10.1016/j.celrep.2019.12.025.

Gard, D. L. and M. W. Kirschner (1987). 'A Microtubule-Associated Protein from Xenopus Eggs That Specifically Promotes Assembly at the plus-End'. *J Cell Biol* 105.5, pp. 2203–2215. DOI: 10.1083/jcb.105.5.2203.

Gard, D. L., B. E. Becker and S. Josh Romney (2004). 'MAPping the Eukaryotic Tree of Life: Structure, Function, and Evolution of the MAP215/Dis1 Family of Microtubule-Associated Proteins'. *Int Rev Cytol* 239, pp. 179–272. DOI: 10.1016/S0074-7696(04)39004-2.

Gergely, F., V. M. Draviam and J. W. Raff (2003). 'The Ch-TOG/XMAP215 Protein Is Essential for Spindle Pole Organization in Human Somatic Cells'. *Genes Dev* 17.3, pp. 336–341. DOI: 10.1101/gad.245603.

Gergely, F., C. Karlsson, I. Still, J. Cowell, J. Kilmartin and J. W. Raff (2000a). 'The TACC Domain Identifies a Family of Centrosomal Proteins That Can Interact with Microtubules'. *Proc Natl Acad Sci U S A* 97.26, pp. 14352–14357. DOI: 10.1073/pnas.97.26.14352.

Gergely, F., D. Kidd, K. Jeffers, J. G. Wakefield and J. W. Raff (2000b). 'D-TACC: A Novel Centrosomal Protein Required for Normal Spindle Function in the Early Drosophila Embryo.' *The EMBO journal* 19.2, pp. 241–52. DOI: 10.1093/emboj/19.2.241.

Glotzer, M. (2017). 'Cytokinesis in Metazoa and Fungi'. *Cold Spring Harb Perspect Biol* 9.10, a022343. DOI: 10.1101/cshperspect.a022343.

Godinho, S. A. and D. Pellman (2014). 'Causes and Consequences of Centrosome Abnormalities in Cancer'. *Philos Trans R Soc Lond B Biol Sci* 369.1650, p. 20130467. DOI: 10.1098/rstb.2013.0467.

Grimaldi, A. D., M. Fomicheva and I. Kaverina (2013). 'Ice Recovery Assay for Detection of Golgi-Derived Microtubules'. *Methods Cell Biol* 118, pp. 401–415. DOI: 10.1016/B978-0-12-417164-0.00024-0.

Gudimchuk, N. B. and J. R. McIntosh (2021). 'Regulation of Microtubule Dynamics, Mechanics and Function through the Growing Tip'. *Nat Rev Mol Cell Biol*. DOI: 10.1038/s41580-021-00399-x.

Guglielmi, L. and P. Martineau (2009). 'Intrabody Expression in Eukaryotic Cells'. *Methods Mol Biol* 562, pp. 195–203. DOI: 10.1007/978-1-60327-302-2_15.

Gulluni, F., M. Martini, M. C. De Santis, C. C. Campa, A. Ghigo, J. P. Margaria, E. Ciraolo, I. Franco, U. Ala, L. Annaratone, D. Disalvatore, G. Bertalot, G. Viale, A. Noatynska, M. Compagno, S. Sigismund, F. Montemurro, M. Thelen, F. Fan, P. Meraldi, C. Marchiò, S. Pece, A. Sapino, R. Chiarle, P. P. Di Fiore and E. Hirsch (2017). 'Mitotic Spindle Assembly and Genomic Stability in Breast Cancer Require PI3K-C2α Scaffolding Function'. *Cancer Cell* 32.4, 444–459.e7. DOI: 10.1016/j.ccell.2017.09.002.

Guo, Y., C. L. Partch, J. Key, P. B. Card, V. Pashkov, A. Patel, R. K. Bruick, H. Wurdak and K. H. Gardner (2013). 'Regulating the ARNT/TACC3 Axis: Multiple Approaches to Manipulating Protein/Protein Interactions with Small Molecules'. *ACS Chem Biol* 8.3, pp. 626–635. DOI: 10.1021/cb300604u.

Gutierrez-Caballero, C., S. G. Burgess, R. Bayliss and S. J. Royle (2015). 'TACC3-ch-TOG Track the Growing Tips of Microtubules Independently of Clathrin and Aurora-A Phosphorylation'. *Biology Open* 4.2, pp. 170–179. DOI: 10.1242/bio.201410843.

Hamers-Casterman, C., T. Atarhouch, S. Muyldermans, G. Robinson, C. Hamers, E. B. Songa, N. Bendahman and R. Hamers (1993). 'Naturally Occurring Antibodies Devoid of Light Chains'. *Nature* 363.6428, pp. 446–448. DOI: 10.1038/363446a0.

Hartwell, L. H., J. Culotti and B. Reid (1970). 'Genetic Control of the Cell-Division Cycle in Yeast. I. Detection of Mutants'. *Proc Natl Acad Sci U S A* 66.2, pp. 352–359. DOI: 10.1073/pnas.66.2.352.

Hayashi, I. and M. Ikura (2003). 'Crystal Structure of the Amino-Terminal Microtubule-Binding Domain of End-Binding Protein 1 (EB1)'. *J Biol Chem* 278.38, pp. 36430–36434. DOI: 10.1074/jbc.M305773200.

Hepler, P. K., J. R. McIntosh and S. Cleland (1970). 'Intermicrotubule Bridges in Mitotic Spindle Apparatus'. *J Cell Biol* 45.2, pp. 438–444. DOI: 10.1083/jcb.45.2.438.

Herman, J. A., M. P. Miller and S. Biggins (2020). 'chTOG Is a Conserved Mitotic Error Correction Factor'. *Elife* 9, e61773. DOI: 10.7554/eLife.61773.

Hirst, J. and M. S. Robinson (1998). 'Clathrin and Adaptors'. *Biochim Biophys Acta* 1404.1-2, pp. 173–193. DOI: 10.1016/s0167-4889(98)00056-1.

Holder, J., E. Poser and F. A. Barr (2019). 'Getting out of Mitosis: Spatial and Temporal Control of Mitotic Exit and Cytokinesis by PP1 and PP2A'. *FEBS Lett* 593.20, pp. 2908–2924. DOI: 10.1002/1873-3468.13595.

Holland, A. J., D. Fachinetti, J. S. Han and D. W. Cleveland (2012). 'Inducible, Reversible System for the Rapid and Complete Degradation of Proteins in Mammalian Cells'. *Proc Natl Acad Sci U S A* 109.49, E3350–3357. DOI: 10.1073/pnas.1216880109.

Honnappa, S., S. M. Gouveia, A. Weisbrich, F. F. Damberger, N. S. Bhavesh, H. Jawhari, I. Grigoriev, F. J. A. van Rijssel, R. M. Buey, A. Lawera, I. Jelesarov, F. K. Winkler, K. Wüthrich, A. Akhmanova and M. O. Steinmetz (2009). 'An EB1-binding Motif Acts as a Microtubule Tip Localization Signal'. *Cell* 138.2, pp. 366–376. DOI: 10.1016/j.cell.2009.04.065.

Hood, F. E. and S. J. Royle (2009). 'Functional Equivalence of the Clathrin Heavy Chains CHC17 and CHC22 in Endocytosis and Mitosis'. *J Cell Sci* 122.Pt 13, pp. 2185–2190. DOI: 10.1242/jcs.046177.

Hood, F. E., S. J. Williams, S. G. Burgess, M. W. Richards, D. Roth, A. Straube, M. Pfuhl, R. Bayliss and S. J. Royle (2013). 'Coordination of Adjacent Domains Mediates TACC3-ch-TOG-clathrin Assembly and Mitotic Spindle Binding'. *Journal of Cell Biology* 202.3, pp. 463–478. DOI: 10.1083/jcb.201211127.

Hopkins, A. L. and C. R. Groom (2002). 'The Druggable Genome'. *Nat Rev Drug Discov* 1.9, pp. 727–730. DOI: 10.1038/nrd892.

Hubner, N. C., A. W. Bird, J. Cox, B. Splettstoesser, P. Bandilla, I. Poser, A. Hyman and M. Mann (2010). 'Quantitative Proteomics Combined with BAC TransgeneOmics Reveals in Vivo Protein Interactions.' *The Journal of cell biology* 189.4, pp. 739–54. DOI: 10.1083/jcb.200911091.

Hwang, H. C. and B. E. Clurman (2005). 'Cyclin E in Normal and Neoplastic Cell Cycles'. *Oncogene* 24.17, pp. 2776–2786. DOI: 10.1038/sj.onc.1208613.

Kanaseki, T. and K. Kadota (1969). 'The "Vesicle in a Basket". A Morphological Study of the Coated Vesicle Isolated from the Nerve Endings of the Guinea Pig

Brain, with Special Reference to the Mechanism of Membrane Movements'. *J Cell Biol* 42.1, pp. 202–220. DOI: 10.1083/jcb.42.1.202.

Kastan, M. B. and J. Bartek (2004). 'Cell-Cycle Checkpoints and Cancer'. *Nature* 432.7015, pp. 316–323. DOI: 10.1038/nature03097.

Khodjakov, A. and C. L. Rieder (1999). 'The Sudden Recruitment of Gamma-Tubulin to the Centrosome at the Onset of Mitosis and Its Dynamic Exchange throughout the Cell Cycle, Do Not Require Microtubules'. *J Cell Biol* 146.3, pp. 585–596. DOI: 10.1083/jcb.146.3.585.

Kiewisz, R., G. Fabig, W. Conway, D. Needleman and T. Müller-Reichert (2021). *Three-Dimensional Structure of the Kinetochore-Fibers in Human Mitotic Spindles*. DOI: 10.1101/2021.11.13.468347.

Kinoshita, K., T. L. Noetzel, L. Pelletier, K. Mechtler, D. N. Drechsel, A. Schwager, M. Lee, J. W. Raff and A. A. Hyman (2005). 'Aurora A Phosphorylation of TACC3/Maskin Is Required for Centrosome-Dependent Microtubule Assembly in Mitosis'. *J Cell Biol* 170.7, pp. 1047–1055. DOI: 10.1083/jcb.200503023.

Kirchhausen, T. and S. C. Harrison (1981). 'Protein Organization in Clathrin Trimers'. *Cell* 23.3, pp. 755–761. DOI: 10.1016/0092-8674(81)90439-6.

Köhler, G. and C. Milstein (1975). 'Continuous Cultures of Fused Cells Secreting Antibody of Predefined Specificity'. *Nature* 256.5517, pp. 495–497. DOI: 10.1038/256495a0.

Küey, C., G. Larocque, N. I. Clarke and S. J. Royle (2019). 'Unintended Perturbation of Protein Function Using GFP Nanobodies in Human Cells'. *J Cell Sci* 132.21, jcs234955. DOI: 10.1242/jcs.234955.

Lane, H. A. and E. A. Nigg (1996). 'Antibody Microinjection Reveals an Essential Role for Human Polo-like Kinase 1 (Plk1) in the Functional Maturation of Mitotic Centrosomes'. *J Cell Biol* 135.6 Pt 2, pp. 1701–1713. DOI: 10.1083/jcb.135.6.1701.

Lawo, S., M. Bashkurov, M. Mullin, M. G. Ferreria, R. Kittler, B. Habermann, A. Tagliaferro, I. Poser, J. R. A. Hutchins, B. Hegemann, D. Pinchev, F. Buchholz, J.-M. Peters, A. A. Hyman, A.-C. Gingras and L. Pelletier (2009). 'HAUS, the 8-Subunit Human Augmin Complex, Regulates Centrosome and Spindle Integrity'. *Curr Biol* 19.10, pp. 816–826. DOI: 10.1016/j.cub.2009.04.033.

Ledbetter, M. C. and K. R. Porter (1963). 'A "MICROTUBULE" IN PLANT CELL FINE STRUCTURE'. *J Cell Biol* 19.1, pp. 239–250. DOI: 10.1083/jcb.19.1.239.

Lee, K.-Y., T. Davies and M. Mishima (2012). 'Cytokinesis Microtubule Organisers at a Glance'. *J Cell Sci* 125.Pt 15, pp. 3495–3500. DOI: 10.1242/jcs.094672.

Lee, K. and K. Rhee (2011). 'PLK1 Phosphorylation of Pericentrin Initiates Centrosome Maturation at the Onset of Mitosis'. *J Cell Biol* 195.7, pp. 1093–1101. DOI: 10.1083/jcb.201106093.

Lee, M. J., F. Gergely, K. Jeffers, S. Y. Peak-Chew and J. W. Raff (2001). 'Msps/XMAP215 Interacts with the Centrosomal Protein D-TACC to Regulate Microtubule Behaviour'. *Nature Cell Biology* 3.7, pp. 643–649. DOI: 10.1038/35083033.

Lens, S. M. A. and R. H. Medema (2019). 'Cytokinesis Defects and Cancer'. *Nat Rev Cancer* 19.1, pp. 32–45. DOI: 10.1038/s41568-018-0084-6.

LeRoy, P. J., J. J. Hunter, K. M. Hoar, K. E. Burke, V. Shinde, J. Ruan, D. Bowman, K. Galvin and J. A. Ecsedy (2007). 'Localization of Human TACC3 to Mitotic Spindles Is Mediated by Phosphorylation on Ser558 by Aurora A: A Novel Pharmacodynamic Method for Measuring Aurora A Activity'. *Cancer Res* 67.11, pp. 5362–5370. DOI: 10.1158/0008-5472.CAN-07-0122.

Lin, C. H., C. K. Hu and H. M. Shih (2010). 'Clathrin Heavy Chain Mediates TACC3 Targeting to Mitotic Spindles to Ensure Spindle Stability'. *Journal of Cell Biology* 189.7, pp. 1097–1105. DOI: 10.1083/jcb.200911120.

Lopata, A., R. Hughes, C. Tiede, S. M. Heissler, J. R. Sellers, P. J. Knight, D. Tomlinson and M. Peckham (2018). 'Affimer Proteins for F-actin: Novel Affinity Reagents That Label F-actin in Live and Fixed Cells'. *Scientific Reports* 8.1, pp. 1–15. DOI: 10.1038/s41598-018-24953-4.

Los, G. V., L. P. Encell, M. G. McDougall, D. D. Hartzell, N. Karassina, C. Zimprich, M. G. Wood, R. Learish, R. F. Ohana, M. Urh, D. Simpson, J. Mendez, K. Zimmerman, P. Otto, G. Vidugiris, J. Zhu, A. Darzins, D. H. Klaubert, R. F. Bulleit and K. V. Wood (2008). 'HaloTag: A Novel Protein Labeling Technology for Cell Imaging and Protein Analysis'. *ACS Chem Biol* 3.6, pp. 373–382. DOI: 10.1021/cb800025k.

Lu, R.-M., Y.-C. Hwang, I.-J. Liu, C.-C. Lee, H.-Z. Tsai, H.-J. Li and H.-C. Wu (2020). 'Development of Therapeutic Antibodies for the Treatment of Diseases'. *J Biomed Sci* 27.1, p. 1. DOI: 10.1186/s12929-019-0592-z.

Mabuchi, I. and M. Okuno (1977). 'The Effect of Myosin Antibody on the Division of Starfish Blastomeres'. *J Cell Biol* 74.1, pp. 251–263. DOI: 10.1083/jcb.74.1.251.

Mack, G. J. and D. A. Compton (2001). 'Analysis of Mitotic Microtubule-Associated Proteins Using Mass Spectrometry Identifies Astrin, a Spindle-Associated Protein'. *Proc Natl Acad Sci U S A* 98.25, pp. 14434–14439. DOI: 10.1073/pnas.261371298.

Maiato, H., A. M. Gomes, F. Sousa and M. Barisic (2017). 'Mechanisms of Chromosome Congression during Mitosis'. *Biology (Basel)* 6.1, E13. DOI: 10.3390/biology6010013.

Maiato, H. and E. Logarinho (2014). 'Mitotic Spindle Multipolarity without Centrosome Amplification'. *Nat Cell Biol* 16.5, pp. 386–394. DOI: 10.1038/ncb2958.

Maiato, H., C. L. Rieder and A. Khodjakov (2004). 'Kinetochore-Driven Formation of Kinetochore Fibers Contributes to Spindle Assembly during Animal Mitosis'. *J Cell Biol* 167.5, pp. 831–840. DOI: 10.1083/jcb.200407090.

Malumbres, M. and M. Barbacid (2005). 'Mammalian Cyclin-Dependent Kinases'. *Trends Biochem Sci* 30.11, pp. 630–641. DOI: 10.1016/j.tibs.2005.09.005.

Mastronarde, D. N., K. L. McDonald, R. Ding and J. R. McIntosh (1993). 'Interpolar Spindle Microtubules in PTK Cells'. *J Cell Biol* 123.6 Pt 1, pp. 1475–1489. DOI: 10.1083/jcb.123.6.1475.

Maurer, S. P., N. I. Cade, G. Bohner, N. Gustafsson, E. Boutant and T. Surrey (2014). 'EB1 Accelerates Two Conformational Transitions Important for Microtubule Maturation and Dynamics'. *Curr Biol* 24.4, pp. 372–384. DOI: 10.1016/j.cub.2013.12.042.

McInnes, C., A. Mazumdar, M. Mezna, C. Meades, C. Midgley, F. Scaerou, L. Carpenter, M. Mackenzie, P. Taylor, M. Walkinshaw, P. M. Fischer and D. Glover (2006). 'Inhibitors of Polo-like Kinase Reveal Roles in Spindle-Pole Maintenance'. *Nat Chem Biol* 2.11, pp. 608–617. DOI: 10.1038/nchembio825.

McIntosh, J. R. (2016). 'Mitosis'. *Cold Spring Harb Perspect Biol* 8.9, a023218. DOI: 10.1101/cshperspect.a023218.

Meraldi, P. (2019). 'Bub1-the Zombie Protein That CRISPR Cannot Kill'. *EMBO J* 38.7, e101912. DOI: 10.15252/embj.2019101912.

Meunier, S. and I. Vernos (2012). 'Microtubule Assembly during Mitosis - from Distinct Origins to Distinct Functions?' *J Cell Sci* 125.Pt 12, pp. 2805–2814. DOI: 10.1242/jcs.092429.

Mishima, M., S. Kaitna and M. Glotzer (2002). 'Central Spindle Assembly and Cytokinesis Require a Kinesin-like Protein/RhoGAP Complex with Microtubule Bundling Activity'. *Dev Cell* 2.1, pp. 41–54. DOI: 10.1016/s1534-5807(01)00110-1.

Mitchison, T. J. (1989). 'Polewards Microtubule Flux in the Mitotic Spindle: Evidence from Photoactivation of Fluorescence'. *J Cell Biol* 109.2, pp. 637–652. DOI: 10.1083/jcb.109.2.637.

Mitchison, T. and M. Kirschner (1984). 'Dynamic Instability of Microtubule Growth'. *Nature* 312.5991, pp. 237–242. DOI: 10.1038/312237a0.

Mohri, H. (1968). 'Amino-Acid Composition of "Tubulin" Constituting Microtubules of Sperm Flagella'. *Nature* 217.5133, pp. 1053–1054. DOI: 10.1038/2171053a0.

Mollinari, C., J.-P. Kleman, W. Jiang, G. Schoehn, T. Hunter and R. L. Margolis (2002). 'PRC1 Is a Microtubule Binding and Bundling Protein Essential to Maintain the Mitotic Spindle Midzone'. *J Cell Biol* 157.7, pp. 1175–1186. DOI: 10.1083/jcb.200111052.

Monte, M., L. Collavin, D. Lazarevic, R. Utrera, T. Dragani and C. Schneider (2000). 'Cloning, Chromosome Mapping and Functional Characterization of a Human Homologue of Murine Gtse-1 (B99) Gene'. *Gene* 254.1-2, pp. 229–236. DOI: 10.1016/S0378-1119(00)00260-2.

Moritz, M., M. B. Braunfeld, J. W. Sedat, B. Alberts and D. A. Agard (1995). 'Microtubule Nucleation by Gamma-Tubulin-Containing Rings in the Centrosome'. *Nature* 378.6557, pp. 638–640. DOI: 10.1038/378638a0.

Mullard, A. (2021). 'Targeted Protein Degraders Crowd into the Clinic'. *Nat Rev Drug Discov* 20.4, pp. 247–250. DOI: 10.1038/d41573-021-00052-4.

Muyldermans, S. (2021). 'A Guide to: Generation and Design of Nanobodies'. *FEBS J* 288.7, pp. 2084–2102. DOI: 10.1111/febs.15515.

Nasmyth, K. and C. H. Haering (2009). 'Cohesin: Its Roles and Mechanisms'. *Annu Rev Genet* 43, pp. 525–558. DOI: 10.1146/annurev-genet-102108-134233.

Nigg, E. A. and A. J. Holland (2018). 'Once and Only Once: Mechanisms of Centriole Duplication and Their Deregulation in Disease'. *Nat Rev Mol Cell Biol* 19.5, pp. 297–312. DOI: 10.1038/nrm.2017.127.

Nigg, E. A. and T. Stearns (2011). 'The Centrosome Cycle: Centriole Biogenesis, Duplication and Inherent Asymmetries'. *Nat Cell Biol* 13.10, pp. 1154–1160. DOI: 10.1038/ncb2345.

Nishimura, K., T. Fukagawa, H. Takisawa, T. Kakimoto and M. Kanemaki (2009). 'An Auxin-Based Degron System for the Rapid Depletion of Proteins in Nonplant Cells'. *Nat Methods* 6.12, pp. 917–922. DOI: 10.1038/nmeth.1401.

Nixon, F. M., C. Gutiérrez-Caballero, F. E. Hood, D. G. Booth, I. A. Prior and S. J. Royle (2015). 'The Mesh Is a Network of Microtubule Connectors That Stabilizes Individual Kinetochore Fibers of the Mitotic Spindle'. *Elife* 4. DOI: 10.7554/eLife.07635.

Novais, P., P. M. A. Silva, I. Amorim and H. Bousbaa (2021). 'Second-Generation Antimitotics in Cancer Clinical Trials'. *Pharmaceutics* 13.7, p. 1011. DOI: 10.3390/pharmaceutics13071011.

Nurse, P., P. Thuriaux and K. Nasmyth (1976). 'Genetic Control of the Cell Division Cycle in the Fission Yeast Schizosaccharomyces Pombe'. *Mol Gen Genet* 146.2, pp. 167–178. DOI: 10.1007/BF00268085.

Nwagbara, B. U., A. E. Faris, E. A. Bearce, B. Erdogan, P. T. Ebbert, M. F. Evans, E. L. Rutherford, T. B. Enzenbacher and L. A. Lowery (2014). 'TACC3 Is a Microtubule plus End-Tracking Protein That Promotes Axon Elongation and Also Regulates Microtubule plus End Dynamics in Multiple Embryonic Cell Types'. *Mol Biol Cell* 25.21, pp. 3350–3362. DOI: 10.1091/mbc.E14-06-1121.

O'Connell, C. B. and Y. L. Wang (2000). 'Mammalian Spindle Orientation and Position Respond to Changes in Cell Shape in a Dynein-Dependent Fashion'. *Mol Biol Cell* 11.5, pp. 1765–1774. DOI: 10.1091/mbc.11.5.1765.

Okamoto, C. T., J. McKinney and Y. Y. Jeng (2000). 'Clathrin in Mitotic Spindles'. *Am J Physiol Cell Physiol* 279.2, pp. C369–374. DOI: 10.1152/ajpcell.2000.279.2.C369.

Paweletz, N. (2001). 'Walther Flemming: Pioneer of Mitosis Research'. *Nat Rev Mol Cell Biol* 2.1, pp. 72–75. DOI: 10.1038/35048077.

Pearse, B. M. (1976). 'Clathrin: A Unique Protein Associated with Intracellular Transfer of Membrane by Coated Vesicles'. *Proc Natl Acad Sci U S A* 73.4, pp. 1255–1259. DOI: 10.1073/pnas.73.4.1255.

Peset, I., J. Seiler, T. Sardon, L. A. Bejarano, S. Rybina and I. Vernos (2005). 'Function and Regulation of Maskin, a TACC Family Protein, in Microtubule Growth during Mitosis'. *Journal of Cell Biology* 170.7, pp. 1057–1066. DOI: 10.1083/jcb.200504037.

Peset, I. and I. Vernos (2008). 'The TACC Proteins: TACC-ling Microtubule Dynamics and Centrosome Function'. *Trends in Cell Biology* 18.8, pp. 379–388. DOI: 10.1016/j.tcb.2008.06.005.

Peters, J.-M. (2006). 'The Anaphase Promoting Complex/Cyclosome: A Machine Designed to Destroy'. *Nat Rev Mol Cell Biol* 7.9, pp. 644–656. DOI: 10.1038/nrm1988.

Petry, S. (2016). 'Mechanisms of Mitotic Spindle Assembly'. *Annu Rev Biochem* 85, pp. 659–683. DOI: 10.1146/annurev-biochem-060815-014528.

Prosser, S. L. and L. Pelletier (2017). 'Mitotic Spindle Assembly in Animal Cells: A Fine Balancing Act'. *Nat Rev Mol Cell Biol* 18.3, pp. 187–201. DOI: 10.1038/nrm.2016.162.

Qian, J., B. Lesage, M. Beullens, A. Van Eynde and M. Bollen (2011). 'PP1/Repo-man Dephosphorylates Mitotic Histone H3 at T3 and Regulates Chromosomal Aurora B Targeting'. *Curr Biol* 21.9, pp. 766–773. DOI: 10.1016/j.cub.2011.03.047.

Raff, J. W. (2019). 'Phase Separation and the Centrosome: A Fait Accompli?' *Trends Cell Biol* 29.8, pp. 612–622. DOI: 10.1016/j.tcb.2019.04.001.

Raff, J. W. and R. Basto (2017). 'Centrosome Amplification and Cancer: A Question of Sufficiency'. *Dev Cell* 40.3, pp. 217–218. DOI: 10.1016/j.devcel.2017.01.009.

Rajeev, R., P. Singh, A. Asmita, U. Anand and T. K. Manna (2019). 'Aurora A Site Specific TACC3 Phosphorylation Regulates Astral Microtubule Assembly by Stabilizing γ-Tubulin Ring Complex'. *BMC Molecular and Cell Biology* 20.1, pp. 1–13. DOI: 10.1186/s12860-019-0242-z.

Ramadan, K., R. Bruderer, F. M. Spiga, O. Popp, T. Baur, M. Gotta and H. H. Meyer (2007). 'Cdc48/P97 Promotes Reformation of the Nucleus by Extracting the Kinase Aurora B from Chromatin'. *Nature* 450.7173, pp. 1258–1262. DOI: 10.1038/nature06388.

Ran, F. A., P. D. Hsu, J. Wright, V. Agarwala, D. A. Scott and F. Zhang (2013). 'Genome Engineering Using the CRISPR-Cas9 System'. *Nat Protoc* 8.11, pp. 2281–2308. DOI: 10.1038/nprot.2013.143.

Rieder, C. L. (1981). 'The Structure of the Cold-Stable Kinetochore Fiber in Metaphase PtK1 Cells'. *Chromosoma* 84.1, pp. 145–158. DOI: 10.1007/BF00293368.

Robinson, M. S. (2015). 'Forty Years of Clathrin-coated Vesicles'. *Traffic* 16.12, pp. 1210–1238. DOI: 10.1111/tra.12335.

Robinson, M. S., D. A. Sahlender and S. D. Foster (2010). 'Rapid Inactivation of Proteins by Rapamycin-Induced Rerouting to Mitochondria'. *Developmental Cell* 18.2, pp. 324–331. DOI: 10.1016/j.devcel.2009.12.015.

Rogers, G. C., S. L. Rogers, T. A. Schwimmer, S. C. Ems-McClung, C. E. Walczak, R. D. Vale, J. M. Scholey and D. J. Sharp (2004). 'Two Mitotic Kinesins Cooperate to Drive Sister Chromatid Separation during Anaphase'. *Nature* 427.6972, pp. 364–370. DOI: 10.1038/nature02256.

Rondelet, A., Y.-C. Lin, D. Singh, A. T. Porfetye, H. C. Thakur, A. Hecker, P. Brinkert, N. Schmidt, S. Bendre, F. Müller, L. Mazul, P. O. Widlund, T. Bange, M. Hiller, I. R. Vetter and A. W. Bird (2020). 'Clathrin's Adaptor Interaction Sites Are Repurposed to Stabilize Microtubules during Mitosis'. *The Journal of Cell Biology* 219.2, e201907083. DOI: 10.1083/jcb.201907083.

Rostkova, E., S. G. Burgess, R. Bayliss and M. Pfuhl (2018). 'Solution NMR Assignment of the C-terminal Domain of Human chTOG.' *Biomolecular NMR assignments* 12.2, pp. 221–224. DOI: 10.1007/s12104-018-9812-9.

Roth, T. F. and K. R. Porter (1964). 'YOLK PROTEIN UPTAKE IN THE OOCYTE OF THE MOSQUITO AEDES AEGYPTI. L'. *J Cell Biol* 20, pp. 313–332. DOI: 10.1083/jcb.20.2.313.

Rothbauer, U., K. Zolghadr, S. Tillib, D. Nowak, L. Schermelleh, A. Gahl, N. Backmann, K. Conrath, S. Muyldermans, M. C. Cardoso and H. Leonhardt

(2006). 'Targeting and Tracing Antigens in Live Cells with Fluorescent Nanobodies'. *Nat Methods* 3.11, pp. 887–889. DOI: 10.1038/nmeth953.

Roux, K. J., D. I. Kim, B. Burke and D. G. May (2018). 'BioID: A Screen for Protein-Protein Interactions'. *Curr Protoc Protein Sci* 91, pp. 19.23.1–19.23.15. DOI: 10.1002/cpps.51.

Royle, S. J., N. A. Bright and L. Lagnado (2005). 'Clathrin Is Required for the Function of the Mitotic Spindle'. *Nature* 434.7037, pp. 1152–1157. DOI: 10.1038/nature03502.

Royle, S. J. and L. Lagnado (2006). 'Trimerisation Is Important for the Function of Clathrin at the Mitotic Spindle'. *J Cell Sci* 119.Pt 19, pp. 4071–4078. DOI: 10.1242/jcs.03192.

Ruigrok, V. J. B., M. Levisson, M. H. M. Eppink, H. Smidt and J. van der Oost (2011). 'Alternative Affinity Tools: More Attractive than Antibodies?' *Biochem J* 436.1, pp. 1–13. DOI: 10.1042/BJ20101860.

Rusan, N. M., U. S. Tulu, C. Fagerstrom and P. Wadsworth (2002). 'Reorganization of the Microtubule Array in Prophase/Prometaphase Requires Cytoplasmic Dynein-Dependent Microtubule Transport'. *J Cell Biol* 158.6, pp. 997–1003. DOI: 10.1083/jcb.200204109.

Ryan, E. L., J. Shelford, T. Massam-Wu, R. Bayliss and S. J. Royle (2021). 'Defining Endogenous TACC3–chTOG–Clathrin–GTSE1 Interactions at the Mitotic Spindle Using Induced Relocalization'. *J Cell Sci* 134.3, jcs255794. DOI: 10.1242/jcs.255794.

Sakamoto, K. M., K. B. Kim, A. Kumagai, F. Mercurio, C. M. Crews and R. J. Deshaies (2001). 'Protacs: Chimeric Molecules That Target Proteins to the Skp1-Cullin-F Box Complex for Ubiquitination and Degradation'. *Proc Natl Acad Sci U S A* 98.15, pp. 8554–8559. DOI: 10.1073/pnas.141230798.

Salisbury, J. L. (2003). 'Centrosomes: Coiled-Coils Organize the Cell Center'. *Curr Biol* 13.3, R88–90. DOI: 10.1016/s0960-9822(03)00033-2.

Sapkota, H., J. D. Wren and G. J. Gorbsky (2020). 'CSAG1 Maintains the Integrity of the Mitotic Centrosome in Cells with Defective P53'. *J Cell Sci* 133.10, jcs239723. DOI: 10.1242/jcs.239723.

Schindelin, J., I. Arganda-Carreras, E. Frise, V. Kaynig, M. Longair, T. Pietzsch, S. Preibisch, C. Rueden, S. Saalfeld, B. Schmid, J.-Y. Tinevez, D. J. White, V. Hartenstein, K. Eliceiri, P. Tomancak and A. Cardona (2012). 'Fiji: An Open-Source Platform for Biological-Image Analysis'. *Nat Methods* 9.7, pp. 676–682. DOI: 10.1038/nmeth.2019.

Schooley, A., B. Vollmer and W. Antonin (2012). 'Building a Nuclear Envelope at the End of Mitosis: Coordinating Membrane Reorganization, Nuclear Pore

Complex Assembly, and Chromatin de-Condensation'. *Chromosoma* 121.6, pp. 539–554. DOI: 10.1007/s00412-012-0388-3.

Schuyler, S. C. and D. Pellman (2001). 'Microtubule "plus-End-Tracking Proteins": The End Is Just the Beginning'. *Cell* 105.4, pp. 421–424. DOI: 10.1016/s0092-8674(01)00364-6.

Scolz, M., P. O. Widlund, S. Piazza, D. R. Bublik and S. Reber (2012). 'GTSE1 Is a Microtubule Plus-End Tracking Protein That Regulates EB1-Dependent Cell Migration'. *PLoS ONE* 7.12, pp. 51259–51259. DOI: 10.1371/journal.pone.0051259.

Shamsuddin, S. H., D. G. Jayne, D. C. Tomlinson, M. J. McPherson and P. A. Millner (2021). 'Selection and Characterisation of Affimers Specific for CEA Recognition'. *Sci Rep* 11.1, p. 744. DOI: 10.1038/s41598-020-80354-6.

Shelford, J. and S. J. Royle (2020). *Comparing Antibodies for the Detection of Ch-TOG/CKAP5 in Mitotic HeLa Cells by Indirect Immunofluorescence*. DOI: 10.6084/M9.FIGSHARE.13395554.V1.

Sherr, C. J. and J. M. Roberts (1999). 'CDK Inhibitors: Positive and Negative Regulators of G1-phase Progression'. *Genes Dev* 13.12, pp. 1501–1512. DOI: 10.1101/gad.13.12.1501.

Sikirzhytski, V., V. Magidson, J. B. Steinman, J. He, M. Le Berre, I. Tikhonenko, J. G. Ault, B. F. McEwen, J. K. Chen, H. Sui, M. Piel, T. M. Kapoor and A. Khodjakov (2014). 'Direct Kinetochore-Spindle Pole Connections Are Not Required for Chromosome Segregation'. *J Cell Biol* 206.2, pp. 231–243. DOI: 10.1083/jcb.201401090.

Singh, D., N. Schmidt, F. Müller, T. Bange and A. W. Bird (2020). 'Destabilization of Long Astral Microtubules via Cdk1-Dependent Removal of GTSE1 from Their Plus Ends Facilitates Prometaphase Spindle Orientation'. *Current Biology*, S0960982220317528. DOI: 10.1016/j.cub.2020.11.040.

Singh, P., G. E. Thomas, K. K. Gireesh and T. K. Manna (2014). 'TACC3 Protein Regulates Microtubule Nucleation by Affecting γ-Tubulin Ring Complexes.' *The Journal of biological chemistry* 289.46, pp. 31719–35. DOI: 10.1074/jbc.M114.575100.

Škrlec, K., B. Štrukelj and A. Berlec (2015). 'Non-Immunoglobulin Scaffolds: A Focus on Their Targets'. *Trends Biotechnol* 33.7, pp. 408–418. DOI: 10.1016/j.tibtech.2015.03.012.

Slautterback, D. B. (1963). 'CYTOPLASMIC MICROTUBULES. I. HYDRA'. *J Cell Biol* 18, pp. 367–388. DOI: 10.1083/jcb.18.2.367.

Smith, G. P. (1985). 'Filamentous Fusion Phage: Novel Expression Vectors That Display Cloned Antigens on the Virion Surface'. *Science* 228.4705, pp. 1315–1317. DOI: 10.1126/science.4001944.

So, C., K. B. Seres, A. M. Steyer, E. Mönnich, D. Clift, A. Pejkovska, W. Möbius and M. Schuh (2019). 'A Liquid-like Spindle Domain Promotes Acentrosomal Spindle Assembly in Mammalian Oocytes'. *Science* 364.6447, eaat9557. DOI: 10.1126/science.aat9557.

Spittle, C., S. Charrasse, C. Larroque and L. Cassimeris (2000). 'The Interaction of TOGp with Microtubules and Tubulin'. *J Biol Chem* 275.27, pp. 20748–20753. DOI: 10.1074/jbc.M002597200.

Stiff, T., F. R. Echegaray-Iturra, H. J. Pink, A. Herbert, C. C. Reyes-Aldasoro and H. Hochegger (2020). 'Prophase-Specific Perinuclear Actin Coordinates Centrosome Separation and Positioning to Ensure Accurate Chromosome Segregation'. *Cell Reports* 31.8, p. 107681. DOI: 10.1016/j.celrep.2020.107681.

Still, I. H., M. Hamilton, P. Vince, A. Wolfman and J. K. Cowell (1999a). 'Cloning of TACC1, an Embryonically Expressed, Potentially Transforming Coiled Coil Containing Gene, from the 8p11 Breast Cancer Amplicon'. *Oncogene* 18.27, pp. 4032–4038. DOI: 10.1038/sj.onc.1202801.

Still, I. H., P. Vince and J. K. Cowell (1999b). 'The Third Member of the Transforming Acidic Coiled Coil-Containing Gene Family, TACC3, Maps in 4p16, Close to Translocation Breakpoints in Multiple Myeloma, and Is Upregulated in Various Cancer Cell Lines'. *Genomics* 58.2, pp. 165–170. DOI: 10.1006/geno.1999.5829.

Sugizaki, A., K. Sato, K. Chiba, K. Saito, M. Kawagishi, Y. Tomabechi, S. B. Mehta, H. Ishii, N. Sakai, M. Shirouzu, T. Tani and S. Terada (2021). 'POLArIS, a Versatile Probe for Molecular Orientation, Revealed Actin Filaments Associated with Microtubule Asters in Early Embryos'. *Proc Natl Acad Sci USA* 118.11, e2019071118. DOI: 10.1073/pnas.2019071118.

Tang, A. A.-S., C. Tiede, D. J. Hughes, M. J. McPherson and D. C. Tomlinson (2017). 'Isolation of Isoform-Specific Binding Proteins (Affimers) by Phage Display Using Negative Selection'. *Sci Signal* 10.505, eaan0868. DOI: 10.1126/scisignal.aan0868.

Thadani, R., F. Uhlmann and S. Heeger (2012). 'Condensin, Chromatin Crossbarring and Chromosome Condensation'. *Curr Biol* 22.23, R1012–1021. DOI: 10.1016/j.cub.2012.10.023.

Tiede, C., R. Bedford, S. J. Heseltine, G. Smith, I. Wijetunga, R. Ross, D. AlQallaf, A. P. Roberts, A. Balls, A. Curd, R. E. Hughes, H. Martin, S. R. Needham, L. C. Zanetti-Domingues, Y. Sadigh, T. P. Peacock, A. A. Tang, N. Gibson, H. Kyle, G. W. Platt, N. Ingram, T. Taylor, L. P. Coletta, I. Manfield, M. Knowles, S. Bell, F. Esteves, A. Maqbool, R. K. Prasad, M. Drinkhill, R. S. Bon, V. Patel, S. A. Goodchild, M. Martin-Fernandez, R. J. Owens, J. E. Nettleship, M. E. Webb, M. Harrison, J. D. Lippiat, S. Ponnambalam,

M. Peckham, A. Smith, P. K. Ferrigno, M. Johnson, M. J. McPherson and D. C. Tomlinson (2017). 'Affimer Proteins Are Versatile and Renewable Affinity Reagents'. *Elife* 6, e24903. DOI: 10.7554/eLife.24903.

Tiede, C., A. A. S. Tang, S. E. Deacon, U. Mandal, J. E. Nettleship, R. L. Owen, S. E. George, D. J. Harrison, R. J. Owens, D. C. Tomlinson and M. J. McPherson (2014). 'Adhiron: A Stable and Versatile Peptide Display Scaffold for Molecular Recognition Applications'. *Protein Engineering, Design and Selection* 27.5, pp. 145–155. DOI: 10.1093/protein/gzu007.

Toure, M. and C. M. Crews (2016). 'Small-Molecule PROTACS: New Approaches to Protein Degradation'. *Angew Chem Int Ed Engl* 55.6, pp. 1966–1973. DOI: 10.1002/anie.201507978.

Tovell, H., A. Testa, C. Maniaci, H. Zhou, A. R. Prescott, T. Macartney, A. Ciulli and D. R. Alessi (2019). 'Rapid and Reversible Knockdown of Endogenously Tagged Endosomal Proteins via an Optimized HaloPROTAC Degrader'. *ACS Chem Biol* 14.5, pp. 882–892. DOI: 10.1021/acschembio.8b01016.

Utrera, R., L. Collavin, D. Lazarević, D. Delia and C. Schneider (1998). 'A Novel P53-Inducible Gene Coding for a Microtubule-Localized Protein with G2-phase-specific Expression'. *The EMBO Journal* 17.17, pp. 5015–5025. DOI: 10.1093/emboj/17.17.5015.

van der Vaart, B., C. Manatschal, I. Grigoriev, V. Olieric, S. M. Gouveia, S. Bjelic, J. Demmers, I. Vorobjev, C. C. Hoogenraad, M. O. Steinmetz and A. Akhmanova (2011). 'SLAIN2 Links Microtubule plus End-Tracking Proteins and Controls Microtubule Growth in Interphase'. *J Cell Biol* 193.6, pp. 1083–1099. DOI: 10.1083/jcb.201012179.

Vincke, C. and S. Muyldermans (2012). 'Introduction to Heavy Chain Antibodies and Derived Nanobodies'. *Methods Mol Biol* 911, pp. 15–26. DOI: 10.1007/978-1-61779-968-6_2.

Visconti, R., R. Della Monica and D. Grieco (2016). 'Cell Cycle Checkpoint in Cancer: A Therapeutically Targetable Double-Edged Sword'. *Journal of Experimental & Clinical Cancer Research* 35.1, p. 153. DOI: 10.1186/s13046-016-0433-9.

Vukušić, K. and I. M. Tolić (2021). 'Anaphase B: Long-standing Models Meet New Concepts'. *Semin Cell Dev Biol* 117, pp. 127–139. DOI: 10.1016/j.semcdb.2021.03.023.

Wang, R., C. Ascanelli, A. Abdelbaki, A. Fung, T. Rasmusson, I. Michaelides, K. Roberts and C. Lindon (2021). 'Selective Targeting of Non-Centrosomal AURKA Functions through Use of a Targeted Protein Degradation Tool'. *Commun Biol* 4.1, p. 640. DOI: 10.1038/s42003-021-02158-2.

Widlund, P. O., J. H. Stear, A. Pozniakovsky, M. Zanic, S. Reber, G. J. Brouhard, A. A. Hyman and J. Howard (2011). 'XMAP215 Polymerase Activity Is Built by Combining Multiple Tubulin-Binding TOG Domains and a Basic Lattice-Binding Region'. *Proceedings of the National Academy of Sciences* 108.7, pp. 2741–2746. DOI: 10.1073/PNAS.1016498108.

Willox, A. K. and S. J. Royle (2012). 'Functional Analysis of Interaction Sites on the N-terminal Domain of Clathrin Heavy Chain'. *Traffic* 13.1, pp. 70–81. DOI: 10.1111/j.1600-0854.2011.01289.x.

Wollman, R., E. N. Cytrynbaum, J. T. Jones, T. Meyer, J. M. Scholey and A. Mogilner (2005). 'Efficient Chromosome Capture Requires a Bias in the 'search-and-Capture' Process during Mitotic-Spindle Assembly'. *Curr Biol* 15.9, pp. 828–832. DOI: 10.1016/j.cub.2005.03.019.

Wong, Y. L., J. V. Anzola, R. L. Davis, M. Yoon, A. Motamedi, A. Kroll, C. P. Seo, J. E. Hsia, S. K. Kim, J. W. Mitchell, B. J. Mitchell, A. Desai, T. C. Gahman, A. K. Shiau and K. Oegema (2015). 'Cell Biology. Reversible Centriole Depletion with an Inhibitor of Polo-like Kinase 4'. *Science* 348.6239, pp. 1155–1160. DOI: 10.1126/science.aaa5111.

Wood, L. A., G. Larocque, N. I. Clarke, S. Sarkar and S. J. Royle (2017). 'New Tools for "Hot-Wiring" Clathrin-Mediated Endocytosis with Temporal and Spatial Precision'. *J Cell Biol* 216.12, pp. 4351–4365. DOI: 10.1083/jcb.201702188.

Woodruff, J. B. (2018). 'Assembly of Mitotic Structures through Phase Separation'. *J Mol Biol* 430.23, pp. 4762–4772. DOI: 10.1016/j.jmb.2018.04.041.

Woodruff, J. B. (2021). 'The Material State of Centrosomes: Lattice, Liquid, or Gel?' *Curr Opin Struct Biol* 66, pp. 139–147. DOI: 10.1016/j.sbi.2020.10.001.

Woodruff, J. B., B. Ferreira Gomes, P. O. Widlund, J. Mahamid, A. Honigmann and A. A. Hyman (2017). 'The Centrosome Is a Selective Condensate That Nucleates Microtubules by Concentrating Tubulin'. *Cell* 169.6, 1066–1077.e10. DOI: 10.1016/j.cell.2017.05.028.

Woodruff, J. B., O. Wueseke and A. A. Hyman (2014). 'Pericentriolar Material Structure and Dynamics'. *Philos Trans R Soc Lond B Biol Sci* 369.1650, p. 20130459. DOI: 10.1098/rstb.2013.0459.

Woods, J. (2019). 'Selection of Functional Intracellular Nanobodies'. *SLAS Discov* 24.7, pp. 703–713. DOI: 10.1177/2472555219853235.

Wurdak, H., S. Zhu, K. H. Min, L. Aimone, L. L. Lairson, J. Watson, G. Chopiuk, J. Demas, B. Charette, R. Halder, E. Weerapana, B. F. Cravatt, H. T. Cline, E. C. Peters, J. Zhang, J. R. Walker, C. Wu, J. Chang, T. Tuntland, C. Y. Cho and P. G. Schultz (2010). 'A Small Molecule Accelerates

Neuronal Differentiation in the Adult Rat'. *Proc Natl Acad Sci U S A* 107.38, pp. 16542–16547. DOI: 10.1073/pnas.1010300107.

Yang, D., N. Rismanchi, B. Renvoisé, J. Lippincott-Schwartz, C. Blackstone and J. H. Hurley (2008). 'Structural Basis for Midbody Targeting of Spastin by the ESCRT-III Protein CHMP1B'. *Nat Struct Mol Biol* 15.12, pp. 1278–1286. DOI: 10.1038/nsmb.1512.

Yao, R., Y. Kondoh, Y. Natsume, H. Yamanaka, M. Inoue, H. Toki, R. Takagi, T. Shimizu, T. Yamori, H. Osada and T. Noda (2014). 'A Small Compound Targeting TACC3 Revealed Its Different Spatiotemporal Contributions for Spindle Assembly in Cancer Cells'. *Oncogene* 33.33, pp. 4242–4252. DOI: 10.1038/onc.2013.382.

Yao, R., Y. Natsume, Y. Saiki, H. Shioya, K. Takeuchi, T. Yamori, H. Toki, I. Aoki, T. Saga and T. Noda (2012). 'Disruption of Tacc3 Function Leads to in Vivo Tumor Regression'. *Oncogene* 31.2, pp. 135–148. DOI: 10.1038/onc.2011.235.

Zanic, M., J. H. Stear, A. A. Hyman and J. Howard (2009). 'EB1 Recognizes the Nucleotide State of Tubulin in the Microtubule Lattice'. *PLoS One* 4.10, e7585. DOI: 10.1371/journal.pone.0007585.

Zhai, Y., P. J. Kronebusch and G. G. Borisy (1995). 'Kinetochore Microtubule Dynamics and the Metaphase-Anaphase Transition'. *J Cell Biol* 131.3, pp. 721–734. DOI: 10.1083/jcb.131.3.721.

Zimmerman, W. C., J. Sillibourne, J. Rosa and S. J. Doxsey (2004). 'Mitosis-Specific Anchoring of Gamma Tubulin Complexes by Pericentrin Controls Spindle Organization and Mitotic Entry'. *Mol Biol Cell* 15.8, pp. 3642–3657. DOI: 10.1091/mbc.e03-11-0796.

Appendix 1

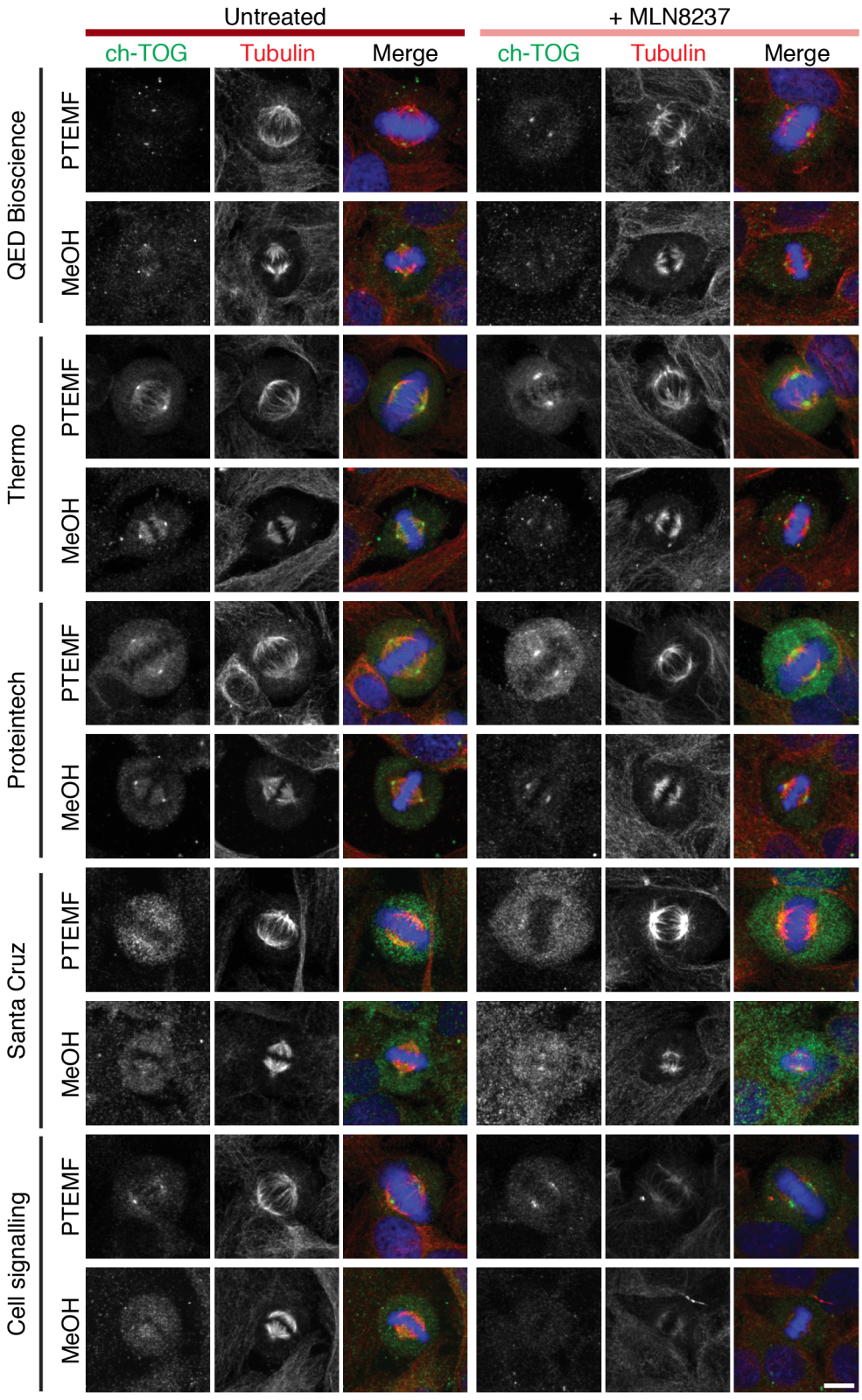

Figure 5.1. Comparing antibodies for the detection of ch-TOG in mitotic HeLa cells by indirect immunofluorescence. Confocal micrographs of fixed HeLa cells in metaphase stained with antibodies to detect ch-TOG (see table 5.1 for details), α-tubulin and DNA. Cells were fixed in PTEMF or ice-cold methanol (MeOH), as indicated. Cells were treated with MLN8237 (0.3 µM, 40 min) before fixing to test for antibody specificity. Scale bar = 10 µm.

Table 5.1. Comparing antibodies for the detection of ch-TOG in mitotic HeLa cells by indirect immunofluorescence.

Antibody name	**Working concentration**	**Supplier**	**Cat No.**
Rabbit anti-ch-TOG	1:5000	QED Bioscience	34032
Mouse anti-ch-TOG	1:50	Santa Cruz	sc-374394
Rabbit anti-ch-TOG	1:50	Proteintech	26457-1-AP
Rabbit anti-ch-TOG	1:800	Thermo	PA5-59150
Rabbit anti-ch-TOG	1:50	Biorbyt	orb418091
Rabbit anti-ch-TOG	1:1000	Cell signalling	67774S

Appendix 2

© 2021. Published by The Company of Biologists Ltd | Journal of Cell Science (2021) 134, jcs255794. doi:10.1242/jcs.255794

RESEARCH ARTICLE

Defining endogenous TACC3–chTOG–clathrin–GTSE1 interactions at the mitotic spindle using induced relocalization

Ellis L. Ryan[1,*], James Shelford[1,*], Teresa Massam-Wu[1], Richard Bayliss[2] and Stephen J. Royle[1,‡]

ABSTRACT

A multiprotein complex containing TACC3, clathrin and other proteins has been implicated in mitotic spindle stability. To disrupt this complex in an anti-cancer context, we need to understand its composition and how it interacts with microtubules. Induced relocalization of proteins in cells is a powerful way to analyze protein–protein interactions and, additionally, monitor where and when these interactions occur. We used CRISPR/Cas9 gene editing to add tandem FKBP–GFP tags to each complex member. The relocalization of endogenous tagged protein from the mitotic spindle to mitochondria and assessment of the effect on other proteins allowed us to establish that TACC3 and clathrin are core complex members and that chTOG (also known as CKAP5) and GTSE1 are ancillary to the complex, binding respectively to TACC3 and clathrin, but not each other. We also show that PIK3C2A, a clathrin-binding protein that was proposed to stabilize the TACC3–chTOG–clathrin–GTSE1 complex during mitosis, is not a member of the complex. This work establishes that targeting the TACC3–clathrin interface or their microtubule-binding sites are the two strategies most likely to disrupt spindle stability mediated by this multiprotein complex.

KEY WORDS: GTSE1, TACC3, Clathrin, Knocksideways, Mitosis, Mitotic spindle

INTRODUCTION

During mitosis, chromosomes are segregated with high precision to generate two genetically identical daughter cells. This segregation is driven by the mitotic spindle, a bipolar microtubule array with associated motor and non-motor proteins (Manning and Compton, 2008). One non-motor protein complex that binds spindle microtubules contains TACC3, chTOG (also known as CKAP5) and clathrin (Fu et al., 2010; Hubner et al., 2010; Lin et al., 2010; Booth et al., 2011). This complex is important for stabilizing the bundles of microtubules that attach to kinetochores (kinetochore-fibers, k-fibers) by physically crosslinking them (Booth et al., 2011; Hepler et al., 1970; Nixon et al., 2015, 2017). Uncovering the molecular details of how proteins of this complex bind to one another and to microtubules is important to understand how mitotic spindles are stabilized and how we can target spindle stability in an anti-cancer context.

Mitotic phosphorylation of TACC3 on serine 558 by Aurora kinase A (referred to here as Aurora A) controls the interaction between clathrin and TACC3 (Booth et al., 2011; Cheeseman et al., 2011, 2013; Hood et al., 2013; Burgess et al., 2018). This interaction brings together the N-terminal domain of clathrin heavy chain and the TACC domain of TACC3 to make the microtubule-binding surface (Hood et al., 2013). Despite having a microtubule-lattice binding domain, chTOG is not needed for the complex to bind microtubules and interacts with the TACC3–clathrin complex via its TOG6 domain, binding to a stutter in the TACC domain of TACC3 (Booth et al., 2011; Hood et al., 2013; Gutiérrez-Caballero et al., 2015).

Despite this detail, the exact composition of the complex on kinetochore microtubules is uncertain. Besides TACC3, clathrin and chTOG, two further proteins, GTSE1 and phosphatidylinositol 4-phosphate 3-kinase C2 domain-containing subunit α (PI3K-C2α, also known as PIK3C2A) have been proposed to be members. Both were originally identified as binding partners for mitotic TACC3–clathrin (Hubner et al., 2010). Biochemical evidence convincingly shows that GTSE1 binds the N-terminal domain of clathrin heavy chain and that this interaction localizes GTSE1 to spindle microtubules (Rondelet et al., 2020). Like chTOG, GTSE1 has the capacity to bind microtubules, but it appears to use TACC3–clathrin to bind the spindle (Monte et al., 2000; Scolz et al., 2012; Bendre et al., 2016). By contrast, PIK3C2A is a component of clathrin-coated vesicles where it acts as a lipid kinase (Gaidarov et al., 2001). It was recently proposed to act as a scaffolding protein in the TACC3–chTOG–clathrin complex by binding to both TACC3 and clathrin (Gulluni et al., 2017). PIK3C2A and GTSE1 bind to the same sites on the N-terminal domain of clathrin heavy chain (Gaidarov et al., 2001; Rondelet et al., 2020), and although clathrin has the capacity to bind multiple proteins (Smith et al., 2017; Willox and Royle, 2012), this raises the question of whether the binding of PIK3C2A and GTSE1 to TACC3–clathrin at the spindle is mutually exclusive.

Dissecting this multiprotein complex is further complicated by each putative member being able to form subcomplexes that have different subcellular localizations (Gutiérrez-Caballero et al., 2015). TACC3–chTOG (without clathrin) localizes to the plus ends of microtubules (Nwagbara et al., 2014; Gutiérrez-Caballero et al., 2015). Similarly, GTSE1 binds plus ends and can also stabilize astral microtubules of the mitotic spindle by inhibiting the microtubule depolymerase MCAK (also known as KIF2C; Scolz et al., 2012; Bendre et al., 2016; Tipton et al., 2017). PIK3C2A and clathrin are found in clathrin-coated vesicles away from the mitotic spindle (Gaidarov et al., 2001). Biochemical approaches do not have the capacity to discriminate these subcomplexes from the multiprotein complex on k-fibers. Therefore, subcellular investigation of protein interactions are required to answer this question.

[1]Centre for Mechanochemical Cell Biology, Warwick Medical School, Gibbet Hill Road, Coventry CV4 7AL, UK. [2]School of Molecular and Cellular Biology, Astbury Centre for Structural Biology, Faculty of Biological Sciences, University of Leeds, Leeds LS2 9JT, UK.
*These authors contributed equally to this work

‡Author for correspondence (s.j.royle@warwick.ac.uk)

E.L.R., 0000-0001-7426-2036; J.S., 0000-0002-4546-9844; T.M.-W, 0000-0002-4364-8734; R.B., 0000-0003-0604-2773; S.J.R., 0000-0001-8927-6967

Handling Editor: Michael Way
Received 15 October 2020; Accepted 14 December 2020

Knocksideways is a method to acutely and inducibly relocalize a protein to mitochondria in order to inactivate that protein (Robinson et al., 2010). In the original method, the target protein is depleted by RNAi, and an FKBP-tagged version is expressed alongside MitoTrap (an FRB domain targeted to mitochondria); relocalization is achieved by the addition of rapamycin. This method has many advantages over slow inactivation methods such as RNAi-mediated knockdown or gene disruption (knockout) approaches (Royle, 2013). We have previously used knocksideways in mitotic cells to investigate protein–protein interactions, because any proteins that are in a complex with the target protein also become mislocalized to the mitochondria (Cheeseman et al., 2013; Hood et al., 2013). This approach has the added advantage that the subcellular location of proteins can also be tracked during the experiment, and that it can be done at specific times, allowing us to pinpoint where and when interactions occur.

In this study, we applied a knocksideways approach to investigate how proteins of the TACC3–chTOG–clathrin–GTSE1 complex bind to one another and to microtubules of the mitotic spindle. Instead of overexpression and RNAi, we sought to tag each target protein with FKBP and GFP at their endogenous locus using CRISPR/Cas9-mediated gene editing. This strategy allowed us to study these subcellular interactions at the endogenous level for the first time. The cell lines we have created are a multi-purpose 'toolkit' for studying microtubule-crosslinking proteins by live-cell imaging, biochemistry or electron microscopy (Clarke and Royle, 2018).

RESULTS

Generation and validation of clathrin, TACC3, chTOG and GTSE1 knock-in HeLa cell lines

Our first goal was to tag four proteins with FKBP and GFP at their endogenous loci using CRISPR/Cas9 gene editing. Clathrin (targeting clathrin light chain A, LCa, also known as CLTA), TACC3, chTOG (CKAP5) and the clathrin-interacting protein GTSE1 were edited in HeLa cells so that they had a GFP–FKBP tag at their N-terminus or an FKBP–GFP tag at their C-terminus (Fig. 1A). The dual FKBP and GFP tag allows direct visualization of the protein as well as its spatial manipulation using knocksideways (Cheeseman et al., 2013; Robinson et al., 2010). Following editing, GFP-positive cells were isolated by FACS and were validated using a combination of PCR, sequencing, western blotting and fluorescence microscopy (Fig. 1B,C; Figs S1, S2). These validation steps yielded a cell line for each protein that could be used for all future analyses. Homozygous knock-in was achieved for CLTA–FKBP–GFP, GFP–FKBP–TACC3 and GTSE1–FKBP–GFP. Despite multiple attempts to generate a homozygous knock-in for chTOG–FKBP–GFP, we only recovered heterozygous lines (more than twenty heterozygous clones in three separate attempts). Although there is a report of homozygous knock-in of chTOG–FKBP–GFP in HCT116 cells (Cherry et al., 2019), we assume that homozygous knock-in of chTOG–FKBP–GFP in HeLa cells is lethal.

The localization of tagged proteins in all cell lines was normal. In mitotic cells, clathrin was located on the spindle, in the cytoplasm and at coated pits; TACC3 was located exclusively on the spindle; chTOG was located on the spindle but was more pronounced on the centrosomes and kinetochores; and GTSE1 was localized throughout the spindle and the cytoplasm (Fig. 1C; Fig. S2A,C), consistent with previous observations (Gergely et al., 2000, 2003; Royle et al., 2005; Foraker et al., 2012; Bendre et al., 2016; Herman et al., 2020). Overexpression of TACC3 can result in the formation of aggregates (Gergely et al., 2000; Hood et al., 2013), which have recently been described as liquid-like phase-separated structures (So et al., 2019). We note that at endogenous levels in HeLa cells, GFP–FKBP–TACC3 did not form these structures (Fig. 1C; Fig. S2A). GTSE1–FKBP–GFP could be seen tracking microtubule plus ends in interphase, as previously reported (Scolz et al., 2012), but also during all stages of mitosis (Fig. S2D).

As a further validation step, we assessed mitotic timings in each knock-in cell line and found progression to be comparable to that of their respective parental HeLa cells. These observations indicate that the addition of an FKBP and GFP tag did not affect the mitotic function of clathrin, TACC3, chTOG or GTSE1, and that clonal selection did not adversely affect mitosis in the four cell lines (Fig. S3). In summary, the generation and validation of these four knock-in cell lines represents a toolkit that can be used to study clathrin, TACC3, chTOG and GTSE1 at endogenous levels (see Table S1).

Knocksideways of endogenous proteins in knock-in cell lines

We next performed knocksideways experiments to assess the functionality of the FKBP tag that was introduced (Fig. 2A). Each cell line, expressing mCherry–MitoTrap, was imaged live during the application of 200 nM rapamycin. At metaphase, CLTA–FKBP–GFP, GFP–FKBP–TACC3, chTOG–FKBP–GFP and GTSE1–FKBP–GFP were all removed from the spindle and relocalized to the mitochondria by rapamycin addition (Fig. 2B). The timecourse of relocalization was variable but was complete by 10 min (Movies 1–4). The efficiency of relocalization in all four cell lines was 100% (clathrin, 28/28; TACC3, 26/26; chTOG, 22/22; GTSE1, 20/20).

To test whether relocating the tagged protein from the spindle to the mitochondria was sufficient to induce a mitotic phenotype, we analyzed progression through mitosis. Each knock-in cell line, transiently expressing mCherry–MitoTrap(T2098L), a rapalog-sensitive MitoTrap, was imaged overnight by light microscopy following application of 1 µM rapalog AP21967 or control. Relocalization of endogenous clathrin (CLTA–FKBP–GFP) caused a prolonged mitosis (median nuclear envelope breakdown-to-anaphase timing of 73.5 min versus 57.75 min in control conditions), with only 55% of cells exiting metaphase during the movie compared with 100% of control (Fig. 2C). Similarly, TACC3 relocalization prolonged the time to reach anaphase by 2.2-fold compared to the time taken by the control, with delays in reaching metaphase and reaching anaphase, and 72% of cells exiting metaphase. Relocalization of chTOG (chTOG–FKBP–GFP) also caused a delay of 1.5-fold, with 80% of cells entering anaphase. This phenotype was more mild than that following clathrin or TACC3 relocalization, although we note that some chTOG is likely to remain on the spindle due to the heterozygosity of this cell line. Finally, relocalization of GTSE1–FKBP–GFP had a smaller effect on mitotic progression, with 96% of cells exiting metaphase and a 1.2-fold delay in the timing from nuclear envelope breakdown to anaphase (Fig. 2C). These experiments show that relocalization of each protein is possible in live cells using knocksideways and that functional mitotic consequences of this mislocalization can be observed.

Defining mitotic clathrin, TACC3, chTOG and GTSE1 interactions using knocksideways of endogenously tagged proteins

Acute manipulation of protein localization using knocksideways can be used to uncover interactions in living cells (Hood et al., 2013). To examine mitotic interactions between clathrin, TACC3, chTOG and GTSE1, we set out to relocalize each endogenous protein in mitotic knock-in cells and ask whether this manipulation affects the localization of the other proteins, detected by indirect immunofluorescence (Fig. 3). Relocalization of endogenous clathrin (CLTA–FKBP–GFP) caused the removal of TACC3,

Journal of Cell Science (2021) 134, jcs255794. doi:10.1242/jcs.255794

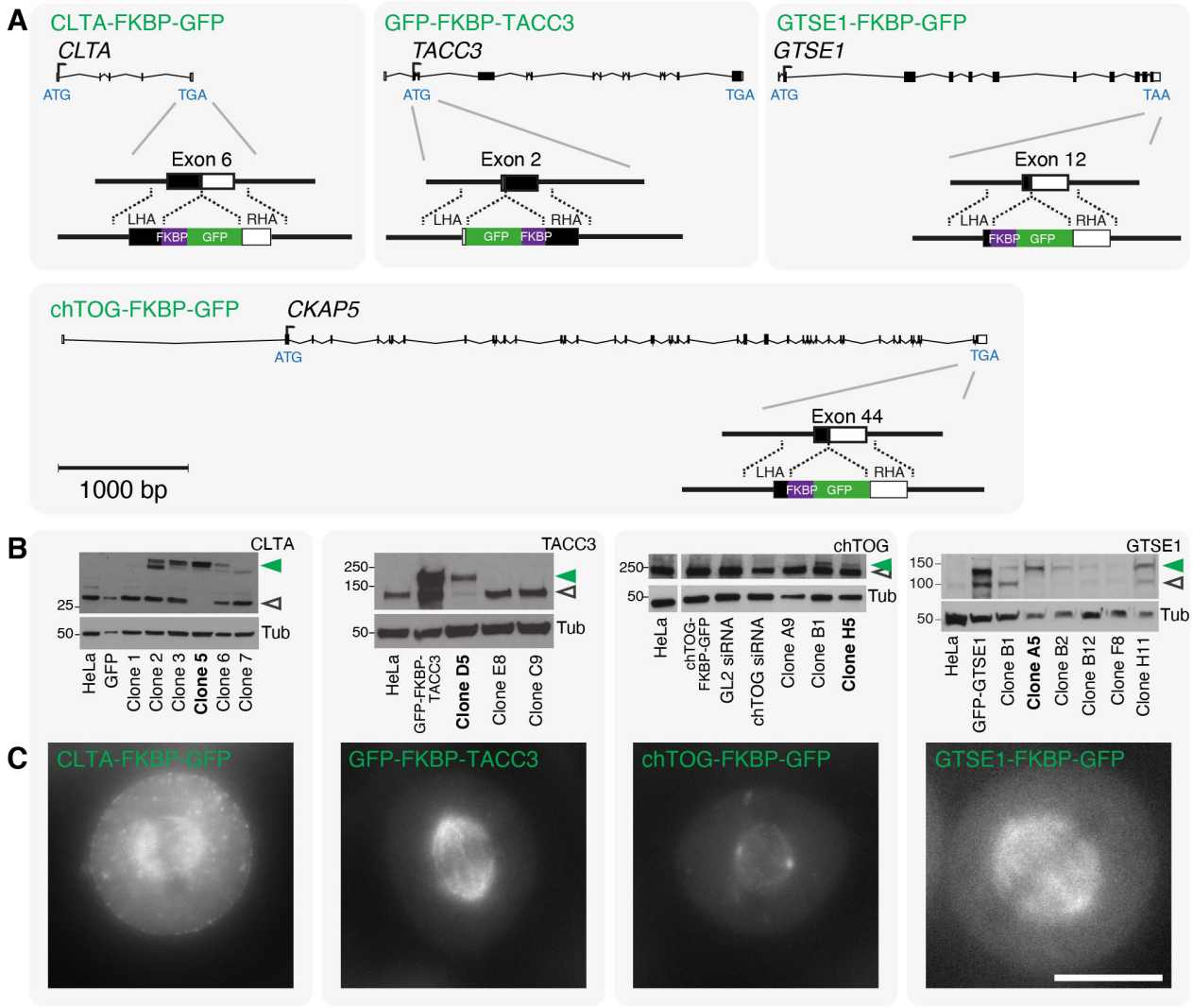

Fig. 1. Generation of knock-in HeLa cell lines using gene editing. (A) Strategy to tag clathrin (CLTA), TACC3, chTOG (CKAP5) and GTSE1 with FKBP and GFP at their endogenous loci. Cas9n D10A nickase was used to target the indicated site, and a repair template with FKBP–GFP or GFP–FKBP tag flanked by left and right homology arms (LHA and RHA, respectively) was used as indicated. GFP-positive cells were individually sorted by FACS and validated using a combination of western blotting, imaging and DNA sequencing (not shown). (B) Western blotting showed negative clones and positive clones that were either homozygous (single band, shifted by ∼30 kDa) or heterozygous (two bands, one at expected size and the other shifted by ∼30 kDa) knock-in cell lines. The tagged and untagged proteins are denoted by filled green and open gray arrowheads, respectively. Clones used in this work are highlighted in bold. Molecular mass markers are shown in kDa for each blot. Control lanes show parental HeLa (HeLa) or parental HeLa overexpressing the indicated protein. HeLa cells may have more than two alleles of the targeted gene. We use the term homozygous to indicate editing of all alleles and heterozygous to indicate that at least one allele was edited and that an unedited allele remained. PCR and DNA sequencing confirmed that: CLTA–FKBP–GFP (clone 5) is homozygous, GFP–FKBP–TACC3 (clone D5) is homozygous, chTOG–FKBP–GFP (clone H5) is heterozygous and GTSE1–FKBP–GFP (clone A5) is homozygous. (C) Micrographs showing GFP fluorescence of each tagged cell line indicating the correct localization of each tagged protein. Scale bar: 10 µm.

GTSE1 and chTOG from the spindle (Fig. 3A). On the other hand, relocalization of endogenous GFP–FKBP–TACC3 resulted in removal of chTOG but only small reduction in clathrin and GTSE1 (Fig. 3B). By contrast, relocalization of chTOG–FKBP–GFP had no effect on the spindle localization of the other three proteins (Fig. 3C). We also detected small changes in clathrin, TACC3 and chTOG localization following relocalization of GTSE1–FKBP–GFP (Fig. 3D). Although these experiments were designed to examine interactions between endogenous proteins, it is only possible to measure relocalization and removal in different populations of cells.

We next sought to repeat these experiments using a single-cell live-imaging approach. To do this, the knock-in cell lines were transfected with dark MitoTrap and either mCherry–CLTA, mCherry–TACC3, chTOG–mCherry or tdTomato–GTSE1. Metaphase cells were imaged live as rapamycin was added (Fig. 4). Relocalization of endogenous clathrin caused the removal of mCherry–TACC3, chTOG–mCherry and tdTomato–GTSE1 from the spindle (Fig. 4A). Similarly, relocalization of endogenous TACC3 also caused the removal of the other three proteins from the spindle, but to a lesser extent than with clathrin relocalization (Fig. 4B). Again, relocalization of either chTOG or GTSE1 had no effect on the spindle localization of the other three proteins (Fig. 4C,D). A semi-automated analysis procedure was used to measure induced relocalization of both proteins (see Materials and Methods). All movement was from the mitotic spindle to the mitochondria, without significant loss to the cytoplasm, suggesting that the complex is either relocalized en masse

Journal of Cell Science (2021) 134, jcs255794. doi:10.1242/jcs.255794

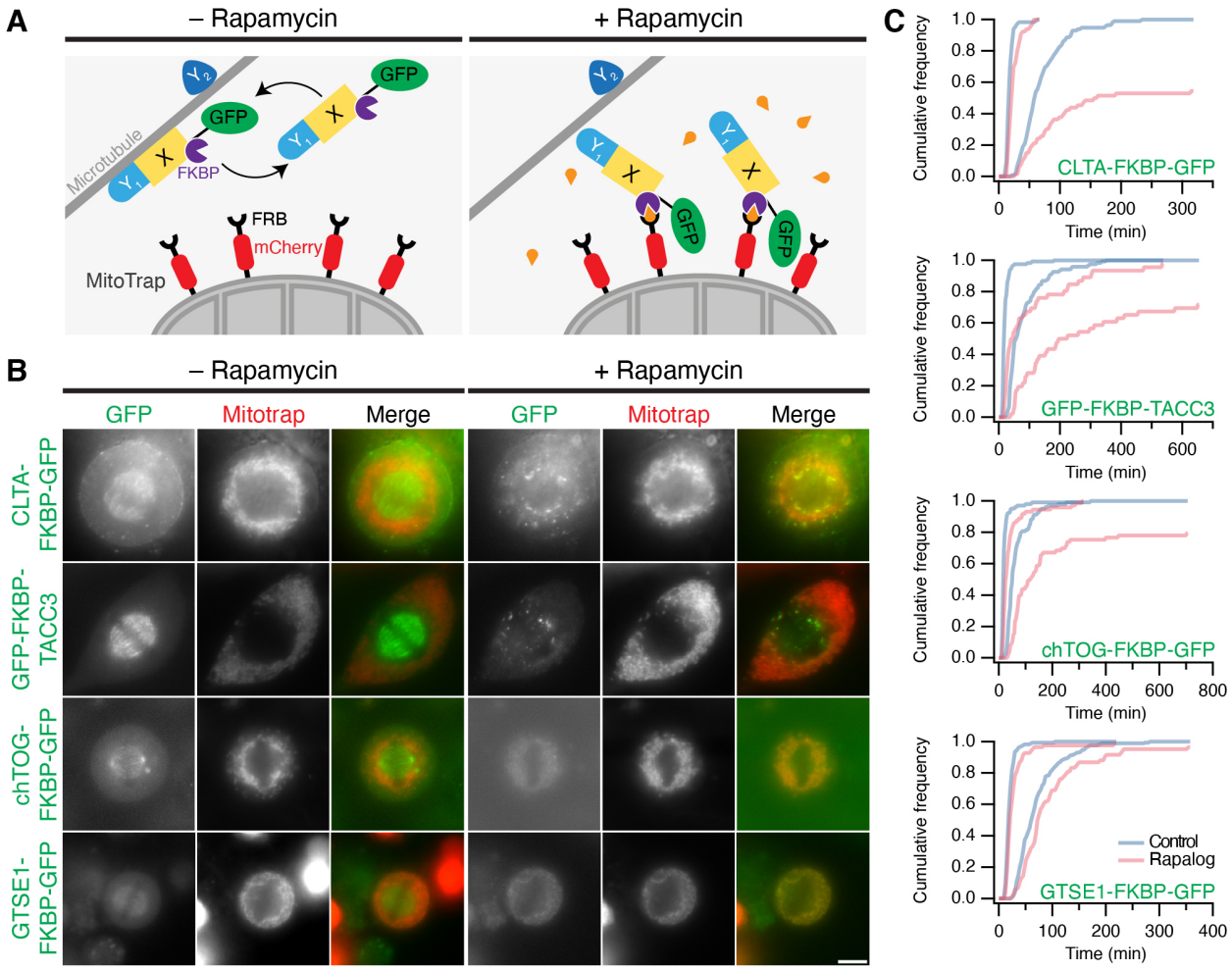

Fig. 2. Generation of knock-in HeLa cell lines using gene editing. (A) Schematic diagram of knocksideways in gene edited cells. A microtubule-binding protein X is fused to FKBP and GFP. MitoTrap, an FRB domain targeted to mitochondria, tagged with mCherry, is transiently expressed. Addition of rapamycin causes the relocalization of proteins to the mitochondria (Robinson et al., 2010). This strategy can also be used to assess whether another protein Y, co-reroutes with X to the mitochondria. Y_1 co-reroutes with X, indicating that they form a complex, whereas Y_2 does not. (B) Live-cell imaging of knocksideways of gene-edited cell lines. The indicated tagged cell lines expressing mCherry-tagged MitoTrap were imaged on a widefield microscope. Stills from a movie where metaphase cells were treated with rapamycin (200 nM) are shown. The post-rapamycin images (+ Rapamycin) are 10–15 min after treatment. Scale bar: 10 µm. (C) Mitotic progression following knocksideways. Cumulative histograms of timings from nuclear envelope breakdown (NEB) to metaphase (short duration plots) and NEB to anaphase (long duration plots). Gene-edited cells expressing mCherry–MitoTrap(T2098L) were pre-treated with 1 µM rapalog as indicated. All imaging experiments were repeated three times. Number of cells analyzed (control and rapalog, respectively): CLTA–FKBP–GFP, 115 and 66; GFP–FKBP–TACC3, 122 and 46; chTOG–FKBP–GFP, 104 and 73; GTSE1–FKBP–GFP, 176 and 84.

or not. Two-dimensional arrow plots were therefore used to visualize the results of these experiments (Fig. 4E,F). As previously reported, mCherry–TACC3 expression distorted the localization of the complex prior to knocksideways (Booth et al., 2011; Nixon et al., 2015), enhancing the amount of clathrin, chTOG and GTSE1 on the spindle (Fig. 4F, note the rightward shift of the starting point in the arrow plots when mCherry–TACC3 was expressed). This likely reflects the importance of TACC3 in loading the complex onto the spindle (Hood et al., 2013). The expression of other partner proteins, mCherry–CLTA, chTOG–mCherry and tdTomato–GTSE1, had no effect on the localization of the knock-in protein.

The lack of removal of complex members after relocalization of chTOG–FKBP–GFP could be due to the heterozygosity of this knock-in cell line, since the untagged copy may prevent removal. In order to verify this result, we performed knocksideways using transient expression of chTOG–FKBP–GFP in unedited HeLa cells that were depleted of endogenous chTOG by RNAi. These experiments showed that clathrin, TACC3 and GTSE1 all remain in place following the relocalization of chTOG–GFP–FKBP to the mitochondria (Fig. S4).

The results of both knocksideways approaches are summarized in Table S2. Overall, the relocalization of either clathrin or TACC3 during metaphase results in removal of the entire TACC3–chTOG–clathrin–GTSE1 complex. The efficiency of this removal is higher with clathrin than TACC3, yet overexpression of TACC3 can load more complex members onto the spindle. Relocalization of either chTOG or GTSE1 has no effect on the rest of the complex, suggesting that these proteins are ancillary to TACC3–chTOG–clathrin–GTSE1, while TACC3 and clathrin are core members.

Role of LIDL motifs in recruitment of GTSE1 to the TACC3–chTOG–clathrin complex

In order to test if GTSE1 is an ancillary complex member, we sought to disrupt its interaction with clathrin and assess whether or not the

Journal of Cell Science (2021) 134, jcs255794. doi:10.1242/jcs.255794

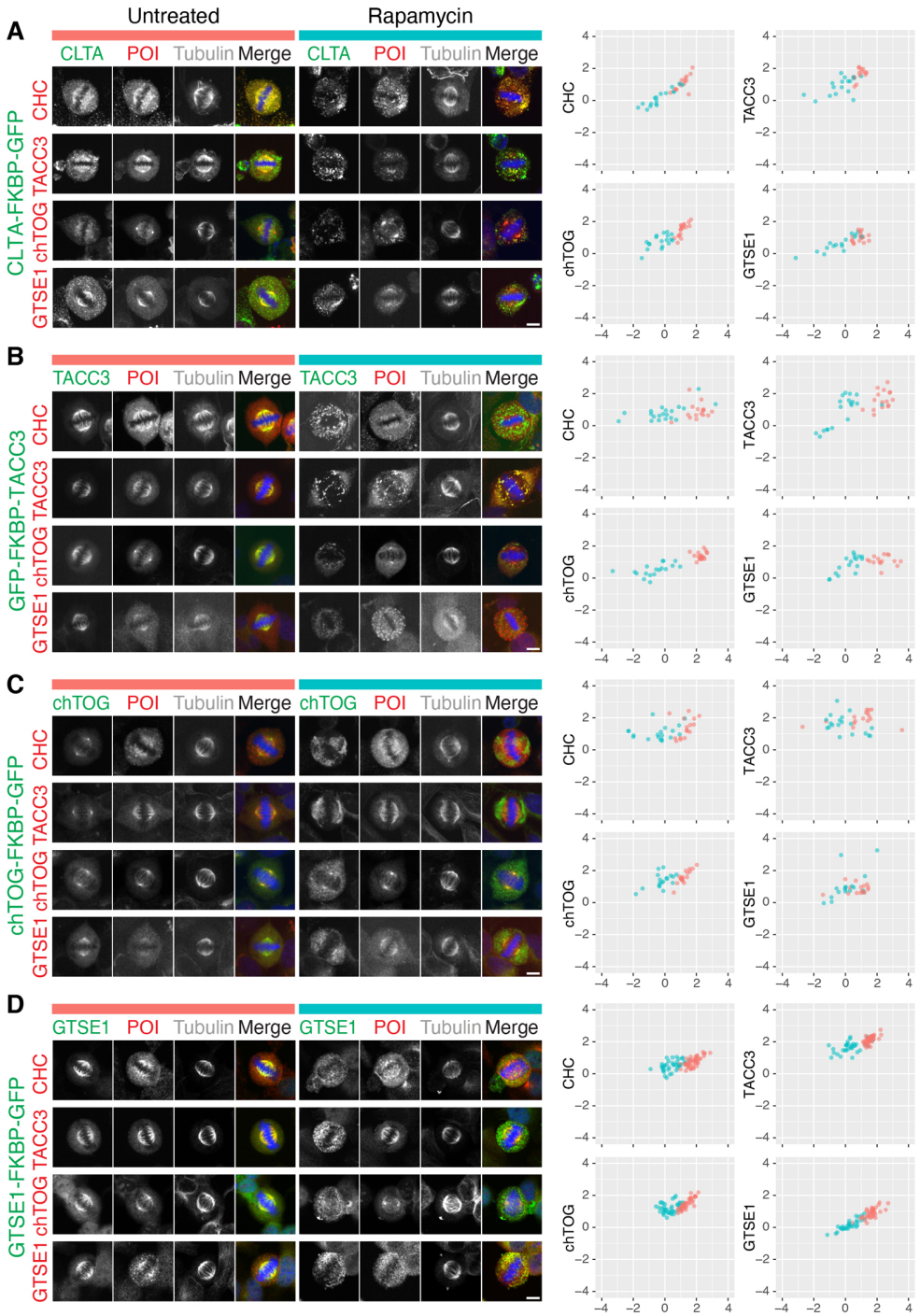

Fig. 3. Co-rerouting of endogenous complex members following knocksideways in knock-in cell lines. (A–D) Knocksideways experiments using each knock-in cell line expressing dark MitoTrap. (A) CLTA–FKBP–GFP cells. (B) GFP–FKBP–TACC3 cells. (C) chTOG–FKBP–GFP cells. (D) GTSE1–FKBP–GFP cells. Representative confocal micrographs of cells that were either untreated or treated with rapamycin (200 nM) for 30 min, fixed and stained for tubulin and either CHC, TACC3, chTOG or GTSE1 (protein of interest, POI; red). Scale bars: 10 µm. Right, quantification of images. Spindle localization of the target protein (*x*-axis) and the POI (*y*-axis) in control (red) and knocksideways (turquoise) cells. Spindle localization is the ratio of spindle to cytoplasmic fluorescence shown on a $\log_2$ scale (where a value of 1 is twice the amount of fluorescence signal in the spindle regions of interest as in the cytoplasmic regions of interest, and −1 indicates half the amount of fluorescence in the spindle regions of interest versus in the cytoplasmic regions of interest). Quantification of cells from three or more experiments is shown.

spindle-binding of these two proteins was interdependent. To examine the effect on the mitotic localization of both proteins, mCherry-tagged GTSE1 constructs were expressed in GTSE1-depleted CLTA–FKBP–GFP cells (Fig. 5). GTSE1 has a previously mapped clathrin-interaction domain (CID; amino acids 639–720) containing five clathrin box-like motifs (LI[DQ][LF]; hereafter referred to as LIDL motifs), which was targeted for disruption (Wood et al., 2017; Rondelet et al., 2020). We found that deletion of the entire CID

Journal of Cell Science (2021) 134, jcs255794. doi:10.1242/jcs.255794

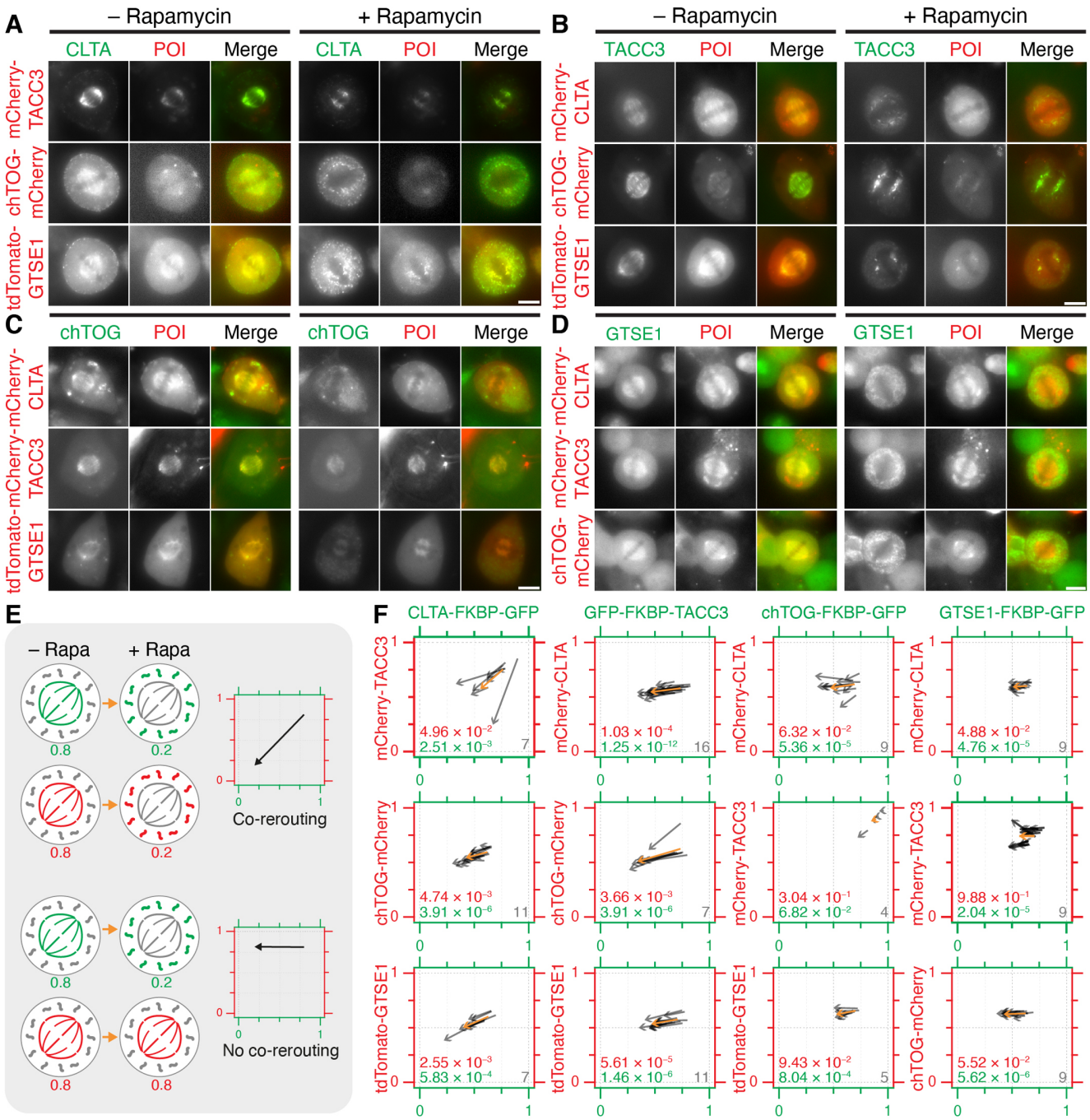

Fig. 4. Co-rerouting of complex members during live-cell knocksideways experiments in knock-in cell lines. (A–F) Knocksideways experiments using each knock-in cell line expressing dark MitoTrap and one of the three other complex proteins tagged with a red fluorescent protein (mCherry–CLTA, mCherry–TACC3, chTOG–mCherry or tdTomato–GTSE1) as indicated. (A) CLTA–FKBP–GFP cells. (B) GFP–FKBP–TACC3 cells. (C) chTOG–FKBP–GFP cells. (D) GTSE1–FKBP–GFP cells. Still images are shown before (– Rapamycin) and 10 min after rapamycin (200 nM; + Rapamycin) treatment. In merge panels, GFP fluorescence is shown in green and protein of interest (POI) fluorescence is shown in red. Scale bars: 10 µm. (E) Explanation of 'arrow plots' to analyze co-rerouting. Arrows show the fraction of combined spindle and mitochondria fluorescence that is at the spindle (i.e. 1=completely spindle-localized, 0=mitochondria-localized) for green and red fluorescence channels, moving from pre- to post-rapamycin localization. Examples are shown of two mCherry-tagged proteins that do (top) or do not (bottom) co-reroute with an FKBP–GFP-tagged protein. (F) Arrow plots of live-cell knocksideways experiments. Gray arrows represent individual cells measured across three experimental repeats (*n* is shown bottom right), orange arrow indicates the mean. Bottom left of each plot, *P*-values from Student's paired *t*-tests to compare the effect of rapamycin on the two proteins in that condition.

resulted in a reduction in GTSE1 on the spindle. Mutation of LIDL motifs 1 and 2, 3, or 4 and 5 to alanines did not result in reduction, but when mutated in combination resulted in a loss of GTSE1 that was similar to deletion of the CID. However, under all conditions the spindle localization of clathrin was unaffected. These findings were corroborated by a live-cell knocksideways approach (Fig. S5).

To test whether the reduction in GTSE1 spindle localization represented a block of recruitment, cells were treated with 0.3 µM

Journal of Cell Science (2021) 134, jcs255794. doi:10.1242/jcs.255794

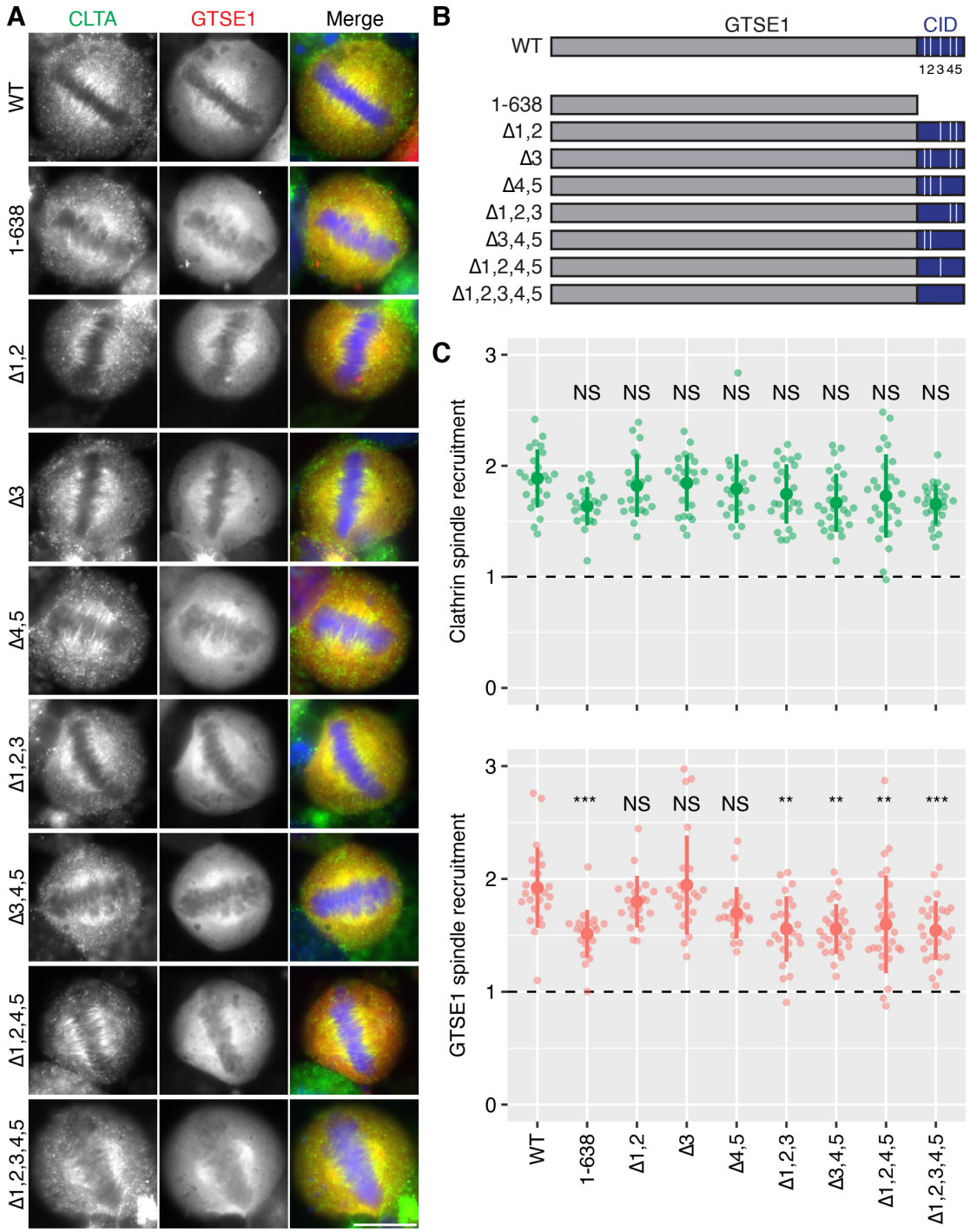

Fig. 5. Role of LIDL motifs in GTSE1 spindle localization. (A) Representative widefield micrographs of GTSE1–mCherry constructs (red) in GTSE1-depleted CLTA–FKBP–GFP cells at metaphase. Cells expressing the indicated constructs, as described in B, were fixed and stained using DAPI (blue) and a GFP-boost antibody to enhance the signal of CLTA–FKBP–GFP (green). Scale bar: 10 µm. (B) Schematic diagram of full-length GTSE1 (WT, 1–720), truncated GTSE1 lacking the CID (1–638) and mutant forms. The five LIDL motifs (white) are numbered 1 to 5. Mutation of the corresponding motifs by replacement of each motif sequence with four alanine residues is denoted by Δ. (C) Quantification of the spindle localization of clathrin (top) and GTSE1 (bottom). Each dot represents a single cell, *n*=21–28 cells per construct over three separate experiments. The dashed horizontal line represents no enrichment on the spindle. The large dot and error bars show the mean±s.d., respectively. ANOVA with Tukey's post-hoc test was used to compare the means between each group. The *P*-value level is shown compared to WT: ****P*<0.001; ***P*<0.01; NS, *P*>0.05.

MLN8237 to inhibit Aurora A activity and provide a reference for minimal recruitment (Hood et al., 2013; Booth et al., 2011). Spindle localization of both clathrin and wild-type GTSE1 (WT) was abolished by drug treatment (Fig. S6). Again, spindle localization of GTSE1 with LIDL motifs 1–5 mutated to alanine (GTSE1Δ1,2,3,4,5) was lower than that of WT in untreated cells,

Journal of Cell Science (2021) 134, jcs255794. doi:10.1242/jcs.255794

and was not reduced further by MLN8237 treatment (P=0.08). These data are consistent with the idea that GTSE1 is recruited to the spindle by clathrin via multiple LIDL motifs in GTSE1 (Rondelet et al., 2020). Moreover, they suggest that there is no interdependent spindle localization of clathrin–GTSE1 and that GTSE1 is an ancillary member of the complex.

The ability to bind clathrin is necessary for GTSE1 to localize to the spindle, but is it sufficient? To address this question we examined the subcellular localization of a panel of GTSE1 fragments in mitosis and in interphase cells (Fig. 6). A GTSE1 fragment comprising the CID containing all five LIDL motifs was unable to bind the mitotic spindle. Progressively adding more N-terminal sequence to the CID eventually yielded a construct that bound the spindle (amino acids 161–720; Fig. 6A–C). This experiment demonstrated that the CID alone is not sufficient for spindle localization. Interphase microtubule binding was seen for the GTSE1 fragment 161–720 and to a lesser extent for 1–354, 335–720 and 400–720 (Fig. 6A,D). This suggests that the region 161–638 contains one or more regions that can bind

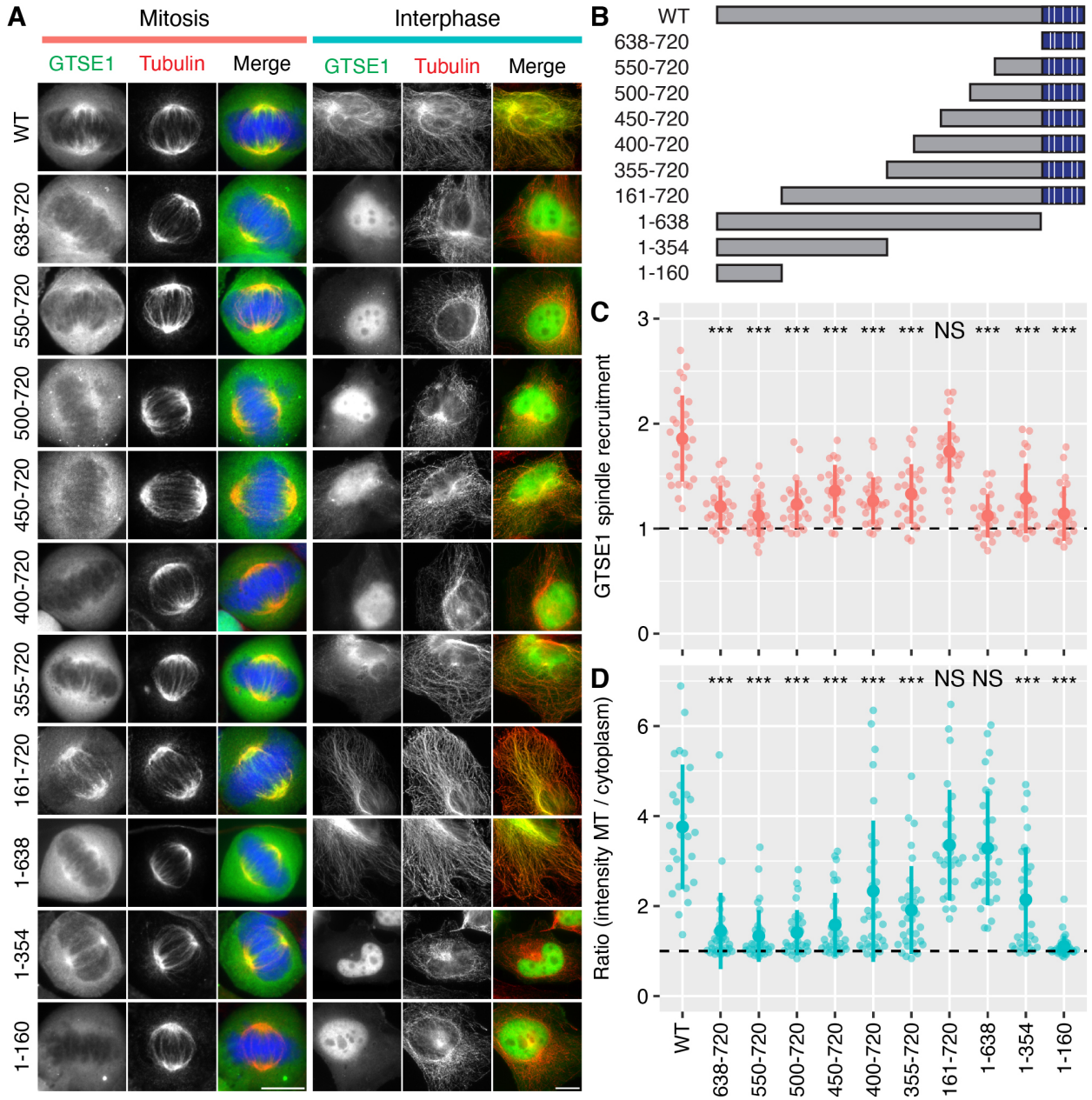

Fig. 6. Localization of GTSE1 fragments in interphase and mitosis. (A) Representative widefield micrographs of GTSE1–FKBP–GFP constructs (green), as described in B, expressed in cells in mitosis or interphase. Cells were stained to show α-tubulin (red) and DNA (cells in mitosis only; DAPI, blue). Scale bars: 10 µm. (B) Schematic diagram of full-length GTSE1 (WT, 1–720) and fragments of GTSE1 used in this figure. The CID is shown in blue, with LIDL motifs indicated by white lines. Quantification of GTSE1 localization on mitotic spindles (C) or interphase microtubules (D). Each dot represents a single cell, n=23–28 cells per construct (mitosis) and n=27–33 cells per construct (interphase) pooled from three independent experiments. The dashed horizontal line represents no enrichment. The large dot and error bars show the mean±s.d., respectively. ANOVA with Tukey's post-hoc test was used to compare the means between each group. The P-value level is shown compared to WT: ***P<0.001; NS, P>0.05.

Journal of Cell Science (2021) 134, jcs255794. doi:10.1242/jcs.255794

microtubules and that these regions, together with the five LIDL motifs in the CID, are required for spindle localization.

PIK3C2A is not a component of the TACC3–chTOG–clathrin–GTSE1 complex

We next investigated whether or not PIK3C2A is a component of the TACC3–chTOG–clathrin–GTSE1 complex, since PIK3C2A has been proposed to bind TACC3 and clathrin, and therefore stabilize the complex (Gulluni et al., 2017). If PIK3C2A binds the complex, we would predict that it should also localize to the mitotic spindle. We imaged GFP–PIK3C2A in live cells and found no evidence for spindle localization (Fig. 7A). The construct localized to clathrin-coated pits, suggesting that the GFP tag had not interfered with its normal localization. We next overexpressed mCherry–TACC3 to concentrate the TACC3–chTOG–clathrin–GTSE1 complex on the spindle and maximize our chances of seeing any GFP–PIK3C2A signal on microtubules but, again, we saw no spindle localization of GFP–PIK3C2A (Fig. 7B).

To further explore any mitotic role for PIK3C2A, we generated a PIK3C2A-knockout cell line using CRISPR/Cas9. This generated a clone with a premature stop codon in both alleles, resulting in truncation after 87 and 72 residues for the two alleles, that we termed PIK3C2A null (Fig. S7C). It was previously shown that PIK3C2A knockout in primary mouse embryo fibroblasts (MEFs) altered their mitotic progression (Gulluni et al., 2017). We analyzed mitotic timings of our PIK3C2A-null cell line, compared to those of

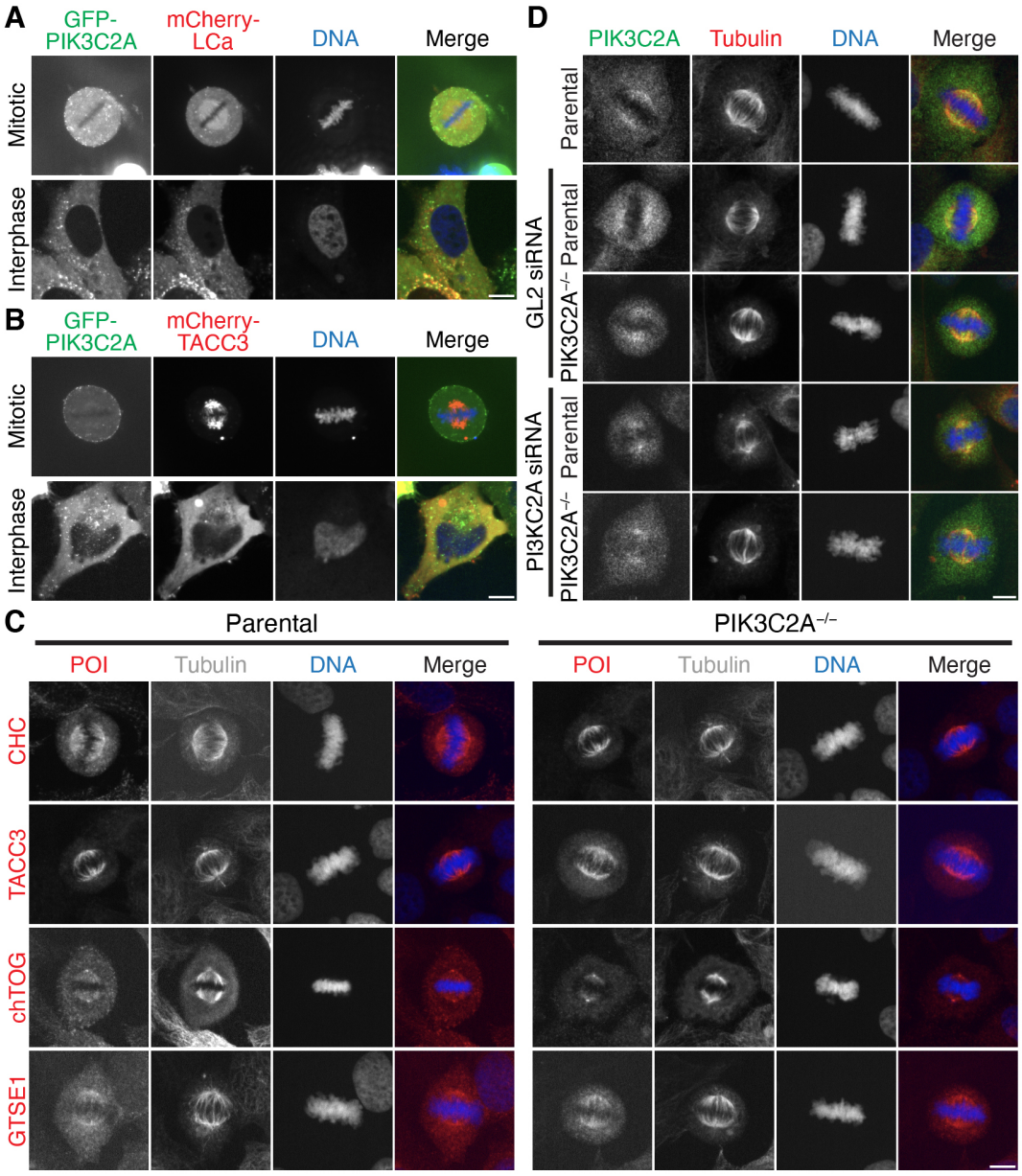

Fig. 7. PIK3C2A is not a component of the TACC3–chTOG–clathrin–GTSE1 complex. (A,B) Representative confocal micrographs of mitotic and interphase HeLa cells expressing GFP–PIK3C2A and either (A) mCherry–CLTA (mCherry–LCa) or (B) mCherry–TACC3. (C) Representative widefield micrographs of parental HeLa and PIK3C2A-null (PIK3C2A$^{-/-}$) cells stained for tubulin and either CHC, TACC3, chTOG or GTSE1 (red; protein of interest, POI). (D) Representative widefield micrographs of parental HeLa and PIK3C2A$^{-/-}$ cells treated with GL2 (control) or PIK3C2A siRNA, stained with an anti-PIK3C2A antibody (Proteintech; green) and an anti-tubulin antibody (red). DNA was stained with DAPI (blue). Scale bars: 10 µm.

Journal of Cell Science (2021) 134, jcs255794. doi:10.1242/jcs.255794

parental HeLa cells, and found no differences in mitotic timings (Fig. S7D).

If PIK3C2A was a scaffold protein for the TACC3–chTOG–clathrin–GTSE1 complex, we would expect some disruption of the spindle localization of clathrin, TACC3, chTOG or GTSE1 in the PIK3C2-null cells. However, immunostaining of parental HeLa and PIK3C2A-null cells with antibodies against clathrin heavy chain (CHC), TACC3, chTOG and GTSE1 revealed a similar distribution of all four complex members during mitosis (Fig. 7C). In the original paper, immunostaining of PIK3C2A at the mitotic spindle was shown (Gulluni et al., 2017).

We immunostained parental HeLa cells and the PIK3C2A-null cells with the same anti-PI3KC3A antibody used in the original report and found that there was a signal at the mitotic spindle, but that it was non-specific, because it was also detected in the PIK3C2A-null cells (Fig. 7D). We also used RNAi of PIK3C2A in parental and PIK3C2A-null cells to rule out the possibility that the antibody signal resulted from residual expression of PIK3C2A. Again, the spindle fluorescence remained after RNAi treatment, indicating that the antibody is non-specific for immunofluorescence. Taken together, our results suggest that PIK3C2A is not a component of the TACC3–chTOG–clathrin–GTSE1 complex.

DISCUSSION

Inducible relocalization is a powerful method to investigate protein–protein interactions in cells and to pinpoint where and when they occur. We generated a number of cell lines to study the interactions between members of the TACC3–chTOG–clathrin–GTSE1 complex on mitotic spindles at metaphase. This approach showed that TACC3 and clathrin are core complex members, while chTOG and GTSE1 are ancillary. Our current picture of this multiprotein complex is outlined in Fig. 8.

It has been reported that PIK3C2A is a component of the TACC3–chTOG–clathrin–GTSE1 complex, where it has been proposed to act as a scaffold protein binding both TACC3 and clathrin (Gulluni et al., 2017). This proposal is consistent with several observations. First, PIK3C2A has been found to interact with clathrin, GTSE1 and TACC3 in a proteomic analysis of immunoprecipitations with each of these three proteins from mitotic lysate (Hubner et al., 2010). In that study, immunoprecipitation of PIK3C2A brought down clathrin, GTSE1 and components of the membrane trafficking machinery, but notably neither TACC3 nor chTOG co-immunoprecipitated with PIK3C2A. Second, PIK3C2A binds clathrin heavy chain via an N-terminal region that contains a clathrin box-like motif (LLLDD; Gaidarov et al., 2001). These motifs bind to grooves in the seven-bladed β-propeller that constitutes the N-terminal domain of clathrin heavy chain (Smith et al., 2017). The N-terminal domain is required for clathrin–TACC3 to localize at the spindle (Royle et al., 2005), and mutations in one of the grooves is sufficient to reduce spindle binding (Hood et al., 2013). However, while the proposal that PIK3C2A is a component of the complex makes sense, we found no evidence to suggest that PIK3C2A was even present on mitotic spindles. GFP-tagged PIK3C2A was found in clathrin-coated vesicles, as expected, but was absent from the mitotic spindles of HeLa cells. We also found that the PIK3C2A antibody used in the original study to detect the protein at the spindle gave a false signal that remained after knockout and/or knockdown of PIK3C2A. Finally, a PIK3C2A-null cell line we generated had no mitotic delays, and all members of the TACC3–chTOG–clathrin–GTSE1 complex had normal localization. We conclude that PIK3C2A is not a component of the complex and any mitotic function for this protein is doubtful.

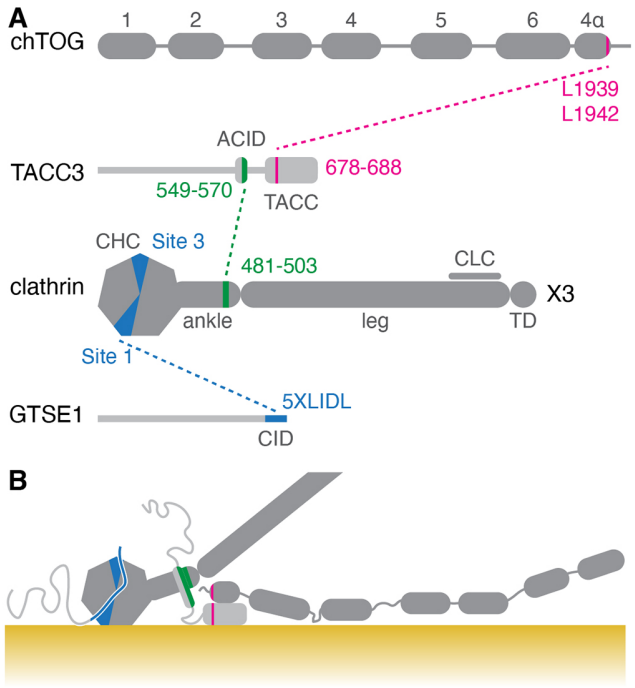

Fig. 8. Summary diagram of interactions between TACC3–chTOG–clathrin–GTSE1 complex members and microtubules. (A) Primary structure of chTOG, TACC3, clathrin and GTSE1, showing the interactions between each protein (dashed lines). ACID, Aurora-A and clathrin interaction domain; CHC, clathrin heavy chain; CLC, clathrin light chain; TD, trimerization domain. The TOG domains of chTOG are numbered. Interactions were mapped previously (Gutiérrez-Caballero et al., 2015; Hood et al., 2013; Burgess et al., 2018; Rondelet et al., 2020). (B) Proposed topology of the complex on a microtubule (yellow). TACC3 and clathrin bind each other and form a composite microtubule-interaction surface. GTSE1 and chTOG bind to clathrin and TACC3, respectively. Both proteins can interact with microtubules: chTOG in a domain between TOG4 and TOG5 (Widlund et al., 2011), GTSE1 in a diffuse region between residues 161–638, although neither interaction is necessary for the complex to bind microtubules.

PIK3C2A has a well-established role in clathrin-mediated membrane traffic (Posor et al., 2013), and it seems likely that the presence of PIK3C2A among other membrane-trafficking factors in the original proteomic work was due to association with a fraction of clathrin that was not associated with the spindle, or erroneous binding during purification (Hubner et al., 2010).

Recent work has shown that GTSE1 contains five conserved LIDL motifs – an intrinsically disordered C-terminal region that can bind to the N-terminal domain of clathrin heavy chain (Rondelet et al., 2020). In agreement with this, we found that these motifs are redundant and that mutations reducing the total number of motifs to below three significantly impaired spindle binding. We also found that GTSE1 was an ancillary protein not required for the localization of the complex on microtubules and that inducing its mislocalization did not affect the other complex members. This interpretation is consistent with other work on GTSE1 (Rondelet et al., 2020; Bendre et al., 2016). It is a mystery why mutation of one groove of the N-terminal domain of clathrin heavy chain results in loss of the complex from the spindle, since it appears that this domain recruits GTSE1 to k-fibers but that GTSE1 is not needed for localization of the complex (Hood et al., 2013). One explanation is that this groove interacts directly with microtubules and that GTSE1 may also bind other sites on the N-terminal domain of clathrin heavy chain. Another is that the GTSE1–clathrin interaction may be

important for the formation of the complex, but not for its stability once loaded onto microtubules.

The ancillary nature of GTSE1 and chTOG binding to the complex via association with clathrin and TACC3, respectively, is intriguing. Especially because GTSE1 and chTOG each have the ability to bind microtubules themselves (Monte et al., 2000; Spittle et al., 2000). Rondelet et al. have proposed that clathrin–TACC3 could be forming a 'scaffold' for the recruitment of other factors, such as GTSE1, to the spindle so that they can in turn perform specific functions (Rondelet et al., 2020; Bendre et al., 2016). Our work is consistent with this idea, that clathrin–TACC3 are core to spindle microtubule binding and that other ancillary factors may be recruited through this complex. In this work, we mapped a constitutive microtubule-binding region in GTSE1 to residues 161–638, whereas chTOG likely binds the microtubule lattice through a region between TOG4 and TOG5 domains. The criterion for binding clathrin–TACC3 at the spindle may include the ability to bind microtubules, which would explain the selectivity for ancillary partners and mean that clathrin adaptors, for example, are not recruited to the spindle.

Our work establishes that, in order to disrupt the TACC3–chTOG–clathrin–GTSE1 complex, agents that target (1) the TACC3–clathrin interaction or (2) the interface between TACC3–clathrin and microtubules are required. In the first case, preventing the helix that is formed by phosphorylation of TACC3 on serine 558 from binding to the helical repeat in the ankle region of clathrin heavy chain is predicted to disrupt the complex (Burgess et al., 2018). To address the second case, the microtubule interface needs to be mapped at high resolution using cryo-electron microscopy. The endogenously tagged cell lines we have developed will be useful for investigating these interactions. Besides fluorescence microscopy and knocksideways, the cells are well suited for visualizing proteins at the ultrastructural level using inducible methodologies such as FerriTagging (Clarke and Royle, 2018).

MATERIALS AND METHODS

Molecular biology

The following plasmids were available from previous work: MitoTrap (pMito-mCherry-FRB), dark MitoTrap (pMito-mCherryK70N-FRB), rapalog-sensitive MitoTrap (pMito-mCherry-FRB-T2098L), mCherry–α-tubulin, mCherry–CLTA (mCherry–LCa), mCherry–TACC3, chTOG–GFP, and pBrain-chTOG-GFP-shchTOG (Booth et al., 2011; Cheeseman et al., 2013; Hood et al., 2013; Wood et al., 2017; Clarke and Royle, 2018). Plasmid to express chTOG–mCherry was made by ligating a BamHI–NotI fragment from chTOG–GFP into pmCherry-N1 (made by substituting mCherry for EGFP in pEGFP-N1 at NheI and NotI). For tdTomato–GTSE1, a GFP–GTSE1 construct was first made by PCR of human GTSE1 (IMAGE: 4138532) with the addition of EcoRI–BamHI and cloning into pEGFP-C1 (Clontech) and then ligating the EcoRI–BamHI fragment from GFP–GTSE1 into ptdTomato-C1 (made by substituting tdTomato for EGFP in pEGFP-C1 at NheI and XhoI). Note that our GTSE1 constructs use the 720 residue isoform as their basis. Therefore our residue numbers differ from other work that uses the 739 residue isoform with an alternative start codon as the full-length GTSE1 (Rondelet et al., 2020). For GFP–PIK3C2A a ScaI–BstEII fragment from full-length human PIK3C2A in PCR-XL-Topo (IMAGE: 8322710) was cloned into pEGFP-C1. The mCherry-tagged GTSE1 constructs were made by PCR amplification of GTSE1 (IMAGE: 4138532) followed by insertion into pmCherry-N1 between SalI and BamHI, and using site-directed mutagenesis to introduce each mutation.

Cell culture

HeLa cells (Health Protection Agency/European Collection of Authenticated Cell Cultures, #93021013) were maintained in Dulbecco's Modified Eagle's Medium (DMEM) supplemented with 10% FBS and 100 U ml^{-1} penicillin/streptomycin in a humidified incubator at 37°C and 5% CO_2. Cell cultures were checked for mycoplasma contamination at six-week intervals.

Knock-in cell lines were generated by CRISPR/Cas9 gene editing. The orientation of tags (N-terminal or C-terminal) was guided by previous work on CLTA (Doyon et al., 2011), TACC3 (Cheeseman et al., 2013), chTOG (Gutiérrez-Caballero et al., 2015) and GTSE1 (Scolz et al., 2012). Briefly, HeLa cells were transfected with a Cas9n D10A nickase plasmid [pSpCas9n(BB)-2A-Puro, pX462; Addgene #48141] and a repair template. The following guide pairs were used: CLTA–FKBP–GFP cell line (guide 1, 5′-CACCGCAGATGTAGTGTTTCCACA-3′; guide 2, 5′-CACCGTGAAGCTCTTCACAGTCAT-3′), GFP–FKBP–TACC3 cell line (guide 1, 5′-CACCGGCACGACCACTTCCCACAC-3′; guide 2, 5′-CACCGACGTCTGTGTCTGGACAATG-3′), chTOG–FKBP–GFP cell line (guide 1, 5′-CACCGAAGATCCTCCGACAGCGATG-3′; guide 2, 5′-CACCGCCAGACCACATCGCTGTCGG-3′), FKBP–GFP–GTSE1 cell line (guide 1, 5′-CACCGGGAGCTCAGGTCTATGAGC-3′; guide 2, 5′-CACCGTGAGGCTGACAAGGAGAACG-3′). Details of the repair templates are available (see Data availability). Ten days after transfection, single GFP-positive cells were selected by fluorescence-activated cell sorting (FACS), expanded and validated using microscopy, western blotting, PCR and DNA sequencing. The PIK3C2A-knockout cell line was generated by transfecting HeLa cells with pSpCas9(BB)-2A-GFP (pX458; Addgene #48138) into which a single guide (5′-CACCGAGCACAGGTTTATAACAAGC-3′) had been cloned. GFP-positive cells were isolated by FACS and then single cell clones were validated using western blotting and genome sequencing. Briefly, a genomic region encompassing the target site was amplified (forward primer, 5′-CCAGTTGTGTCAGGAAATGGG-3′; reverse primer, 5′-TCCAAATCAGTCCTTGCTTTCCC-3′) and TA-cloned into pGEM-T Easy vector (Promega). Ten bacterial transformants were picked and sequenced, revealing a 1:1 ratio of the two alleles, shown in Fig. S7.

For knockdown of endogenous GTSE1 in spindle recruitment experiments, CLTA–FKBP–GFP CRISPR knock-in HeLa cells were transfected with 100 nM siRNA targeting the 3′UTR of GTSE1 [GTSE1, 5′-GCCTGGGAAATATAGTGAAACTCCT-3′; GL2 (control), 5′-CGTACGCGGAATACTTCGA-3′]. For knockdown of PIK3C2A in HeLa, RNAi was performed by transfecting 60 nM siRNA [siPIK3C2A '1', 5′-GAAACTATTGCTGGATGACAGT-3′; GL2 (control), 5′-CGTACGCGGAATACTTCGA-3′], using Lipofectamine 2000 (Invitrogen), according to the manufacturer's instructions.

For DNA plasmid transfections, cells were transfected with a total of 1000–1500 ng DNA in 35 mm fluorodishes or 6-well plates using Genejuice, as per the manufacturer's instructions (Merck Millipore). Cells were typically imaged 48 h after transfection. For knocksideways experiments, cells were transfected with plasmids to express MitoTrap alone or dark MitoTrap in combination with other constructs as indicated. For the expression of GTSE1–mCherry mutants, cells were transfected with DNA 24 h after siRNA treatment using Genejuice (Merck Millipore), following the manufacturer's protocol. Cells were fixed 64 h after siRNA transfection and 40 h after DNA transfection.

Knocksideways was via the application of rapamycin (Alfa Aesar) to a final concentration of 200 nM; either live on the microscope or, in the case of immunofluorescence experiments, for 30 min prior to fixation. Successful relocalization in edited cells depends on the optimal expression of MitoTrap and the efficient application of rapamycin to cells. For Aurora-A inhibition, MLN8237 (Apexbio) was added at a final concentration of 300 nM for 40 min.

Immunofluorescence

For immunofluorescence, cells were fixed at room temperature using PTEMF (20 mM PIPES, pH 6.8, 10 mM EGTA, 1 mM $MgCl_2$, 0.2% Triton X-100 and 4% paraformaldehyde) for 10 min and permeabilized at room temperature in 0.5% Triton-X100 in phosphate-buffered saline (PBS) for 10 min. Cells were blocked in 3% BSA in PBS for 30 min. Cells were incubated for 1 h at room temperature with primary antibodies as follows: rabbit anti-α-tubulin (PA5-19489, Invitrogen; 1:1000), mouse anti-α-tubulin (B-5-1-2; Sigma; 1:1000), mouse anti-CHC (X22; CRL-2228, ATCC; 1:1000), rabbit anti-CKAP5 (PA5-59150, Thermo Fisher Scientific; 1:400), rabbit anti-chTOG

(Fig. 7 only; 34032, QED Biosciences; 1:5000), mouse anti-TACC3 (ab56595, Abcam; 1:1000), mouse anti-GTSE1 (H00051512-B01P, Abnova; 1:1000) and rabbit anti-PIK3C2A (22028-1-AP, Proteintech; 1:1000). Cells were washed three times with PBS, then incubated for 1 h with Alexa Fluor 568- or Alexa Fluor 647-conjugated secondary antibodies (Molecular Probes). Finally, coverslips were rinsed with PBS and mounted with Mowiol containing DAPI (Sigma). In some experiments it was necessary to boost the GFP signal of the knock-in cells. To do this, GFP-booster (Alexa Fluor 488, Chromotek) or GFP rabbit anti-Tag, Alexa Fluor 488 (Invitrogen) 1:200 was used during the primary incubations.

Biochemistry

For western blotting, cell lysates were prepared by scraping cells in RIPA buffer containing cOmplete EDTA-free protease inhibitor cocktail (Sigma-Aldrich), incubation on ice for 30 min and clarification in a benchtop centrifuge (20,800 ***g***) for 15 min at 4°C. Lysates were boiled in 4× Laemmli buffer for 10 min and resolved on a precast 4–15% polyacrylamide gel (Bio-Rad). Proteins were transferred to nitrocellulose using a Trans-Blot Turbo Transfer System (Bio-Rad). Primary antibodies used were mouse anti-α-tubulin (DM1A, Sigma) 1:10,000, rabbit anti-CLTA (sc-28276, Santa Cruz) 1:1000, goat anti-TACC3 (AF5720, Novus Biologicals) 1 µg ml^{-1}, rabbit anti-chTOG (34032, QED Biosciences) 1:2000, mouse anti-GTSE1 (H00051512-B01P, Abnova) 1:500 and rabbit anti-PIK3C2A (22028-1-AP, Proteintech) 1:1000. Secondary antibodies used were anti-mouse, -rabbit and -goat IgG HRP conjugates. For detection, enhanced chemiluminescence detection reagent (GE Healthcare) and manual exposure of Hyperfilm (GE Healthcare) was performed.

Microscopy

For live-cell imaging, medium was changed to Leibovitz (Gibco) L-15 CO_2-independent medium supplemented with 10% FBS. Imaging was performed on a Nikon Ti epifluorescence microscope with standard filter sets and 100× or 60× (both 1.4 NA, oil, PlanApoVC) objectives, equipped with a heated environmental chamber (OKOlab) and either a CoolSnap MYO or 95B Prime camera (Photometrics), using NIS elements AR software.

For overnight mitotic imaging, asynchronously growing cells were incubated with 0.5 µM SiR-DNA (Spirochrome) for 60 min to visualize DNA. Image stacks (7×2 µm optical sections; 1×1 binning) were acquired every 3 min for 12 h with a 40× oil-immersion 1.3 NA objective using an Olympus DeltaVision Elite microscope (Applied Precision, LLC) equipped with a CoolSNAP HQ2 camera (Roper Scientific). Images were acquired at 10% neutral density using a Cy5 filter and an exposure time of 100 ms. A stage-top incubator maintained cells at 37°C and 5% CO_2, with further stabilization from a microscope enclosure (Weather station, PrecisionControl) held at 37°C. To analyze mitotic progression after knocksideways, cells were transfected with mCherry–MitoTrap(T2098L), and asynchronously growing cells were treated (or not) with 1 µM rapalog AP21967 prior to 30 min SiR-DNA labeling and overnight imaging. Rapalog was used for these experiments because we found that rapamycin treatment affected mitotic timing, whereas in parental HeLa cells, control versus rapalog-treated timings were unaffected (nuclear envelope breakdown-to-metaphase: 13.2 min versus 12.6 min, respectively; metaphase-to-anaphase: 20.8 min versus 20.6 min, respectively).

To image fixed cells, image stacks (5×1 µm optical sections) were acquired on a spinning-disk confocal system. Either an Ultraview (Perkin Elmer) system or a Nikon CSU-W1 spinning-disk confocal with SoRa upgrade was used with a 60×1.4 NA oil-immersion objective (Nikon) and Hamamatsu Orca-R2 (Ultraview) or 95B Prime (Photometrics) camera.

Data analysis

Analysis of knocksideways movies was done by extracting a pre- and a post-rapamycin multichannel image from the sequence. An automated procedure in Fiji (https://imagej.net/Fiji) measured three regions in each of the following areas: spindle, cytoplasm and mitochondria, after registration of the pre- and post-rapamycin images. A background measurement and a whole cell fluorescence measurement were also taken. The average value for each region, after background subtraction, was corrected for bleach using the whole cell fluorescence measurement (background-subtracted) for the respective channel. Data were exported in csv format and read into IgorPro (WaveMetrics), where a custom-written procedure analyzed the data and generated all the plots. Ternary diagrams of spindle, mitochondria and cytoplasm fluorescence revealed that knocksideways resulted in movement mainly between spindle and mitochondria (Fig. S8). Therefore, the fraction of fluorescence at the spindle and mitochondria were used to generate the arrow plots.

For spindle localization analysis of fixed cells, a 31×31 pixel (1.4 $µm^2$) region of interest was used to measure three regions of the spindle, the cytoplasm and one region outside of the cell as background, using Fiji. Following background subtraction, the average spindle fluorescence was divided by the cytoplasm fluorescence to give a measure of spindle enrichment. To quantify the microtubule localization of GTSE1 fragments, a line-scan analysis method adapted from Hooikaas et al. (2019) was used. Using an automated procedure in Fiji, average fluorescence intensities from three lines, 1–3 µm length, along microtubules stained for α-tubulin and three adjacent lines (not coincident with microtubules) were measured. Following background subtraction, the average fluorescence intensity of the microtubule line scan was divided by the average fluorescence intensity of the adjacent control line scan to generate a microtubule enrichment ratio. Analysis was done by an experimenter blind to the conditions of the experiment. All figures were made in Fiji, R or Igor Pro 8 and assembled using Adobe Illustrator. All code used in this article is available at https://github.com/quantixed/p053p030.

Acknowledgements

We thank Computing and Advanced Microscopy Unit (CAMDU) for their support and assistance in this work. We are also grateful to Nuria Ferrándiz, Vishakha Karnawat and Laura Downie for commenting on the manuscript.

Competing interests

The authors declare no competing or financial interests.

Author contributions

Conceptualization: S.J.R.; Software: J.S., S.J.R.; Formal analysis: E.L.R., J.S., S.J.R.; Investigation: E.L.R., J.S.; Resources: E.L.R., J.S., T.M.-W.; Writing - original draft: E.L.R., S.J.R.; Writing - review & editing: J.S., R.B., S.J.R.; Visualization: S.J.R.; Supervision: R.B., S.J.R.; Funding acquisition: R.B., S.J.R.

Funding

The work was supported by a Programme Award from Cancer Research UK (C25425/A27718). J.S. was supported by a studentship from the Biotechnology and Biological Sciences Research Council Midlands Integrative Biosciences Training Partnership (MIBTP) (BB/M01116X/1). Deposited in PMC for immediate release.

Data availability

Sequences for repair templates and source data are available at https://github.com/quantixed/p053p030.

Supplementary information

Supplementary information available online at
https://jcs.biologists.org/lookup/doi/10.1242/jcs.255794.supplemental

Peer review history

The peer review history is available online at
https://jcs.biologists.org/lookup/doi/10.1242/jcs.255794.reviewer-comments.pdf

References

Bendre, S., Rondelet, A., Hall, C., Schmidt, N., Lin, Y.-C., Brouhard, G. J. and Bird, A. W. (2016). GTSE1 tunes microtubule stability for chromosome alignment and segregation by inhibiting the microtubule depolymerase MCAK. *J. Cell Biol.* **215**, 631-647. doi:10.1083/jcb.201606081

Booth, D. G., Hood, F. E., Prior, I. A. and Royle, S. J. (2011). A TACC3/ch-TOG/clathrin complex stabilises kinetochore fibres by inter-microtubule bridging. *EMBO J.* **30**, 906-919. doi:10.1038/emboj.2011.15

Burgess, S. G., Mukherjee, M., Sabir, S., Joseph, N., Gutiérrez-Caballero, C., Richards, M. W., Huguenin-Dezot, N., Chin, J. W., Kennedy, E. J., Pfuhl, M. et al. (2018). Mitotic spindle association of TACC3 requires Aurora-A-dependent stabilization of a cryptic α-helix. *EMBO J.* **37**, e97902. doi:10.15252/embj.201797902

Cheeseman, L. P., Booth, D. G., Hood, F. E., Prior, I. A. and Royle, S. J. (2011). Aurora a kinase activity is required for localization of TACC3/ch-TOG/clathrin inter-microtubule bridges. *Commun. Integr. Biol.* **4**, 409-412. doi:10.4161/cib.15250

Cheeseman, L. P., Harry, E. F., McAinsh, A. D., Prior, I. A. and Royle, S. J. (2013). Specific removal of TACC3-ch-TOG-clathrin at metaphase deregulates kinetochore fiber tension. *J. Cell Sci.* **126**, 2102-2113. doi:10.1242/jcs.124834

Cherry, A. E., Vicente, J. J., Xu, C., Morrison, R. S., Ong, S.-E., Wordeman, L. and Stella, N. (2019). GPR124 regulates microtubule assembly, mitotic progression, and glioblastoma cell proliferation. *Glia* **67**, 1558-1570. doi:10.1002/glia.23628

Clarke, N. I. and Royle, S. J. (2018). FerriTag is a new genetically-encoded inducible tag for correlative light-electron microscopy. *Nat. Commun.* **9**, 2604. doi:10.1038/s41467-018-04993-0

Doyon, J. B., Zeitler, B., Cheng, J., Cheng, A. T., Cherone, J. M., Santiago, Y., Lee, A. H., Vo, T. D., Doyon, Y., Miller, J. C. et al. (2011). Rapid and efficient clathrin-mediated endocytosis revealed in genome-edited mammalian cells. *Nat. Cell Biol.* **13**, 331-337. doi:10.1038/ncb2175

Foraker, A. B., Camus, S. M., Evans, T. M., Majeed, S. R., Chen, C.-Y., Taner, S. B., Corrêa, I. R., Doxsey, S. J. and Brodsky, F. M. (2012). Clathrin promotes centrosome integrity in early mitosis through stabilization of centrosomal ch-TOG. *J. Cell Biol.* **198**, 591-605. doi:10.1083/jcb.201205116

Fu, W., Tao, W., Zheng, P., Fu, J., Bian, M., Jiang, Q., Clarke, P. R. and Zhang, C. (2010). Clathrin recruits phosphorylated TACC3 to spindle poles for bipolar spindle assembly and chromosome alignment. *J. Cell. Sci.* **123**, 3645-3651. doi:10.1242/jcs.075911

Gaidarov, I., Smith, M. E. K., Domin, J. and Keen, J. H. (2001). The class II phosphoinositide 3-kinase C2α is activated by clathrin and regulates clathrin-mediated membrane trafficking. *Mol. Cell* **7**, 443-449. doi:10.1016/S1097-2765(01)00191-5

Gergely, F., Karlsson, C., Still, I., Cowell, J., Kilmartin, J. and Raff, J. W. (2000). The TACC domain identifies a family of centrosomal proteins that can interact with microtubules. *Proc. Natl. Acad. Sci. USA* **97**, 14352-14357. doi:10.1073/pnas.97.26.14352

Gergely, F., Draviam, V. M. and Raff, J. W. (2003). The ch-TOG/XMAP215 protein is essential for spindle pole organization in human somatic cells. *Genes Dev.* **17**, 336-341. doi:10.1101/gad.245603

Gulluni, F., Martini, M., De Santis, M. C., Campa, C. C., Ghigo, A., Margaria, J. P., Ciraolo, E., Franco, I., Ala, U., Annaratone, L. et al. (2017). Mitotic spindle assembly and genomic stability in breast cancer require PI3K-C2α scaffolding function. *Cancer Cell* **32**, 444-459.e7. doi:10.1016/j.ccell.2017.09.002

Gutiérrez-Caballero, C., Burgess, S. G., Bayliss, R. and Royle, S. J. (2015). TACC3-ch-TOG track the growing tips of microtubules independently of clathrin and Aurora-A phosphorylation. *Biol. Open* **4**, 170-179. doi:10.1242/bio.201410843

Hepler, P. K., McIntosh, J. R. and Cleland, S. (1970). Intermicrotubule bridges in mitotic spindle apparatus. *J. Cell Biol.* **45**, 438-444. doi:10.1083/jcb.45.2.438

Herman, J. A., Miller, M. P. and Biggins, S. (2020). chTOG is a conserved mitotic error correction factor. *eLife* **9**, e61773. doi:10.7554/eLife.61773

Hood, F. E., Williams, S. J., Burgess, S. G., Richards, M. W., Roth, D., Straube, A., Pfuhl, M., Bayliss, R. and Royle, S. J. (2013). Coordination of adjacent domains mediates TACC3-ch-TOG-clathrin assembly and mitotic spindle binding. *J. Cell Biol.* **202**, 463-478. doi:10.1083/jcb.201211127

Hooikaas, P. J., Martin, M., Mühlethaler, T., Kuijntjes, G.-J., Peeters, C. A. E., Katrukha, E. A., Ferrari, L., Stucchi, R., Verhagen, D. G. F., van Riel, W. E. et al. (2019). MAP7 family proteins regulate kinesin-1 recruitment and activation. *J. Cell Biol.* **218**, 1298-1318. doi:10.1083/jcb.201808065

Hubner, N. C., Bird, A. W., Cox, J., Splettstoesser, B., Bandilla, P., Poser, I., Hyman, A. and Mann, M. (2010). Quantitative proteomics combined with BAC TransgeneOmics reveals in vivo protein interactions. *J. Cell Biol.* **189**, 739-754. doi:10.1083/jcb.200911091

Lin, C.-H., Hu, C.-K. and Shih, H.-M. (2010). Clathrin heavy chain mediates TACC3 targeting to mitotic spindles to ensure spindle stability. *J. Cell Biol.* **189**, 1097-1105. doi:10.1083/jcb.200911120

Manning, A. L. and Compton, D. A. (2008). Structural and regulatory roles of nonmotor spindle proteins. *Curr. Opin. Cell Biol.* **20**, 101-106. doi:10.1016/j.ceb.2007.11.004

Monte, M., Collavin, L., Lazarevic, D., Utrera, R., Dragani, T. A. and Schneider, C. (2000). Cloning, chromosome mapping and functional characterization of a human homologue of murine gtse-1 (B99) gene. *Gene* **254**, 229-236. doi:10.1016/S0378-1119(00)00260-2

Nixon, F. M., Gutiérrez-Caballero, C., Hood, F. E., Booth, D. G., Prior, I. A. and Royle, S. J. (2015). The mesh is a network of microtubule connectors that stabilizes individual kinetochore fibers of the mitotic spindle. *eLife* **4**, e07635. doi:10.7554/eLife.07635

Nixon, F. M., Honnor, T. R., Clarke, N. I., Starling, G. P., Beckett, A. J., Johansen, A. M., Brettschneider, J. A., Prior, I. A. and Royle, S. J. (2017). Microtubule organization within mitotic spindles revealed by serial block face scanning electron microscopy and image analysis. *J. Cell Sci.* **130**, 1845-1855. doi:10.1242/jcs.203877

Nwagbara, B. U., Faris, A. E., Bearce, E. A., Erdogan, B., Ebbert, P. T., Evans, M. F., Rutherford, E. L., Enzenbacher, T. B. and Lowery, L. A. (2014). TACC3 is a microtubule plus end-tracking protein that promotes axon elongation and also regulates microtubule plus end dynamics in multiple embryonic cell types. *Mol. Biol. Cell* **25**, 3350-3362. doi:10.1091/mbc.e14-06-1121

Posor, Y., Eichhorn-Gruenig, M., Puchkov, D., Schöneberg, J., Ullrich, A., Lampe, A., Müller, R., Zarbakhsh, S., Gulluni, F., Hirsch, E. et al. (2013). Spatiotemporal control of endocytosis by phosphatidylinositol-3,4-bisphosphate. *Nature* **499**, 233-237. doi:10.1038/nature12360

Robinson, M. S., Sahlender, D. A. and Foster, S. D. (2010). Rapid inactivation of proteins by rapamycin-induced rerouting to mitochondria. *Dev. Cell* **18**, 324-331. doi:10.1016/j.devcel.2009.12.015

Rondelet, A., Lin, Y.-C., Singh, D., Porfetye, A. T., Thakur, H. C., Hecker, A., Brinkert, P., Schmidt, N., Bendre, S., Müller, F. et al. (2020). Clathrin's adaptor interaction sites are repurposed to stabilize microtubules during mitosis. *J. Cell Biol.* **219**, e201907083. doi:10.1083/jcb.201907083

Royle, S. J. (2013). Protein adaptation: mitotic functions for membrane trafficking proteins. *Nat. Rev. Mol. Cell Biol.* **14**, 592-599. doi:10.1038/nrm3641

Royle, S. J., Bright, N. A. and Lagnado, L. (2005). Clathrin is required for the function of the mitotic spindle. *Nature* **434**, 1152-1157. doi:10.1038/nature03502

Scolz, M., Widlund, P. O., Piazza, S., Bublik, D. R., Reber, S., Peche, L. Y., Ciani, Y., Hubner, N., Isokane, M., Monte, M. et al. (2012). GTSE1 is a microtubule plus-end tracking protein that regulates EB1-dependent cell migration. *PLoS ONE* **7**, e51259. doi:10.1371/journal.pone.0051259

Smith, S. M., Baker, M., Halebian, M. and Smith, C. J. (2017). Weak molecular interactions in clathrin-mediated endocytosis. *Front. Mol. Biosci.* **4**, 72. doi:10.3389/fmolb.2017.00072

So, C., Seres, K. B., Steyer, A. M., Mönnich, E., Clift, D., Pejkovska, A., Möbius, W. and Schuh, M. (2019). A liquid-like spindle domain promotes acentrosomal spindle assembly in mammalian oocytes. *Science* **364**, eaat9557. doi:10.1126/science.aat9557

Spittle, C., Charrasse, S., Larroque, C. and Cassimeris, L. (2000). The interaction of TOGp with microtubules and tubulin. *J. Biol. Chem.* **275**, 20748-20753. doi:10.1074/jbc.M002597200

Tipton, A. R., Wren, J. D., Daum, J. R., Siefert, J. C. and Gorbsky, G. J. (2017). GTSE1 regulates spindle microtubule dynamics to control Aurora B kinase and Kif4A chromokinesin on chromosome arms. *J. Cell Biol.* **216**, 3117-3132. doi:10.1083/jcb.201610012

Widlund, P. O., Stear, J. H., Pozniakovsky, A., Zanic, M., Reber, S., Brouhard, G. J., Hyman, A. A. and Howard, J. (2011). XMAP215 polymerase activity is built by combining multiple tubulin-binding TOG domains and a basic lattice-binding region. *Proc. Natl. Acad. Sci. USA* **108**, 2741-2746. doi:10.1073/pnas.1016498108

Willox, A. K. and Royle, S. J. (2012). Functional analysis of interaction sites on the N-terminal domain of clathrin heavy chain. *Traffic* **13**, 70-81. doi:10.1111/j.1600-0854.2011.01289.x

Wood, L. A., Larocque, G., Clarke, N. I., Sarkar, S. and Royle, S. J. (2017). New tools for "hot-wiring" clathrin-mediated endocytosis with temporal and spatial precision. *J. Cell Biol.* **216**, 4351-4365. doi:10.1083/jcb.201702188

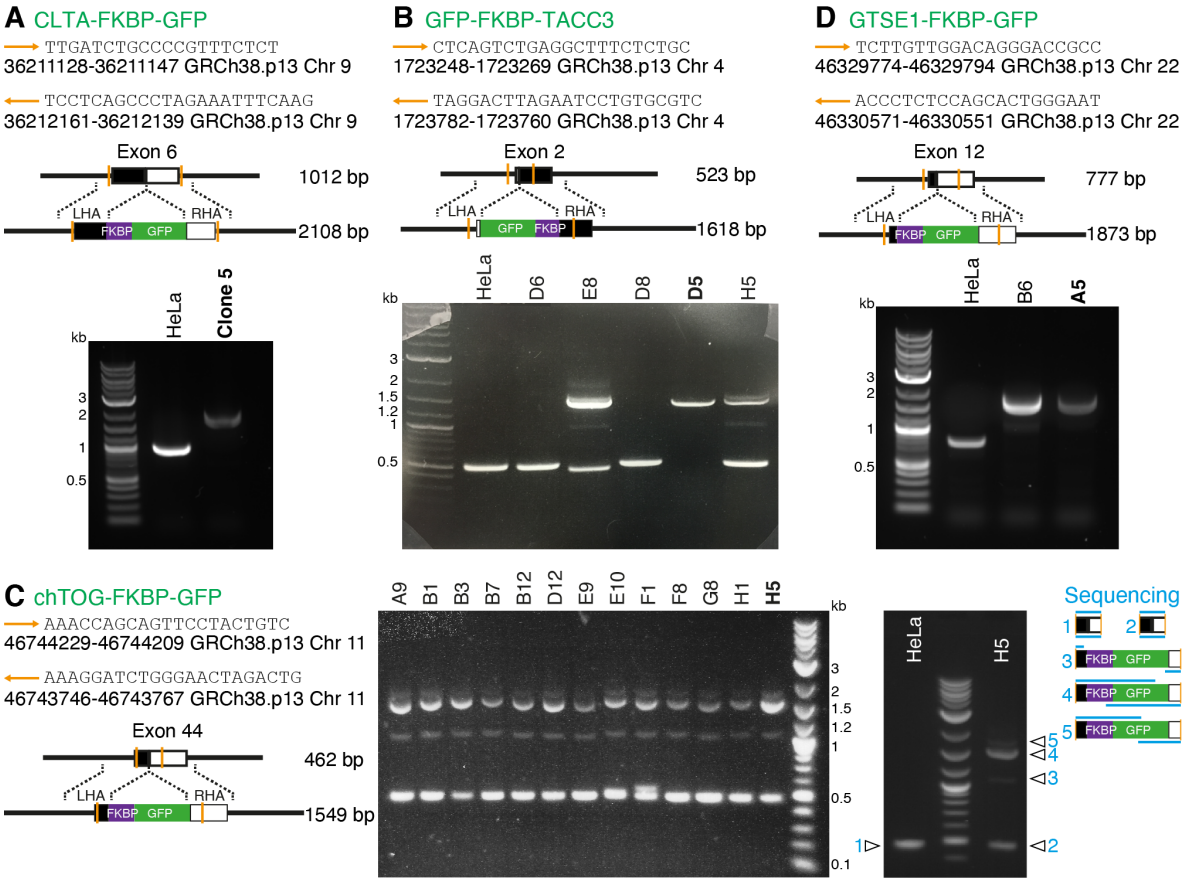

Figure S1: Genotyping gene-edited cell lines

PCR analysis to confirm insertion of tandem FKBP-GFP tag at each locus. (**A-D**) For each indicated cell line, a schematic diagram of the gene targeting event is shown with primers that anneal to left and right homology arms (orange lines); the amplicon for wild-type and successful insertion of tandem tag is shown. SyBr-stained agarose gels of PCR from genomic DNA isolated from parental HeLa or from recovered clones. Bold labels indicate the clone used in this study. (**C**) A sample of recovered clones displaying heterozygosity. Sequencing of amplicons from clone H5 revealed tagged and untagged alleles.

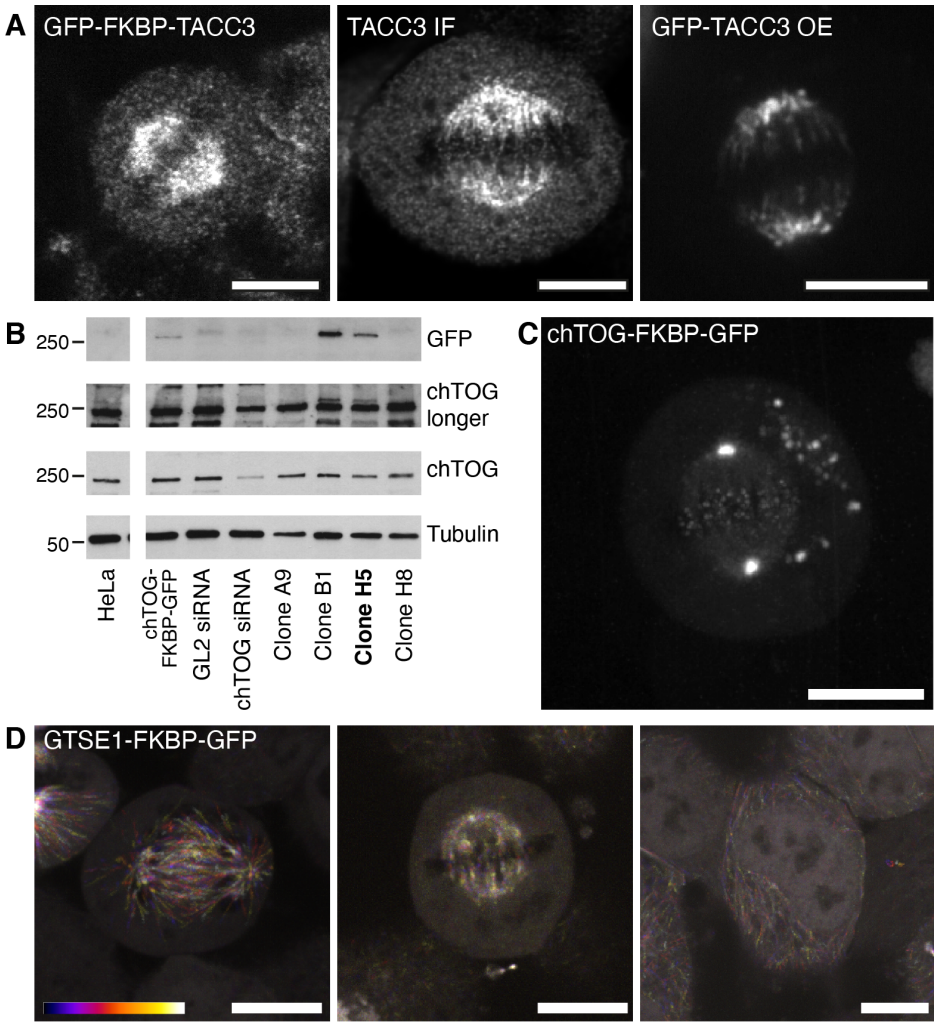

Figure S2: Further validation of gene-edited cell lines
(**A**) Representative confocal micrographs of the GFP-FKBP-TACC3 cell line (with GFP booster), anti-TACC3 immunofluorescence in unedited HeLa cells, and over-expression of GFP-TACC3 in unedited HeLa. (**B**) Western blots of four representative chTOG-FKBP-GFP clones. For comparison, parental HeLa are shown, untransfected (HeLa) or expressing chTOG-FKBP-GFP, or transfected with siRNA as described. A single gel is shown probed with a chTOG antibody (two different exposures), tubulin as a loading control, the upper blot was reprobed with a GFP antibody. The chTOG antibody does not appear to detect the tagged protein with the same efficiency as the unedited protein. (**C**) Maximum intensity projection of a stack of confocal images of a live chTOG-FKBP-GFP knock-in cell at metaphase. (**D**) Temporal color coded stacks of GTSE1-FKBP-GFP cells to show fluorescence at microtubule plus-ends. Three examples are shown of cells in anaphase (61 s), metaphase (10 s), and interphase (61 s). Scale bars, 10 µm.

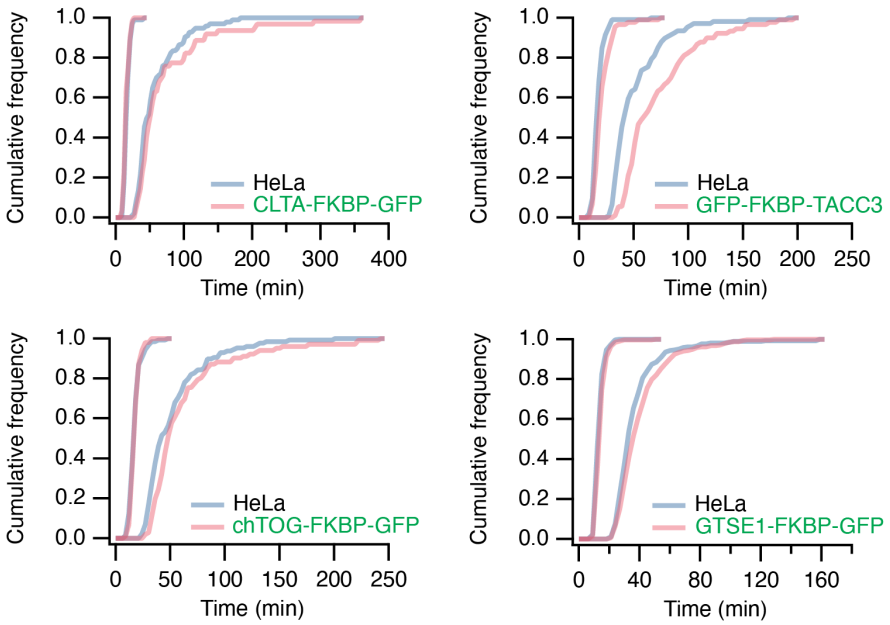

Figure S3: Mitotic progression of gene-edited cell lines
Cumulative histograms of timings from nuclear envelope breakdown (NEB) to metaphase (short duration) and NEB to anaphase (long duration). Gene-edited cells are as indicated and were imaged alongside their respective unedited parental HeLa counterpart. All imaging experiments were done three times. Number of cells analyzed (edited line and parental) = CLTA-FKBP-GFP: 62 and 97; GFP-FKBP-TACC3: 90 and 106; chTOG-FKBP-GFP: 102 and 128; GTSE1-FKBP-GFP: 265 and 319.

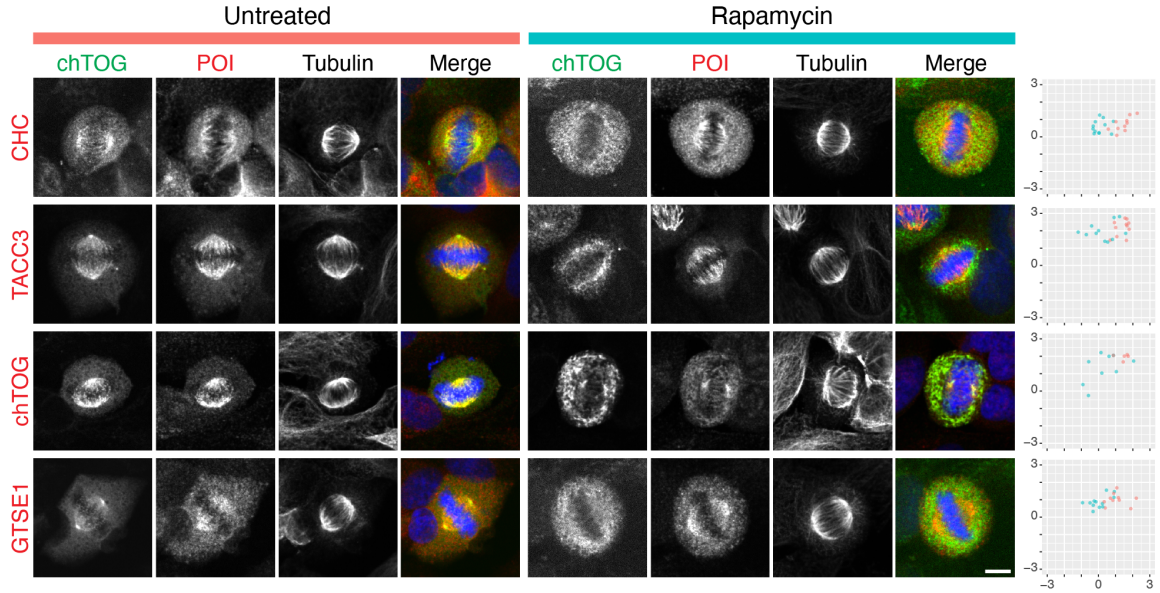

Figure S4: Verification of chTOG knocksideways results
Knocksideways experiments using transiently expressing chTOG-FKBP-GFP and dark MitoTrap in HeLa cells depleted of endogenous chTOG by RNAi. Representative widefield micrographs of cells that were treated with rapamycin (200 nM) for 30 min, fixed and stained for tubulin and either CHC, TACC3, chTOG, or GTSE1 (protein-of-interest, POI, red). Scale bar, 10 µm. Right, quantification of images. Spindle localization of the target protein (x-axis) and the protein-of-interest (y-axis) in control (salmon) and knocksideways (turquoise) cells. Spindle localization is the ratio of spindle to cytoplasmic fluorescence shown on a log2 scale (1 is twice the amount of protein on the spindle as the cytoplasm, -1 indicates half the amount on spindle versus cytoplasm). Quantification of cells from a single experiment are shown.

Journal of Cell Science • Supplementary information

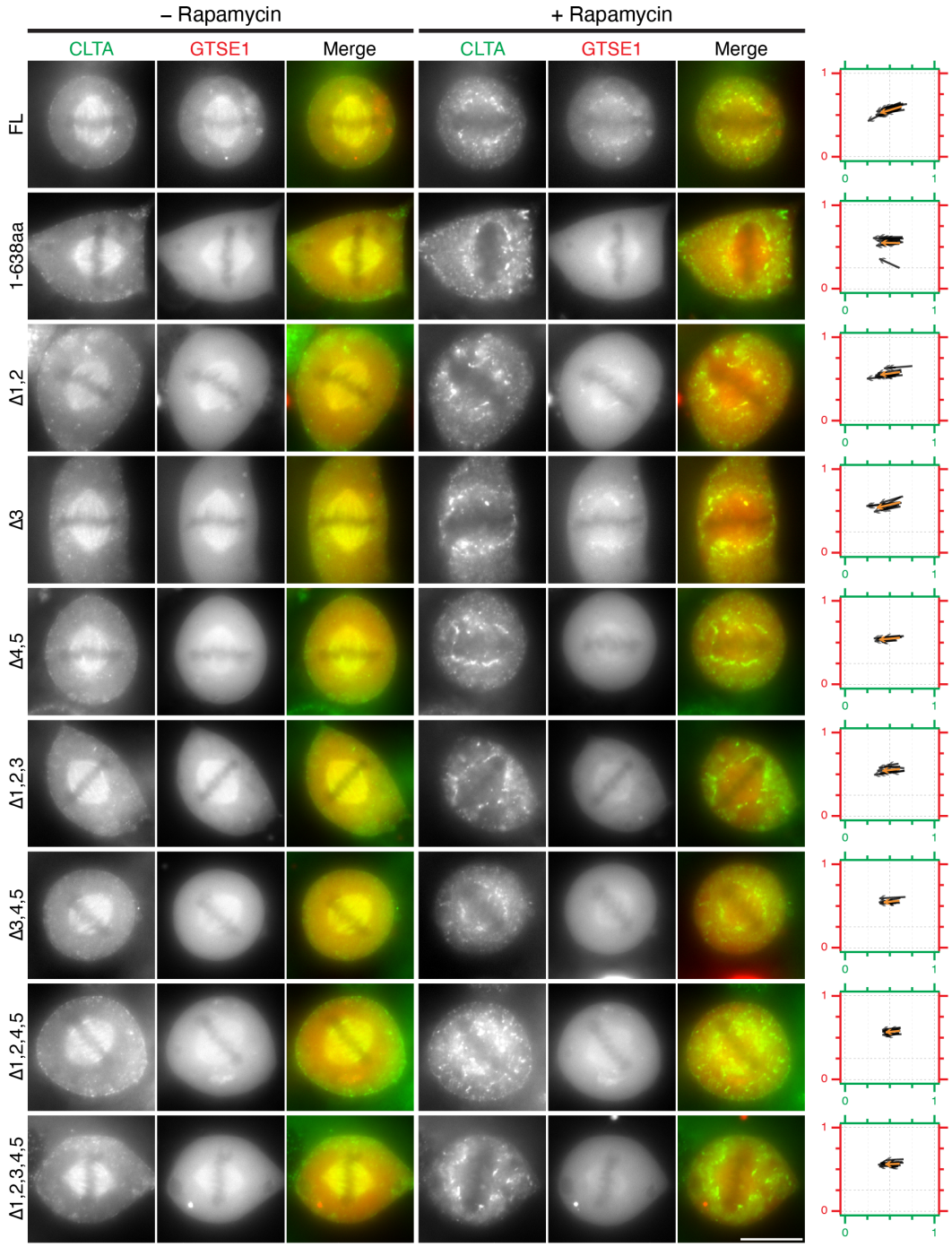

Figure S5: Live cell imaging of knocksideways in CLTA-FKBP-GFP cells expressing GTSE1 LIDL mutants. Stills from live cell imaging of clathrin knocksideways in metaphase CLTA-FKBP-GFP cells expressing the indicated GTSE1-mCherry constructs. Rapamycin (200 nM) was added to induce removal of clathrin and imaged for a total of 10 min to visualize co-rerouting of GTSE1 mutants. Scale bar, 10 µm. (Right) Quantification of GTSE1 co-rerouting shown as arrow plots. Arrows show the fraction of spindle and mitochondria fluorescence that is at the spindle (i.e. 1 = completely spindle-localized, 0 = mitochondria-localized), for both channels, moving from pre to post rapamycin localization. Black arrows represent individual cells, the orange arrow is the mean. n = 7-12 cells per condition.

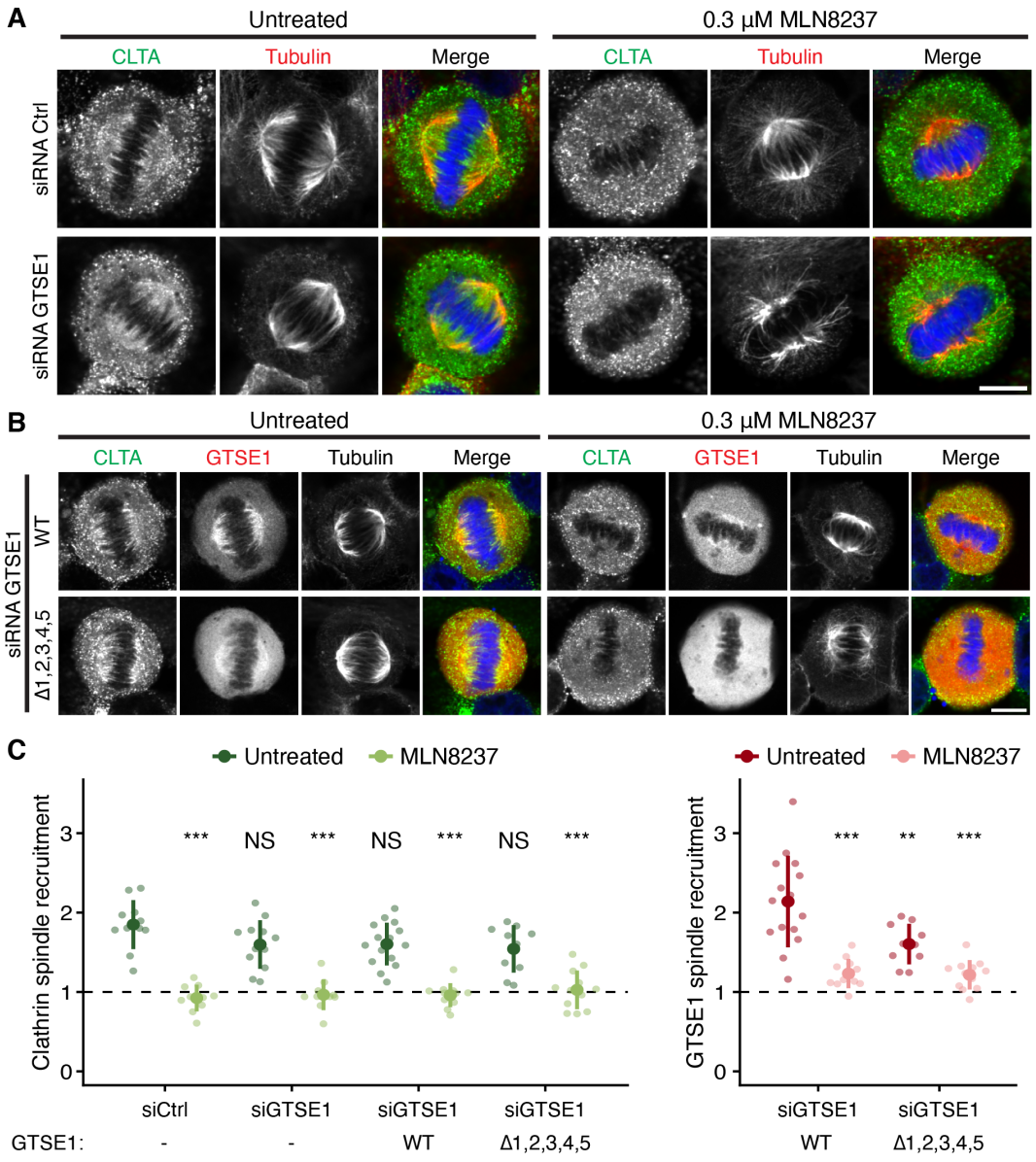

Figure S6: Comparison of GTSE1 LIDL motif ablation with the effect of Aurora-A inhibition on spindle localization of clathrin and GTSE1.
Representative widefield micrographs of CLTA-FKBP-GFP cells at metaphase to show the spindle localization of clathrin (**A**), or GTSE1-mCherry construct (WT or Δ1,2,3,4,5, red) and clathrin (**B**). Cells were treated with control (GL2, Ctrl) or GTSE1 siRNA and Aurora-A kinase was inhibited with MLN8237 (0.3 µM, 40 min) as indicated. Cells were stained for tubulin (red in A, not shown in merge in B) and DNA (blue). A GFP-boost antibody was used to enhance the signal of CLTA-FKBP-GFP (green). Scale bar, 10 µm. (**C**) Quantification of clathrin and GTSE1 spindle recruitment. Each dot represents a single cell, n = 10-15 cells per condition. The large dot and error bars show the mean and the mean ±SD, respectively. Analysis of variance (ANOVA) with Tukey's post-hoc test was used to compare the means between each group, using the untreated cells + siRNA Ctrl (clathrin) and untreated cells + WT GTSE1 (GTSE1) for comparison. The p-value level is shown compared to WT: ***, $p < 0.001$; **, $p < 0.01$; NS, $p > 0.05$.

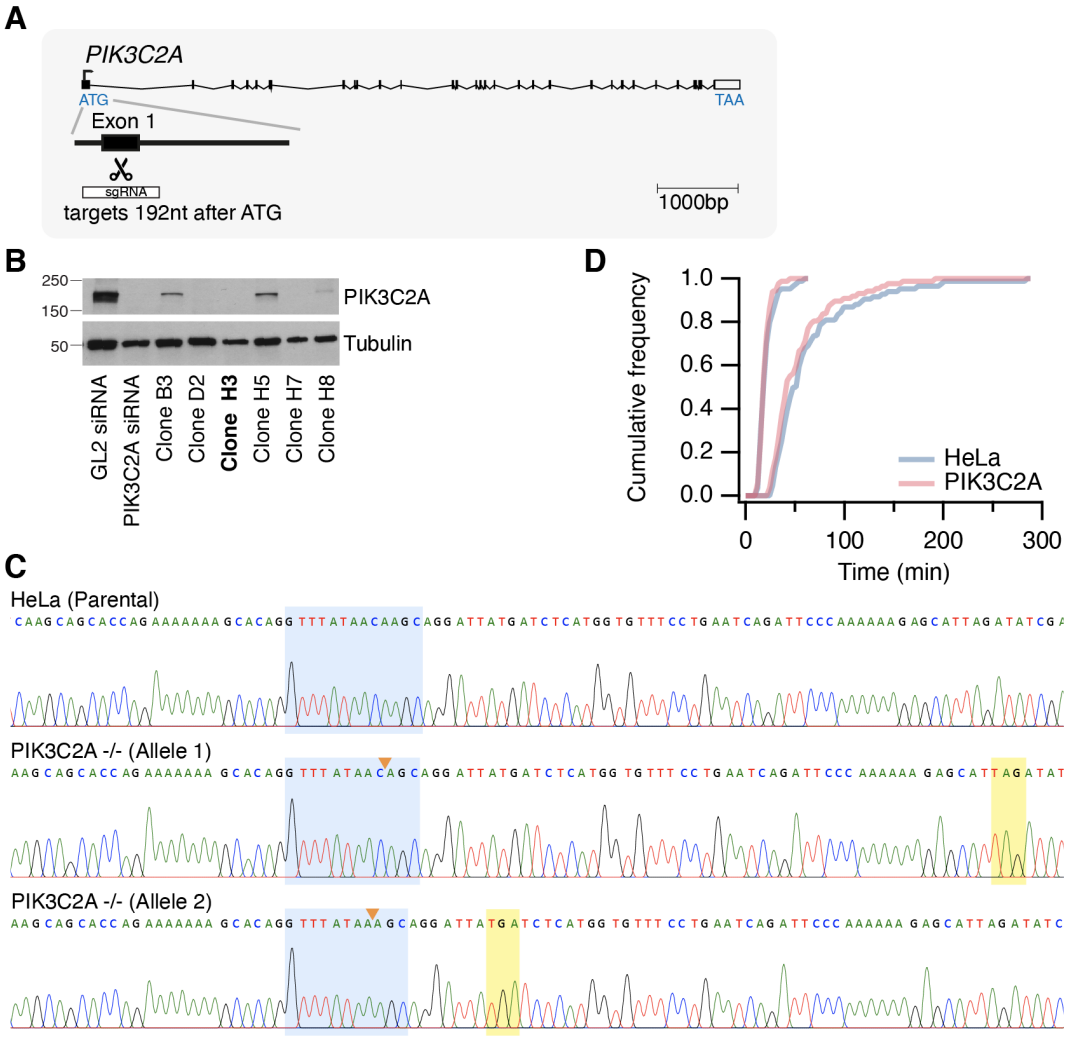

Figure S7: Generation of PIK3C2A-null HeLa cells.
(**A**) Targeting strategy for generation of a PIK3C2A-null cell line. HeLa cells were transfected with plasmid to express GFP coupled Cas9 nuclease and sgRNA targeting 192 bp from the start codon of the PIK3C2A gene. Scale bar, 1000 bp. (**B**) Western blot of a selection of clones grown after expansion of GFP-expressing cells sorted by FACS. Presence of a band for PIK3C2A was assessed compared parental HeLa cells treated with PIK3C2A siRNA or control, GL2. Tubulin, loading control. Clone H3, was used in this study (bold). (**C**) A genomic fragment from clone H3 was cloned into a cloning vector and 20 bacterial clones were picked and sequenced to assess the status of PIK3C2A alleles. We found two sequences, indicating two alleles and both had deletions (orange arrows) which resulted in premature truncation of the PI3KC2A gene after 87 and 72 residues, respectively. Stop codon is highlighted in yellow. Blue window highlights the edited region. (**D**) Mitotic progression of PIK3C2A-null cells compared to parental HeLa cells. Cumulative histograms of timings from nuclear envelope breakdown-to-metaphase (NEB-M, long duration) and metaphase-to-anaphase (M-A, short duration). Progression experiments were done three times. Number of cells analyzed = PIK3C2A$^{-/-}$: 87; parental: 84.

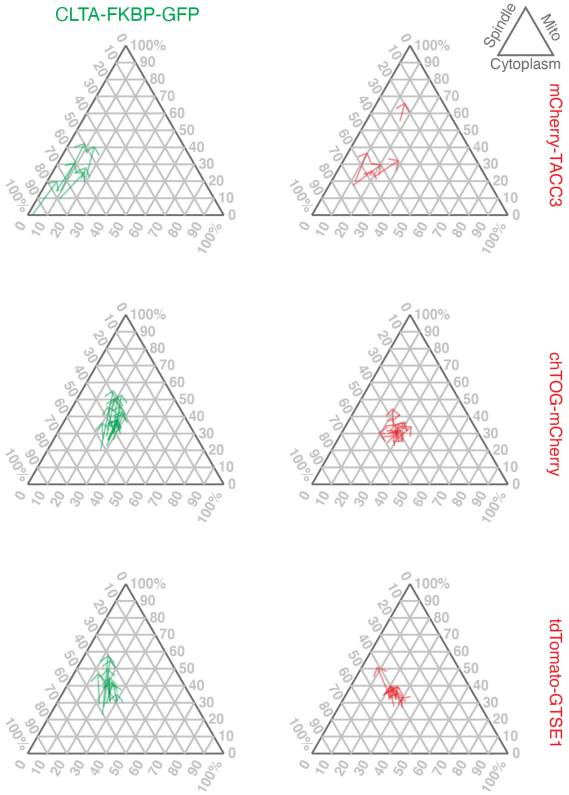

Figure S8: Ternary diagrams of live CLTA-FKBP-GFP spatial relocalization experiments.
Localization before and after addition of rapamycin is shown by an arrow for each cell. Ternary diagrams can be read using the key. For example, a protein that is localized entirely on the miochondria and is absent from the spindle would be at the top corner of the triangle. Generally, movement (if it occurs) is from the bottom left corner to the upper corner with cytoplasmic signal staying approximately constant.

Cell line	Clone	Genomic status	Western band-shift	Western endogenous	Insertion	Unedited allele(s)	Expected localization	KSW	Mitosis	Notes
CLTA-FKBP-GFP	5	Homozygous	Yes	No	Yes	No	Yes	Yes	Normal	Clathrin triskelia are CLTC with CLTA and CLTB. In HeLa, CLTA > CLTB expression
GFP-FKBP-TACC3	D5	Homozygous	Yes	No	Yes	No	Yes	Yes	Slight delay	–
chTOG-FKBP-GFP	H5	Heterozygous	Yes	Yes	Yes	Yes	Yes	Yes	Normal	>20 heterozygous clones, 0 homozygous recovered from three attempts
GTSE1-FKBP-GFP	A5	Homozygous	Yes	No	Yes	No	Yes	Yes	Normal	–

Table S1: Summary of knock-in cell lines used in this study.
Details of each cell line used. Insertion and unedited allele(s) were detected using PCR and genomic sequencing. KSW, Knocksideways.

	Protein of interest			
Cell line	**clathrin**	**TACC3**	**chTOG**	**GTSE1**
CLTA-FKBP-GFP	-1.04 [-1.51, -0.673] * –	-1.21 [-1.69, -0.704] * -0.181 [-0.336, -0.0768] *	-1.16 [-1.55, -0.755] * -0.0535 [-0.0911, -0.009] *	-0.399 [-0.733, -0.0903] * -0.0991 [-0.161, -0.0547] *
GFP-FKBP-TACC3	-0.136 [-0.708, 0.375] -0.0352 [-0.0568, -0.0144] *	-1.06 [-1.94, -0.267] * –	-1.19 [-1.47, -0.94] * -0.115 [-0.223, -0.0582] *	-0.248 [-0.62, 0.128] -0.0418 [-0.0759, -0.013] *
chTOG-FKBP-GFP	-0.65 [-1.35, 0.0585] -0.0331 [-0.105, 0.022]	-0.745 [-1.48, 0.314] -0.0198 [-0.146, 0.0762]	-0.45 [-0.989, 0.098] –	0.698 [-0.138, 2.36] -0.033 [-0.0663, 0.00429]
GTSE1-FKBP-GFP	-0.267 [-0.416, -0.125] * -0.00823 [-0.0356, 0.0205]	-1.17 [-1.52, -0.829] * 0.000224 [-0.0544, 0.0563]	-0.484 [-0.757, -0.205] * -0.00675 [-0.0249, 0.0106]	-0.775 [-0.938, -0.613] * –

Table S2: Summary of knocksideways experiments.
Each row is a cell line and the effect of relocalization of the tagged protein to mitochondria on the spindle localization of each protein-of-interest is indicated. Effect sizes for immunofluorescence (upper) and live cell (lower) knocksideways experiments, are presented with bias-corrected and accelerated bootstrap 95% confidence intervals. *, interval is less than 0.

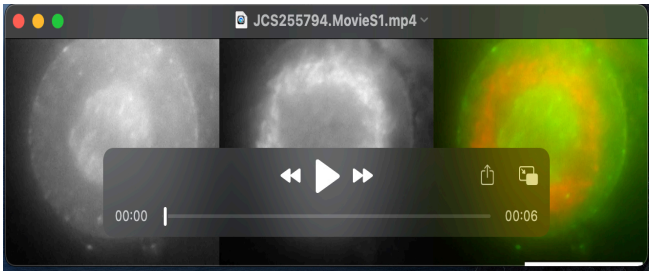

Movie 1: Knocksideways of CLTA-FKBP-GFP. Typical widefield movie of relocalization in response to rapamycin (200 nM) in cells co-expressing mCherry-MitoTrap.
Time, mm:ss. Scale bar, 10 µm.

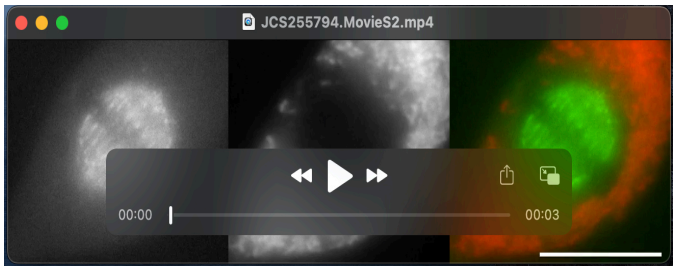

Movie 2: Knocksideways of GFP-FKBP-TACC3. Typical widefield movie of relocalization in response to rapamycin (200 nM) in cells co-expressing mCherry-MitoTrap.
Time, mm:ss. Scale bar, 10 µm.

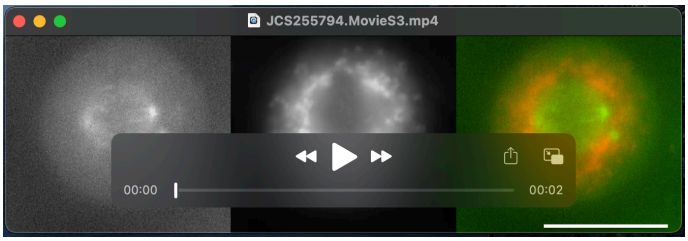

Movie 3: Knocksideways of chTOG-FKBP-GFP. Typical widefield movie of relocalization in response to rapamycin (200 nM) in cells co-expressing mCherry-MitoTrap.
Time, mm:ss. Scale bar, 10 µm.

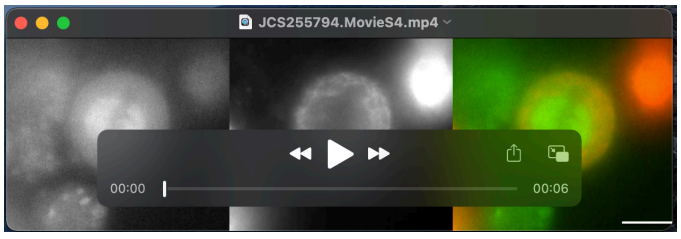

Movie 4: Knocksideways of GTSE1-FKBP-GFP. Typical widefield movie of relocalization in response to rapamycin (200 nM) in cells co-expressing mCherry-MitoTrap.
Time, mm:ss. Scale bar, 10 µm.

Journal of Cell Science • Supplementary information